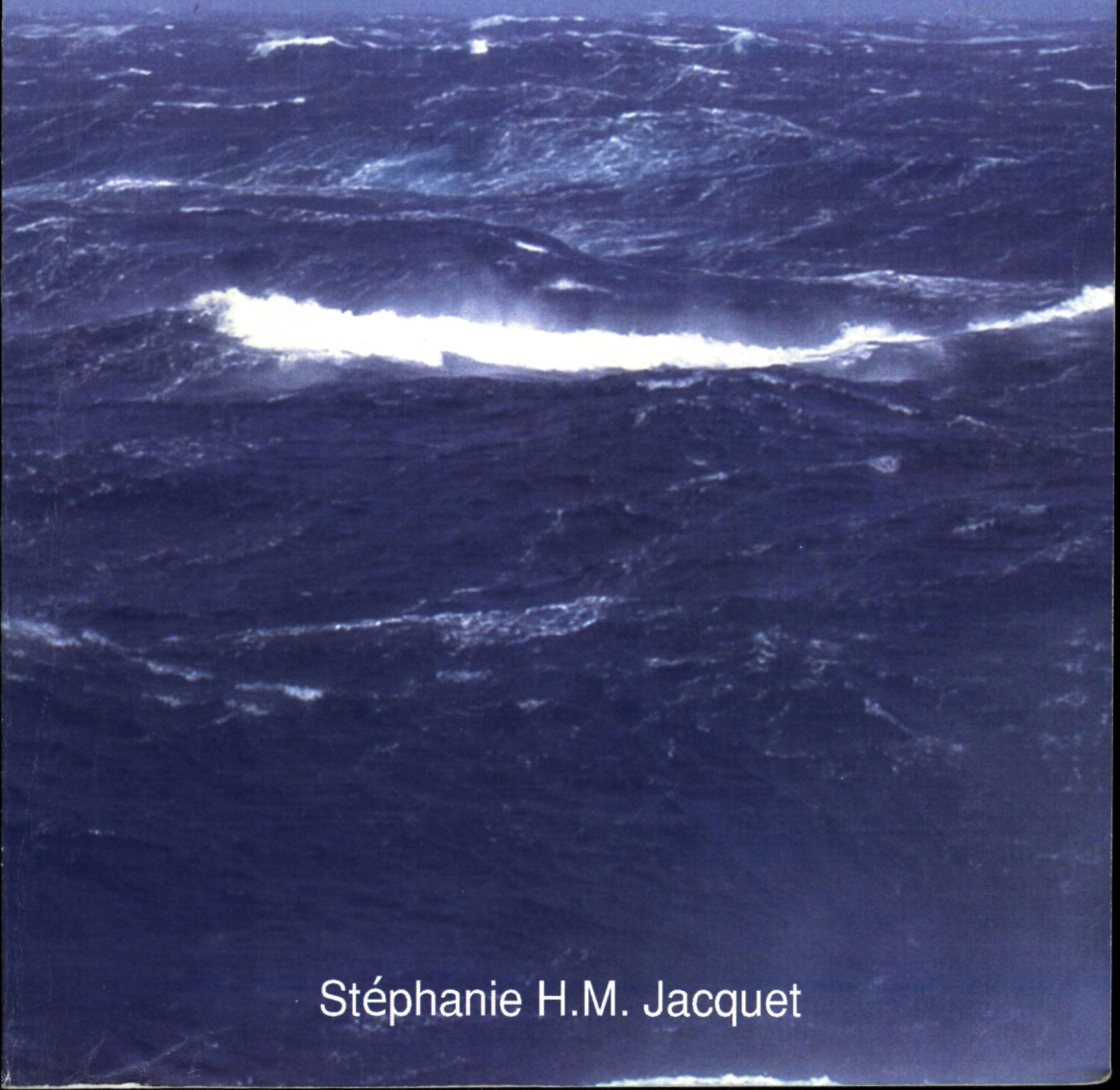
Barium in the Southern Ocean: Towards an estimation of twilight zone C mineralization



Stéphanie H.M. Jacquet

www.baiteco.com

Stef

Vrije Universiteit Brussel - Faculty of Science
Laboratory of Analytical and Environmental Chemistry

Barium in the Southern Ocean: Towards an estimation of twilight zone C mineralization

Stéphanie H.M. Jacquet

Proefschrift voorgedragen tot het behalen van de graad van
Doctor in the Wetenschappen

Academic year 2006-2007

Advisor
F. Dehairs (VUB)

Co-advisors
B. Quéguiner (LOB-COM, France)
W. Baeyens (VUB)

Committee
M. Elskens (VUB)
G. Laus (VUB)
P. Claeys (VUB)
F. De Ridder (VUB)
C. Jeandel (LEGOS-OMP, France)
D. Cardinal (MRAC)
C. Lancelot (ULB, ESA)

CONTENTS

Acknowledgements 7

Abstract 9

General introduction 11

Section1 – Material and method

Introduction 23

Chapter1 25

Suspended matter, acantharians and barite crystals: a brief overview of the methods used

Chapter2 33

Dissolved barium in seawater

Section 2 - Dissolved barium in the global Ba-cycle dynamics

Introduction 53

Chapter 3 57

Barium distribution in the Crozet-Kerguelen Basin

Chapter 4 77

A high resolution transect of dissolved barium

Chapter 5 87

Seasonal variability of barium signals

Chapter 6 107

Dissolved barium according to a parametric mixing model

Discussion 119

Section 3 - Ba_{xs}-based mesopelagic C mineralization

Introduction 127

Chapter 7 135

Mesopelagic C mineralization in artificial iron fertilization conditions

Chapter 8 149

Mesopelagic C mineralization in the Kerguelen Plateau region

Chapter 9 166

Twilight zone organic C mineralization in the North Pacific

Chapter 10 183

Particulate Ba_{xs}, barite and acantharians

Discussion 203

General conclusion 213

References 219

ACKNOWLEDGEMENTS

This research was supported by the Federal Belgian Science Policy Office under SPSD Programs on Global Change, Ecosystems and Biodiversity, Brussels, Belgium (BELCANTO network contracts EV/37/7C, EV/03/7A, SD/CA/03A), the Vrije Universiteit Brussel under grant GOA22 and the Research Foundation Flanders via contract G. 0021.04. I thank the captains and crews of the R/V *Polarstern, Marion Dufresne, Aurora Australis, Kilo Moana and Revelle*. I'm grateful to the different chief scientists and to colleagues who helped in sampling and made some of the measurements on board during the SAZ-98, CLIVAR SR3, EIFEX, ANTARES-4, VERTIGO and more particularly KEOPS and SAZ-SENSE cruises. I'm grateful to all persons who kindly shared their data during these cruises. Jacques Navez and Laurence Monin are greatly acknowledged for their help during sample processing and element analyses. Thanks also to Anouk de Brauwere for her help in modeling and to Michael Korntheuer for his technical expertise concerning the Riso low B counter. Discussions with Damien Cardinal, Nicolas Savoye and Marc Elskens very much helped shaping this dissertation. The constructive criticisms of various reviewers were also appreciated and greatly improved this work. I also thank all my colleagues and friends at the VUB, ULB, ESA, MRAC, ULG, UA, COM, OMP, LBCM, CSIRO, AWI, WHOI..., for their support; thanks especially to people involved in the BELCANTO network. To finish I would like to thank my co-advisors Prof. Willy Baeyens and Prof. Bernard Quéguiner, and mainly my advisor Prof. Frank Dehairs who made this work possible and enjoyable.

To all I've named, and to the many friends and relatives who have given me inspiration, ideas, and support along the way, I would like to extend a big hug.

Brussels, 7 May 2007
S.H.M. Jacquet

ABSTRACT

[1] The downward export of organic material through the biological pump constitutes the critical process linking the surface to deep ocean and an important mechanism for carbon (C) sequestration. In simulation studies of the Southern Ocean's role in the global C cycle, resolving the issue of the controls on particle transport magnitude and efficiency in the upper 1000 m water column is of particular importance. Assessing C export and mineralization fluxes in the Southern Ocean (S.O.) via a multi-proxies approach represents indeed one of the major objectives of the BELCANTO II project (BELgian research on C uptake in the ANTarctic Ocean; Belspo). Among the different proxies used (i.e. Ba_{xs}-barite, ^{234}Th, biomarkers, $\delta^{15}N$, ^{13}C, $\delta^{29}Si$, bacterial activity and sediment traps data), specific focus in the present work was on the barium proxy.

[2] The great potential of the mesopelagic particulate biogenic Ba_{xs}-barite ($BaSO_4$) as a proxy of C mineralization processes in the S.O. was however shadowed by uncertainties related to the mechanism itself of Ba_{xs}-barite formation in the water column. This issue moreover constitutes the limiting keys for any application of the Ba proxies. In order to further improve the robustness of the Ba_{xs}-barite tool, two pathways were followed in this dissertation: the first one consisted in shedding light on the interaction between the dissolved and particulate Ba phases and the significance of this in the oceanic Ba dynamics. The second pathway consisted in better constraining and calibrating the mesopelagic Ba_{xs} proxy. Two major outcomes of this work are (1) the denial of the active biological mediation as the major factor setting both the dissolved Ba and Ba_{xs}-barite water column distributions and the clear decoupling between dissolved Ba, silicate and alkalinity, and (2) the significant link between mesopelagic particulate biogenic Ba_{xs}-barite and bacterial activity distributions. We demonstrated that the mesopelagic Ba_{xs} build-up reflects the intensity of exported biogenic material degradation by heterotrophic bacteria and that the release of biogenic Ba from acantharia celestite ($SrSO_4$) is only a minor contributor to barite formation. Moreover, the particulate biogenic Ba_{xs}-barite formation/dissolution dynamics overwhelmed by the general circulation appeared as the major mechanism shaping the water column dissolved Ba gradient. Findings allowed us to refine a potential scenario of open Ocean mesopelagic Ba_{xs}-barite formation process.

[3] The present work enabled a better evaluation of the processes controlling transport of sinking particles between surface and deep ocean. Various

environments which significantly differed in terms of ecosystem functioning (intensity of the biological pump and subsequent fate of sinking biogenic materials with depth) were investigated. Mesopelagic Ba_{xs} fluxes were translated into C mineralization rates using a relationship relating Ba_{xs} to O_2 consumption as reported by Dehairs et al. [1997]. The Ba_{xs} residual content (Ba_{xs} signal at zero oxygen consumption, i.e. zero organic C demand) which depends on the saturation state of the water for barite was adjusted for each study area. We moreover showed that Ba_{xs}-based mesopelagic C mineralization fluxes compare well with results obtained with modes of C utilization assessment (i.e. bacterial carbon demand and POC flux decrease from Neutrally Buoyant Sediment Traps). From the different environments studied, the outcome of the C export, not only dependent on its magnitude, appears significantly modified by conditions at intermediate layers. The extent of mesopelagic C mineralization is closely linked to the combination of both the intensity and nature of the blooms, the grazing pressure, the distribution of bacterial activity and the type of biogenic material exported. It is actually difficult to define a single, global response in mineralization processes following bloom developments. Results seem however to indicate that systems where calcium carbonate producing plankton is significant are prone to more important deep export than systems dominated by diatoms. Moreover, in diatom dominated systems thriving in Fe replete conditions, it seems that blooms are less prone to mesopelagic C mineralization when surface productivity is particularly intense and the materials exported composed by larger diatoms and fast sinking pellets. On the contrary, mesopelagic processing of organic matter appears higher in HNLC's systems dominated by smaller diatoms, lower grazing pressure and deeper bacterial activity. Moreover, at the Southern Ocean's scale, the biological pump and undergoing C mineralization at intermediate depths appear more intense (in absolute values) in the subantarctic and polar front zones, coinciding with regions of atmospheric CO_2 sink. The intensity of mesopelagic C mineralization has moreover been shown to increase during the growth season in these areas. Frontal systems, where hydrodynamics and trophic gradients are well known to enhance productivity, seem also to be site of higher mesopelagic mineralization processes.

GENERAL INTRODUCTION

Mesopelagic carbon mineralization

[4] In studying the key role played by the oceans in the global carbon (C) cycle and climatic changes, efforts have gone into understanding the biological pump. The biological pump is a combination of processes that result in the transfer of CO_2 from the surface of the ocean, where it is fixed by phytoplankton, to the deep ocean through the sinking of particles, thus redistributing the ocean's C content [Sarmiento et al., 1988; Honjo, 1996; Battle et al., 2000; see further Section 3]. The Southern Ocean (S.O.), as a result of its circumpolar circulation and its active hydrological and ecological dynamics, is a crucial component of this C pump [François et al., 1997; Trull et al., 2001-a; Takahashi et al., 2002]. For some decades, studies have mainly focused on understanding/quantifying the processes acting in the upper mixed layer (upper 100 m). However, most (~90%) of the biogenic particles exported from the latter layer are remineralized at mesopelagic depths (~100-1000 m) and only a small fraction (<1%) of the particle flux reaches the seafloor. Less than 0.1% of the surface C export carried to the sea bed is buried to become sequestered over geological time scales. As the study of the mesopelagic zone (or twilight zone) has all too often been neglected, the efficiency of remineralization processes in this part of the water column remains poorly understood to this very day. This zone is, however, of crucial significance in determining the efficiency of export by the surface biological pump and the fate of biogenic material, since mineralization length scales are important indicators of the capacity of intermediate layers for longer term carbon sequestration.

Particulate biogenic barium and C mineralization: what is the link?

[5] In order to resolve the remineralization curve (or also mineralization length scale) in the mesopelagic zone, studies of downward particle flux have mainly focused on the particulate organic carbon (POC) flux change with depth by using sediment traps at depths generally >1000 m and by reconstructing the export flux and mineralization length scale using empirical functions [e.g. Martin et al., 1987; Bendtsen et al., 2002; Boyd and Trull, in press; see further Section 3]. Earlier studies of C fluxes were first conducted from a geological perspective with the aim of linking C accumulation patterns to productivity, and thus, by developing empirical algorithms, to obtain proxies for paleoproductivity. However, due to the rapid and extensive degradation of exported organic matter and to hydrodynamics [Honjo and Manganini, 1996;

Siegel and Deuser, 1997], sediment traps are not reliable in the upper 1000 m of the ocean [Yu et al., 2001]. The use of the previous approach to resolve the mineralization curve has led to obvious errors [Buesseler et al., 1994]. During the last decade, studies focused on more refractory proxies of C export of which particulate biogenic barium, also called excess Ba or Ba_{xs} (total particulate Ba minus the lithogenic part; mainly constituted of barite crystals, $BaSO_4$; Dehairs et al., 1980; Robin et al., 2006) appeared a good candidate. The Ba_{xs} stock in mesopelagic water is built up during the phytoplankton growth season as a result of the transfer and degradation of biogenic aggregates from the mixed layer [Dehairs et al., 1997; Cardinal et al., 2005; see further Sections 2 and 3]. Observations support that in a World Ocean mostly under-saturated with $BaSO_4$ [Monnin et al., 1999; Rushdi et al., 2000; Monnin and Cividini, 2006], these biogenic aggregates provide the necessary thermodynamic conditions for barite precipitation during organic matter mineralization [Dehairs et al., 1980, 2000; Collier and Edmond, 1984; Bishop, 1988; Stroobants et al., 1991; Bertram and Cowen, 1997; Ganeshram et al, 2003]. The Ba_{xs}–barite distribution (see further sections 2 and 3) reflects production of particulate Ba to take place below the upper mixed layer and to be ongoing in the twilight zone, as recently emphasized in Van Beek et al. [2007]. Barite in sediments was first used as a paleo-productivity proxy. This application is based on the strong relationship between Ba_{xs} and organic carbon fluxes observed in sediment traps [Bishop, 1988; Dymond et al., 1992; Francois et al., 1995] and the high barite accumulation rate in sediment underlying areas of high productivity [Goldberg and Arrhenius, 1958; Paytan et al., 1993, 1996-a; Gingele and Dahmke, 1994; Eagle et al., 2003]. Here, the association of barite formation with bacterial degradation of organic matter at mesopelagic depths, followed by the release of discrete barite micro-crystals in the ambient water, led to the use of discrete barite crystals as an indirect proxy for the mesopelagic mineralization of exported biogenic material [Dehairs et al., 1980, 1990, 1991, 1997; Cardinal et al., 2001, 2005]; the mesopelagic Ba_{xs} (meso-Ba_{xs}) stock can be translated into POC fluxes by using a relationship empirically relating Ba_{xs} to O_2 consumption [Shopova and al., 1995; Dehairs et al., 1997; see further Section 1].

Improving the link

[6] Despite the great potential of the meso-Ba_{xs} proxy, its use remained limited. This is in part due to uncertainties about the mechanism of barite precipitation itself in the water column. The scenario outlined above suggests a passive barite ($BaSO_4$) precipitation in micro-environments through

enrichment of sulfates and/or barium in decomposing organic material, which is itself still largely unexplained [Dehairs et al., 1980, 2000; Collier and Edmond, 1984; Bishop, 1988; Stroobants et al., 1991; Bertram and Cowen, 1997; Ganeshram et al, 2003]. Sulfate would be produced by the reduction of sulphur from proteinaceous phytoplankton material during the degradation of organic matter [Bishop, 1988], and barium, adsorbed or incorporated to plankton material, would be released during the breakdown inside such micro-environments. Indeed, experimental work has shown that production of barite is induced during phytoplankton aggregation and subsequent mineralization [Ganeshram et al., 2003], corroborating hypotheses issued earlier [Bishop, 1988; Dehairs et al., 1991].

[7] Some questions remain regarding the involvement of the dissolved Ba (Ba_d) phase in Ba_{xs}-barite dynamics: dissolved Ba from ambient water must be involved, but the difficulty resides in finding evidence of this process. To date, only a small number of studies have addressed the Ba cycle from the angle of Ba_d [e.g. Chan et al., 1977; Falkner et al., 1994; Jeandel et al., 1996]- a difficult task considering the difference in stock and oceanic residence time of dissolved Ba (few tens of nM; ~10,000 years; Broecker and Peng, 1982) compared to particulate Ba (few hundreds of pM; ~10 years; Dehairs et al., 1980). Since Ba_d in the open ocean behaves as a bio-intermediate element presenting lower concentration in the upper 1000 m without, however, reaching total depletion in surface waters [Chow and Goldberg, 1960; Broeker and Peng, 1982; see further Section 2], a large number of studies concluded that the apparent correlation of Ba_d with silicate and alkalinity involves a direct link with biological processes [Wolgemuth and Broeker, 1970; Li et al., 1973; Chan et al., 1977; Lea and Boyle, 1989; Bruland, 1983]. However, other studies clearly indicated that dissolved Ba is not controlled by the processes which control silicate and alkalinity [Edmond, 1974]. This conclusion was subsequently corroborated by the observed close relationship between barite with productivity [Cronan, 1974; Dehairs et al., 1980, 1987; Dymond et al., 1992; François et al., 1995; Dymond and Collier, 1996; McManus et al., 1998], suggesting that the dissolved Ba distribution does not reflect a direct link with biological activity, but a potential link with the Ba_{xs}-barite dynamics [Collier and Edmond, 1984; Bishop, 1988; Jeandel et al., 1996; Dehairs et al., 1990, 1991, 1992; Stroobants et al., 1991; Stecher et al., 1999; see further Section 2]. Various studies thus focused on determining whether planktonic organisms could directly incorporate or precipitate Ba from solution, thus explaining surface Ba_d removal and Ba fluxes in the water column [Collier

and Edmond, 1984; Bernstein et al., 1987, 1992, 1998; Dehairs et al., 1980; Ganeshram et al., 2003; Bernstein and Byrne, 2004; Sternberg et al., 2005-a, accepted]. The specific role of different planktonic organisms such as coccolithophorids ($CaCO_3$), diatoms (opal) or acantharians ($SrSO_4$) has been debated [Dehairs et al., 1980; Bernstein et al., 1998; Esser and Volpe, 2002; Ganeshram et al. 2003; Bernstein and Byrne, 2004; Sternberg et al., 2005; see further Section 3]. Association of barite crystals and biota is well documented in the case of the Xenophyophora (benthic Rhizopods) carrying barite crystals inside their protoplasm [Tendal, 1972; Hopwood et al., 1997], as well as in the case of agglutinating benthic foraminifera [Gooday et al., 1995; Bertram and Cowen, 1997]. However, it is not clear whether these organisms synthesize the barite or incorporate barite crystals originally present in the sediment [Gooday et al., 1995; Hopwood et al., 1997]. Similarity in morphology between sedimentary barite and barites inside Xenophyophora suggests uptake of the crystals from the sediments [Hopwood et al., 1997]. Presence of barite has also been reported in cultured Prymnesiophyte algae (*Exanthemachrysis gayraliae*) originally collected from the Mediterranean [Fresnel et al. 1979; Gayral and Fresnel, 1979]. For the freshwater environment as well, intracellular barite crystals and active synthesis of barite has been observed for desmids (unicellular green algae) [Brook, 1980; Wilcock et al., 1989] as well as for ciliates [Hubert et al., 1975; Finlay et al., 1983; Fenchel and Finlay, 1984]. Nanometer sized barite crystals were observed to be associated with cell surface of benthic algae forming microbial mats in an Antarctic lake [Tazaki et al., 1997]. Some doubt also remains for the implication of Acantharians (marine pelagic plankton), which are celestite ($SrSO_4$) secreting micro-heterotrophs, reported to be involved in Ba uptake and barite formation [Bernstein et al., 1998, 2004; Sternberg et al., accepted].

[8] Overall, further efforts must be made to understand the processes leading to the mesopelagic Ba_{xs} formation; this is crucially important if the barite proxy calibration is to be refined. Indeed, the application of any proxy requires a mechanistic understanding of the pathways leading to that proxy. In many cases, the relationship between dissolved and particulate phases in the water column is not fully understood due to the complexity of the biological processes, lithogenic supplies and physico-chemical processes (varying regionally and with depth) that are acting on their distributions and this is particularly the case for Ba. To validate the proxy calibration, the temporal and spatial variability of both dissolved and particulate barium in the water column (variability of Ba profiles during bloom developments and their examination in contrasting environments), as well as the

relationship between Ba_{xs} and organic C mineralization, need to be investigated further. Optimization of the Ba_{xs}-barite approach would provide a powerful tool to estimate mesopelagic mineralization of exported organic matter.

Objectives

[9] In the present work, the essential achievements after four years of research are discussed. This study forms part of the interdisciplinary network BELCANTO II project (BELgian research on Carbon uptake in the ANTarctic Ocean, funded by BELSPO, Belgian Science Policy) in which the major role of the Southern Ocean in the global biogeochemical cycling of elements (such as C, N, Si, P, Fe) and climate regulation (notably through its capacity to absorb atmospheric CO_2) are studied. Specific attempts were made to assess the C flux exported at the base of the mixed layer and the remineralization flux of organic C at mesopelagic depths via a multi-proxies approach including Ba-barite, ^{13}C, $\delta^{15}N$, ^{234}Th, biomarkers, $\delta^{29}Si$, bacterial activity and sediment traps data (see further Section 3). In particular, the aim of our contribution in using the barium proxy via a systematic study of both its dissolved and particulate phases, was double: (**1**) shed light on the interaction between dissolved and particulate Ba and the significance of this in the oceanic Ba dynamics, and (**2**) better validate and calibrate the meso-Ba_{xs} proxy to make it a powerful tracer of the mesopelagic C mineralization. This will also help to strengthen applications of the Ba proxy, e.g. for reconstructing modern and past ocean carbon export (for which barite precipitation and its fate in the water column constitute the limiting keys for robust interpretation). Moreover, in the context of global climate dynamics, this work - via its multi-pronged approach - is of considerable importance in assessing the capacity of intermediate layers for longer term carbon sequestration.

Study areas

[10] Various environments, which differed significantly in terms of ecosystem functioning, were investigated both in the S.O. and in the North Pacific Ocean. Respectively, we confront results from the following cruises: SAZ-98, CLIVAR SR3, ANTARES-4, KEOPS and EIFEX (Figure A-a), and VERTIGO 1-ALOHA and VERTIGO 2-K2 (Figure A-b). These data are also compared to results obtained during previous S.O. cruises (ANTX/6, ANTX/7, CIVA-1, Prydz Bay, ANT IX/2, EPOS-2, ANTARES 2, INDIGO 3; Frank Dehairs's data base). We give here only a brief overview on the cruises carried out in the context of this dissertation:

- **SAZ-98** (Subantarctic Zone) and **CLIVAR SR3** (Climate Variability) expeditions were carried out at ~145°E in the Australian sector of the S.O. along north–south transects between Tasmania and Antarctica (R/V *Aurora Australis*). SAZ-98 (AU9706; summer; Feb.–Apr. 1998) and CLIVAR-SR3 (AU0103; spring; October – December 2001) are part of several cruises in this sector aiming at identifying and quantifying the seasonal and interannual variations of the S.O. dynamics and biogeochemistry, with particular focus on the Subantarctic Zone and Polar Front areas.

- **ANTARES-4** (Antarctic Research, SO-JGOFS France program) was a meso-scale study in the Indian sector of the S.O., north-west of the Kerguelen archipelago in the Crozet-Kerguelen basin (43°S-46°S and 62°E-65°E; Jan.-Feb. 1999; R/V *Marion Dufresne*). This zone is characterized by particularly strong gradients in physico-chemical and biological characteristics due to the confluence in a latitudinal restricted zone of frontal systems. This cruise aimed at understanding and quantifying C and biogenic elements export fluxes in the water column of a region known to be a major CO_2 sink.

- The **KEOPS** project (KErguelen: compared study of the Ocean and the Plateau in Surface water) was carried out on the Kerguelen continental shelf (~51°S-75°E; Polar front zone, Indian sector of the S.O.) during Jan.-Feb. 2005 (R/V *Marion Dufresne*). In this sector known to be a HNLC region, the shelf is a site experiencing quasi-continuous natural iron fertilization resulting in high biological productivity; the Kerguelen Plateau thus served as a natural laboratory for comparisons with short term iron-induced blooms. The goal was to refine assessment of C sequestration by the ocean under natural iron fertilization conditions.

- The **EIFEX** experiment (European Iron Fertilization Experiment) was carried out in a mesoscale cyclonic eddy located in a meander of the Antarctic Circumpolar Current during Jan.-Mar. 2004 (R/V *Polarstern* ANT XXI/3; ~50°S-2°E, Atlantic sector). The main aim of this experiment was to study the growth and demise of a phytoplankton bloom induced by iron fertilization with special emphasis on the fate of the bloom: biomass transfer to higher trophic levels and export out of the surface mixed layer.

- The **VERTIGO** project (VERtical Transport In the Global Ocean) focused on the efficiency of particle transport between the surface and deep ocean.

VERTIGO 1 (station **ALOHA**, oligotrophic NE Pacific; R/V *Kilo Moana*) was carried out in Jun.-Jul. 2004 and VERTIGO 2 (station **K2**, mesotrophic NW Pacific; R/V *Revelle*) in Jul.-Aug. 2005. The project more specifically addressed the fate of sinking particles leaving the upper ocean and the factors that influence mineralization length scales for different particles types.

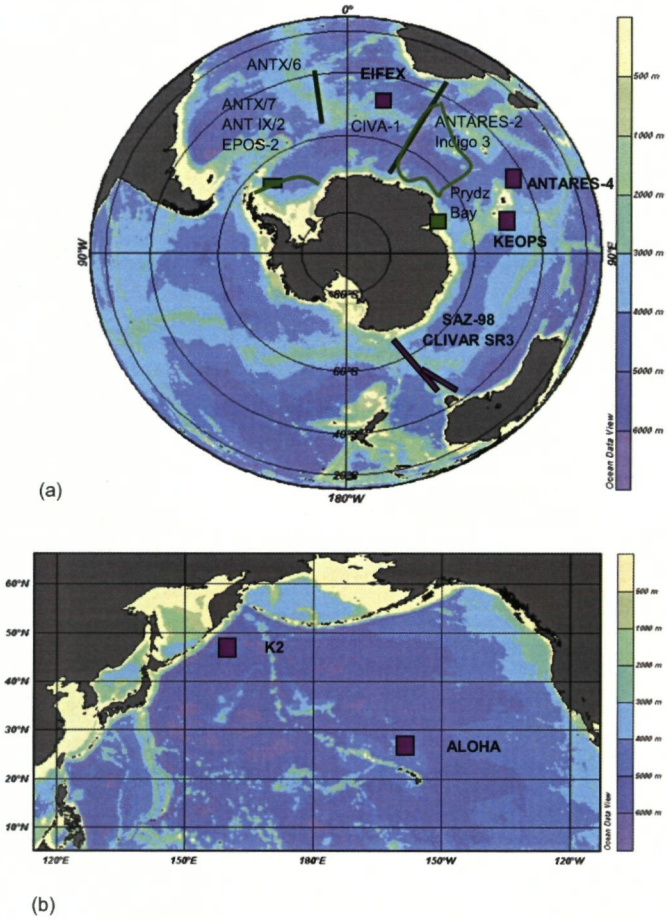


Figure A: Location of the cruises (a) in the Southern Ocean and (b) in the North Pacific.

Chapter outline

[11] This work is divided in three major sections. Section 1 (Chapters 1 and 2) focuses on the analytical/methodology part. We present the different methods used in this work to determine Ba in the dissolved and particulate phases. Special emphasis is given to dissolved Ba measurements in seawater for which two methods are confronted. In Section 2 (Chapter 3 to 6), we investigate the importance of the dissolved Ba phase in the Ba dynamics and in Section 3 (Chapter 7 to 10), we concentrate on the calibration of Ba_{xs} to estimate mesopelagic C remineralization fluxes. In sections 2 and 3, a general introduction is given on the existing literature and on our particular contribution to the questions addressed, before discussing results from the different cruises reported above. An effort is made both for Section 2 and Section 3 to combine the data presented and to expend these conclusions in a more general context. To finish, we provide an integrated overview of the whole results, in order to present an overall image of this work (General conclusion). Some gaps in the current knowledge will be pointed out where relevant, along with suggestions for future research.

Publications of the author related to this work

[12] The results and ideas expressed in this dissertation are derived from the following publications:

- **Jacquet S.H.M.**, F. Dehairs and S. Rintoul (2004). A high resolution transect of dissolved barium in the Southern Ocean. Geophys. Res. Lett., 31, L14301, doi: 10,1029/2004GL20016
- **Jacquet S.H.M.**, F. Dehairs, D. Cardinal, J. Navez and B. Delille (2005). Barium distribution across the Southern Ocean Frontal system in the Crozet-Kerguelen Basin. Mar. Chem., 95(3-4), 149-162
- **Jacquet S.H.M.**, F. Dehairs, M. Elskens, N. Savoye and D. Cardinal (2007). Barium cycling along WOCE SR3 line in the Southern Ocean. In press, Mar.Chem.
- de Brauwere A., **S.H.M. Jacquet**, F. De Ridder, F. Dehairs, R. Pintelon, J. schoukens and W. Baeyens (2007). Water mass distributions in the Southern Ocean derived from a parametric analysis of mixing water masses. J. of Geophys. Res.-Ocean, 112, C02021, doi:10;1029/2006JC003742
- Blain and **al.** (2007). The effect of natural iron fertilization on carbon sequestration in the Southern Ocean. Nature, doi:10.1038/05700
- **Jacquet S.H.M.**, F. Dehairs, N. Savoye, I. Obernosterer, U. Christaki, C. Monnin and D. Cardinal. Mesopelagic organic carbon mineralization in the

Kerguelen Plateau region tracked by biogenic particulate Ba. Accepted with minor revisions, Deep Sea Res. II

- N. Savoye, T. Trull, **S.H.M. Jacquet**, J. Navez and F. Dehairs. ^{234}Th-derived export fluxes during a natural iron fertilization experiment (KEOPS). Accepted with minor revisions, Deep Sea Res. II
- **Jacquet S.H.M.**, N. Savoye, F. Dehairs, V. Strass and D. Cardinal. Mesopelagic carbon mineralization during the European Iron Fertilization Experiment (EIFEX). Accepted with minor revisions, Glob. Biogeochem. Cycles
- **Jacquet S.H.M.**, A. de Brauwere, F. De Ridder and F. Dehairs. Investigating dissolved barium behavior in the Southern Ocean using a parametric mixing model. In review, Geophys. Res. Lett.
- **Jacquet S.H.M.**, J. Henjes, F. Dehairs, A. Maeyer-Worobiec, N. Savoye and D. Cardinal. Particulate barium-barite and acantharians in the Southern Ocean during the European Iron Fertilization Experiment (EIFEX). In review, J. of Geophys. Res.-Biogeosciences
- F. Dehairs, **S.H.M. Jacquet**, D. Cardinal and J. Bishop et al.. Barium in twilight zone suspended matter as proxy for organic carbon mineralization: results for the North Pacific. In preparation, Deep Sea Res. II

Section 1

Material and method

INTRODUCTION

[13] This section presents the sampling procedures and analytical techniques used in this work to analyze Ba in dissolved and particulate phases, along with other major and trace elements. Dissolved Ba was measured from seawater samples and particulate Ba from suspended matter and acantharians individual's skeletons. These measurements constitute our own expertise; in parallel, barite crystals and acantharian abundance measurements were performed in collaboration with A. Worobiec (U. Antwerpen, Belgium) and J. Henjes (AWI, Germany), respectively. Here we briefly present suspended matter, acantharian and barite analyses (Chapter 1) before focusing on dissolved Ba in seawater for which two methods are confronted (Chapter 2). These methods constitute the major analytical development achieved in the context of this work.

[14] Our "work-horses" instruments were the following:

- An ICP-AES (inductively coupled plasma- atomic emission spectrometry): Thermo Optek Iris Advantage
- An ICP-QMS (inductively coupled plasma- quadrupole mass spectrometry, often referred to as ICP-MS): VG Plasma Quad 2+ Thermo Elemental
- An SF-ICP-MS (sector field -inductively coupled plasma- mass spectrometry, often referred to as high resolution HR-ICP-MS): Element 2 Thermo Finnigan

Chapter 1

Suspended matter, acantharians and barite crystals: a brief overview of the methods used

Foreword

[15] Particulate Ba and other trace and majors elements in suspended matter were measured systematically during the different cruises presented in this dissertation. Measurements of acantharian abundances and Ba/Sr skeletons contents, as well as barite crystals in suspended matter, were performed during the EIFEX cruise only. We give in Chapter 1 a brief overview of the sampling and analytical protocols used.

1.1. SUSPENDED MATTER

Sampling

[16] Sampling of suspended materials in seawater was done using CTD Rosettes equipped with 24 12 L Niskin bottles. 4 to 8 L of seawater were transferred to gauged filtration unit and filtered under pressure of filtered air (0.4 µm porosity) on polycarbonate membranes of 0.4 µm-porosity (47 and 90 mm-diameter). Samples were subsequently rinsed with Milli-Q grade water (10 to 20 mL) to remove sea-salt, dried at 50°C and stored in Petri dishes.

Chemical processing

[17] The detailed procedure used in this study for suspended matter is given in Cardinal et al. [2001]. Briefly, in the home based laboratory filtered particulate material was completely digested in sealed Teflon beakers using a $HCl/HNO_3/HF$ mixture (1.5 mL/1 mL/0.5 mL respectively; all Suprapur grade) heated at 90°C, in a clean pressurized room. After evaporation to dryness, the residue was dissolved in 3 mL of 2% HNO_3 and made to volume 10 mL with Milli-Q water. Blank were processed in the same conditions as samples and their analytical signals were subtracted.

[18] Trace elements (e.g. ^{86}Sr, ^{90}Zr, ^{135}Ba, ^{138}Ba, ^{139}La, ^{140}Ce, ^{141}Pr, ^{146}Nd, ^{172}Yb, ^{175}Lu, ^{181}Ta, ^{208}Pb, ^{232}Th and ^{238}U) were analyzed by ICP-QMS. Matrix and instrumental drift effects were continuously monitored and corrected by measuring the fluctuations of 4 internal standards (Ru, In, Re and Bi) added to the sample. Major elements (Al, Ca, Fe, K, Mn, Na, P, S and Ti) were measured by ICP-AES. Y and Au internals standards were used to correct the instrumental drift. Both for trace and major elements, external calibrations were performed using artificial standard solutions and dilute mineralized natural rock standards (e.g. BHVO-1, SGR-1, CCH-1, DWA; Govindaraju, 1994). Barium contents were measured both by ICP-AES and ICP-QMS. The two techniques gave indistinguishable Ba concentrations within the 5% accuracy as monitored by analyses of the above-mentioned standards and solutions. Among the whole elements analyzed, particular interest is given on Al and Ti (for lithogenic correction; see further), and Ca and Sr measurements. Since we choose to rinse the sample after filtration to remove sea-salts, the sea-salt particulate Ca, Sr and Ba (Ca_p, Sr_p and Ba_p) contents is negligible as can be checked using element/Na seawater ratio. For instance, the Ba_p:Na_p ratio is usually 50000 times higher compared to seawater ratio.

Lithogenic correction

[19] Particulate biogenic Ba in excess (i.e. excess Ba or Ba_{xs}) was calculated by subtracting the lithogenic contribution from total Ba_p. Lithogenic Ba was estimated using Post Archean Australian Shale Ba/Al and Ba/Ti ratio as the lithogenic reference [Taylor and McLennan, 1985, Murray et al., 1993, Dymond et al., 1992; Taylor and McLennan, 1985]. The difference between the two calculations (Al, Ti) is generally less than 10%. Because a better accuracy was obtained on Al analyses, we preferred the correction based on molar Ba/Al ratios (Ba/Al= 0.00135). However, even if Ti could sometimes be used instead of Al, we should be careful at potential authigenic fraction of Ti, which thus would exclude Ti as a lithogenic reference element [Cardinal et al., 2001]. Particulate Al was analyzed by ICP-AES with an average relative standard error of 14 % due to low contents. Since the lithogenic correction is usually very small in our various study areas in the Southern Ocean (Ba_{xs} represented more than 95 % of total particulate Ba), such relatively larger uncertainty does not have a significant impact on the precision of the Ba_{xs} calculation. For Sr_p and Ca_p, the lithogenic supply estimated was also low (≤10%) in our various study areas. Since crustal Ca and Sr contents are less homogeneous than Al and Ba (Taylor and McLennan, 1985; average molar crustal ratios Ca/Al= 0.251 and Sr/Al= 0.00134), to avoid approximate correction, we assumed that Sr_p and Ca_p have a marine origin only.

Ba_{xs}-based C mineralization fluxes

[20] As the mesopelagic (100-1000 m) Ba_{xs} signal builds up during the growth season in association with particulate organic matter mineralization, the mineralized C in the mesopelagic layer could be estimated using an algorithm relating meso-Ba_{xs} contents to oxygen consumption (Figure 1.1), as established by Shopova et al. [1995] and Dehairs et al. [1997] (see Eq. 1 and 2 below). This relationship was deduced from a 1D advection-diffusion model applied on highly resolved, precise oxygen profiles, during the ANTX/6 cruise in the PF region of Atlantic sector of the Southern Ocean.

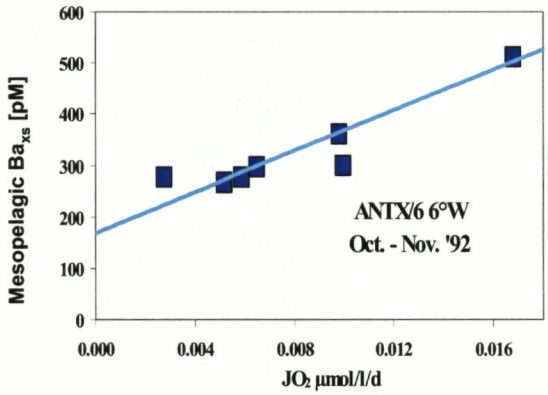


Figure 1.1: Mesopelagic Ba_{xs} vs. JO_2 in the Southern as reported by Dehairs et al. [1997].

[21] In this dissertation we used the following equations to convert meso-Ba_{xs} fluxes into C mineralization rates [Dehairs et al., 1997]:

$$J_{O_2} = (mesoBa_{xs} - Ba_{residual})/17200 \qquad \text{Eq.1}$$

$$C_{respired} = Z \times J_{O_2} \times RR \qquad \text{Eq.2}$$

where JO_2 is the O_2 consumption (µmol L^{-1} d^{-1}), $C_{respired}$ is the carbon mineralized rate (in mmolC/m^2/d; further expressed in mgC/m^2/d), Z is the thickness of the depth layer over which meso-Ba_{xs} is calculated, RR is the Redfield O_2:C mole ratio (175:127; Broecker and Peng, 1982), meso-Ba_{xs} is the Ba_{xs} amount that accumulates over the growth season and $Ba_{residual}$ is the background Ba_{xs} signal at zero oxygen consumption, i.e. zero organic C demand. The residual Ba_{xs} depends on the saturation state of the water with respect to barite. For the S.O. south of the PF, shown by Monnin et al. [1999] and Monnin and Cividini [2006] to be saturated for $BaSO_4$ from surface to 2500 m, this residual Ba_{xs} is close to 180 pM [Dehairs et al., 1997].

1.2. ACANTHARIANS ABUNDANCES AND Ba/Sr SKELETONS CONTENTS

Sampling

[22] For quantitative assessment of acantharian abundance (EIFEX cruise), seawater samples were taken using Niskin bottles. The entire content of one or two Niskin bottle(s) (12 or 24 L) depending on depth were gently passed through a 20 µm mesh plankton net and concentrated to a final volume of 50 mL. The concentrated samples were preserved with hexamine buffered formalin solution to a final concentration of 2% and stored at 4°C in the dark for

subsequent counting in the home laboratory. 2 mL of strontium chloride were also added to the samples to prevent acantharian skeletons from dissolution.

[23] For Ba/Sr skeletons measurements, individual acantharians were sampled from the surface water using an Apstein hand-net. Between 1 and 9 individuals (average size of 100 µm) of the most abundant genera (Acanthostaurus spp, Gigartacon spp.) were isolated onto 3 µm Isopore membranes (Wheatman), rinsed quickly with deionised water to wash of all seawater, dried and stored in a polypropylene centrifuge tubes for analytical measurements.

Analytical method

[24] For quantitative assessment of acantharians, on return to the home-based laboratory, a volume of 3 mL (10–150 m depth) and 10 mL (200–550 m) was settled in sedimentation chambers (Hydrobios, Kiel, Germany) for 6 and 24 hours respectively. Organisms were identified to genus level and enumerated using inverted light and epifluorescence microscopy (Axiovert 135 and Axiovert 200) according to the method of Utermöhl [1958]. Prior to counting 35 µL of stock solution of the nuclear fluorochrome 4', 6-diamidino-2-phenylindole (DAPI) [Porter and Feig, 1980] was added to the samples to stain the nucleus. Cells with stained nuclei were considered alive at the time of capture. Organisms were counted in the whole chamber at magnifications of x200. For each station, abundance are trapezoidal depth-integrated values for the upper 150 m and between 150 to 350 and 550 m of the water column, respectively: Nt =((∫0-150N)/Z), where Nt is the average abundance at time t, ∫0-150N the depth integral and Z the depth (150 m). Abundances are not given per m^{-2} but for a better comparison as the mean indiv. density m^{-3} between 150 m depth and the surface. The sample processing above has been performed by J. Hejnes (AWI; Germany).

[25] For Ba/Sr skeletons measurements, in the ANCH-VUB-Brussels laboratory, acantharians celestite ($SrSO_4$) skeletons were completely digested using 5% HNO_3 as described in Bernstein et al. [1998]. Ba and Sr contents were analyzed by SF-ICP-MS. An Indium solution was added to each sample tube as an internal standard and we used SLRS-4 (National Research Council Canada) as reference water for Ba and Sr; repeated analysis yielded average Ba values of 12.5± 0.4 µg/L (σ) with RSD of 2.90% and Sr values of 26.6± 1.7 µg/L (σ) with RSD of 6.4%, values which are within the range of the certified values (Ba=

12.2± 0.6 µg/L and Sr= 26.3± 3.2 µg/L). Blanks (less than 2% of total signal) were subtracted from both standard and samples. Ba/Sr mole ratios of individual acantharians skeletons were calculated.

1.3. BARITE CRYSTALS

[26] We focused on the identification of Ba-rich particles in filtered suspended matter at 6 depths from different stations from the surface layers to the mesopelagic zone (EIFEX cruise; 20, 80, 90, 400, 800 and 1000 m). A small fraction of the filter (~7%) was fixed with double-sided tape on a plastic plate. Electron probe microanalyses of the particle were done on a small part of this filter fraction (<0.2‰ of the whole filter). Samples were covered with a thin layer of carbon to avoid sample charging during the electron beam bombardment.

[27] The single particle analysis was performed by EPMA (electron probe microanalysis), using a JEOL JSM 6300 Scanning Electron Microscope (JEOL, Tokyo, Japan) equipped with backscattered (BSE) and secondary electron (SE) detectors and an energy dispersive X-ray detection system was used. A Si(Li) X-ray detector (FWHM=150 eV at E=5.898 keV) coupled to a PGT (Princeton Gamma Tech, Princeton, NJ, USA) – system was employed for acquiring the X-ray spectra (acquisition time was 20 s). For analysis of the samples, a typical electron beam energy of 20 keV and a beam current of 1 nA were applied. Magnification was set at 2000x, enabling analysis of particles as small as 0.35 µm in diameter. The average diameter of the particles was determined from the BSE image. The controlling software localised the particles from the BSE image and performed an X-ray measurement at 1 central point of the particle. The intensities of the characteristic peaks in the spectra were determined by the top-hat filter method [Van Espen and Janssens, 1992; Van Espen, 1984]; a home written program, PRODPP, was used for peak identification. Next, from the diameter [µm] of each barite particles, we estimated the Ba mass carried by the particle assuming the diameter was the one of an equivalent spheres (as described in Dehairs et al., 1980) and considering pure barite particles (molar fraction of Ba in barite f= 0.59 and barite density ρ= 4.5 g/cm^3). Ba contents will be confronted to results obtain by ICP-MS. It is possible that in some cases, Ba content as estimated by EPMA exceed values obtained by ICP measurements; differences up to 250% have been reported for suspended matter samples from mesopelagic depths by Sternberg et al. [accepted]. The mode of calculation (considering the mass of Ba of equivalent sphere and pure barite particles) could in part lead to an overestimation of Ba

contents. Moreover, we also consider that the particles are homogenously spread over the filter area, whereas the total surface scanned represents a very small fraction (<0.2‰) of the whole filter, thus multiplying the imprecision. So, we caution the EPMA results are rather semi-quantitative. The sample processing above has been performed by A. Worobiec (Universiteit Antwerpen).

Chapter 2

Dissolved barium in seawater

Foreword

[28] In Chapter 2 we focus on dissolved Ba measurements in seawater for which two methods are confronted. The purpose of this work was an analytical development as such, aiming at establishing a procedure which provides accurate, precise, simple and fast determination of Ba contents using isotopic dilution. Acquiring such expertise in our department (ANCH-VUB-Brussels) was crucial for constructing high quality large dissolved Ba data bases for the global Ocean.

SUMMARY

[29] Two isotope dilution approaches for high-precision determination of dissolved barium in seawater are compared, based on the use of ICP-QMS and SF-ICP-MS instruments (inductively coupled plasma; respectively quadrupole and sector field - mass spectrometry). When analyzing with the ICP-QMS, we observed erratic variations of the Ba mass bias. The most accurate results were obtained by adding an external element with the same mass bias behavior as the analyte, for internal mass bias correction. For $^{138}Ba/^{135}Ba$ isotopic ratio, we showed that $^{146}Nd/^{143}Nd$ fulfils these conditions. Nd and Ba isotopes were measured quasi simultaneously, and we used the Nd mass bias to correct this of Ba. When analyzing with the SF-ICP-MS, Nd and Ba mass biases slightly differed, but since Ba mass bias remained remarkably constant, Nd spiking proved unnecessary. In the latter case Ba mass bias correction was achieved by analyzing regularly natural Ba solutions each few samples (12). Comparison of Ba results for reference water solutions and open ocean water column profiles obtained via both approaches indicate that they both achieve the same precision. However, the SF-ICP-MS based method proved to be simpler and faster.

2.1. INTRODUCTION

[30] Correct assessment of the weak surface to deep gradients of dissolved Ba concentrations (a few µg/L-ppb over a few Km of water column) in the Southern Ocean water column requires that concentrations are measured with a precision close to 0.1 µg/L. The use of isotopic dilution (ID) method as described by Klinkhammer and Chan [1990] and Freydier et al. [1995] allows to reach such precision. This method is a technique whereby a known quantity of an enriched isotope (spike) of the analyte that has a low natural abundance, is added to an unknown amount of a sample with a known isotopic composition. By measuring the perturbation in the isotopic composition of the sample/spike, the concentration can be back extracted. In this work, two types of ICP-MS are used (a quadrupole and a sector field - mass spectrometer); these instruments are sensitive enough to detect barium in diluted sea water.

[31] One of the crucial points for which ID requires care at achieving high accuracy, consists in an accurate monitoring and correction of the mass bias (i.e. difference between measured isotopic ratio and true ratio). Other points imply an accurate knowledge of isotope ratio [Boulyga et al., 2005], spike composition and quantities of sample and spike, and a good control of the blank; potential matrix effect could also hampered the procedure. Here, we compare two methodologies based on different instruments.

2.2. SAMPLING

[32] During all cruises presented in this work, sampling of seawater was done using a CTD Rosette equipped with Niskin bottles. 15 mL of unfiltered seawater were sampled in polypropylene vials (Nalgene; rinsed three times with the seawater sample), acidified using Suprapur HCl (15 µL) and stored at room temperature till analysis.

2.3. THEORETICAL

Isotope dilution

[33] For dissolved Ba seawater, isotope dilution technique is well described [Klinkhammer et al., 1990; Freydier et al., 1995; Falkner et al., 1993]. Here, the spike consisted of a ^{135}Ba enriched solution (EURISO-top, $BaCO_3$). It is crucial that the isotopic composition and concentration of the spike be accurately

known, as well as the added amounts of sample and spike (see below the Eq. 1,2,3 and 4). The isotopic composition and concentration of the Ba spike were: 94.07% ^{135}Ba, ^{138}Ba/^{135}Ba = 0.0241 and Ba= 14.2 µg/L, as assessed via thermal ionization mass spectrometry (TIMS; ULB-Brussels-Belgium; J.P. Liegeois). Considering that we aim at achieving a precision of ~1% on Ba contents and that the seawater samples (approx. salinity 34) have to be diluted ~30 fold, since ICP analysis imposes samples not to contain more than 0.2% salt, it is crucial that the instrument be sensitive. Diluting the samples reduces the level of Ba to the sub µg/L level and requires that water used for dilution is of high purity: we used Milli-Q water (deionized filtered water produced by Milli-Q system; Millipore). Moreover in order to achieve better precision, spiking and dilution of the samples were done gravimetrically (<0.1% of error).

[34] As outlined above, it is essential to monitor and correct mass discrimination during ICP-MS analysis of ^{138}Ba/^{135}Ba isotopic ratio. Mass bias can be expressed by the following linear law:

$$Rm = Rn(1 + n \times \delta) \quad (1)$$

where *Rm*= measured ^{138}Ba/^{135}Ba ratio, *Rn*= true ^{138}Ba/^{135}Ba ratio (71.69/6.59= 10.87) [Rosman et al., 1998], δ = mass bias per atomic mass unit (amu) and *n*= number of amu's. (difference between both isotopes *n*= 3).

[35] To determine the Ba concentration in the sample we start with the general equation (2) for quantitative interpretation of isotope dilution results. The measured ratio takes in account isotopes of the spike and the sample:

$$\left(\frac{138Ba}{135Ba}\right)measured = \frac{(138Ba)\ spike + (138Ba)\ sample}{(135Ba)\ spike + (135Ba)\ sample} \quad (2)$$

(^{138}Ba)spike and (^{135}Ba)spike = quantity of isotopes 138 and 135 provided by the spike

(^{138}Ba)sample and (^{135}Ba)sample= quantity of isotopes 138 and 135 provided by the sample.

[36] The following expression (3) is derived from (2). We obtain the dissolved barium concentration (µg/L) after correction of the mass bias as described in [Klinkhammer et al., 1990; Freydier et al., 1995]:

$$CBa = \frac{(Rv - Rspk) \times C(135Ba)spk \times Wspk}{\left(1 - Rv/Rn\right) \times A138 \times Wsamp} \quad (3)$$

where *CBa*= barium concentration in the sample (µg/L), *Rv*= mass bias corrected $^{138}Ba/^{135}Ba$ ratio of the solution analyzed (i.e. a mixture of sample + spike), *Rspk*= $^{138}Ba/^{135}Ba$ ratio in the spike, *Rn*= true natural ratio of $^{138}Ba/^{135}Ba$ (10.87), A138 = natural abundance of ^{138}Ba (71.69%) [Rosman et al., 1998], *Wspk* and *Wsamp*= weight of spike and sample, respectively and $C(^{135}Ba)spk$ = ^{135}Ba concentration in the spike (Ba = 14.2 µg/L).

[37] The final barium concentration (µg/L) is obtained after blank correction:

$$CBacorr = \frac{(CBa \times Wsamp) - (VolMQ \times Cblc)}{WMQ} \qquad (4)$$

where *CBacorr*= blank corrected Ba concentration (µg/L), *CBa*= Barium concentration obtained from eq. 2 (µg/L), *VolMQ*= volume of Milli-Q water added (g) and *CBlk*= Ba concentration in the blank (µg/L). Blank solutions are made from the same Milli-Q water used for sample dilution.

Mass bias monitoring

[38] Assessing mass bias is critical and should ideally be done synchronously with acquisition of the analyte signal. However, when using a sequential device such as the ICP-MS instruments we dispose of, perfect synchronicity is not possible. In this case several approaches for mass bias correction can be considered:

(**1**) In case the mass bias is stable (isotope ratios fluctuate within the error bar range) a Ba solution with natural isotope distribution can be analyzed every few unknown samples and we take the mean of the 2 mass biases bracketing the samples series or we take the mean of all mass biases measured during the day;

(**2**) In case mass bias is unstable (isotope ratios are scattered widely) a natural Ba solution should be analyzed before and after each unknown (standard-sample bracketing method). This approach also assumes that the mass bias variations are linear in between the sample and standard;

(**3**) A third approach consists in spiking the unknown sample with an external element which behaves similarly to Ba during measurements. This internal standard should be an external element with atomic mass close to the one of the analyte. It should also have at least two stable isotopes and should be present in negligible concentrations in the original samples; it is not however a limiting

condition as long as the element has a known isotopic composition. Although the ICP-MS operates sequentially and therefore mass bias for the internal standard may not exactly apply to the Ba isotopes as well, this latter approach comes closest to a real synchronous mass bias correction in reason of the calculation mode itself: during 1 run the results for each isotopes are the average of ±40 successive measures of all the isotopes during a selected time. We will show further that Nd ($^{146}Nd/^{143}Nd$) fulfils these conditions.

2.4. EXPERIMENTAL

Instrumentation

[39] All measurements were carried out on an ICP-QMS VG Plasma Quad 2+ Thermo Elemental and on a SF-ICP-MS Element 2 Thermo Finnigan. Detailed operating conditions for both instruments are given in Table 2.1 and Table 2.2, respectively.

Instrument	VG Elemental PlasmaQuad PQ 2 +
Forward power	1350 W
Reflected power	< 2 W
Nebuliser	Quartz, concentric
Solution uptake rate	1.3 mL min^{-1} (peristaltic pump)
Spray chamber	Quartz, cyclonic
Sampling cone	Ni, ø 1 mm
Skimmer cone	Ni, ø 0.7 mm
Nebuliser argon flow rate	0.850 L min^{-1}
Cool argon flow rate	13 L min^{-1}
Auxiliary argon flow rate	1 L min^{-1}
Sensitivity	(2-3) $\times 10^5$ cps per 10 ng mL^{-1} ^{138}Ba
Acquisition time	15 s
Number of acquisition/sample	10
Up-take time	80 s
Each sample is measured in ~7 min	

Table 2.1: ICP-QMS instrumental operating conditions.

Instrument	Element 2 Thermo Finnigan
Forward power	1200 W
Reflected power	<2 W
Nebuliser	Quatz, concentric
Solution uptake rate	1 mL min^{-1} (peristaltic pump)
Spray chamber	Quartz, cyclonic
Sampling and skimmer cones	Ni (Thermo Finnigan)
Sample gas flow	1 to 1.5 L min^{-1}
Cool argon flow rate	16 L min^{-1}
Auxiliary argon flow rate	1.5 L min^{-1}
Sensitivity	1 $\times 10^6$ cps per 1 ng mL^{-1} ^{138}Ba
Up-take time	50 s
Wash time	15 s
Number of acquisition	18 (3 runs and 6 pass)
Sample time	0.05 s for each isotope
Search window	60%
Integration window	40%
Scan type	E Scan
Integration type	Average for each isotope

Each sample is measured in 3 min

Table 2.2: SF-ICP-MS instrumental operating conditions.

[40] Sensitivity of the ICP-QMS instrument was generally around 20000 to 25000 cps (counts per second) for 1 µg/L ^{138}Ba. Seawater diluted 30-fold contains between 0.17 and ~0.73 µg/L of ^{138}Ba and yielded analyte intensities ranging between 3400 to 14600 cps. Since blank signals (Milli-Q water) were low and fluctuated between 50 to 100 cps, the analyte signal stayed well above the analytical detection limit (~3 ng/L in the solution measured, i.e. 0.09 µg/L in the seawater sample). Although progressive clogging of the cones could often gradually decrease the sensitivity to reach 4000 cps for 1 µg/L ^{138}Ba at the end of the day, sensitivity was still sufficient, ensure operating within the quantitative domain. With the SF-ICP-MS, the problem of the number of counts (sensitivity) decrease during the day does not occur, providing a better continuity between different analyses days. Moreover, note that the sensitivity of the ICP-SFMS exceeds the one of ICP-QMS by at least 100. The ICP-SFMS was operated in low resolution mode ($m/\Delta m$= 300). The detection limit is around few pg/L-ppq. Control of the blank is also crucial and blank Ba contents should not exceed 5 to 10 pg/L.

Sample preparation

[41] Depending on mass bias behavior, two protocols for sample preparation were finally applied:

(**1**) when mass bias is stable (all values are within the error bar range; see below), 1 g of seawater is spiked with 0.7 g of ^{135}Ba-spike solution to obtain a $^{138}Ba/^{135}Ba$ ratio between 0.7 and 1 to minimize error propagation [Webster, 1960; Klinkenberg et al., 1996]. Subsequently the sample is diluted with Milli-Q grade water to a final weight of 30 g. Blanks used in stable conditions consist of acidified (nitric acid) Milli-Q water;

(**2**) when mass bias is unstable (not all values are within the error bar space; see below), the procedure described under (1) is adapted by also adding 0.3 g of a 10 µg/L Nd solution with natural abundance ($^{146}Nd/^{143}Nd$ = 1.4113, Rosman et al., 1998). Blanks used in unstable conditions consist of 0.3 g of the Nd spike solution diluted with acidified Milli-Q grade water to a final weight of 30 g. Spiking and dilution of the samples were done gravimetrically.

[42] Reference waters for sample bracketing and inter-calibration exercises are prepared following the same protocol used for the unknown samples. References used were SLRS-3 (river water, Canadian certified reference material, Ba= 13.4 ±0.6 µg/L), an in-house Mediterranean Sea water standard (OMP; recommended value Ba= 10.4 ± 0.2 µg/L) prepared by C. Jeandel (LEGOS, Toulouse, France) and a second artificial standard (OSU, recommended value Ba = 4.96 µg/L) prepared by K.K. Falkner (Oregon State University).

2.5. RESULTS AND DISCUSSION

Mass bias determination

ICP-QMS - VG PQ 2+

[43] We followed the temporal evolution of mass bias for a 10 µg/L natural Ba solution (Figure 2.1) and noted that while mass bias was occasionally constant (Figure 2.1-a), it was mostly drifting (Figure 2.1-b). Moreover mass bias variation along the mass discrimination line was erratic and thus correction of the mass bias by averaging Ba mass bias values measured before and after each sample does not yield accurate results in our case. As outline above, potential explanation of mass bias change could imply the clogging and contamination of the instrument with salt from the sample, leading to a higher ion density and therefore unstable mass discrimination. However, we took care at enough diluting the seawater sample (see above). Moreover control of temperature is crucial for the mass bias; it is made trough the plasma stability, itself linked to the

generator. During our work, evidences have risen that radio frequency generator dysfunction may in part explain the mass bias variability.

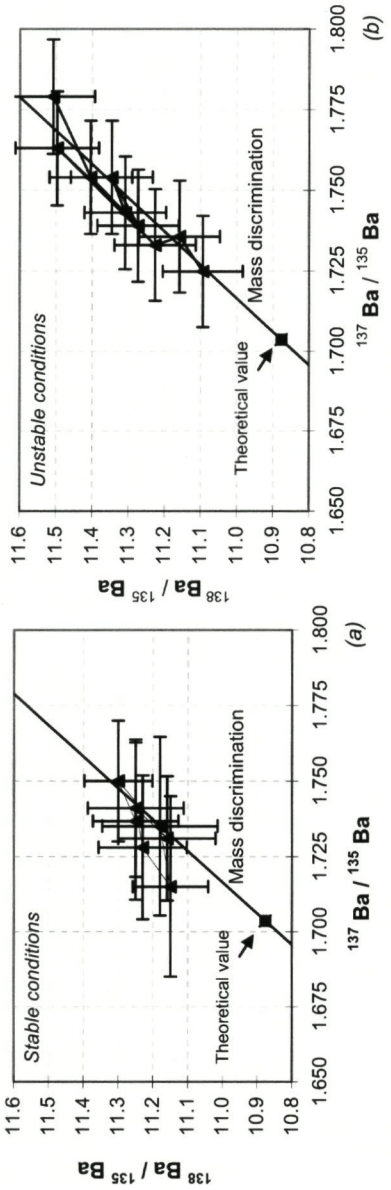


Figure 2.1: Measured $^{138}Ba/^{135}Ba$ vs. $^{137}Ba/^{135}Ba$ ratios during ICP-MS analysis of natural Ba solutions under stable (a) and unstable (b) conditions. The line represents the theoretical mass bias evolution.

[44] Overall, these results prompted us to look for an external element with the same behavior as Ba, which could serve as an internal standard for mass bias correction. We selected Nd as a potential candidate based on criteria exposed above: ^{146}Nd, ^{143}Nd are close in mass to ^{138}Ba, ^{135}Ba and Nd concentration in the ocean is of the order of the pg/L [Jeandel et al., 1995]. Although ^{143}Nd isotopic abundances will vary with age of the sample and the sample's initial Sm contents (^{147}Sm and ^{143}Nd daughter are used for geochronological studies), it is negligible for our analyses. We followed the Ba and Nd mass bias by analyzing a simple solution containing 10 µg/L each of Ba and Nd (Figure 2.2). Results showed that Ba and Nd mass biases were not significantly different during stable (Figure 2.2-a) and unstable (Figure 2.2-b) conditions occurring over 8 hours of ICP-QMS operation. These results indicate that Nd can be used for correcting Ba mass bias by ICP-QMS.

[45] Moreover, over 15 days time, we analyzed some 87 aliquots of OSU standard by ICP-QMS with mass bias corrected via Nd spiking and via natural Ba solution for 19 of these aliquots (Figure 2.3 and Table 2.3). We deduced an average Ba concentration of 4.97 ± 0.12 µg/L (σ, n= 87, Figure 2.3-a). RSD was 2.4% and offset of the mean data relative to the reference value (4.96 µg/L) was 0.2%. In addition, for samples with both correction approaches (numbers 1 to 19, Figure 2.3-b), we found that the mean result obtained with Nd spiking (4.97 ± 0.13 µg/L, σ) was closer to the certified value than for natural Ba solution correction (4.92 ± 0.14 µg/L, σ). Our results showed that when using the ICP-QMS instrument the most precise method can be achieved by adding an internal standard (Nd) to monitor and correct Ba mass discrimination. This method is adopted throughout when analyzing with the ICP-QMS device.

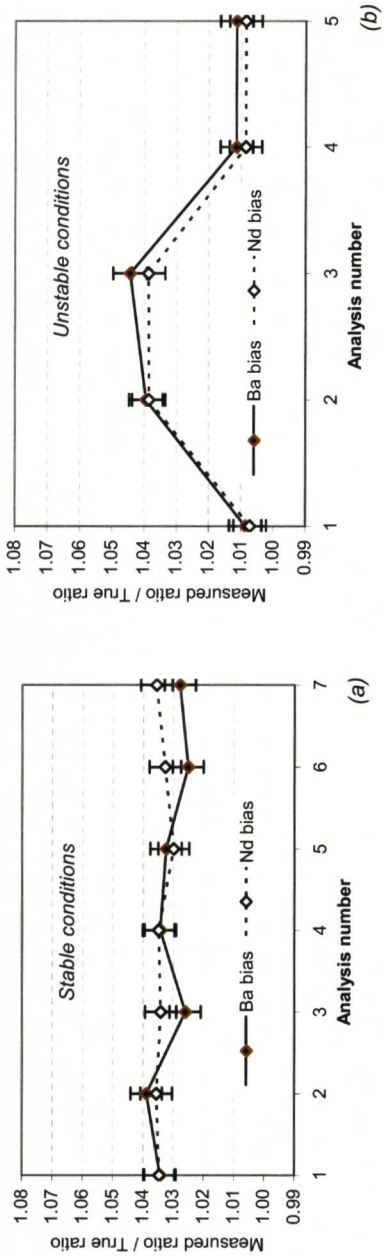


Figure 2.2: Evolution of Ba and Nd mass bias (measured isotope ratio/true isotope ratio) during a full (a) stable and (b) unstable day of ICP-QMS analysis (~8 hours) of a mixed Ba and Nd solution (each of 10µg/L).

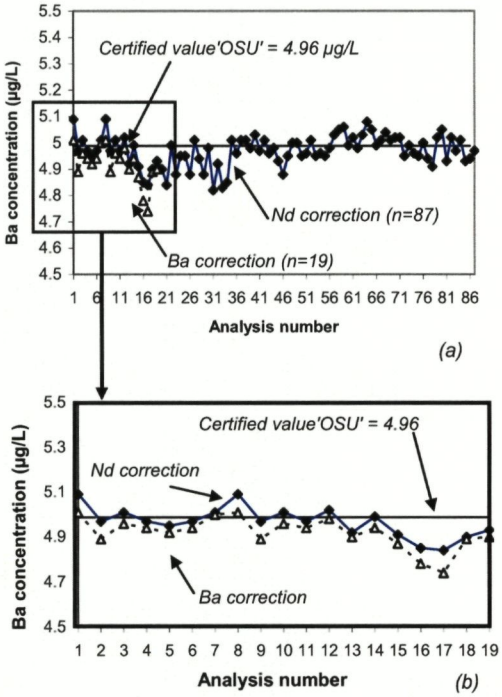


Figure 2.3: Ba concentrations for 'OSU' artificial standard (certified value of 4.96 µg/L) measured over 12 days with ICP-QMS with both Nd and Ba correction.

ICP-QMS VG PQ 2+	**Nd** correction	**Ba** correction
Certified value (OSU, µg/L)	**4.96**	
Mean value (µg/L) **n= 19**	**4.97**	**4.92**
Standard deviation (2σ)	0.13	0.14
RSD %	2.7	2.86
Mean value (µg/L) **n= 87**	**4.97**	-
Standard deviation (2σ)	0.12	-
RSD %	2.4	-

Table 2.3: Comparison between our measurements of Ba concentration and certified values for OSU standard (4.96 µg/L). Correction of the mass bias via Nd on the ICP-QMS and correction via Ba on the SF-ICP-MS.

SF-ICP-MS – Element 2

[46] The evolution of Ba and Nd mass bias was followed over 3 days of analysis, using a simple MQ solution containing 1 µg/L of both Ba and Nd. Figure 2.4 shows that mass bias for both Ba and Nd is smaller (ratio closer to 1; 1.008± 0.01 (σ) and 1.003± 0.01 (σ) for Ba and Nd respectively) as compared to the ICP-MS results, but also that on occasions Ba and Nd mass bias variations differ. As outline above conditions inherent to the instrument, e.g. temperature control, plasma and frequency generator stability, could induce these variations. The latter situation in fact precludes better mass bias correction based on Nd addition.

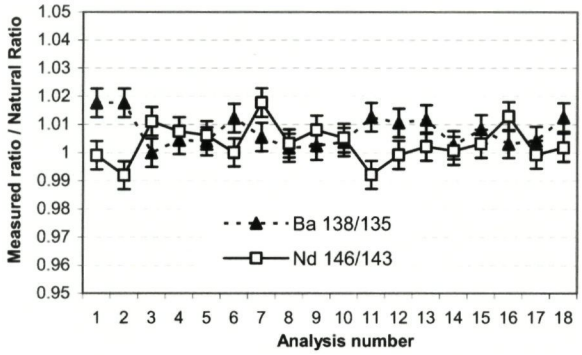


Figure 2.4: Evolution of Ba and Nd mass bias (measured isotope ratio/natural isotope ratio) during SF-ICP-MS analysis of a mixed Ba and Nd solution (each of 1 µg/L).

However, the evolution of the Ba mass bias ($^{138}Ba/^{135}Ba$ vs. $^{137}Ba/^{137}Ba$ ratios) during the 3 days of machine operation revealed a stable signal (Figure 2.5). Therefore, to correct mass bias we can apply the average mass bias as obtained from the analysis of a Ba solution with natural abundance, bracketing every few samples or we can take the mean value of all a day. This method is adopted throughout when analyzing with the ICP-SFMS device.

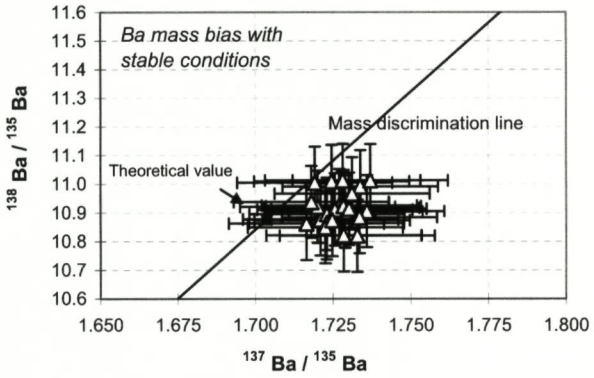


Figure 2.5: Measured $^{138}Ba/^{135}Ba$ vs. $^{137}Ba/^{135}Ba$ ratios during 3 days of SF-ICP-MS analyzes of natural Ba solutions and comparison with theoretical mass bias line.

Precision, reproducibility, repeatability and accuracy

[47] In the following discussion we compare results obtained by the two methods proposed (correction of the mass bias via Nd on the ICP-QMS and correction via Ba on the SF-ICP-MS) for reference water solutions and open ocean water column profiles.

[48] Repeated analysis of SLRS-3 (certified value of 13.4± 0.6 µg/L) and 'OMP' (certified value of 10.4± 0.2 µg/L) reference solutions yielded average Ba values of 13.25± 0.38 µg/L (σ, n=12) with RSD of 2.89 % and 10.21± 0.24 µg/L (σ, n=14) with RSD of 2.38% for SLRS-3 and OMP respectively. These results are in good agreement with the certified values (Figure 2.6-a; Table 2.4). On the SF-ICP-MS (Ba mass bias correction) average Ba values obtained for reference waters SLRS-3 and OMP were 13.48± 0.21 µg/L (σ) with RSD of 1.55% and 10.49± 0.29 µg/L (σ) with RSD of 2.75% respectively (Figure 2.6-b), again in good agreement with certified values.

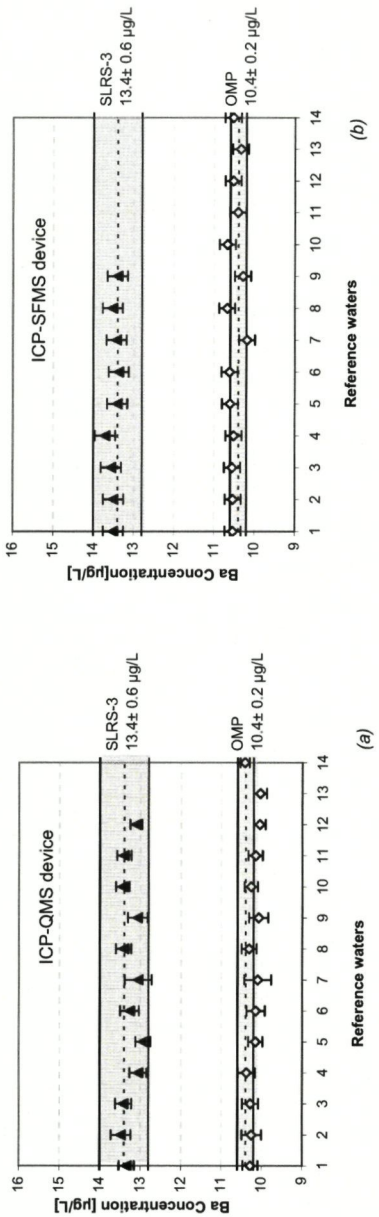


Figure 2.6: SLRS-3 (certified Ba value = 13.4± 0.6 µg/L) and 'OMP' (certified Ba value = 10.4± 0.2 µg/L) reference waters analyzed (a) with the ICP-QMS and (b) with the SF-ICP-MS.

The two methodologies give average values which are not significantly different and achieve similar repeatability. This inter-calibration thus validates our two methodologies which achieve very similar precision.

Instrument	ICP-QMS VG PQ2+		SF- ICP-MS Element 2	
Standard solution	*SLRS*	*OMP*	*SLRS*	*OMP*
Recommended value (µg/L)	13.4	10.4	13.4	10.4
Average measured value (µg/L)	**13.25**	**10.21**	**13.48**	**10.49**
Standard deviation (2σ)	0.38	0.24	0.21	0.29
RSD %	2.89	2.38	1.55	2.75

Table 2.4: Comparison between our measurements of Ba concentration and certified values for SLRS3 (Ba = 13.4 ±0.6 µg/L) and OMP (Ba = 10.4 ± 0.2 µg/L) standards. Correction of the mass bias via Nd on the ICP-MS and correction via Ba on the SF-ICP-MS.

[49] Ba_d water column profiles were measured at station ALOHA (Figure 2.7-a, VERTIGO cruise, June 2004) and at 49.5°S – 1.8°E (Figure 2.7-b, Atlantic sector of the Southern Ocean, EIFEX cruise, Jan. 2004). Clearly, profiles obtained via both methods are indistinguishable, highlighting the fact that excellent precision can be achieved with both machines provided mass bias is properly assessed.

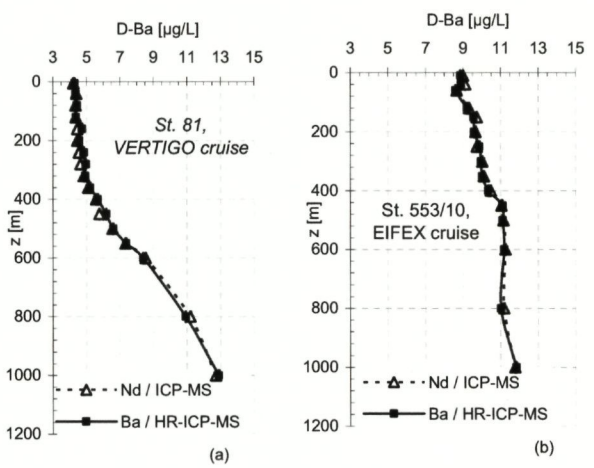


Figure 2.7: Comparisons of dissolved Ba profiles (µg/L) obtained by mass bias correction via Nd (ICP-QMS) and natural Ba (SF-ICP-MS) at (a) Station Aloha, North pacific, VERTIGO cruise, July 2004 and (b) 49.5°S – 1.8°E, Southern Ocean EIFEX cruise, Jan 2004. The sizes of the symbols correspond to the errors bar.

[50] The variability of measurement (sampling precision) was estimated at station ALOHA (VERTIGO 1; June-July 2004) using the SF-ICP-MS (Ba mass bias correction). 6 casts were sampled at the same site over 3 weeks time (Figure 2.8) using 12L Niskin bottles mounted in a CTD rosette. Steady state conditions prevailed at station ALOHA. On average, the sampling precision equals ±0.3 µg/L (σ) with RSD of 5%.

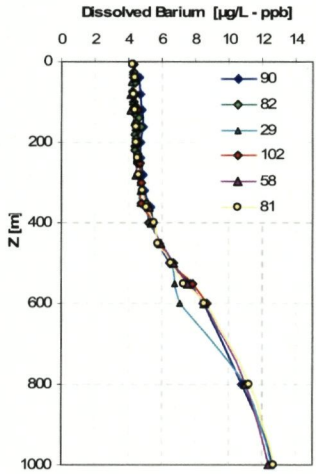


Figure 2.8: Dissolved Ba profiles (µg/L- ppb) at station ALOHA.

2.6. CONCLUDING REMARKS

[51] The aim of this study was to develop an analytical methodology that is accurate, precise, simple and fast. Using the ICP-QMS VG Plasma Quad 2+, the most accurate method consists in correcting the mass bias via an external element (Nd spiking) while using the SF-ICP-MS Element 2, the method proposed corrects the mass bias by bracketing every few samples with a natural Ba solution. Results showed that both methodologies achieve the same precision, but using the SF-ICP-MS allows faster analyses (twice more samples per day compared to the ICP-QMS), since the protocol for sample preparation is simpler (no need for Nd spiking) and machine analysis time is shorter (see Table 2.1 and 2.2). Thus SF-ICP-MS method appears as an ideal procedure for processing large dissolved Ba sample sets.

Section 2

Dissolved barium in the global Ba-cycle dynamics

INTRODUCTION

Dissolved Ba distribution

[52] Dissolved Ba (Ba_d) profiles in the S.O. were first documented during the GEOSECS [Chan et al., 1977; Östlund et al., 1987] and INDIGO [Poisson et al., 1990; Jeandel et al., 1996] programs. Studies have shown that Ba_d behaves as a bio-intermediate element which is present in lowered concentrations in the upper 1000 m water column without, however, reaching total depletion in surface water (Figure B-1).

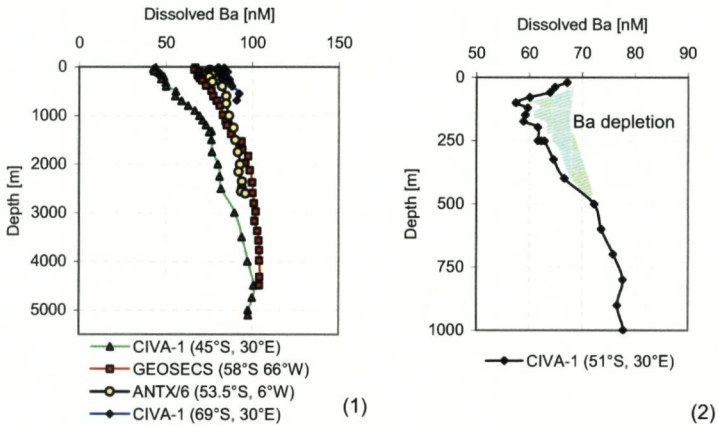


Figure B: (1) Dissolved Ba profiles in the upper 5000 m water column of the Southern Ocean; (2) Focus on dissolved Ba depletion in the upper 1000 m.

Though in the Arctic basin conservative mixing clearly appears to be the main control on the Ba_d distribution (Ba_d is used as a water mass tracer; Falkner et al., 1994; Taylor et al., 2003), Ba_d distributions in other locations, and in particular in the S.O., reflect evidence for non-conservative behavior. At first, straight Ba-Nutrient relationships may suggest the direct involvement of Ba in biological processes. However, although the Ba_d distribution shows strong similarities with those of silicate and alkalinity, discrepancies have surfaced that indicate that the biogeochemical cycling of Ba is unique [Edmond, 1974; Chan et al., 1977, Lea and Boyle, 1989, Lea, 1993, Jeandel et al. 1996] and involves a potential link with the particulate Ba_{xs}-barite dynamics [Dehairs et al., 1980; Stroobants et al., 1991].

Potential dissolved Ba depletion

[53] Barite constitutes the major part of excess particulate biogenic Ba in suspended matter [Dehairs et al., 1980; Bishop, 1988] despite the fact that most of the World Ocean is undersaturated for $BaSO_4$ [Monnin et al., 1999; Rushdi et al., 2000; Monnin and Cividini, 2006]. This implies that barite is formed under specific conditions, provided directly or indirectly by biological systems [Bertram and Cowen, 1997]. Although the exact mechanism of barite formation is still being debated, results support the idea that microenvironments (biogenic aggregates) provide the necessary thermodynamic conditions for passive barite precipitation, through enrichment of sulfates and/or barium in decomposing organic material [Dehairs et al., 1980, 2000; Collier and Edmond, 1984; Bishop, 1988; Stroobants et al., 1991; Bertram and Cowen, 1997; Dehairs et al., 2000 Ganeshram et al, 2003] (Figure C); alternative pathways are discussed in Section 3. Studies have shown that the Ba_{xs} stock is built up during the growth season as a result of export and degradation of biogenic aggregates from the mixed layer in the mesopelagic zone (~100-1000 m) [Dehairs et al., 1997; Cardinal et al., 2005]. Considering this scenario of barite precipitation, we wondered whether potential Ba_d subtraction in ambient water during barite formation in micro-environments could lead to a measurable impact on Ba_d profiles and thus explain the upper 1000 m Ba_d gradient referred to above (Figure B-1). This hypothesis was moreover based on observation of mesopelagic depletions on Ba_d profiles in the Atlantic sector of the Southern Ocean (Figure B-2) [Dehairs et al., in preparation-a] and on Edmond and Collier's works [1984] on Pacific Ocean Ba profiles, concluding that significant local uptake of Ba_d was required to maintain mesopelagic Ba maximum. Addressing the question of the Ba cycle from the angle of the dissolved phase [Chan et al., 1977; Falkner et al., 1994; Jeandel et al., 1996] is not an easy work; differences in turn over between the two Ba phases constitute the main difficulty in confronting fluxes.

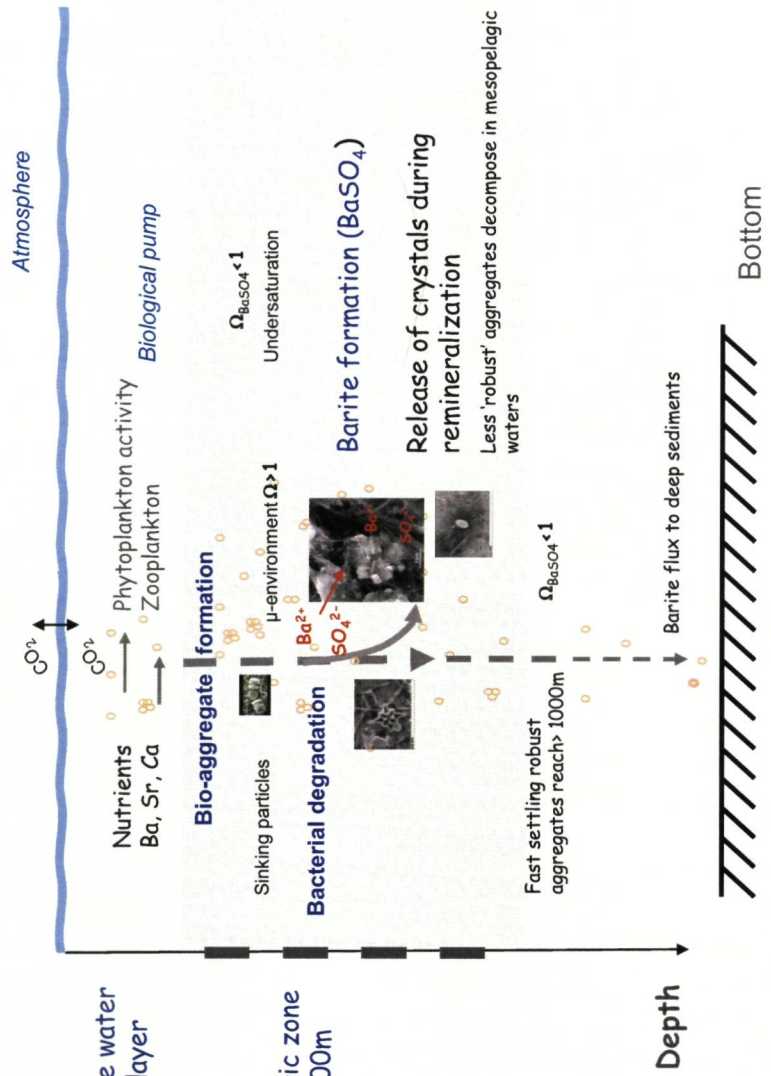


Figure C: Particulate biogenic Ba_{xs}- barite formation process in the water column.

Objectifs

[54] In this section, we investigated the importance of dissolved Ba in the global Ba cycle dynamics; the main aim was to evaluate the factors controlling the oceanic Ba_d distribution. We confronted the major results from the SAZ-98 and CLIVAR SR3 cruises (Australian sectors) and the ANTARES-4 cruise (Indian sector). We examined the details of Ba_d profiles in the hydrodynamical context of the different study areas. Ba_d distributions were compared to frontal structures and characteristics of the water masses and were confronted to physical properties (e.g. temperature, salinity, density). We also discussed the correlative behaviors of dissolved Ba with other biogeochemical water mass properties (e.g. dissolved oxygen, nutrients and alkalinity). Finally, confronting dissolved and particulate Ba profiles from different seasonal situations allowed us to investigate both the sensitivity of Ba_d to the onset of the phytoplankton growth season and the strata where the Ba uptake occurs.

Chapter outline

[55] Overall, this second section has attempted to address the question as to whether it is possible to define what the exact processes are (physical and/or biological control) that act upon Ba_d distribution in the Southern Ocean. Determining the importance of dissolved Ba in the Ba cycle dynamics will in turn lead to better uses of the Ba proxy, for both dissolved and particulate Ba phases. First (Chapter 3), we presented corresponding dissolved and particulate Ba profiles in the Crozet-Kerguelen basin (ANTARES-4); such confrontation had never been done before and we emphasized on the occurrence of Ba_d depletions. Moreover, we also investigated nutrients, alkalinity and Ba_d correlations in order to shed light on the processes controlling their distributions. Secondly (Chapter 4), we presented Ba_d along a high resolution transect (CLIVAR SR3) and confronted in details its distribution to frontal structures. Thirdly (Chapter 5), we studied the seasonality effect on both dissolved and particulate Ba (SAZ-98 and CLIVAR SR3) and we checked the degree of Ba mass conservation through flux calculation. We also examined nutrients, alkalinity and Ba_d correlative behaviours. Fourthly (Chapter 6), by performing a modeling approach - POMP (parametric optimum multi-parameter) analysis, we quantified which part of the Ba_d signal could be attributed to mixing only and which one to non-conservative processes (SAZ-98 and CLIVAR SR3); again we focused on the occurrence of mesopelagic Ba_d depletions. Finally, in a General discussion, we provided an overview of the whole results presented in Section 2.

Chapter 3

Barium distribution in the Crozet-Kerguelen Basin

Foreword

[56] In this chapter, the question whether it is possible to separate the effects of hydrodynamics from biogeochemical processes (in a situation where both seem implicated in controlling the Ba distribution) is investigated through a detailed comparison of Ba (dissolved and particulate), oxygen, silicate and alkalinity distributions. ANTARES-4 is one of the first cruises for which the dissolved and particulate Ba phases could be compared simultaneously in contrasting zones of a S.O. frontal system. The frontal system investigate here is the "Crozet Front" and stands as one of the strongest in the world ocean.

SUMMARY

[57] We investigated the dissolved and excess particulate Ba distribution across the complex frontal system of the Crozet-Kerguelen Basin (Southern Ocean; 42–47°S, 62–65°E). Ba_{xs} profiles show the characteristic mesopelagic maximum (depth range between 150–400 m) reaching up to 1000 pM in the Subantarctic Zone and Subtropical Front, the highest value observed for Southern Ocean mesopelagic waters. Dissolved Ba (concentrations between 38 and 104 nM) correlates with silicate and alkalinity, but the regression is not perfect, reflecting the involvement of different biogenic carriers in the control of the water column distribution of these compounds. Dissolved Ba in the upper 500 m appears strongly influenced by cross frontal exchanges, involving both northward and southward transport of water masses. In the mesopelagic waters (150–400 m) of the Polar Front Zone, a dissolved Ba depletion faces the Ba_{xs} maximum. This depletion appears mainly maintained by cross frontal advection of waters containing less Ba and originating north of the Subantarctic Front. Overall, no clear evidence was found that precipitation of barite reflected by the occurrence of Ba_{xs} maxima does measurably influence the distribution of dissolved Ba.

3.1. INTRODUCTION

[58] Productivity in S.O. systems is closely linked to hydrodynamic and trophic conditions along oceanic fronts [Arrigo et al., 1998; Fiala et al. 1998; Moore et al., 1999; Landry et al., 2002], which are regions well known to represent a significant CO_2 sink [Metzl et al., 1998, 1999; Poisson et al., 1990]. This is particularly true for the subantarctic region studied here (Crozet-Kerguelen Basin) characterized by strong gradients in physico-chemical and biological characteristics due to the confluence in a latitudinal restricted zone of three major fronts [Metzl et al., 1998; Fiala et al., 2003]. In an attempt to determine the complex mechanisms governing the S.O. dissolved Ba distribution, we examined summer dissolved and particulate Ba data and confront these with physico-chemical conditions of different divides of the "Crozet front". Samples were collected during the ANTARES-4 cruise in the Crozet-Kerguelen basin, between 43°S-46°S and 62°E-65°E in the Subtropical, Subantarctic and Polar Front Zones of the Southern Ocean; location of the stations is shown in Figure 3.1.

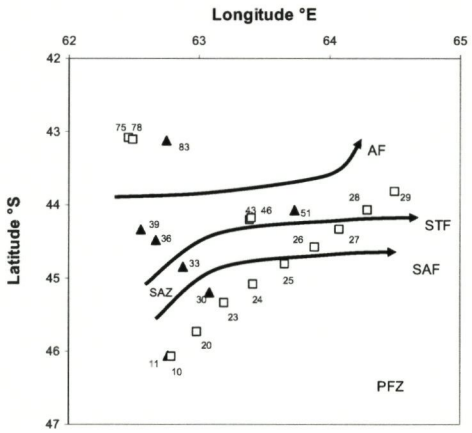


Figure 3.1: Detailed location of stations sampled for dissolved Ba (squares) and particulate Ba (triangles) and position of hydrological fronts [Park et al., 2002]. Fronts reported are from north to south: the Agulhas Return Current Front (AF), the Subtropical Front (STF) and the Subantarctic Front (SAF). The Subtropical Zone (STZ) extends to the north of the STF; the Subantarctic Zone (SAZ) extends between the STF and the SAF, and the Polar Front Zone (PFZ) between the SAF and the Polar Front (PF, located further south outside the study area).

ANTARES-4 is one of the first cruises for which the two Ba phases could be compared simultaneously. The main aim of Chapter 3 consists in investigating what the exact processes are, that drive the dissolved Ba distribution. Here, we first present dissolved and particulate Ba and then confront them to dissolved oxygen, silicate and alkalinity, as well as to water masses characteristics (e.g. temperature, salinity, density).

3.2. FRONTAL STRUCTURES AND WATER MASSES

[59] The study area is characterized by the presence of three fronts compressed in a frontal zone no wider than 200 km (Figure 3.1) [Park et al., 2002]. These fronts are, from north to south: the Agulhas Return Current Front (AF), the Subtropical Front (STF) and the Subantarctic Front (SAF). The Subtropical Zone (STZ) extends to the north of the STF, the Subantarctic Zone (SAZ) between the STF and the SAF, and the Polar Front Zone (PFZ) between the SAF and the Polar Front (PF) located further south outside the study area.

[60] Water masses were identified on the basis of their potential temperature (Tpot), salinity (S) and O_2 characteristics (Figure 3.2) as defined by Park et al. [1993, 2001, 2002], Park and Gamberoni [1997] and Read and Pollard [1993]. Inspection of the Tpot-S and Tpot-O_2 diagrams (Figure 3.2-a, b) reveals the following:

(**1**) North of the AF (stations 78/75, 83), Subtropical Surface Water (STSW) is characterized by Tpot >12°C and S>35.1;

(**2**) Between AF and SAF (stations 26, 27, 28, 29, 33, 36, 39, 43/46, 51) surface waters result from the mixing of STSW and Subantarctic Surface Water (SASW). Note that characteristics of stations 26, 27 and 33 are intermediary between those observed for the PFZ and SAF stations to the south, and STF stations to the north. Northward advection (Ekman drift) of SASW (which is fresher, colder and oxygen-enriched) across the STF is significant and is characterized by a local O_2 maximum in the upper 80 m. Between 80 m and 125 m a local shallow O_2 minimum appears sandwiched between this northward advection of SASW and northward intrusion of oxygen rich Mode Water (MW) occupying the depth range from 150 m to 200 m. The advection of fresher SASW induces also a salinity maximum at about 150 m. Below this surface layer there is strong variability in

the Tpot and S plots (wiggles in the Tpot-S diagram; Figure 3.2-a) reflecting interleaving between Subantarctic and Subtropical waters;

(**3**) In the area just south of the SAF, in the northernmost PFZ, Subantarctic Surface Water (Tpot<9°C, S<34 and O_2>267.8 µM) extends from the surface to about 200 m (i.e., around isopycnal 26.6; see stations 10/20, 11, 23, 24, 25 and 30). A broad oxygen maximum is present between ~50 m and 150 m, the basis of the surface mixed layer. The slightly lower O_2 concentrations in the upper 50 m are chiefly the result of summer heating decreasing the O_2 saturation of surface waters [Toole and Warren, 1993]. Below 150 m, O_2 decreases strongly to a minimum of about 179 µM at 1000 m in Circumpolar Deep water (CDW). Mixing between cold, fresh, oxygen-rich Subantarctic Water (SAW) and intruded warm, salty, oxygen-poor Subtropical Water (STW) takes place below the upper 150 m as indicated by the strong variability of the Tpot and S profiles (wiggles in the Tpot-S plot around isopycnal 27.1; Figure 3.2-a) reflecting interleaving;

(**4**) Antarctic Intermediate Water (AAIW) is characterized by a salinity minimum that is centered on σ_θ = 27.2 for the Crozet Basin;

(**5**) Below 1000 m water characteristics are generally similar throughout the entire study zone. From the Tpot-S and Tpot-O_2 diagrams we can identify CDW with an O_2 minimum, the North Atlantic Deep Water (NADW) with a salinity maximum and the Antarctic Bottom Water (AABW) with lowest temperatures and increased O_2 content.

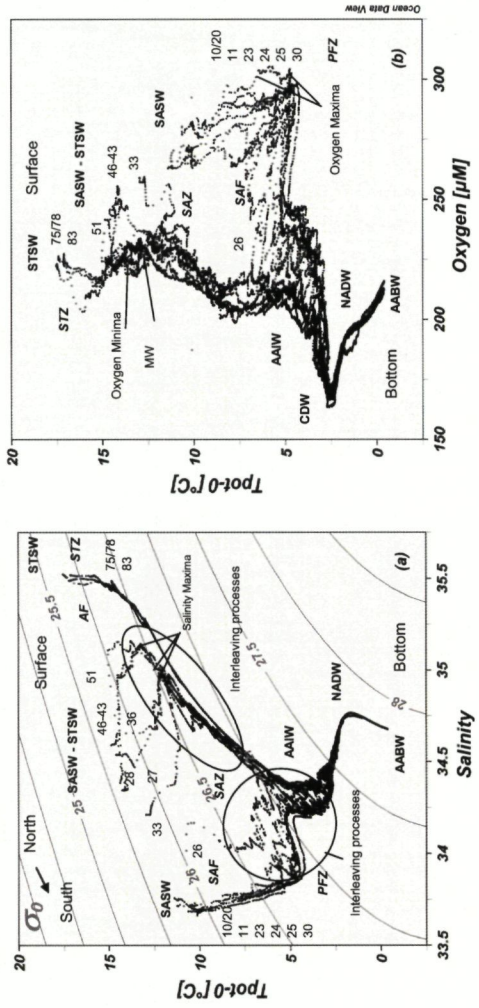


Figure 3.2: (a) Potential Temperature - Salinity plots with isopycnals; (b) Potential Temperature - Dissolved Oxygen plots. Major water masses identified from Tpot-S-O_2 characteristics are: Subtropical Surface Water (STSW); Subantarctic Surface Water (SASW); Mode Water (MW); Antarctic Intermediate Water (AAIW); Circumpolar Deep Water (CDW); North Atlantic Deep Water (NADW) and Antarctic Bottom Water (AABW). Numbers refer to stations. Circled parts = impact of interleaving processes. Graph constructed using Ocean Data View [Schlitzer R., 2003].

3.3. RESULTS

[61] We present results for 13 dissolved Ba and 7 particulate Ba profiles. These will be discussed in relation with Tpot, Salinity, O_2, Nutrients and Alkalinity. For dissolved Ba, profiles 10/20, 43/46 and 75/78 are a combination of data from two different CTD casts sampled closely in time and space. One CTD cast sampled the upper 300 m, while the second one sampled the deeper water column. Pair wise inspection of the Tpot-S and Tpot-O_2 data for these profiles and comparison with nearby single cast profiles warranted the combination of the dissolved Ba data into single vertical profiles. Dissolved and particulate Ba were not analyzed for the same CTD casts, but data were obtained for casts sampled close by in time and space. Pair wise inspection of the Tpot-S and Tpot-O_2 data for these profiles warrants comparison between profiles of dissolved and particulate Ba. Casts suitable for comparisons are: 10/20 (dissolved) and 11 (particulate), 23 (dissolved) and 30 (particulate), 46/46 (dissolved) and 51 (particulate), 78/75 (dissolved) and 83 (particulate). We also show data for 3 other particulate excess Ba profiles (stations 33, 36 and 39) not associated with Ba_d data and 6 other dissolved Ba profiles (stations 24, 25, 26, 27, 28 and 29). For both dissolved and particulate Ba profiles we also reproduce the corresponding O_2 and density profiles.

Dissolved Ba

[62] The vertical and latitudinal Ba_d variations observed during ANTARES-4 (Figure 3.3-a) are consistent with those observed for other cruises in the Southern Ocean: INDIGO 3 in the Indian sector [Poisson et al., 1990; Jeandel et al., 1996], CIVA 1 at 30°E in the Atlantic sector [Dehairs et al., in preparation-a] and GEOSECS in the Atlantic and Indian sectors [Chan et al., 1977; Östlund et al., 1987]. In surface and subsurface waters a positive gradient of Ba_d concentrations appears from north to south (Figure 3.3-a).

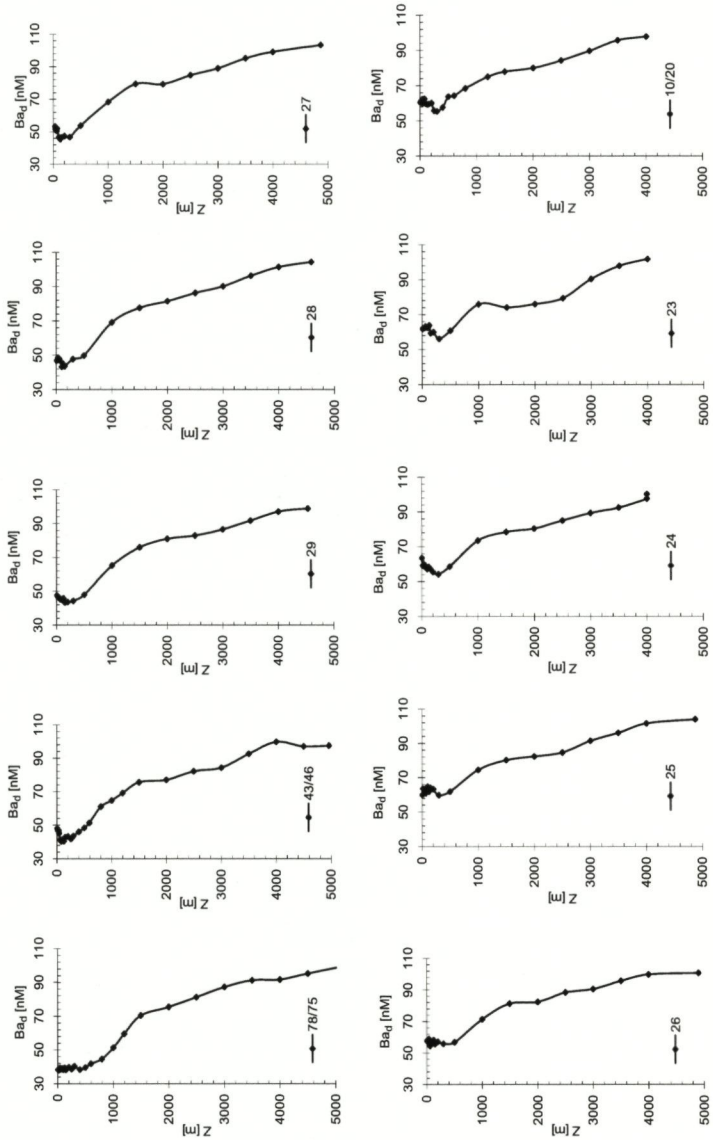


Figure 3.3-a: Dissolved Ba profiles (full squares; nM) in the whole water column. Note the scale differences between stations.

Surface water is most depleted in Ba_d in the STZ north of the AF (38 nM) and is most enriched in the PFZ south of the SAF (62 nM). In deep and bottom waters Ba_d concentrations reach up to 100 nM and more. In the STZ (station 78/75), Ba_d contents increase from 38 nM in surface to 98 nM at depth. Between AF and STF (stations 43/46, 28 and 29), concentrations increase from 47 nM in the surface to 104 nM at depth. In the SAZ (stations 26 and 27), concentrations increase from 55 nM in the surface to 100 nM at depth. In the PFZ (stations 10/20, 23, 24 and 25), concentrations increase from 62 nM in surface to 103 nM at depth. Below 2000 m, differences between zones tend to fade away (concentrations range from 75 to 100 nM), consistent with fairly homogenous Tpot-S properties (Figure 3.2).

[63] A closer inspection of the upper 800 m (Figure 3.3-b) reveals differences between the frontal zones (STZ, SAZ, PFZ). North of the AF, Ba_d concentrations are rather constant around 38 nM from the surface to 500 m. Station 43/46 between AF and STF reveals higher Ba_d concentrations in the upper 80 m as well as between 150 and 250 m. The Ba profile appears to closely follow the dissolved oxygen profile (Figure 3.3-b). At stations 29, 28, 27 and to lesser extent at station 26, the upper 80 m of water column also shows enhanced Ba_d concentrations. The Ba_d profile in the upper 250 m at station 27, south of the STF, shows features that are quite similar to those observed at station 43/46 but at station 27 these are less salient and Ba_d concentrations are higher. In particular we note for both stations a decrease of Ba_d with depth through the density gradient defining the bottom of the mixed layer followed by a slight increase around 200 m, the latter coinciding with a dissolved O_2 increase. Station 26 reflects the transition from SAZ to SAF-PFZ. As observed also for dissolved oxygen, the Ba_d profiles south of the SAF, in the PFZ (profiles 10/20, 23, 24 and 25), show a decrease in Ba_d concentrations between surface and 300 m, where a minimum is reached with Ba_d values 3 to 6 nM lower than in surface water. This depletion is significant, considering that the precision of the method is 1.2%. Deeper in the water column concentrations increase and at about 500 m reach the values observed at ~100 m.

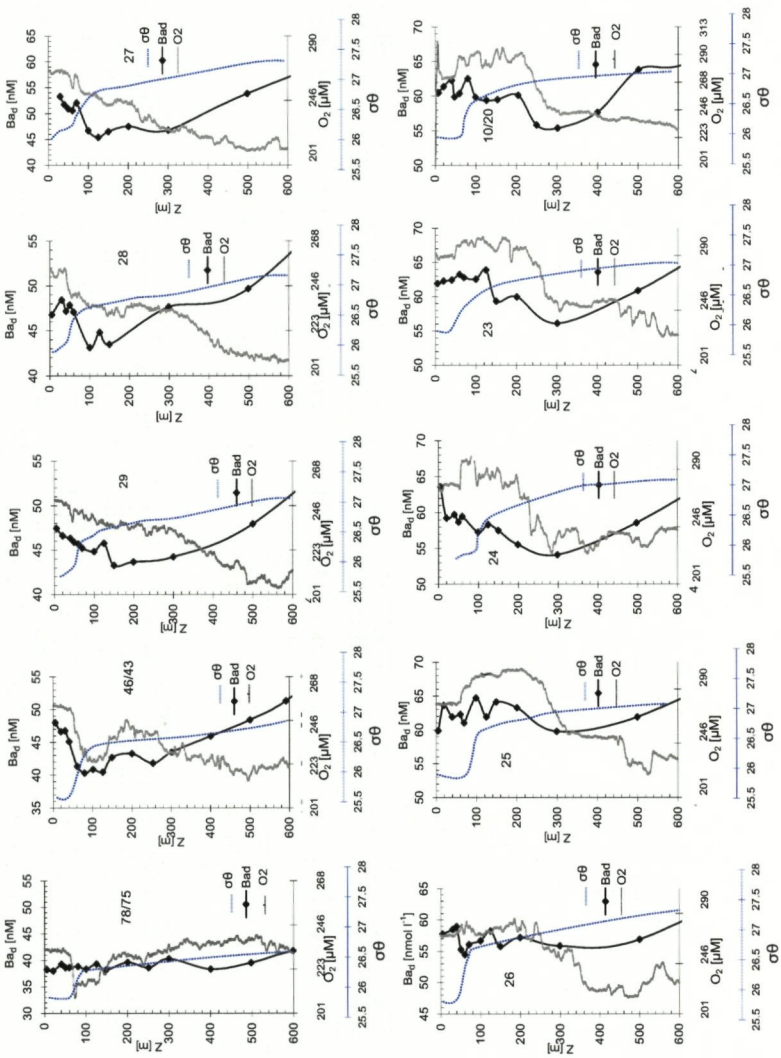


Figure 3.3-b: Dissolved Ba profiles (full squares; nM) in the upper 600 m with corresponding O_2 (continuous curve; µM) and σ_θ (dashed curve; kg m^{-3}) profiles. Note the scale differences between stations.

Particulate Ba

[64] The general shape of the Ba_{xs} profiles (Figure 3.4) is similar to the one observed during earlier work in the SAZ and PFZ [Dehairs et al., 1991, 1997; Cardinal et al., 2001, 2005]. Most profiles show higher concentrations between 100 m and 600 m and this feature is particularly salient for stations 30, 33 and 51. Depth weighted Ba_{xs} averages for the 100 to 600 m depth interval range from 312 pM (station 83) to 693 pM (station 33). While for station 83 north of the AF, the Ba_{xs} peak is weak (Ba_{xs} maximum not exceeding 400 pM), for the area between STF and SAF mesopelagic Ba_{xs} maxima reach up to 1000 pM (station 33 and 51) and are amongst the highest observed for Southern Ocean systems [see Dehairs et al., 1990, 1991, 1997; Cardinal et al., 2001, 2005]. This broad maximum often faces a negative gradient of dissolved O_2, but the increase of Ba_{xs} starts on from the bottom of the mixed layer, at a somewhat shallower depth than the decrease of oxygen (Figure 3.4). The Ba_{xs} profile at station 51 has two maxima: one at about 75 m in surface water and a second at 300 m. Ba_{xs} concentrations tend to decrease again in the deeper part of the water column. For stations 11 and 36, Ba_{xs} peaks are less salient, with Ba_{xs} concentrations showing larger variability in the upper 500 m.

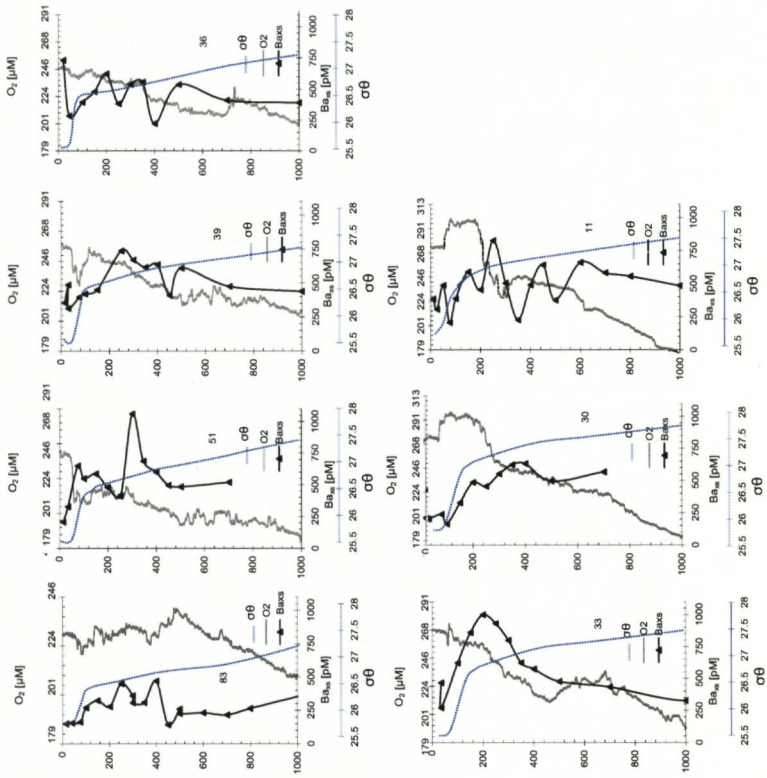


Figure 3.4: Excess particulate Ba profiles (full squares; pM) in the upper 1000 m with corresponding O_2 (continuous curve; µM) and σ_θ (dashed curve; kg m^{-3}) profiles.

3.4. DISCUSSION

Dissolved Ba, silicate and alkalinity

[65] At first sight vertical and latitudinal Ba_d distributions are remarkably similar to those for silicates: they show depletion in surface waters, enrichment at depth and upper water column concentrations which increase from north to south (nutrient profiles not shown here, but discussed in Leblanc et al., 2002). The slopes of the silicate vs. Ba_d regressions (Figure 3.5-a) are similar to those reported by Jeandel et al. [1996] for the Indian sector. Although for the whole area the correlation between Ba_d and $Si(OH)_4$ is tight, for the PFZ an uncoupling is evident between silicates and Ba_d in the upper 500 to 600 m, with Ba_d remaining high and constant as opposed to silicate reaching depletion (silicate

in surface water is very low: <1 µM for the whole study area, but especially in STZ surface water). A similar decoupling of Ba and silicate has been reported previously for the Atlantic and Pacific Oceans [Chan et al., 1977; Collier and Edmond, 1984]. This decoupling reflects the non-limiting, bio-intermediary status of Ba versus the bio-limiting status of silicate in this SAZ area. With biological control being minimized after major nutrient depletion (e.g. silicate) hydrodynamic control is likely to become predominant in setting the distribution of the left over Ba_d.

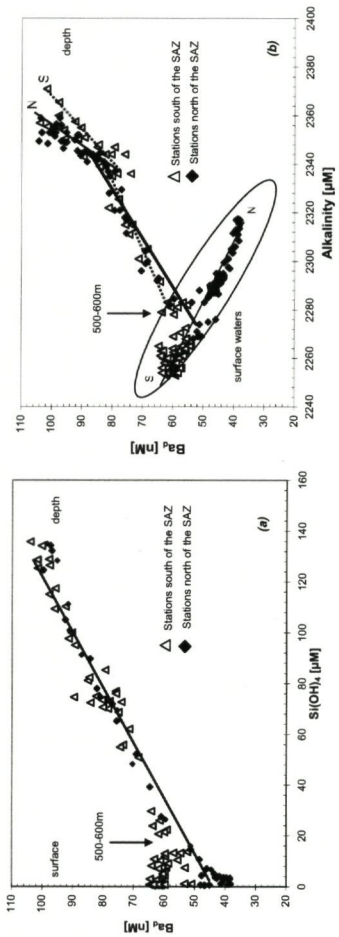


Figure 3.5: Regressions of dissolved Ba (nM) vs. (a) $Si(OH)_4$ (µM) and (b) Alkalinity (µM). Stations south of the SAZ are 10/20, 23, 24, 25, 26; stations north of the SAF are 27, 28, 29, 43/46, 78/75.

[66] The regression of Ba_d vs. alkalinity shows a quite complex picture (Figure 3.5-b). Below 600 m alkalinity correlates positively with Ba_d, but the slope of the regression decreases slightly from north to south. Jeandel et al. [1996] report a similar spatial variability of the Ba_d/alkalinity relationship. Ba_d vs. salinity regressions for deep waters (not shown) do show a similar latitudinal change. Ca and Ba being both bio-intermediate elements [Broecker and Peng, 1982], their oceanic cycles, which include uptake of Ca and Ba (the latter mostly passive) and redissolution at depth of $CaCO_3$ and $BaSO_4$ results in parallel oceanic distributions of Ba and alkalinity. In contrast, for surface waters (upper 500-600 m) an inverse relationship is apparent between Ba_d and alkalinity. From south to north alkalinity values range between 2250 and 2320 μM and Ba_d between 64 and 38 nM. A similar south to north trend of increasing surface water alkalinity is reported by Millero et al. [1998] for the Indian Ocean between 50°S and 30°S and by Goyet et al. [1991, 1999]. In Figure 3.6-a,-b the cross-frontal change in Ba_d vs. alkalinity and alkalinity vs. salinity is highlighted for representative stations of the area north of the SAF (stations 75/78), south of the SAF (station 24) and the transition zone between both (station 27). Comparing the vertical distribution of Ba_d and alkalinity in the upper 500 m of water column at station 27, the following is noted (Figure 3.6-c): the upper 100 m shows the presence of low alkalinity, high Ba_d water, probably reflecting advection of SASW from south of the SAF. Between 100 and 300m we observe higher alkalinity and lower Ba_d waters, characteristic for the area north of the SAF and STF. In this broad alkalinity maximum the slight decrease at 200 m (associated with a Ba_d increase) is likely associated with intrusion of Mode Water (Figure 3.6-c).

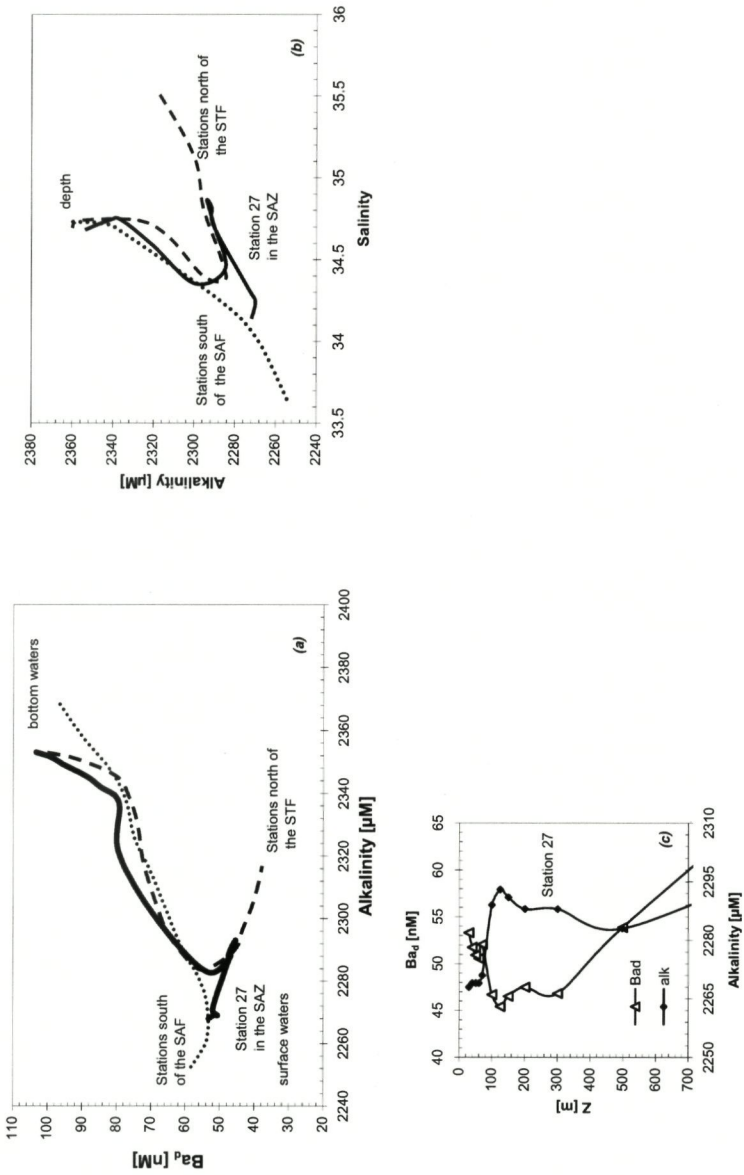


Figure 3.6: The cross-frontal change in Ba_d vs. alkalinity (a) and alkalinity vs. salinity (c) is highlighted for representative stations of the area north of the SAF (station 75/78, dashed line), south of the SAF (station 24, dotted line) and the transition zone between both (station 27, plain line). The vertical distributions of Ba_d and alkalinity in the upper 500 m of water column at station 27 are shown in (c).

[67] The above discussed relationships highlight that Ba is not mechanistically coupled neither with alkalinity nor silicate. The observed relationships rather result from the spatial coherence of parallel carriers over-printed by hydrodynamics, confirming, in general, results from earlier work [Lea, 1993, 1995; Jeandel et al., 1996; McManus et al., 1999; Rubin et al., 2003].

Dissolved and particulate Ba distributions

[68] Earlier work has evidenced the close relationship between biological activity and water column particulate Ba contents. In particular the Ba_{xs} maximum, commonly observed in the mesopelagic waters of the Southern Ocean [e.g. Dehairs et al., 1980; 1992; 1997; Jeandel et al., 2000; Cardinal et al., 2001] and also now during the ANTARES-4 cruise (e.g. station 30; see Figure 3.3) has been associated with mineralization of exported organic matter [Dehairs et al., 1997; Cardinal et al., 2005]. Examining a Pacific Ocean profile of particulate and dissolved Ba, Collier and Edmond [1984] concluded that significant local uptake of dissolved Ba was required to maintain the mesopelagic particulate Ba maximum. Their conclusion rests on the observation that the particulate Ba maximum was associated with a significant enrichment of Ba relative to biogenic components such as Si, Sr, Ca (and also relative to Al) which could not be explained by preferential regeneration of the latter components nor by the amount of Ba present in upper mixed layer suspended matter [Collier and Edmond, 1984]. Such uptake of Ba would then occur in the degrading biogenic aggregates or flocs where it leads to Ba_{xs} – barite production. Overall this picture also fits with the observations from sediment traps often showing increasing fluxes of Ba_{xs} with depth, an indication that Ba is continuously subtracted from solution during the vertical transport of the aggregates [e.g. Dymond et al., 1992].

[69] The ANTARES-4 cruise is one of the few Southern Ocean cruises for which both dissolved and particulate Ba were measured. It therefore offers a unique opportunity to investigate whether the subsurface subtraction of Ba invoked above leads to a measurable impact on the dissolved Ba profile. Focus here will be on the mesopelagic zone where the Ba_{xs} maximum is located. Stations suitable for comparisons are from south to north: 10/20 (dissolved) - 11 (particulate) and 23 (dissolved) - 30 (particulate) in the PFZ; 46/46 (dissolved) - 51 (particulate) between AF and STF; 78/75 (dissolved) - 83 (particulate), north of the AF.

[70] Stations 10/20 and 23 in the PFZ show a Ba_d depletion between 125 and 500 m and 200 and 500 m, respectively, with minima located at 300 m (Figure 3.7).

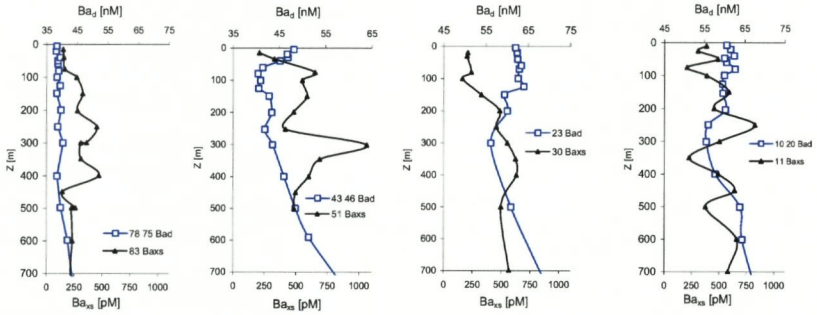


Figure 3.7: Comparison of particulate excess Ba (full triangles curve, pM) and dissolved Ba (open squares curve, nM) profiles for the upper 700 m of the PFZ (Stations 23 and 30 and stations 10/20 and 11).

Stations 24 and 25 for which there are no corresponding Ba_{xs} profiles, also present a Ba_d depletion between 150 and 500 m with a minimum at 300 m (see Figure 3.3-b). The depth interval of this Ba_d minimum in the PFZ is sandwiched between isopycnals 26.6 and 27.1, where the Tpot-Sal diagram shows pronounced intrusive layering, reflecting interleaving between SAW and STW (see Figure 3.2). Furthermore, in the depth range of the broad Ba_d minimum there is an occasional small alkalinity maximum (stations 10/20 and 25; not shown) consistent with the possibility of an intrusion of alkalinity enriched waters from the north. Since many features in the PFZ appear to result from interleaving processes through the SAF, we performed a multiple regression analysis to determine whether the Ba_d depletion between ~ 150 and 500 m in the PFZ could be obtained by intrusion and mixing of waters poorer in Ba_d, originating north of the SAF. Therefore we considered the region between SAF and AF as the source region (i.e., stations 43/46, 26, 27, 28, 29). Then we expressed Ba_d for these stations as a function of other parameters including: alkalinity, nitrate, salinity, silicate and Tpot (contributions of pressure and O_2 are not significant):

$Ba = 293.34 + 0.183*Alk - 0.244*NO_3 - 18.85*Sal + 0.300*Si - 0.744*Tpot$

(R-squared = 98.066; p-Value < 0.01).

[71] Subsequently, Ba_d profiles in the PFZ were recalculated based on the regression coefficients defined for the selected source region and on local PFZ conditions for alkalinity, nitrate, salinity, silicate and Tpot. For stations 10/20, 23, 24 and 25 the model closely reconstructs the Ba_d minimum between ~ 150 and

500 m suggesting that the observed Ba_d depletion in the PFZ has not a local origin, but is maintained by the combined effect of hydrodynamics and biogeochemical processing elsewhere. However, at station 23 two data points (150 and 200 m) in the Ba_d minimum are not reproduced by the model results. Although we are confident that this discrepancy is real, it represents far from strong evidence for an impact of barite production on the dissolved the Ba pool.

[72] The zone between AF and STF is also particularly marked by cross frontal advections and intrusions. The Ba_{xs} profile at station 51 shows two maxima coinciding with large density and O_2 gradients. One local Ba_{xs} maximum occurs at the bottom of the mixed layer (~75 m) below the O_2 enriched surface layer and a second one at 300 m, below the O_2 enriched Mode Water. It is well known that organic aggregates and flocs tend to form and accumulate in association with density gradients [e.g., Lampitt et al., 1993; MacIntyre et al., 1995; Simon et al., 2002]. Therefore, a scenario of local Ba_{xs} production associated with enhanced abundances of micro-environments favored by physico-chemical gradients (indicated by salinity, Tpot, O_2 clines) induced by cross-frontal water exchange and associated shear, appears plausible here. Ba_d in the upper 200 m at station 43/46 evolves inversely to Ba_{xs}. Ba_d concentrations show a local maximum in the low salinity upper 50 m (O_2= 250 µM; Ba_d= 48 nM) as well as between 150 m to 300 m (O_2= 236.6 µM; Ba_d= 43 nM) and Ba_d and O_2 profiles are strikingly similar (Figure 3.3). This may reflect the northward advection of fresher and O_2 rich SASW (upper 90 m) and Mode Water at 200 m (Figure 3.2) reported by Park et al. [1993, 2002]. Similar Ba_d - O_2 patterns are observed for station 27 (Figure 3.3). A scenario of combined hydrodynamic and biogeochemical control on the Ba_{xs} distribution (station 51) seems likely and does not conflict with our discussion about advection controlling the Ba_d (and also O_2) distributions in the upper 300 m at station 43/46. Overall, our results suggest that hydrodynamics in combination with local productivity provide the appropriate conditions for Ba_{xs} production.

[73] North of the AF, the Ba_{xs} peak occurring between ~75 and 450 m is weak and Ba_d concentrations are quite uniform over the upper 400 m (Figure 3.7). The weak Ba_{xs} peak reflects weak export in the area, what is in agreement with the intensive recycling of biogenic Si in this surface water reported by Leblanc et al. [2002].

3.5. CONCLUDING REMARKS

[74] The Polar Front, Subantarctic Front and Subtropical Front Zones in the Crozet-Kerguelen Basin, each exhibited characteristic distributions of dissolved and particulate Ba as well as different correlative behavior of Ba with silicate, alkalinity and dissolved O_2. While showing some similarity with the distribution of silicate and alkalinity, the Ba distribution presents unique features, highlighting that specific biogeochemical processes are operating which are different from those controlling silicate and alkalinity. In general these findings corroborate existing knowledge on Ba_{xs}-barite formation in the oceanic water column. We also investigated the link between the dissolved and particulate phases of Ba, and except for the PFZ, we did not observe a systematic occurrence of dissolved Ba minima coinciding with maxima of mesopelagic particulate Ba which reflect barite precipitation associated with organic matter mineralization. However, the Ba_d minima in the PFZ appear largely influenced by cross frontal advection of SAZ waters and no clear evidence was found that precipitation of barite, reflected by the occurrence of Ba_{xs} maxima, does measurably influence the distribution of dissolved Ba. It is likely that strong mixing in this complex frontal system of the Crozet-Kerguelen Basin ultimately precludes that a measurable Ba_d depletion establishes. Overall, our observations suggest that since control of hydrodynamics on dissolved Ba appears overwhelming, spatially well resolved profiles of dissolved and particulate Ba, measured with great precision, are required to de-convolve the biogeochemical from the hydrodynamical effects on the barium distribution.

Chapter 4

A high resolution transect of dissolved barium

Foreword

[75] As outlined in the preceding chapter, a high spatial resolution of Ba profiles in complex S.O. frontal systems is necessary to better understand the relative contribution of conservative vs. non conservative processes in the control of the Ba_d distribution. In Chapter 4, a high sampling resolution is thus described with special emphasize on the relation between dissolved Ba, frontal structures and water masses; the whole water column is sampled at 53 stations separated by ~½ degree of latitude, along the WOCE SR3 line (43-68°S; CLIVAR SR3 cruise).

SUMMARY

[76] The dissolved Barium distribution in the whole water column was examined along the WOCE SR3 line in the Southern Ocean (Australian sector, late winter-spring 2001). The high sampling resolution offered an excellent opportunity to relate the Ba_d distribution to frontal structures and the water masses. Such a high resolution was not achieved in previous Southern Ocean studies and showed the tight overprinting of the frontal zones by Ba_d gradients. Hydrodynamic control on Ba_d is evident in the case of Antarctic Bottom Water formation, westward flow of Tasman Sea waters and return flow of an eddy of the SubAntarctic Front. However biogeochemical processes are also acting, as witnessed by enhanced Ba_d contents in deep waters of the SubAntarctic Front zone and by a local mesopelagic minimum in the Inter Polar Front Zone. These features are respectively ascribed to the dissolution of Ba-rich phases and Ba transfer from solution to particulate.

4.1. INTRODUCTION

[77] Zonal coverage of Ba_d data in the Southern Ocean is still limited today, especially for the major frontal systems through which strong physico-chemical gradients occur [Arrigo et al., 1998; Moore et al., 1999]. As outline above in the study of the Ba distribution in the Crozet-Kerguelen basin, spatially well resolved profiles of Ba_d are required, especially in these complex S.O. frontal systems, to de-convolve the biogeochemical from the hydrodynamical effects on the barium distribution. The high sampling resolution along WOCE SR3 line in the Australian sector of the Southern Ocean, achieved during the CLIVAR-SR3 cruise, offered a unique opportunity to compare the Ba_d distribution in a late winter-spring situation with frontal structures and characteristics of the water masses present and to shed more light on the relative importance of physico-chemical versus biogeochemical controls. The whole water column was sampled at 53 stations separated by ~½ degree of latitude, along the 140-142°E meridian (43-68°S) in the Australian sector of the Southern Ocean.

4.2. RESULTS AND DISCUSSION

[78] Definitions and positions of zones and fronts discussed here (Figures 4.1 and 4.2) are mainly based on potential temperature (θ) and salinity (S) characteristics, as discussed by Sokolov and Rintoul [2002] and Rintoul and Bullister [1999]. Nutrient conditions encountered during the cruise were rather typical of the area and season [Trull et al., 2001-a]. Sampled zones and fronts were from north to south: the Subtropical Zone (STZ), the Subtropical Front (STF), the SubAntarctic Zone (SAZ), the SubAntarctic Front (SAF, northern and southern branch), the Polar Front Zone (PFZ), the Polar Front (northern and southern branch, with the InterPolar Front Zone (IPFZ) between the two branches), the southern Antarctic Zone (AZ-S), the Southern Antarctic Circumpolar Current Front (SACCF, northern and southern branch), the Southern Boundary (SB) and the zone under Sea Ice influence (SI).

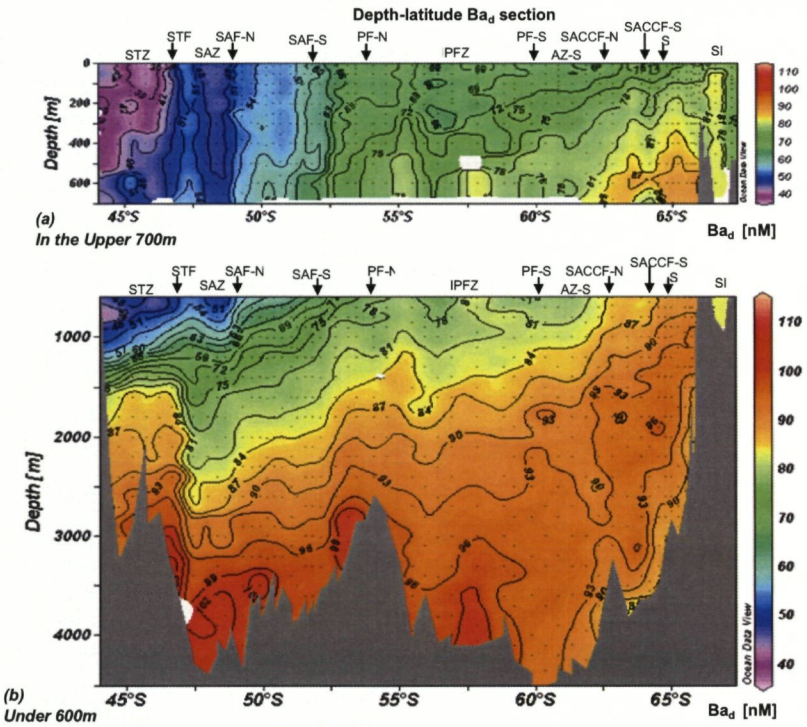


Figure 4.1: High resolution whole water column Ba_d distribution (nM) along SR3 transect from Tasmania to Antarctica (October-November 2001); (a) in the upper 700 m and (b) between 600 m and seafloor. STZ = the Subtropical Zone, STF = the Subtropical Front, SAZ = the SubAntarctic Zone, SAF-N and SAF-S = the SubAntarctic Front northern and southern branches, PFZ = the Polar Front Zone, PF-N and PF-S = the Polar Front northern and southern branches, IPFZ = InterPolar Front Zone, AZ-S = the southern Antarctic Zone, SACCF = the Southern Antarctic Circumpolar Current Front, SB = the Southern Boundary and SI = the zone under Sea Ice influence. Figure elaborated using Ocean Data View [Schlitzer R., 2003].

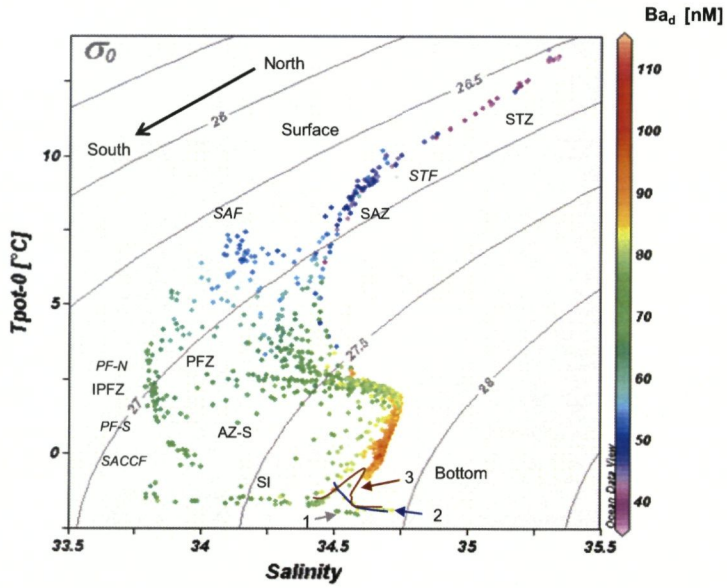


Figure 4.2: θ-S diagram superposed with Ba_d concentration ranges (nM). STZ, STF, SAZ, SAF, PFZ (PF-N, -S), IPFZ, AZ-S, SACCF, SI: as in Figure 1. Arrows 1, 2 and 3 represent stations on the Antarctic shelf discussed in paragraph [79]. Figure elaborated using Ocean Data View [Schlitzer R., 2003].

[79] The observed vertical and latitudinal Ba_d variations are consistent with those observed elsewhere in the Southern Ocean [Chan et al., 1977; Östlund et al., 1987; Jeandel et al., 1996]. Figure 4.1 shows the Ba_d distribution along the CLIVAR-SR3 transect.

Upper 1000 m

[80] The general picture for the upper 1000 m shows a Ba_d increase from north to south, similar to what is commonly observed for nutrients. This general latitudinal pattern is overprinted by sharp gradients of Ba_d, coinciding with the different frontal structures. From north to south the following features are observed (Figure 4.1-a and Figure 4.2):

(**1**) The STZ surface waters at 45°S present low Ba contents (<45 nM), with a minimum of 35 nM. Water properties and altimeter maps (not shown) indicate the section crossed an eddy of subtropical Tasman Sea water between 45°S and 47°S. The STF (corresponding to a drop in temperature from 11 to 9.5°C and salinity >35.0 to <34.8 from north to south in the upper 300 m) is located at 47°S at the

southern edge of the eddy. The STF coincides with a Ba_d gradient from ~48 to 54 nM in the upper 400 m;

(**2**) At 47°S, just south of the STF, Ba_d values are locally quite high (reaching up to 54 nM in the upper 600 m), similar to values found further south, between the northern and southern branch of the SAF. Water properties and altimetry (not shown) suggest that this water mass coincides with a cold-core eddy pinched off from the SAF. The juxtaposition of these two eddies results in a very strong Ba_d front between the subtropical waters to the north and the SAF waters to the south. South of the cold-core eddy and north of the SAF, a relatively homogeneous water mass, the Subantarctic Mode Water (SAMW), is found between the surface and 700 m depth. Ba_d content in the SAMW is between 45 and 49 nM, greater than the subtropical waters but lower than values found in the SAF and the eddy spawned from the SAF, resulting in a local minimum between 48 and 49°S. Between 49 and 49.3°S a surface water Ba_d gradient from ~47 to 53 nM coincides with the position of the northern branch of the SAF (SAF-N). Here, steep Ba_d isolines extend beyond 600 m in the water column and this is observed also for the other water mass properties. The southern branch of the SAF (SAF-S) is located between ~51.5 and 52°S and coincides with a slightly weaker Ba_d gradient from 60 to 63 nM;

(**3**) The Polar Front, which marks the northern limit of the Antarctic Zone, is also composed of two branches, the PF-North and the PF-South. Taking the northern-most extent of the 2°C water in the temperature minimum as the subsurface expression of the northern branch of the Polar Front, positions the latter at ~54°S. The southern-most extent of the temperature maximum waters warmer than 2.2°C sets the PF-S at ~60°S. Besides small Ba_d gradients through the PF-N (~68 to 69 nM) and the PF-S (71 to 72 nM), no peculiar feature in the Ba_d distribution coincides with the position of the PF. Interestingly, the upper 300 to 400 m in the IPFZ (~54 to 60°S) between the PF-N and PF-S, is relatively homogenous in Ba_d (69 to 70 nM) as it also is for salinity, except for four stations between 55.9 and 57.8°S where slightly lower Ba_d concentrations are observed in the upper 300m (between ~ 65 and 67 nM). The fact that the same Ba_d section plotted versus neutral density instead of depth (not shown) also presents the anomaly indicates that the feature is not associated with differences in water column stratification. It is possible we witness the effect of enhanced translocations of Ba from the dissolved to the particulate phase. This fits also with the observation of higher

particulate Ba concentrations in the mesopelagic waters at ~57°S [Cardinal et al., 2005];

(**4**) The AZ-S is delineated to the south by the SACCF, also characterized by a northern and southern branch, the positions of which are set by the southernmost extension of θ maximum water warmer than 2°C (~62.4°S) and 1.8°C (at 64.2°S), respectively. Surface concentrations in the AZ-S range between 70 and 72 nM. In surface waters the northern branch is not associated with peculiar Ba_d features whereas the southern branch shows slightly lower Ba_d concentrations in the upper 1000 m, reflecting the transition between the two branches of the SACCF and the SB (Southern Boundary). Surface waters at the (SB) of the ACC (set by the southernmost extension of the O_2 minimum waters) and in the Seasonal Ice Zone (SI) south of the SB, have Ba_d contents >75 nM, reaching a maximum of 78 nM. The situation over the Antarctic shelf is discussed later.

Under 1000 m

[81] Concerning the deeper (>1000 m) water column (Figure 4.1-b and Figure 4.2), major features are:

(**1**) North of 45.5°S, deep waters between the Tasmanian shelf and the South Tasman Rise show significant build-up of Ba resulting in quite strong surface to deep Ba_d gradients. The space between Tasmania and the SAZ is occupied by a westward flowing poorly ventilated (low CFC), warm, salty and O_2 poor water coming from the Tasman Sea [Rintoul and Bullister, 1999]. The long residence time of these deep waters from the Tasman Sea could give rise to a build-up of Ba_d from the dissolution of barite and other Ba-rich particles in these undersaturated waters [Monnin et al., 1999; Rushdi et al., 2000];

(**2**) At ~45.5°S near the top of the South Tasman Rise, lower Ba_d values probably reflect the Tasman Sea origin of the subtropical eddy;

(**3**) The upper ocean Ba_d gradients coinciding with the positions of STF, SAF-N and SAF-S reach very deep and clearly extend over most of the water column; between STF and SAF-N (~49°S) a wedge of relatively low Ba_d extends between ~1000 and 3000 m, a feature that is also observed for other physico-chemical characteristics and remains visible in a Ba_d vs. neutral density transect plot;

(**4**) Between 47.5 and 53°S bottom waters reach the highest Ba_d values observed along the whole transect (between 100 and 115 nM). This could reflect dissolution of Ba-rich phases such as barite in the under-saturated deep Southern Ocean waters [Monnin et al., 1999; Rushdi et al., 2000]. However, since deep waters (>2000 m) over the whole latitudinal extent of the Southern Ocean basin are reported to be under-saturated for barite [Monnin et al., 1999; Minnin and Cividini, 2006], the high bottom water concentrations at 47.5-50°S probably also reflect higher export of Ba-rich particles to the seafloor at these latitudes. This is corroborated by sediment trap flux data showing higher Ba fluxes in the deep water column at 47-51°S (traps between 1000 and 3300 m) compared to 54°S (traps between 800 and 1500 m), generally following a north – south decrease in this latitudinal range [Cardinal et al., 2001; 2005]. It is also possible that the high Ba concentrations are due to epibenthic fluxes of Ba, in which case as well they would reflect a larger flux or rain rate of Ba-rich particles to the sea floor in the SAZ region;

(**5**) The presence of the ridge between 52.5 and 55°S clearly affects the deep Ba_d distribution showing a sharp Ba_d gradient on its northern side, coinciding with the position of the SAF-S;

(**6**) Bottom waters in the vicinity of the Antarctic margin, south of 63°S, show decreased Ba_d concentrations. These bottom waters have lower temperatures, increased O_2 and CFC contents [M. Warner, pers. commun., 2003] and reflect the sinking of dense waters over the Antarctic shelf and along the margin, forming Antarctic Bottom Water (AABW). When comparing these bottom waters with waters at 100 m having similar CFC contents (i.e. comparing water masses of same origin and age), we observe for Ba_d a slight enrichment in bottom water. Again, this may indicate release of Ba from settling Ba-enriched particles such as barite, as discussed above.

Antarctic Shelf

[82] We now focus on the Antarctic shelf. Most waters here spread along the freezing line (-1.8°C; see Figure 4.2). The southernmost station (67.15°S; see 1 on Figure 4.2) is homogenous in Ba_d content with concentrations not exceeding 76 nM. The profile at 66.59°S in the central part of the shelf (see 2 on Figure 4.2) contrasts sharply, showing much higher Ba_d values (>83 nM) with deep and bottom waters on the freezing line. The origin of the waters at this shelf station is likely Circumpolar Deep Water upwelling at the Antarctic Divergence

(SB) and (occasionally) spilling over on the shelf, a process recognized as essential to the formation of Antarctic Bottom Water [e.g. Orsi et al., 1999]. This explanation is supported by the physico-chemical characteristics (θ, Salinity, O_2, CFC's, nutrients and Ba_d) of the CDW waters at station at 66°S (see 3 on Figure 4.2) which are similar to the characteristics both at 66.59 and 67.15°S on the shelf.

4.3. CONCLUDING REMARKS

[83] The present work brings information on the Ba_d distribution in the Australian sector of the Southern Ocean along the WOCE SR3 line (140-142°E) during spring 2001. Our results reveal a situation where the Ba_d distribution appears mainly driven by hydrodynamics, while regionally enhanced Ba_d contents in the deep ocean north of the mid-ocean ridge, could reflect the combined effect of a higher particulate Ba flux towards undersaturated deep waters and poorer ventilation of some of these deep basins. From Chapter 3 and Chapter 4, since Ba_d appears partly driven by the particulate Ba-barite dynamics and since this latter is biogeochemically derived, seasonal dynamics is particularly important to be investigated. Determining the sensitivity of Ba_d to the growth season would be of great interest to better de-convolve conservative and non-conservative behavior of Ba.

Chapter 5

Seasonal variability of barium signals

Foreword

[84] At this stage, the reader should have a clear understanding of the complexity in separating biogeochemical vs. hydrodynamics on the Ba_d distribution in S.O. frontal systems. As outlined in the preceding chapter, determining the sensitivity of Ba_d to the phytoplankton growth season could provide new insights on the behavior of Ba. Chapter 5 thus focuses on the seasonal variability of Ba signals (both dissolved and particulate), along the same SR3 transect as presented in Chapter 4; summer 1998 (SAZ-98 cruise) is confronted to spring 2001 (CLIVAR cruise). Additionally, relations between dissolved Ba, nutrients and alkalinity (as investigated in Chapter 3) are also discussed in the contrasting divides along the frontal system.

SUMMARY

[85] Spring and summer profiles of dissolved and particulate Ba from WOCE SR3 line (145°E) in the Southern Ocean are compared and seasonal evolutions discussed. Fluxes are estimated from mass conservation equations and from differences in reservoir contents between seasons. Subtraction of barium is observed at mesopelagic depths (upper 600 m) and appears to exceed up to ten-fold the combined local build-up and the deep ocean fluxes of particulate Ba, pointing towards significant dissolution to take place in intermediate and deep waters. Although regression analyses identify silicate as the major predictor of Ba, Ba and silicate are clearly uncoupled in surface waters where Ba behaves more similar to nitrate, excluding diatoms as consumers of Ba. Moreover, we observe a southward decrease in the Ba vs. silicate regression slopes driven by the conditions in intermediate and deep waters and mainly marked by the location of the Polar Front. These findings corroborate existing knowledge about the predominant control by barite formation and dissolution on the oceanic Ba cycle. It suggests a decreased dissolution of barite south of the Polar Front as compared to the situation in the Polar Front Zone and the Subantarctic Zone. This is in agreement with the fact that, except for deep waters the Antarctic Circumpolar Current water column is oversaturated with respect to barite, in contrast to the situation north of the Polar Front, where the whole water column is undersaturated [Jeandel et al,. 1996; Monnin et al., 1999; Monnin and Cividini, 2006].

5.1. INTRODUCTION

[86] In the study of the Ba distribution in the Crozet-Kerguelen basin (Chapter 3), we underpinned the fact that the Ba_d distribution does not depend on the same particle-solute interaction processes which control alkalinity and silicate. While such results are in line with the fact that formation and dissolution of barite are major processes shaping the oceanic Ba profile, we did not provide clear evidence that barite formation does measurably influence the distribution of dissolved Ba. Moreover, as outline in the study of dissolved Ba along the SR3 transect (Chapter 4), investigating the sensitivity of Ba_d to the onset of the phytoplankton growth season would help to better de-convolve conservative and non-conservative behavior of Ba.

[87] Here, we thus present dissolved and particulate Ba profiles obtained for spring and summer situations during two cruises in the Australian sector, crossing the Southern Ocean south of Tasmania from the Subtropical Zone to the Polar Front zone (SAZ-98 and CLIVAR cruises); focus was put on the SubAntarctic region. We confront dissolved Ba with physico-chemical conditions and investigate the correlative behavior of Ba with nutrients (silicate and nitrate) and alkalinity via multiple regression analysis, in order to improve our understanding of the biogeochemical processes involved in shaping the nutrient-like distribution of dissolved Ba. Then we estimate the subtraction of dissolved Ba in subsurface and mesopelagic waters during the growth season and compare this subtraction with release of particulate Ba and with Ba fluxes in deep waters.

5.2. HYDROLOGICAL SETTING

[88] Dissolved Ba (Ba_d) and particulate Ba (Ba_p) were studied in the Australian sector of the Southern Ocean along north – south transects between Tasmania and Antarctica (Figure 5.1). For the Subtropical, Subantarctic and Polar Front Zones we confront data for summer 1998 (SAZ-98 cruise, AU9706; February - April) and spring 2001 (CLIVAR-SR3 cruise, AU0103; October – December). The CLIVAR-SR3 Ba_d transect is the most resolved spatially (depth, latitude), with 32 stations and 24 depths sampled from the Subtropical Zone (STZ) to the Antarctic Zone AZ. The entire Ba_d data set for CLIVAR-SR3 has been discussed above. Dissolved Ba data for the SAZ-98 cruise have not been presented yet. The particulate Ba data sets for SAZ-98 and CLIVAR-SR3 are discussed in Cardinal et al. [2001] and [2005], respectively. During SAZ-98 we

sampled 8 sites for dissolved Ba and 4 for particulate Ba in the area between the Subtropical Front and the Polar Front Zone. During CLIVAR-SR3, the same area was sampled with 24 sites for dissolved and 3 for particulate Ba.

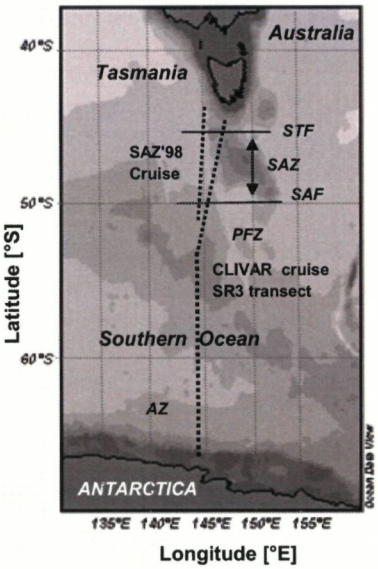


Figure 5.1: Geographical setting of the study areas during the SAZ-98 (summer 1998) and CLIVAR SR3 (spring 2001) cruises along WOCE SR3 line in the Australian sector of the Southern Ocean (~142 °E).

Stations suitable for comparing spring (CLIVAR-SR3) and summer situations (SAZ-98) were selected on the basis of potential temperature - salinity properties (Tpot-S diagram, Figure 5.2). Dissolved and particulate Ba profiles were not obtained from the same CTD casts, but from casts sampled closeby in time and space and having similar Tpot-S data profiles. Deep carbon and Ba export fluxes discussed here are from Trull et al. [2001-b] and Cardinal et al. [2005] respectively. Six sediment traps were deployed between September 1997 and February 1998, in the Subantarctic Zone (46.8°S at 1060, 2050 and 3850 m), the Subantarctic Front (51°S at 3089 m) and the Polar Front Zone (53.8°S at 830 and 1580 m). Ba fluxes were corrected for trapping efficiency via excess ^{230}Th [Trull et al. 2001-b; Cardinal et al., 2005]. Salinity, temperature and nutrients data from CTD bottles have been provided by Marc Rosenberg (Antarctic CRC, Hobart) and alkalinity data (for CLIVAR-SR3 only) by Bronte Tilbrook (CSIRO, Hobart).

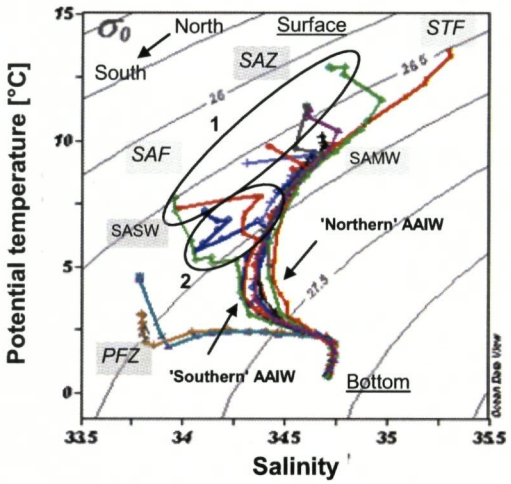


Figure 5.2: Potential Temperature - Salinity plots and isopycnals for SAZ-98 and CLIVAR SR3 profiles. STF = SubTropical Front, SAZ = SubAntarctic Zone, SAF = SubAntarctic Front, PFZ = Polar Front Zone. 1 = northward advection of cold and fresh surface waters; 2 = strong variability in SAF subsurface waters due to cross-frontal exchanges. Graph constructed using Ocean Data View [Schlitzer R., 2003].

[89] Data for CLIVAR-SR3 and SAZ-98 are taken to represent spring (2001) and summer (1998) conditions, respectively. The evolution of the monthly averaged Chl_a contents for the period 1997 to 2006, based on SEAWIFS imagery, reveals a quite regular pattern from year to year with onset of the bloom in September and demise towards March-April [C. Rathbone and B. Griffiths 2006, CSIRO, Hobart, personal communication]. Inter-annual variation in timing of onset and demise of seasonal plankton development did not exceed 3 weeks. Furthermore, the evolution of the 2001-2002 growth season is consistent with observations on seasonal Chl-a evolution reported by Trull et al. [2001-a, 2001-b] for the 1997-1999 period. Therefore, for comparison purposes, we consider that the timing of the season's onset and progress was similar throughout the period 1998 to 2001. We also assume that 100 days have elapsed between spring and summer.

[90] The investigated sections cross the Subtropical Front (STF), the Subantarctic Zone (SAZ), the Subantarctic Front (SAF) and the Polar Frontal Zone (PFZ) (Figure 5.1 and Figure 5.2). Detailed descriptions of the complex physical structure of the area, circulation, water masses and fronts are given in Rintoul and Bullister [1999], Trull et al. [2001-a] and Sokolov and Rintoul [2002]. Briefly,

the main hydrodynamical features observed during both cruises are the following (see Tpot-S diagram, Figure 5.2):

(**1**) The SAZ and SAF are characterized by cool and fresh surface waters (upper 100 m; circle 1 in Figure 5.2);

(**2**) Below the surface layer in the SAF, there is strong variability in the Tpot-S plots reflecting interleaving processes (circle 2 in Figure 5.2);

(**3**) In the subsurface layers between STF and SAF a continuum of Antarctic Intermediate Waters (AAIW) is observed showing decreasing salinities and temperatures from north to south (the northern variety is of Tasman Sea origin; Rintoul and Bullister, 1999);

(**4**) PFZ stations clearly differentiate from the areas to the north, with, very fresh and cold waters at potential densities > 27.5.

5.3. RESULTS – Ba_d AND Ba_{xs} DISTRIBUTIONS

[91] Spring (CLIVAR-SR3) and summer (SAZ-98) Ba_d profiles are reported in Figure 5.3 for representative stations from the STF to PFZ together with potential density profiles. Summer dissolved Ba profiles present similar latitudinal and vertical trends as spring profiles (see above). Ba_d gradients between the surface and 2000 m range from 40 to 80 nM (STF), 45-50 to 80 nM (SAZ), 50-60 to 80 nM (SAF) and 65-70 to 90 nM (PFZ). Deeper in the water column (data not shown here), concentrations increase and values reach up to 110 nM and more in bottom waters at 4000 m. Overall, these SR3 data sets compare well with data reported for other cruises in the Southern Ocean [Chan et al., 1977; Östlund et al., 1987; Poisson et al., 1990; Jeandel et al., 1996].

[92] Summer Ba_d profiles show more variability than spring profiles in the upper 600 m (Figure 5.3), with slight depletions extending over the mesopelagic zone at the STF and the PFZ. The depth where a density gradient sets the lower boundary of the surface mixed layer generally coincides with the depth where summer Ba_d concentrations start to decrease. For both seasons we integrated Ba_d profiles between 100 and 600 m (depth weighted average value; Table 5.1-a) and summer mesopelagic Ba_d values are systematically lower than spring values. With a precision of 1.5% on the measure, the difference between

summer and spring appears significant (t-test). Subsurface depletions are usually not observed for the spring Ba_d profiles (Figure 5.3) except for a slight depletion in the STF where the Ba_d profile is probably influenced by the complex frontal system in the upper 1000 m (see above).

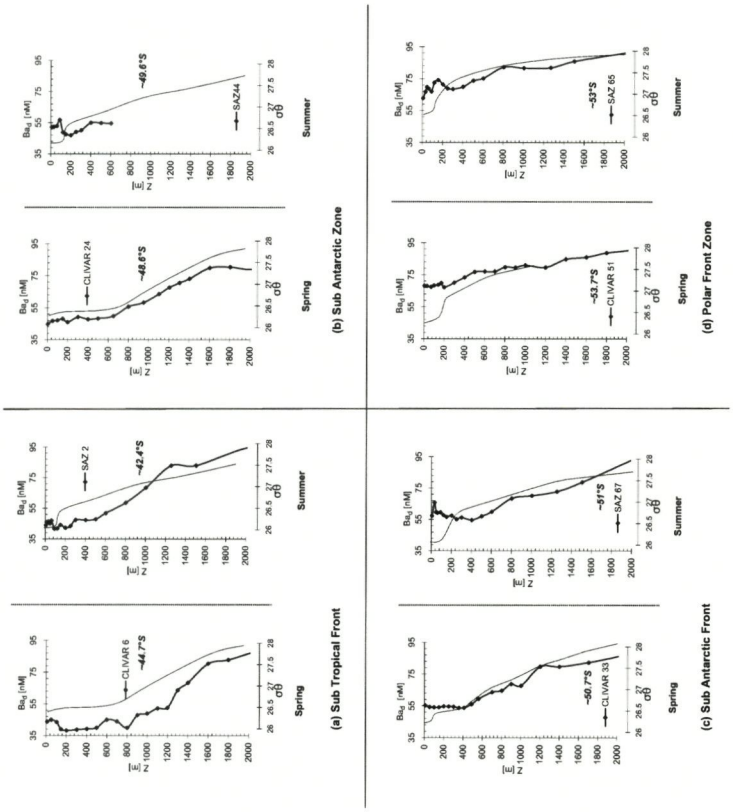


Figure 5.3: Dissolved Ba (nM) in the upper 2000 m of water column during spring (CLIVAR-SR3 cruise, 2001) and summer (SAZ-98 cruise, 1998), shown together with profiles of potential density (thin dotted curve; kg m^{-3}). Station numbers refer to original CTD cast numbers.

[93] Figure 5.4 shows corresponding dissolved and particulate Ba profiles in the upper 700 m during spring and summer. Ba_{xs} concentrations tend to rise on from the depth where a density gradient sets the lower boundary of the surface mixed layer (Figures 5.3 and 5.4). Ba_{xs} profiles display maxima between 100 and 350 m which reach higher values in summer compared to spring (Table 5.1-b; see also Cardinal et al., 2005).

Mesopelagic dissolved Ba stock (nM)

(a) Integration between 100-600m

Location	STF	SAZ	SAF	PFZ
Spring	47.9	55.3	58.7	77.1
Summer	46.1	52.0	56.7	73.6
Δ	1.8 ± 1	3.3 ± 1.1	2.0 ± 1.2	3.5 ± 2.6

Mesopelagic particulate Ba stock (pM)

(b) Integration between 100-600m

Location	STF	SAZ	SAF	PFZ
Spring	-	221	223	305
Summer	328	393	487	516
Δ		171 ± 23	264 ± 27	211 ± 30

Table 5.1: Spring and summer mesopelagic Ba_d (a; nM) and Ba_{xs} (b; pM) depth weighted average values and their seasonal Δ difference (pM); integration between 100–600 m.

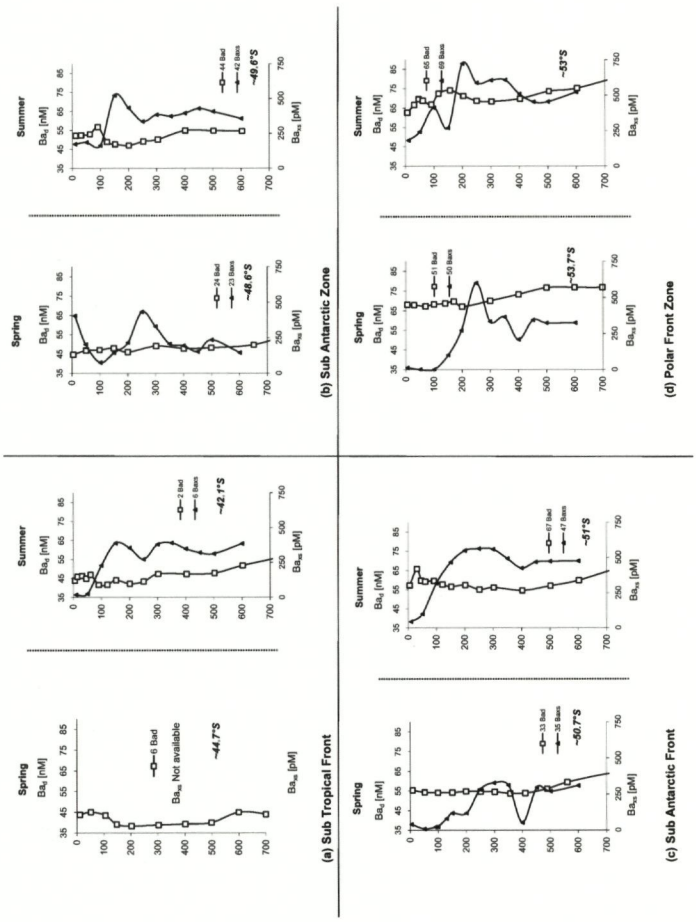


Figure 5.4: Profiles of dissolved Ba (open squares; nM) and particulate Ba (closed triangles; pM) profiles during spring (CLIVAR-SR3 cruise, 2001) and summer (SAZ-98 cruise, 1998) in the upper 700 m of water column. Station numbers refer to original CTD cast numbers.

5.4. DISCUSSION

[94] The precise mechanism shaping the nutrient-like distribution of Ba_d is still debated and this is partly due to the complexity of the processes leading to formation of barite, a major player in the oceanic Ba cycle. Even if, at first, Ba and silicate (Si) are not expected to be coupled [Edmond, 1974], similarities of their distributions tend to indicate control via direct Ba uptake by marine planktonic organisms [Chan et al., 1977, Lea, 1993. Jeandel et al., 1996; see discussion further below]. However, except for a cultured unicellular Prymnesiophyte algae (*Exanthemachrysis gayraliae*; Fresnel et al., 1979) and for Acantharians, which are celestite ($SrSO_4$) secreting micro-heterotrophs [Bernstein et al., 1998, 2004; Sternberg et al., accepted], no other marine pelagic plankton group has been reported to be involved in Ba uptake and barite formation. Indeed, experimental work has shown that production of barite is induced during phytoplankton aggregation and subsequent mineralization [Ganeshram et al., 2003], corroborating hypotheses issued earlier [Bishop, 1988; Dehairs et al., 1991]. Both possible main barite formation loci (Acantharians and decaying plankton) are not just limited to the upper mixed layer but are likely to occur mainly in waters below as shown by the unique feature of Ba_p profiles, i.e. an increase in the mesopelagic layers. The scenario involving aggregation – mineralization appears as being the most consistent with an ubiquitous occurrence of the Ba_{xs} maximum in the mesopelagic waters [e.g. Dehairs et al., 1991, 1997; Cardinal et al., 2001, 2005]. Confronting dissolved and particulate Ba distributions could be a means to identify the strata where the Ba uptake occurs. This is, however, a difficult task considering the 100 to 1000 fold larger concentration of dissolved compared to particulate Ba, which renders it difficult to quantify possible impacts of non-conservative processes on the dissolved phase. In order to understand such effects and the involvement of dead plankton processing on the Ba dynamics, we investigate the correlative behavior of dissolved Ba with nutrients (silicate and nitrate) and alkalinity and then with particulate biogenic Ba.

5.5. DISSOLVED BARIUM BEHAVIOUR IN THE WATER COLUMN

Correlative behaviour of barium with nutrients and alkalinity

[95] Inspecting the barium vs. silicate and alkalinity regressions in intermediate and deep waters ($\sigma_\theta > 27.35$) reveals strong correlations. For the region north of the PF the Ba – silicate correlation is consistent between the SAZ-

98 (1998) and the CLIVAR-SR3 (2001) cruises indicating little year to year variability (see circled part 4 on Figure 5.5).

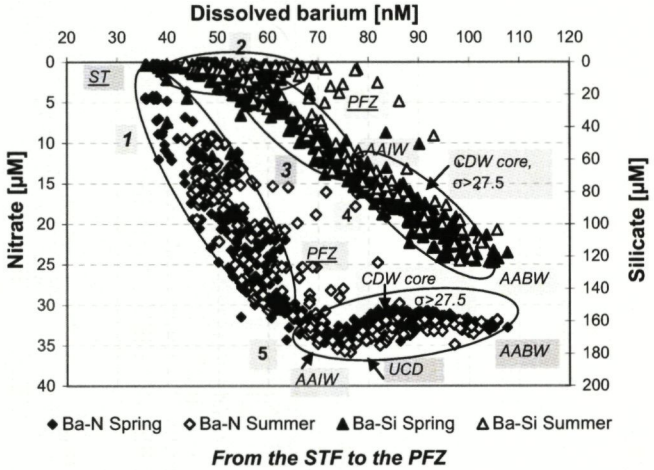


Figure 5.5: Dissolved Ba (nM) versus nutrients (silicate and nitrate; µM) for CLIVAR-SR3 (spring 2001) and SAZ-98 (summer 1998) stations from the STZ to the PFZ. Data are from the whole water column. STZ, STF, SAF, PFZ, as in Figure 2; UCDW = Upper Circumpolar Deep Water; AABW = Antarctic Bottom Water; AAIW = Antarctic Intermediate Water. Circled parts 1, 2 and 3 represent surface and mesopelagic waters, 4 and 5 intermediate and bottom waters.

Focusing on the whole CLIVAR-SR3 data set, which includes the Antarctic Zone south of the PF (see above), we observe the slope of the Ba vs. Si regression to decrease southward (Figure 5.6).

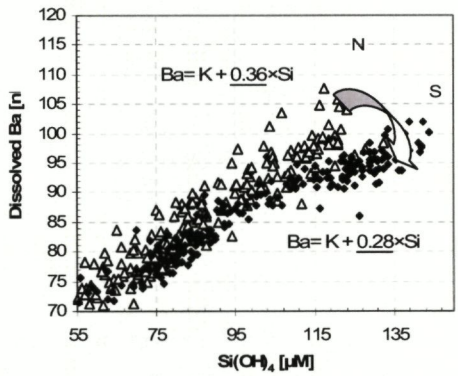


Figure 5.6: Dissolved Ba (nM) versus silicate (µM) for CLIVAR-SR3 (spring 2001) stations from Subtropical Front (STF) to Antarctic Zone (AZ). Only intermediate and deep waters (potential densities > 27.35) are considered. Empty triangles and black diamonds represent stations respectively north

and south of the PF (~54°S); equations indicate the southward decrease of the slope of the Ba vs. Si regression at these two groups of stations.

In contrast, in surface and mesopelagic waters where the action of nutrient uptake takes place (σ_θ < 27.35, ~upper 600 m, see circled parts 2 and 3 on Figure 5.5), the picture (for both cruises) is quite different. Barium and silicate now appear uncoupled, with Ba concentrations remaining high, while silicate reaches depletion (note that the silicate depletion extends more southward in summer compared to spring). In the upper 600 m, silicate subtraction appears as a major process but it does not affect Ba. Ba_d and nitrate, on the contrary, appear to co-vary but Ba never reaches depletion, while nitrate does (see circled part 1 in Figure 5.5). Since Ba in surface waters is uncoupled from silicate, diatoms appear not to consume Ba, at least not in a constant proportion to Si. This is in agreement with observations from laboratory experiments indicating that cultured diatoms do not incorporate barium in significant amounts [see Dehairs et al., 1980 and Sternberg et al., 2005]. Furthermore, the upper 600 m of water column between STZ and PFZ is characterized by an inverse relationship between Ba and alkalinity (see circled part 1 in Figure 5.7), a feature we also observed in the Indian sector of the Southern Ocean (see above) and which reflects the uncoupling of both these parameters. Millero et al. [1998] showed that this latitudinal surface gradient for alkalinity is mainly controlled by evaporation.

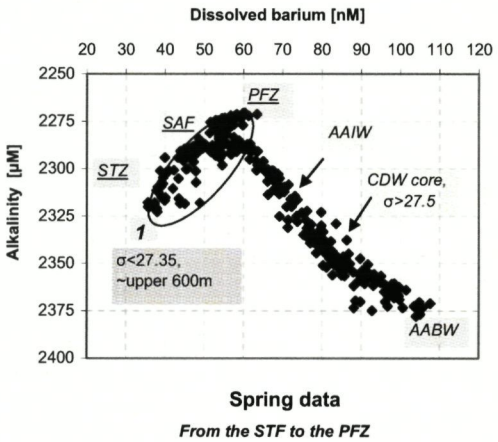


Figure 5.7: Dissolved Ba (nM) versus alkalinity (µM) for CLIVAR-SR3 (spring 2001) stations from STF to AZ. Circled part 1 represents surface and mesopelagic waters.

[96] Clearly, silicate, alkalinity and nitrate all show correlative behaviour with Ba, but to variable extents. In the following we assess this via a multiple regression approach.

Multiple regressions

[97] We applied a multiple regression analysis to assess the relative weight of the above mentioned different nutrient parameters combined with other independent variables, in predicting the Ba distribution. Best subset regressions were used to search for those combinations of independent variables (silicate, nitrate, alkalinity, oxygen, temperature, salinity) providing the best prediction of the dependent variable Ba_d. To that purpose two statistics were used: (**i**) the adjusted R square, providing a measure of how well the regression model describes the data, taking into account the number of independent variables, and (**ii**) the t-statistic which tests the null hypothesis that the partial regression coefficient for each independent variable is zero (a variable is neglected for $p > 0.05$).

[98] Results for CLIVAR-SR3 reveal that silicate and alkalinity are highly correlated. Though no obvious process links silicate and alkalinity, it is likely that biological synthesis of opal and carbonate and subsequent dissolution generate parallel oceanic distributions [Chan et al., 1977; Lea, 1993; Jeandel et al., 1996], thereby inducing multi-colinearity between silicate and alkalinity. This situation implies that only one of these two variables should be used in the multiple regression analysis to avoid a multi-colinearity effect, which may result in unreliable estimates of the dependent parameter (Ba_d). Since alkalinity profiles are less resolved in the deep ocean and since no alkalinity data were available for the SAZ-98 cruise, we choose to include the silicate variable, rather than alkalinity, in the multiple regression analysis.

[99] Regression calculations using the whole CLIVAR-SR3 data set indicate that among the parameters considered, the best predictor of Ba_d is clearly Si, contributing to approximately 88% of the Ba_d variability. Despite the fact that SAZ-98 data are scarcer, best subset regressions provide similar results with Si explaining about 79% of the Ba variability (whole data set). When the regressions are calculated for each individual cast, different groups of stations become apparent both for CLIVAR-SR3 and SAZ-98, again with silicate explaining the major part of the Ba_d variability (Table 5.2; see R squared value).

(a) CLIVAR SR3 - Spring 2001

	STF	SAZ - SAF/N	SAF/S - PFZ	PFZ - AZ
R squared	0.87	0.98	0.91	0.72
Intercept ± SE	42.9 ± 0.9	49.3 ± 0.3	58.7 ± 0.8	64.1 ± 0.7
Slope ± SE	0.50 ± 0.02	0.42 ± 0.01	0.31 ± 0.01	0.23 ± 0.01
p	< 0.001	< 0.001	< 0.001	< 0.001

(b) SAZ'98 - Summer 1998

	STF	SAZ	SAF	PFZ
R squared	0.99	0.99	0.77	0.78
Intercept ± SE	44.0 ± 0.7	48.6± 0.5	55.6 ± 1.7	65.7 ± 1.4
Slope ± SE	0.56 ± 0.11	0.52 ± 0.01	0.32 ± 0.04	0.21 ± 0.03
p	< 0.001	< 0.001	< 0.001	< 0.001

Slope= partial regression coefficient; SE= standard error

Table 5.2: Subset regression analysis results of Si vs. Ba_d: (a) CLIVAR-SR3 cruise (spring 2001) and (b) SAZ-98 cruise (summer 1998). Listed are R squared, intercept, slope and p value; see text for explanations. STF = Subtropical Front; SAZ = Subantarctic Zone, SAF = Subantarctic Front (N: north; S: south), PFZ = Polar Front Zone; AZ = Antarctic Zone.

It is interesting to note that these groups of stations correspond to transition zones along the SR3 line as identified previously and which are similar during spring and summer. From Table 5.2 it appears that the partial regression coefficient for Si (i.e. the slope value) decreases from north to south (see also Figure 5.6) while the intercept increases. Jeandel et al. [1996] and Monnin et al. [1999] report that waters from the upper 2000 to 3000 m of the water column south of the Polar Front are at equilibrium or oversaturated with respect to barite, in contrast to the situation north of the Polar Front where waters are undersaturated. Therefore, decreased slopes of the Ba-silicate regressions south of the PF could reflect reduced dissolution of Ba_{xs} in subsurface and intermediate waters. These results are also in general agreement with earlier work by Jeandel et al. [1996] in the Indian sector of the Southern Ocean. The latter authors also observed decreasing slopes of Ba_d vs. Si regressions from north to south of the PF and likewise concluded that differences in saturation conditions for barite between sites north and south of the front were the main reason for this. Overall it appears that the strong Ba_d-silicate (and Ba_d-alkalinity) correlation we observe when inspecting whole water column profiles are maintained mainly by the situation in intermediate and deep waters, where dissolution of suspended biogenic barium (mainly barite), opal and carbonate parts of plankton are major processes, overprinted by hydrodynamics.

[100] The above-discussed relationships highlight the fact that Ba_d is not controlled by the same biogeochemical processes and thermodynamic conditions

controlling synthesis of opal and carbonate and their dissolution. This emphasizes the unique pseudo-nutrient behavior of dissolved barium.

5.6. SEASONALITY OF DISSOLVED AND PARTICULATE Ba

[101] The mesopelagic waters have been identified as being the site of barite production and its release in the water column as discrete micro-crystals after bacterial degradation of the aggregates in which the precipitation took place [Dehairs et al., 1980; 1997; Stroobants et al., 1991]. Such a process explains why Ba_{xs} accumulation coincides with peak oxygen consumption and can be used as a proxy of organic matter remineralization [Dehairs et al., 1997]. Density and Ba_{xs} gradients are sharp around 100-150 m at the bottom of the mixed layer (Figure 5.3 and Figure 5.4). Since sharp density gradients forming the lower boundary of the mixed layer have been reported as sites of organic aggregate and floc formation and accumulation [MacIntyre et al., 1995; Simon et al., 2002], the coincidence between the increase of mesopelagic Ba_{xs} and the occurrence of this density gradients is consistent with the idea that aggregates and mineralization of organic matter are involved in the process of barite formation as discussed in Cardinal et al. [2005]. Furthermore, according to Collier and Edmond [1984] local uptake of Ba_d in the subsurface waters is required to maintain the mesopelagic Ba_{xs} maximum, which can not be explained solely as a result of regeneration of carriers such as biogenic Si or $SrSO_4$ nor by redistributing the amount of particulate Ba present in upper mixed layer. Thus, the fact that dissolved and particulate Ba summer profiles in mesopelagic waters seem to mirror each other (Figure 5.4) could indeed indicate that the latter is sustained by local Ba_d subtraction. Spring Ba_{xs} maxima, on the contrary, do not appear mirrored by significant Ba_d depletions and it is likely that this reflects differences in the turn-over rates (here seasonal variations) between the particulate and dissolved Ba phases. Since Ba_d concentrations exceed Ba_{xs} concentrations by a factor 100 to 1000, reflecting the faster dynamics of the latter [Dehairs et al., 1980], the time window necessary for Ba_d uptake to become detectable is likely wider than for increases in mesopelagic Ba_{xs} to become detectable. Apparently for CLIVAR-SR3 in spring, insufficient time has elapsed since the onset of the bloom for Ba_d uptake to become detectable. A time window of several months seems necessary for any Ba_d depletion to become apparent. Though Ba_{xs} has a faster turn-over than Ba_d, a clear seasonal build-up of mesopelagic Ba_{xs} occurs, with summer contents systematically exceeding those in spring (Table 5.1 and Figure 5.4; Cardinal et al., 2005). Thus, less Ba subtracted from solution in spring

implies less barite formed. However, exact co-variation of Ba_{xs} and Ba_d in mesopelagic waters is not obvious since the Ba subtracted from solution is not necessarily transferred to the local barite stock, but can become associated with larger aggregates exported deeper in the water column.

Barium fluxes

[102] To determine whether the observed summer Ba_d depletion in the mesopelagic zone can be the result of a Ba subtraction from solution during barite formation, we estimated the seasonal depletion of dissolved Ba and compared this subtraction flux with the build-up of mesopelagic Ba_{xs} as well as with deep water sediment traps derived Ba_{xs} fluxes. We calculated the subtraction of dissolved Ba required to maintain the upper 600 m water column summer depletion by applying a steady state and a non-steady state approach.

[103] The steady state approach is performed on summer profiles (SAZ-98) and assumes the system has been at equilibrium for some time. We apply a simple 1-D box model in which the dissolved Ba subtraction term (J, in μmol m^{-2} d^{-1}) equates the Ba_d input as sustained by vertical advection and turbulent diffusion:

$$J = k(\partial Ba/\partial z)up + k\left(\partial Ba/\partial z\right)down + W[Ba]base - W[Ba]\min \qquad \text{(Eq. 1)}$$

For all the stations, the upper boundary of this box is set by the basis of the mixed layer (100 m) and the lower boundary is taken at 600 m. The turbulent diffusion coefficient k is taken constant and equal to $3*10^{-5}$ m^2 s^{-1} [see Shopova et al., 1995]. Turbulent diffusion transports Ba from the lower ($K(\partial Ba/\partial z)up$) and upper boundaries ($K(\partial Ba/\partial z)down$) of the Ba minimum layer to the center. Vertical advection moves Ba (W[Ba]base) from the lower boundary to the center of the minimum layer and from the center (W[Ba]min) to the upper boundary. The Ba_d minimum is located at 91 m (STF), 201 m (SAZ), 301 m (SAF) and 252 m (PFZ) (Figure 5.4). For the vertical advection transport coefficient W, we use a value of $150*10^{-5}$ cm s^{-1} [Yaremchuck et al. 2001], the choice of which is discussed further below.

[104] The non-steady state approach is based on the comparison of the spring (CLIVAR-SR3) and summer (SAZ-98) situations, assuming year to year variability of the onset of the bloom to be relatively similar (see discussion above, section 5.2). Based on spring Ba-salinity relationships within each zone, the temporal variations of Ba_d values were corrected for ocean mixing effects,

following the rationale Lourey and Trull [2001] applied to estimate seasonal nutrient utilization along the same SR3 transect:

$\Delta Ba_{bio} = \Delta Ba_{tot} - \Delta Ba_{m}$ (Eq. 2)

where ΔBa_{bio} is the estimate of Ba depletion due to the biological activity; ΔBa_{tot} is the overall difference between the spring and summer barium fields; ΔBa_{m} indicates the Ba change due to ocean mixing $\Delta Ba_{m} = \Delta Sal_{m} \times (\Delta Ba / \Delta Sal)$; ΔSal_{m} = Sal (spring) – Sal (summer); $\Delta Ba / \Delta Sal$ = slope of the Ba vs. salinity plots for surface waters (upper 100m) in spring (i.e. supposedly waters still being little affected by biological activity), used to correct for mixing. Depletions of Ba over the growth season (taken as 100 days, see discussion above, section 5.2) were obtained by calculating the summer versus spring difference of Ba_{d} contents integrated over the minimum layer (100-600 m).

[105] Rates of Ba_{d} subtraction calculated via both approaches are given in Table 5.3-a and compared with build-up of Ba_{xs} (Table 5.3-b) in mesopelagic (i.e. seasonal build up of Ba_{xs};) and deep waters (Table 5.3-c; sediment trap Ba_{xs} fluxes covering the period from September 1997 to March 1998, i.e. 153 days; Cardinal et al., 2005). The build-up of Ba_{xs} in mesopelagic waters over the growth season (100 days) was obtained from the difference of mesopelagic Ba_{xs} contents integrated over the Ba_{xs} maximum layer (set equal to the Ba_{d} minimum layer as defined above), between summer and spring.

Location	STF	SAZ	SAF	PFZ
(a) Mesopelagic dissolved Ba subtraction				
Steady state approach	10.5	12.3	6.2	8.3
Non-steady state approach	11.6	18.7	9.3	8.5
(b) Mesopelagic particulate Ba build-up				
Ba_{xs}	–	0.86	1.32	1.06
(c) Deep water particulate Ba flux				
Ba_{xs}*	–	1.50 (1)	0.73 (4)	0.74 (5)
		2.97 (2)		0.68 (6)
		1.43 (3)		

All fluxes in μmol m^{-2} d^{-1}

* Sediment trap derived deep water Ba_{xs} fluxes: values corrected for trapping efficiencies (estimated from ^{230}Thex flux; Trull et al., 2001-b; Cardinal et al., 2005).
Sediment trap depths: 1-1060 m, 2- 2050 m, 3- 3850 m, 4- 3089m, 5 - 800 m and 6- 1580 m.

Table 5.3: (a) Dissolved Ba fluxes obtained via steady state and non steady state approaches; (b) seasonal build up of Ba_{xs} in the mesopelagic zone; (c) deep ocean Ba_{xs} fluxes (sediment trap data from Cardinal et al., 2005). All fluxes in μmol m^{-2} d^{-1}.

Comparing steady state versus non-steady state approaches to assess dissolved Ba fluxes

[106] Overall rates of Ba_d depletions estimated via the steady state (ss) and non-steady state (n-ss) appear to converge (Table 5.3-a). They present the same trend: fluxes are higher in the SAZ compared to STZ and decrease in the SAF and PFZ. However, differences exist. While fluxes in the STF (ss= 10.5 and n-ss= 11.6 μmol m^{-2} d^{-1}) and in the PFZ (ss= 8.3 and n-ss= 8.5 μmol m^{-2} d^{-1}) are quite similar, the steady state approach leads to lower values for the SAZ (ss= 12.3 and n-ss= 18.7 μmol m^{-2} d^{-1}) and the SAF (ss= 6.2 and n-ss= 9.3 μmol m^{-2} d^{-1}). It must be kept in mind that the vertical advection coefficient W, used in the steady state approach, is generally poorly constrained. In this study we used a single value, but obviously, the hydrodynamic complexity along the SR3 transect, make it unlikely that W is constant neither within zones nor with depth. Vertical advection coefficients reported in literature range over two orders of magnitude, from 10^{-5} cm s^{-1} [e.g. Shopova et al., 1995] to $200*10^{-5}$ cm s^{-1} and more [Yaremchuk et al., 2001]. In this study we use a value of $150*10^{-5}$ cm s^{-1} representing the mean of the values reported by Yaremchuk et al. [2001] for the same WOCE SR3 transect. Calculation of depletion fluxes by applying a W value of $200*10^{-5}$ cm s^{-1} [Yaremchuk et al., 2001] for the SAZ and SAF which are particularly marked by an unstable and complex hydrodynamical regime, brings the ss and n-ss fluxes to the same level. Because of poorly constrained transport coefficients, overall, the steady state model is probably the least robust one for predicting subtraction fluxes.

Discrepancies between dissolved Ba subtraction and particulate Ba fluxes

[107] Although the SAZ shows the highest Ba_d subtraction flux and also the highest deep ocean Ba_{xs} flux, the mesopelagic Ba_{xs} build-up is lowest there. The PFZ, on the other hand, has the lowest Ba_d subtraction flux, the lowest deep-ocean Ba_{xs} flux (at 1580 m), but a large mesopelagic Ba_{xs} build-up (slightly lower than the one in the SAF). Trull et al. [2001-b] report that carbon export to the deep ocean in the SAZ sector is larger than in the PFZ and deep-sea Ba_{xs} fluxes have been shown to follow this trend [Cardinal et al., 2005; Table 5.3-c]. Furthermore, there is an inverse latitudinal trend between deep-ocean Ba_{xs} flux and mesopelagic Ba_{xs} contents as discussed in Cardinal et al. [2005]. These conditions potentially reflect the importance of $CaCO_3$ mineral ballast north of the PF and a more intense mineralization in the mesopelagic waters in the PF where diatoms dominate [see Cardinal et al., 2005], in general agreement with the

conclusions by François et al. [2002] and Klaas and Archer [2002] that $CaCO_3$ is the important controller of deep export flux, rather than opal.

[108] A major issue concerning the Ba fluxes is the order of magnitude difference between mesopelagic Ba_d subtraction and Ba_{xs} build-up (Table 5.3-a and b). Balance between Ba_{xs} gain and Ba_d deficit in mesopelagic waters is not really expected since the Ba subtracted from solution is not necessarily transferred to the local barite stock, but can become associated with larger aggregates exported to the deep ocean. This would mean that Ba subtraction fluxes have to be compared with the combined mesopelagic and the deep ocean Ba_{xs} fluxes. However, even adding sediment trap and mesopelagic Ba fluxes does not balance the discrepancy between dissolved and particulate fluxes (Table 5.3-a, b). As already emphasized, the turn-over of particulate Ba is faster than Ba_d and this may in part explain the difference between the two fluxes. We remind that the mesopelagic Ba_{xs} inputs have been integrated over a period of ~3 months during the growth season. Therefore, considering the large difference in turn-over dynamics of the dissolved vs. particulate Ba phases (months vs. weeks, respectively) we also looked at the temporal evolution of the Ba_{xs} signal over a shorter time interval. For the CLIVAR-SR3 cruise (spring) we have data for a station in the Antarctic Zone (60.9°S) visited twice in a time span of 17 days, providing an estimate of the mesopelagic Ba_{xs} flux over a shorter period of time [see Cardinal et al., 2005]. This short term Ba_{xs} build-up integrated between 100 and 600 m amounts to 3.1 μmol m^{-2} d^{-1}. Also Dehairs et al. [1997] report a short term (3 weeks; early spring) mesopelagic particulate Ba build-up of similar magnitude (1.4 μmol m^{-2} d^{-1}) for a Polar Front station in the Atlantic sector of the Southern Ocean (ANTX/6 cruise; 1992). Such values are 2 to 7 times larger than the estimates in the present study, based on the differences between summer 1998 and spring 2001 Ba_{xs} profiles at SR3. As discussed above, this may indicate that while the mesopelagic dissolved Ba depletion reflects uptake integrated over the growth season, the Ba_{xs} stock fluctuates over a shorter time scale, tuned for instance by short term variability of primary production. However, it is unlikely that the discrepancies between dissolved and particulate fluxes are due solely to problems related to the width of the time windows over which signals are integrated. Jeandel et al. [1996] and Monnin et al. [1999] show that the ocean north of the Polar Front is undersaturated for barite over the whole water column, in contrast to waters of the Antarctic Circumpolar Current. Therefore, dissolution of barite, the major carrier of Ba_{xs}, at depths >1000m is likely a main factor

accounting for the discrepancies between the Ba_d subtraction fluxes and the mesopelagic and deep ocean Ba_{xs} fluxes.

[109] We tried to verify whether or not the Ba dissolution rates suggested by the data in Table 5.3-a for the deep ocean are realistic. Comparing our dissolved Ba data for the CIVA-1 section at 30°E (unpublished results; Dehairs et al., in preparation-a) with those for the WOCE SR-3 section at 145°E (see above), we noticed an increase of on average 7 nM for waters deeper than 1000m and having potential densities between 27.70 and 27.83. These are the waters that cover the depth range (i.e. about lower 3000 m of water column) undersaturated for barite [Monnin et al., 1999; Monnin and Cividini, 2006; Jeandel et al., 1996]. Next we performed a simple calculation of dissolved Ba input in the deep sea during water mass transit between 30° and 145°E. Between the SAF and the PF we considered water mass transport to reach 130 Sv, while from the PF to the Antarctic margin only 50 Sv are transported [Rintoul and Sokolov, 2001; Park et al., 2001]. North of the PF the estimated average transit time is 5.3 years (velocity= 4.7 cm s^{-1}), while south of the PF estimated average transit time increases to 18.4 years (velocity= 1.2 cm s^{-1}). The calculated input rate of dissolved Ba to the deep ocean, then ranges between 4 (area south of PF) and 14 µmol m^{-2} d^{-1} (SAZ and PFZ) what is similar to the values obtained for Ba subtraction in the mesopelagic area along SR3 line. Thus, calculations suggest that the discrepancy between particulate Ba fluxes (mesopelagic build-up and deep ocean particle flux) and dissolved Ba subtraction in the mesopelagic waters can be accounted for by intermediate -deep ocean dissolution of particulate Ba that is left 'undetected' by Niskin bottle sampling.

5.7. CONCLUDING REMARKS

[110] Although regression analyses reveal strong similarities between dissolved Ba and silicate distributions along the WOCE SR3 line in the Southern Ocean and identify silicate as the best predictor of Ba_d, this Ba_d-silicate co-variation breaks down in surface waters. Here, Ba_d rather follows the latitudinal trend of nitrate, showing gradual decrease northward, while silicate is depleted over large parts of the SR3 section. Moreover, regression slopes of Ba_d as a function of silicate decrease from north to south, and this is particularly salient for deeper waters known to evolve from undersaturation to oversaturation with respect to barite, across the Polar Front. These facts not only eliminate diatoms as significant consumers of Ba, but also corroborate barite being the main

particulate Ba phase in suspended matter. Moreover, for the SAZ and PFZ the combined seasonal build-up of particulate Ba in mesopelagic waters and deep ocean Ba fluxes underscore estimates of dissolved Ba subtraction in mesopelagic waters. This discrepancy suggests significant dissolution of barite to occur in the deeper water column.

Chapter 6

Dissolved barium according to a parametric mixing model

Foreword

[111] In the preceding chapter, to determine whether the observed summer Ba_d depletion in the mesopelagic zone can be the result of a Ba subtraction from solution during barite formation, mass balance calculations were performed to estimate the seasonal variations of Ba_d. Here in Chapter 6, a different approach is performed to estimate the non-conservative part of the Ba_d signal and its seasonal evolution, using a parametric mixing model called POMP; focus is put on the upper 1000 m of the SAZ region along SR3 line (CLIVAR SR3 and SAZ-98 cruises).

SUMMARY

[112] A parametric extension of Optimum Multi-Parameter analysis (called POMP) is applied to dissolved Barium (Ba_d) datasets from the SR3 line in the Australian sector of the Southern Ocean. Focusing on the subantarctic region and on the upper 1000 m of the water column, this study aims to understand what processes (physical and/or biogeochemical) act upon the Ba_d distribution. Results, based on residual analyses, reveal that the major part of the Ba_d distribution could be reconstructed by mixing only. However, results also show evidence of non-conservative behavior for Ba_d, providing important clues on the relative importance of dissolved Ba in the global Ba cycle. In particular, model calculations suggest that in a sector where intense particulate Ba-barite dynamics have been reported at mesopelagic depths, measurable Ba_d depletions of up to 11 nM occur.

6.1. INTRODUCTION

[113] Though conservative mixing clearly appears to be the main factor controlling the Ba_d distribution in the Arctic basin [Falkner et al., 1994], Ba_d distributions in the S.O. show evidence of non-conservative behavior (see Chapter 5). Although the oceanic distribution of Ba_d shows strong similarities to those of nutrients and alkalinity, the biogeochemical cycling of Ba appears to be unique, involving a strong link with the particulate Ba-barite (Ba_p-$BaSO_4$) dynamics (see Chapter 3 and Chapter 5). Barite precipitation in the mesopelagic zone (~100-1000 m) would occur through enrichment of sulfate and/or barium in decomposing organic material [Bishop, 1988; Dehairs et al., 1980, 1997; Stroobants et al., 1991]. Considering this means of barite precipitation, we wondered whether possible subtraction of Ba_d from the ambient solution during barite formation could lead to a measurable impact on Ba_d profiles. This could explain observed sub-surface Ba_d depletions [Dehairs et al., unpublished results; see also Chapter 3 and Chapter 5]. In the previous chapter, we checked this by contrasting dissolved and particulate Ba water column profiles and calculating the degree of Ba mass conservation. Here, the aim was to establish, through a modeling approach, the relative importance of mixing vs. biogeochemical processing in determining the Ba_d distribution. Estimating the non-conservative part on the Ba_d signal is crucially important in order to better constrain the barite formation process; this issue constitutes to date the limiting keys for robust application of the Ba- barite proxies for reconstructing modern and past ocean export.

[114] Frontal systems in the S.O. are known to sustain intense physico-chemical and biological gradients [Arrigo et al., 1998; Moore et al., 1999]; thus, these systems are suitable sites for investigations of the dependency of Ba_d on (non)-conservative processes. To resolve the question of whether the dissolved Ba signal can be reconstructed by mixing, we performed mixing calculations and residual analyses. We used a modified OMP analysis called Parametric Optimum Multi-Parameter (POMP) as described in de Brauwere et al. [2007]. The POMP analysis was applied on two different seasonal Ba datasets from the 145°E WOCE SR3 line (see Chapter 3 and Chapter 5); we focused on the subantarctic region: this area merits special attention in modelling because it represents a key interface that mediates the influence of the S.O. on the globe (through CO_2 uptake and other exchanges with the atmosphere, intense circulation changes

and critical water mass formation). Here, we present results on the (non)-conservative behavior of Ba_d in the Australian sector of the S.O.; potential dissolved Ba discrepancies of great importance in constraining the Ba-barite dynamics could be revealed. Similar studies, using a classical OMP model, were followed by Kumar and Li [1995] and by Schneider et al [2005]; they evaluated non-conservative issues by estimating the amount of Si and ^{226}Ra added to the water column by decomposing particles and by approximating changes in DIC and nutrients due to remineralization, respectively.

6.2. DATA AND SAMPLING SCHEME

[115] We analyzed Ba_d data for CLIVAR-SR3 (AU0103; Oct. 29 - Dec. 11 2001; R/V Aurora Australis) and SAZ-98 (AU9706; February – April 1998; R/V Aurora Australis) cruises sampled in the Southern Ocean along north – south transects (~142°-145°E) between Tasmania and Antarctica. The first dataset represented the time period between late winter-early spring 2001 (later referred to as spring data) and the second was taken from the summer 1998 (later referred to as summer data). Ba_d datasets have already been discussed and compared to frontal structures and characteristics of water masses in Chapter 3 and Chapter 5. Here we focus on the SubAntarctic Zone (SAZ) located between the SubTropical (STZ) and the Polar Front (PFZ) zones. Furthermore, we limited the analyses to the upper 1000 m of the water column where barite formation in micro-environments is occurring because this layer is relevant for investigating possible seasonal variability.

6.3. METHOD

[116] Optimum Multi-Parameter analysis (OMP) is an inverse modelling technique designed to determine the relative contributions of various source water masses to an investigated target water parcel [Tomczak, 1981; Mackas et al, 1987; Tomczak and Large, 1989]. It is based on the assumption that at a given observation in space all conservative hydrographic parameters can be broken down into a linear combination of the source water characteristics, i.e. for an arbitrary conservative parameter p (like temperature, salinity, etc...) measured at position i one can write

$$pm(i) = x1(i)p1 + x2(i)p2 + \ldots \qquad (1)$$

where p1, p2, etc. stand for the particular parameter value associated with the different source water masses and x_1, x_2, etc. represent the mixing contributions

of the respective source water masses. These latter can be computed by solving a set of mixing equations (each equation has the form of Eq. (1) but represents a different parameter) and imposing a number of physical constraints (for details see Tomczak and Large, 1989). The relative contributions of the source waters vary according to the location in the study area. Hence, if hydrographic parameters are available on a grid, a spatial distribution of the mixing contributions can be computed.

[117] Once these mixing contributions are calculated, they can be used to predict the distributions of another hydrographic parameter under the assumption that it is only influenced by mixing. Eq. (1) shows how the value of a parameter at a given point can be reconstructed if both the mixing fractions (at that position) and the source characteristics for that parameter are known. If measurements of the actual parameter values are available, these can be compared with the reconstructed parameter fields to determine whether areas with systematic discrepancies are present. These discrepancies can be interpreted as the depletion or accumulation of a tracer, due to non-conservative processes, or at least to processes which did not influence the parameters used in the original OMP analysis. The aim of this article is to perform this strategy for the dissolved Barium tracer. However, the OMP analysis has to be performed as precise as possible otherwise we might draw wrong conclusions, based on the interpretation of measurement noise and model errors, rather than a significant measurement information.

[118] The first methodological detail of importance is that the method used in the current paper is not the classical OMP analysis, but a parametric refinement, called POMP. The main advancement in POMP is a parameterization of the mixing fractions, using two dimensional (latitude-depth) spline functions. Essentially, equations in the form of Eq. (1) are still used, but the mixing fractions are now explicitly a function of position (latitude and depth). This approach, combined with an effective choice of spline complexity, leads to smoother, and most importantly, more robust, mixing fraction distributions (i.e. less influenced by measurement noise and thus associated with a lower uncertainty). For an extensive technical outline of the POMP method, please refer to de Brauwere et al. [2007].

[119] The mixing analyses for the study area at the two periods of interest were performed using POMP in de Brauwere et al. [2007] and the results

will not be iterated here. In brief, the POMP method was applied to the above-mentioned spring and summer WOCE SR3 transects, considering only conservative variables, and thus delivering the mixing ratio distributions of the major water masses in the study area (Table 6.1).

Water type	θ /°C	Sal	PO/µM	NO/µM	Ba/nM
AAIW	4.07	34.332	568	403	67
SAMW	9.17	34.655	434	399	45.2
STSW	13.28	35.34	318	297	35.8
CSW	3.3	33.796	609	562	69.3
UCDW	2.52	34.56	555	486	76

(a) CLIVAR - Spring situation

Water type	θ /°C	Sal	PO/µM	NO/µM	Ba/nM
AAIW	3.8	34.25	610	519	74
SAWM	8.6	34.58	468	422	46.3
STSW	12.94	34.71	388	345	44
CSW	4.6	33.6	602	550	63
UCDW	2.275	34.661	566	488	81.64

(b) SAZ-98 - Summer situation

Table 6.1: Sources characteristics for spring (a) and summer (b). For technical details please refer to the text and to de Brauwere et al. [2007]. STSW = SubTropical Surface Water, SAMW = SubAntarctic Mode Water, AAIW = Antarctic Intermediate Water, CSW = CircumPolar Surface Water and UCDW = Upper CircumPolar Deep Water.

The following conservative variables were used: potential temperature (θ), salinity (Sal), PO and NO. PO and NO are tracers based on phosphate and nitrate, but were corrected for non-conservative respiration, according to Broecker [1974]: $PO = 170PO_4 + O_2$ and $NO = 9NO_3 + O_2$. Redfield factors were similar to those used by other studies where OMP analysis was applied to the Southern Ocean [You et al., 2003, Lo Monaco et al., 2005]. The relevant sources for the spring and summer data were selected on the boundaries of the study area. This way of selecting sources was justified since the study area was small and we were concerned with local processes. The following water sources were chosen: the SubTropical Surface Water (STSW), SubAntarctic Mode Water (SAMW), Antarctic Intermediate Water (AAIW) and Upper Circumpolar Deep Water (UCDW) (Table 6.1). Overall, as confirmed by the residuals analysis for θ, Sal, PO and NO, the POMP model allowed reliable reconstitution of the water mass mixing distributions along the study area. To conclude, we have assured ourselves that most insignificant measurement noise is filtered off and that no model error is present.

[120] So, the final step in the procedure was the reconstruction of the theoretical, "mixing only", Ba_d fields. As explained above, these can be computed using the mixing fractions from the (POMP) mixing study, and by attributing Ba_d contents to the above-mentioned water sources (Table 6.1). These latter were selected on the boundaries of the study area, in a similar way as for the other parameters. Subtracting the observed Ba_d concentrations from these «mixing-only» values gives the magnitude of the non-conservative processes influencing Ba_d:

$$Ba_{d,difference} = Ba_{d,reconstructed}(\text{mixing fractions, sources' } Ba_d) - Ba_{d,observed} \quad (2)$$

Only differences which were accepted to be significantly different from zero were interpreted. Significance is defined as larger as than one standard deviation, representing the uncertainty associated with this difference. The uncertainty associated with the reconstructed Ba_d was determined by error propagation using mixing fraction uncertainties from 100 Monte-Carlo simulations (in which both the measurements and the source characteristics were perturbed simultaneously) and a source Ba_d uncertainty of 1 nM, which is the same uncertainty attributed to observed Ba_d. Since the mixing fractions appeared to be subject to a spatial heterogeneous uncertainty, each position is associated with a different uncertainty. Consequently, the same value for the Ba_d difference could be significant at one location and insignificant at another. To summarize, the values presented in the next section (Figure 6.1) exclusively represent systematic features, as determined from this extensive uncertainty analysis. Differences less than the significance level (white area in Figure 6.1) indicate that measured Ba_d could entirely be reconstructed by mixing. Larger differences indicate non-conservative behavior of Ba_d: negative values imply that addition of Ba_d occurs in the water column, while positive values reflect Ba_d depletion. It might be possible that the Ba_d distribution is not entirely reproduced by the model due to a wrong source selection. However, because residuals for θ, Sal, PO and NO indicate that calculated mixing fractions are reliable [cf. de Brauwere et al., 2007] and because we have a rather detailed knowledge of Ba_d source characteristics in the area (see Chapter 4), the possibility of a poor characterization of the source water masses seems unlikely. Finally, note that since local sources were used in the mixing analysis, the Ba_d differences are the result of local processes, which are associated with relatively short time and spatial scales.

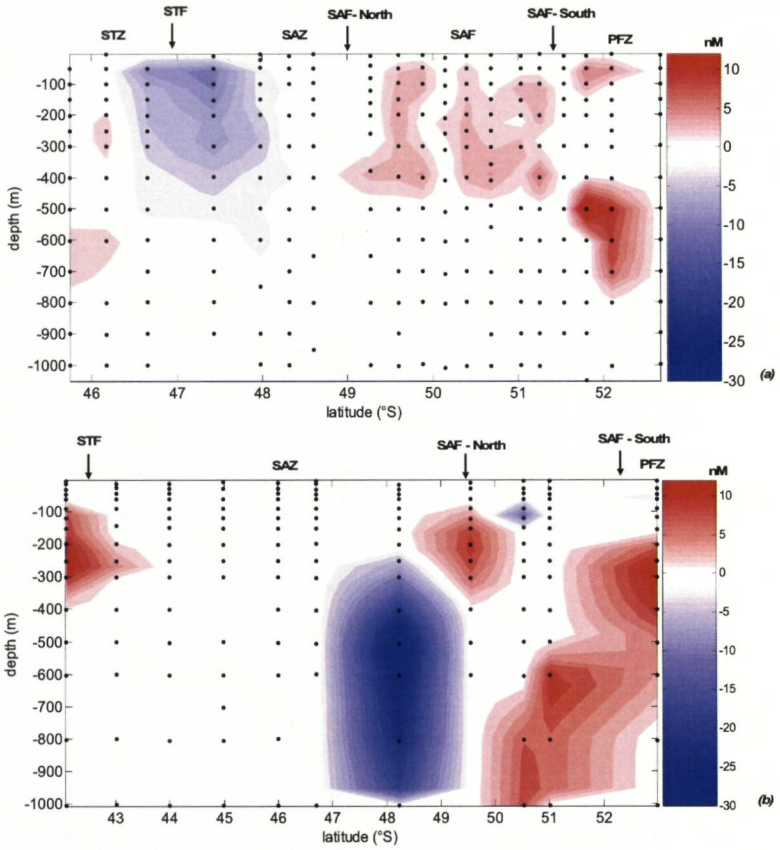


Figure 6.1: Depth distribution of Ba_d differences between reconstructed and measured values vs. latitude for spring (a) and summer (b). STZ = SubTropical Zone, STF = SubTropical Front, SAZ = SubAntarctic Zone, SAF = SubAntarctic Front (north and south) and PFZ = Polar Front Zone.

6.4. RESULTS AND DISCUSSION

[121] Depth distributions of Ba_d differences between reconstructed and measured values are reported vs. latitude in Figure 1 for spring and summer. Figure 6.1-a (spring situation; CLIVAR SR3 cruise) reveals three major features:

(**1**) For most of the section, calculated and observed Ba fields do not differentiate (white patch), thus indicating that the Ba_d distribution at this location is entirely controlled by mixing;

(**2**) Just south of the STF, at ~47°S, negative values (i.e. calculated values < observed values) are apparent in the upper 500 m (up to −11 nM; see blue patch

in Figure 6.1-a). For these latitudes we report quite high Ba_d contents in the upper 600 m (Chapter 4), coinciding with a cold-core eddy pinched off from the SAF. Since low residuals confirmed the reliability of the mixing fractions for that area [de Brauwere et al., in press], results suggest the addition of Ba_d to the water column. It is possible that we witnessed a build-up of Ba_d at these depths, from dissolution of barite and other Ba-rich particles during the northward travel of the eddy;

(**3**) Finally, south of ~49°S, between the northern branch of the SAF and the PFZ, positive values (up to 13 nM; see red patches in Figure 6.1-a) for the difference between calculated and observed Ba distributions appear in the upper 800m (mainly between 150 and 450 m). Again, residual analysis indicated calculated water masses mixing fractions are reliable [de Brauwere et al., 2007], and therefore these positive values reflect subtraction of Ba_d from solution. It is interesting to note these depletions coincide with the presence of higher mesopelagic excess particulate Ba contents and with an increased export of Ba-rich particles to the seafloor [Cardinal et al., 2005]. It is thus very well possible that we observed the effect of Ba translocation from the dissolved to the particulate phase.

[122] Figure 6.1-b (summer situation; SAZ-98 cruise) reveals similar features as in spring:

(**1**) For most of the sampled points, no significant difference exists between calculated and observed Ba fields (white patch), indicating conservative behaviour of Ba_d;

(**2**) At ~48°S, negative values (up to -30 nM; see blue patch Figure 6.1-b) appear below 300 m, mainly in the SAMW and AAIW, indicating enrichment in Ba_d compared to POMP calculations. Again, such results suggest a build-up of Ba_d from the dissolution of Ba-rich phases, potentially linked to the anticyclonic recirculation crossing the SAZ as reported by Rintoul and Trull [2001];

(**3**) Positive values (up to 11 nM; see red patches in Figure 6.1-b) are recorded below 100 m, both north of 43°S in the STF and south of 49°S in the SAF area, indicating Ba_d depletions in the water column. Since quite high Ba_p contents have been recorded at both these latitudes [Cardinal et al., 2001; see also Chapter 5],

these results are consistent with Ba_d subtraction in ambient water during barite formation.

[123] Overall, while the major part of the Ba_d field could be reconstructed by mixing, thus corroborating earlier conclusions that Ba_d gradients showed tight overprinting with frontal zones (Chapter 3), results from the POMP model raised important issues concerning the non-conservative behavior of Ba_d in these areas. At ~47-48°S in the SAZ/SAF area, spring and summer situations show the occurrence of Ba_d contents exceeding those reconstructed by the mixing model; Ba_d input reached up to 30 nM in summer. Particular complex dynamics have been reported for this zone [Rintoul et al., 1997; Rintoul and Sokolov, 2001], and our results suggest that Ba_d enrichment from the dissolution of particulate Ba-rich phases could be achieved during the journey of such mesoscale eddies and meanders. But the major issue of this paper concerns the low occurrence of observed Ba_d compared to that predicted from mixing, occurring mainly south of 49°S in the SAF region. These depletions extend deeper and wider in the mesopelagic zone in the summer compared to the spring, which indicates a potential link with the phytoplankton growth season and emphasizes the non-conservative behavior of Ba_d in this sector. From STZ to PFZ, Ba_p has been reported to be systematically higher in the summer than in the spring, with enhanced Ba_p concentrations reflecting the stronger mesopelagic remineralization that occurs in the SAF-PFZ area [Cardinal et al., 2005]. Our results fit with these observations and suggest that mesopelagic Ba_d depletion could be the result of a Ba subtraction from solution during barite formation over the growth season. Ba_d depletions, as given by the POMP model, reached up to 13 nM. Since such missing dissolved Ba quantities are not balanced by equivalent increases in the particulate phase, the latter ranging between 0.25 and 0.6 nM [Cardinal et al., 2005], this situation implies sinking of particle associated Ba to depths >1000 m (see Chapter 5).

6.5. CONCLUDING REMARKS

[124] This study used a robust model (POMP analysis) to estimate the behavior of dissolved Ba in the S.O. and contributes to a better understanding of the Ba cycle dynamics. Here, it reveals that dissolved Ba could be largely reconstructed by mixing, emphasizing the potential of Ba_d as a water mass tracer. However, it also indicates that at some depths in the water column, the Ba_d distribution displays a non-conservative behavior. Results thus confirm our

hypothesis that processes such as particulate Ba-phases formation and dissolution could lead to a measurable impact on Ba_d water column profiles. Moreover, these results suggest several important issues in the additional application of the Ba_d proxy.

General discussion - Section 2

GENERAL DISCUSSION - Section 2

[125] The main objective of Section 2 was to address the question as to whether it is possible to define what the exact processes are (physical and/or biogeochemical control) that act upon the Ba_d distribution in the Southern Ocean. In particular, we examined Ba_d and Ba_{xs} in various frontal systems and confronted them to the global hydrodynamical and biogeochemical context of our study areas. Overall, investigating the Ba cycle through the angle of the dissolved phase was our strategy to better understand the particulate Ba-barite dynamics; our work will have several important implications for the use of the Ba proxy (see General conclusion). Here, we discuss in a broader context the insight on the importance of Ba_d in the Ba cycle dynamics that our various studies (Chapter 3 to 6) provided.

On dissolved Ba, Nutrients and alkalinity

[126] Since Ba_d in the open ocean behaves as a bio-intermediate element, presenting lower concentration in the upper 1000 m without however reaching total surface depletion [Chow and Goldberg, 1960; Broeker and Peng, 1982], a large number of studies concluded that the apparent correlation of Ba_d with silicate and alkalinity involves a direct link with biological processes [Wolgemuth and Broeker, 1970; Li et al., 1973; Chan et al., 1977; Lea and Boyle, 1989; Bruland, 1983]; this conclusion was moreover strengthened by the association of barite with productivity [Cronan, 1974; Dehairs et al., 1980, 1987; Dymond et al., 1992; François et al., 1995; Dymond and Collier, 1996; McManus et al., 1998]. Various studies thus focused on determining whether planktonic organisms could directly subtract or precipitate Ba and explain surface Ba_d removal and Ba fluxes in the water column [Collier and Edmond, 1984; Bernstein et al., 1987, 1992, 1998; Dehairs et al., 1980; Ganeshram et al., 2003; Bernstein and Byrne, 2004; Sternberg et al., 2005-a, accepted; see also Section 3 of this work]. However, from previous works, discrepancies between Ba, alkalinity and silicate surfaced that dissolved Ba is not controlled by the same processes than nutrients, and that its distribution does not reflect a direct link with biological activity [Edmond, 1974; Collier and Edmond, 1984; Bishop, 1988; Jeandel et al., 1996; Dehairs et al., 1990, 1991, 1992; Stroobants et al., 1991; Stecher et al., 1999].

[127] Here, examining closely nutrients (nitrate and silicate), alkalinity and Ba_d distributions during the ANTARES-4, SAZ-98 and CLIVAR SR3 cruises, we emphasized that they are not mechanistically coupled, neither in surface waters nor at depth, but rather result from the spatial coherence of parallel carriers. During ANTARES-4, although correlation between Ba_d and silicate is tight in the

whole area, for the PFZ an uncoupling is evident in the upper 600 m. Also Ba_d vs. alkalinity in the upper 600 m shows a quite complex relationship during ANTARES-4, with regression slopes decreasing from north to south in surface and getting inverse deeper 600 m. During SAZ-98 and CLIVAR SR3, from the STF to PFZ, although regression analyses identify silicate and alkalinity (being highly correlated) as the major predictors for Ba_d, Ba_d and silicate are uncoupled in surface water where Ba_d behaves more similar to nitrate, and Ba_d and alkalinity are inversely correlated in the upper 600 m. No obvious process links silicate and alkalinity: it is thus likely that biological synthesis of opal and carbonate and subsequent dissolution generate parallel distributions. Moreover, during CLIVAR SR3, the observed relationships for Ba_d, silicate and alkalinity (decreasing slope southward for Ba_d vs. silicate) are mainly maintained by the situation at intermediate and deep waters (where dissolution of suspended biogenic barium, opal and carbonate parts of plankton are major processes) and are marked by the location of the PF. Results suggest a decreased dissolution of barite south of the PF as compared to the situation in the SAZ and PFZ, in agreement with saturation conditions for $BaSO_4$ in these waters. Overall, results highlight the unique pseudo-nutrient behavior of barium and eliminate diatoms as significant consumers of Ba. Moreover, they fit with laboratory experimental work on diatom cultures which show Ba-uptake in diatoms to be relatively small and insufficient to sustain the Ba contents and fluxes in the deeper ocean [Dehairs et al., 1980; Sternberg et al., 2005]. Thus, the surface to deep and north to south positive gradient of Ba_d reported in the Southern Ocean clearly results from the particulate Ba formation/dissolution dynamics, the latter driven by the intensity of biogenic material mineralization processes, the saturation state of the S.O. with respect to barite [Monnin et al., 1999; Monnin and Cividini 2006] and the general circulation. The issue of the Ba removal process in the upper 1000 m water column remains now to be discussed (see further).

On Ba_d conservative vs. non-conservative behavior

[128] Resolving the effects of hydrodynamic and biogeochemical processes on the Ba_d distribution is not an easy task. Cross frontal dynamics is responsible for complex features on both Ba, dissolved oxygen and alkalinity signals (ANTARES-4); such dynamics are especially marked in the Crozet Kerguelen basin due to the presence of the AF, STF and SAF compressed in a narrow front. Moreover, along the highly resolved CLIVAR SR3 transect, Ba_d gradients appear to fit tightly with frontal zones. Hydrodynamic control on Ba_d is evident in the case of AABW formation, Westward flow of Tasman Sea waters and

return flow of an eddy of the SAF. Though in the Arctic basin conservative mixing is being considered as the main control on Ba_d, emphasizing the use of Ba_d as water mass tracer in that region [Falkner et al., 1994; Taylor et al., 2003], the S.O. Ba_d distribution reflects a more complex behavior. Evidences surface that biogeochemical processes are also acting, as witnessed by enhanced Ba_d contents in deep waters north of the mid-ocean ridge (reflecting the combined effect of a higher particulate Ba flux towards undersaturated deep waters and poorer ventilation), and by a local mesopelagic Ba_d minimum in the Inter Polar Front Zone IPFZ (CLIVAR SR3). During ANTARES-4, Ba_d depletions also appear in the PFZ, but results suggest that the effect of hydrodynamics on Ba_d is overwhelming (the depletions seem largely influenced by southward cross-frontal exchanges). Focusing on the subantarctic region and upper 1000 m water column along the SR3 line (145°E; SAZ-98 and CLIVAR SR3 expeditions), parametric optimum multi-parameter model (POMP) results developed by de Brauwere et al. [2007] emphasize that Ba_d distribution can to a large extent be reconstructed by mixing only, thus corroborating that Ba_d gradients show tight overprinting with frontal zones (CLIVAR SR3). However, an important result produced by the POMP model is the quantification of the non-conservative part on the Ba_d signal: Ba_d discrepancies are proved to be significant (SAZ-98 and CLIVAR SR3). Both depletions (reaching 4 to 12 nM) and enrichments (4 to 28 nM) are pin pointed by the POMP approach, these are assigned to particular Ba_{xs}-barite formation and dissolution dynamics, being enrichment in Ba_d during the circulation of an eddy from southern origin and depletions in Ba_d relating to high particulate Ba_{xs} fluxes.

On mesopelagic dissolved Ba depletions

[129] The hypothesis we formulated at the start of this second section concerning the dissolved Ba phase, was whether or not potential Ba_d subtraction in ambient water during barite formation could lead to measurable Ba_d depletion, and thus explain the upper 1000 m Ba_d water column gradient. It was based on the observation of mesopelagic depletions in Ba_d profiles along the 30°E meridian sampling during the CIVA-1 cruise in the S.O. [Dehairs et al., in preparation-a] and on Edmond and Collier's works [1984] on Pacific Ocean Ba profiles, concluding that significant local uptake of Ba_d was required to maintain a mesopelagic particulate Ba maximum. POMP model calculations on both SAZ-98 and CLIVAR datasets suggest that in the SAZ region, where higher particulate Ba_{xs} have been reported at intermediate and deep layers, Ba_d depletions occur, mainly between 200 and 400 m, and reaching as much as 4 to 12 nM over the growth season, occur. Moreover, direct confrontation between Ba profiles during

summer (SAZ-98) and spring (CLIVAR SR3) cruises reveals that the occurrence of mesopelagic Ba_d depletions faces mesopelagic particulate Ba_{xs} maxima. Furthermore, the depth where the density gradient sets the lower boundary of the surface mixed layer generally coincides with the depth where Ba_d contents start to decrease and Ba_{xs} to rise, the latter at a somewhat shallower depth than where the oxygen start to decrease. It is well know that organic aggregates tend to form and accumulate in association with density gradients [Lampitt et al., 1993; MacIntyre et al., 1995; Simon et al., 2002], and therefore, a scenario of local Ba_{xs} production and Ba_d subtraction, associated with enhanced abundances of micro-environments favored by physico-chemical gradients, appears plausible. Results during ANTARES-4 showed no clear evidence that precipitation of barite, reflected by the occurrence of Ba_{xs} maximum, does measurably influence the Ba distribution in the upper 500 m; here, it seems that dynamics preclude measurable depletions to establish. We emphasize the fact that balance between Ba_{xs} gain and Ba_d deficit in mesopelagic waters is not really expected since the Ba subtracted from solution is not necessarily transferred to the local barite stock, but can become associated with larger aggregates exported to the deep ocean. Our results show that combined seasonal build-up of particulate Ba in mesopelagic waters and deep ocean Ba fluxes underscore estimates of dissolved Ba subtraction in mesopelagic waters (SAZ-98 and CLIVAR SR3). This discrepancy suggests significant dissolution of barite to occur in the deeper water column. Values obtained by checking the degree of Ba mass conservation (comparison of in and out fluxes) corroborate those made by the POMP model. Overall, these results emphasize that dissolved Ba subtraction from solution during barite precipitation could lead to measurable impact on Ba_d profiles at mesopelagic depths. From Chapter 3 to 6, considering the scenario through which biogenic aggregates provide the necessary thermodynamic conditions for passive barite precipitation, we thus strengthened the hypothesis that uptake of barium from ambient water (Ba_d subtraction) in decomposing organic material, could explain barite formation; other hypotheses on the barite precipitation process will be confronted further in Section 3.

[130] Overall, this second section provided major improvements in valuing the proxy-role of dissolved Ba in the global Ba-cycle dynamics in the Southern Ocean; several important implications of these results for the use of Ba proxy will be discuss further (see General conclusion).

Section 3

Ba_{xs}-based mesopelagic C mineralization

INTRODUCTION

What happens in the mesopelagic zone?

[131] The downward export of organic material through the biological pump (Figure D), constitutes the critical process linking the surface to deep ocean and an important mechanism for carbon (C) sequestration [Eppley and Peterson, 1979; Sarmiento et al., 1988; Honjo, 1996; Battle et al., 2000].

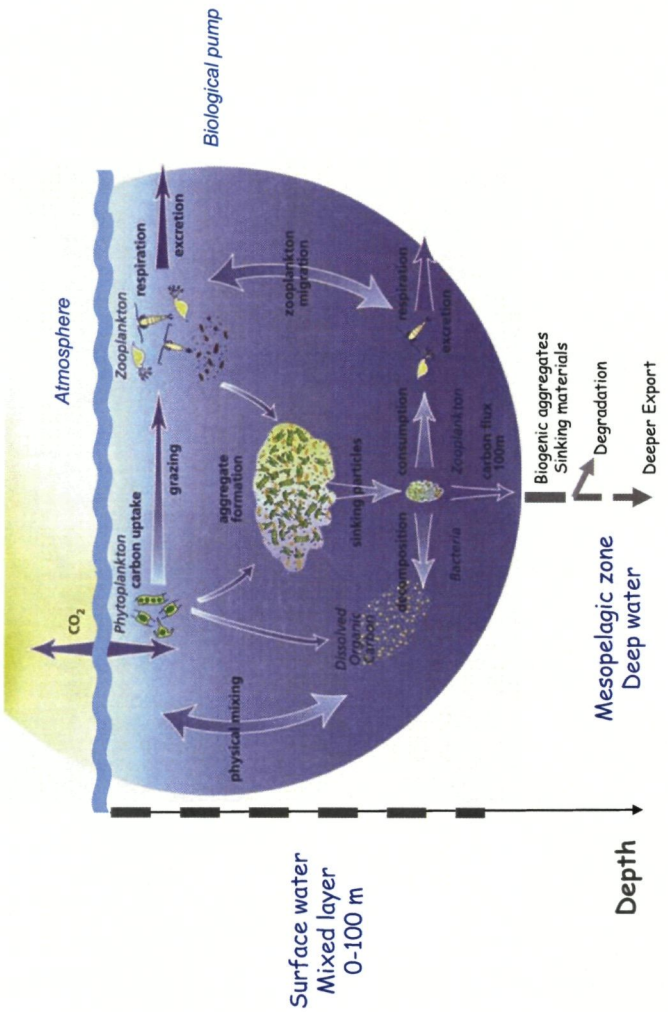


Figure D: The Biologic pump; US JGOFS report.

Only a small part of what is exported out of the mixed layer (~upper 100 m) reaches the seafloor [Lampitt and Antia, 1997].The major part of organic carbon in sinking particles is mineralized (returned to inorganic form) during the transit through the water column, mainly occurring at mesopelagic depths (~100-1000 m) [Martin et al., 1987; Sarmiento et al., 1993; Suess 1980]. These layers have been considered as the largest "heterotrophic digester" of the oceans. The particulate organic matter sinking through the mesopelagic zone is significantly decomposed, transformed, recycled and repackaged in this physically dynamics zone, but the exact physical, chemical and biological mechanisms affecting the downward flux remain to be constrain [Longhurst et al., 1990; Boyd et al., 1999; Kriest and Evans, 1999; François et al., 2002; Jackson and Burd, 2002; Passow and De La Rocha, 2006; VERTIGO 1 & 2 cruises; Boyd and Trull, in press]. The mesopelagic zone is sometimes referred to as the "Twilight zone", partly because it is the transition zone between depths that receive sunlight and those that do not (too dark for photosynthesis), and partly because of the mystery behind many of the processes occurring there [Cindy Lee; 2004]. The nature and extension of the transformation and mineralization processes of sinking biogenic matters through the mesopelagic layer affect the material delivered to deeper depth and seafloor: this zone is thus important to determine the capacity of intermediate layers for longer term C sequestration.

Constraining C mineralization fluxes

[132] In simulations studies of the ocean's role in the global carbon cycle, predicting the depth-distribution for mineralization of particulate organic carbon (POC) is of particular importance. Resolving the particle flux and mineralization curves in the water column is not an easy work. For many years, studies have mainly focused on empirical relationships, based on sediment trap data and power law or exponential functions (Figure E) [Martin et al., 1987; Sarmiento et al., 1993; Bendtsen et al., 2002]. However, the "Martin" curve could not be considered as a single, global relationship between particle flux and depth: remineralization rates clearly change in response to either change in particle source characteristics and/or mesopelagic water processing. Moreover, as sediment traps could strongly be influenced by physical and biological processes [Honjo and Manganini, 1996; Siegel and Deuser, 1997; Yu et al., 2001; Siegel et al., 1997], this could lead to huge errors in reconstructing the POC flux [Lutz et al., 2002].

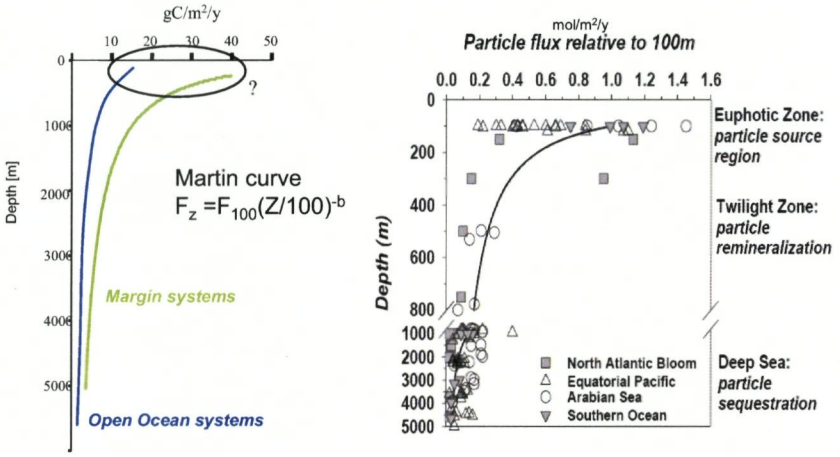


Figure E: Decrease of the particle organic flux with depth; from http://www.whoi.edu/ Vertigo website.

Recent studies also focused on the effect of inorganic materials on fluxes and remineralization of sinking material [Antia et al., 2001; Berelson, 2002; Passow and De La Rocha, 2006]. Based on model simulations [Armstrong et al., 2002], Klass and Archer [2002] studied the relationship between mineral fractions (carbonate, opal or lithogenic material inducing a ballast effect) and the transfer of POC to the deep ocean. Next to flux predictions as reconstructed from sediment traps or modelling, indirect approaches (more mechanistic understanding) could be used to estimate C fluxes in the water column. To resolve the issue of the controls on particles transport efficiency through the twilight zone, studies focused on decomposing the whole processes affecting particles characteristics with depth, time or with location [Longhurst et al., 1990; Lampitt and Antia, 1997; Hoppe and Ullrich, 1999; Graham et al., 2000; Stemmann et al., 2004; Schentzer and Steinberg, 2002-a, -b; Sheridan et al., 2002; Passow and De La Rocha, 2006; VERTIGO 1 & 2 cruises]. Moreover, it is particularly the aim of the BELCANTO II project (BELgian research on Carbon uptake in the ANTarctic Ocean) to constrain the C curve in the upper 1000 m water column, via a multi-proxies approach including Ba-barite, ^{13}C, ^{234}Th, $\delta^{15}N$, biomarkers, $\delta^{30}Si$, bacterial activity and sediment traps data (Figure F).

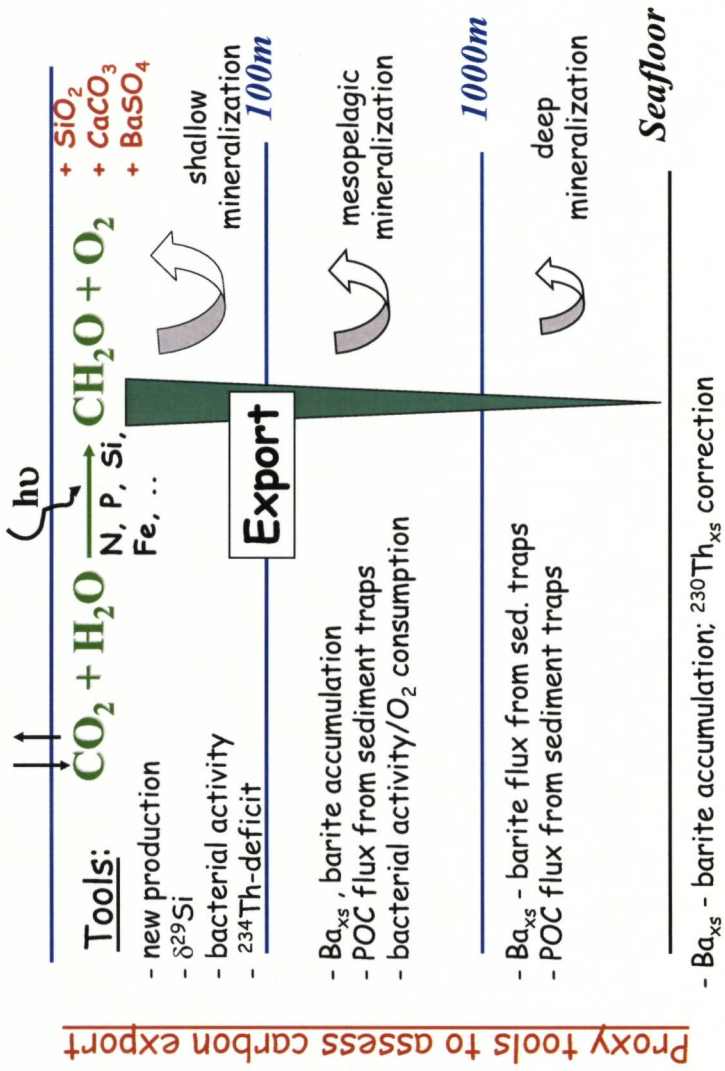


Figure F: Multi-proxies approach to constrain the C curve in the upper 1000 m water column.

Each of these conceptually independent proxies allows reconstructing fragments of the decreasing C flux with depth (Figure G). Some of these C flow rates are thus known; unknown is how these parts fit together to form a consistent picture. The major attenuation of the C curve occurs at mesopelagic depths, between 100 and 1000 m, and this domain belongs to the Ba-barite proxy. As the mesopelagic zone is of considerable significance in determining the export efficiency of the

surface biologic pump and the fate of biogenic material, particular attention is made in this section to better constrain mesopelagic Ba-barite, to make it a robust tool to trace C mineralization processes.

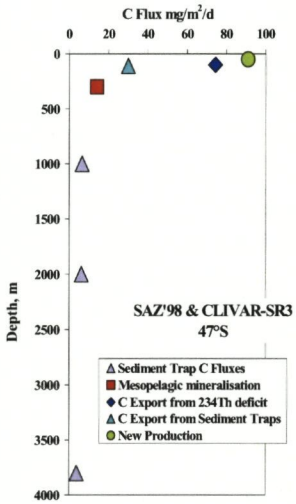


Figure G: Decreasing POC flux with depth as reconstructed by the multi-proxies approach.

The mesopelagic particulate Ba_{xs}- barite tool

[133] Particulate biogenic barium-Ba_{xs} appeared as a good proxy of mesopelagic C mineralization processes [Dehairs et al., 1997; Cardinal et al., 2001; 2005], relying on the formation of barite ($BaSO_4$) in association with sinking organic carbon in decomposition in a World Ocean mostly undersaturated for $BaSO_4$ (see Figure C in Section 2). Ba_{xs} profiles in the S.O. usually display maximum values in the mesopelagic zone (~100-1000 m) (Figure H-a); Ba_{xs} background in the S.O. is set up by the saturation state of the water with respect to barite [Monnin et al., 1999; Monnin and Cividini, 2006]. The mesopelagic Ba_{xs} (meso-Ba_{xs}) builds up during the growth season as a result of the transfer and degradation of biogenic aggregates from the mixed layer (Figure H-b); the association of barite formation with bacterial degradation of organic matter followed by release of discrete barite micro-crystals in the ambient water, led to use discrete barite crystals as an indirect proxy for mesopelagic mineralization of exported biogenic material [Dehairs et al., 1980, 1990, 1991, 1997; Cardinal et al., 2005]. Meso-Ba_{xs} stock is then translated into POC fluxes by using a relationship empirically relating Ba_{xs} to O_2 consumption [Shopova et al., 1995; Dehairs et al., 1997]; equations and further details are given in Section 1, Chapter 1.

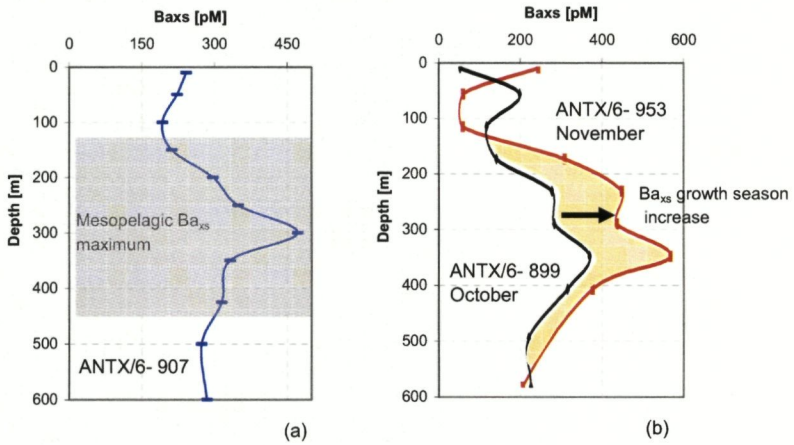


Figure H: Particulate Ba_{xs} profiles (pM): (a) Ba_{xs} mesopelagic maximum, (b) Ba_{xs} growth season increase.

[134] Despite the great potential of the meso-Ba_{xs} proxy, its use remains limited. It is due to uncertainties related in part to the mechanism of Ba_{xs}-barite precipitation in the water column, and in part to the translation of meso-Ba_{xs} into mineralized-C fluxes. (**i**) Indeed, the exact mechanism of barite precipitation in the water column remains to date debated. The scenario above suggests a passive barite precipitation, which is partly unexplained. Barite precipitation inside biogenic aggregates has been proposed as the main mechanism of biogeochemical Ba subtraction [Dehairs et al., 1980; Stroobants et al., 1991] in undersaturated waters for $BaSO_4$ [Monnin et al., 1999; Rushdi et al., 2000]. Inside such micro-environments, Ba subtraction from solution (hypothesis tested in Section 2) and release of biogenic Ba or oxidation of organic sulfur were put forward as the probable processes leading to super-saturation of barite (see Figure C) [Collier and Edmond, 1984; Bishop, 1988; Bertram and Cowen, 1997; Dehairs et al., 2000; Ganeshram et al, 2003]. Moreover, studies by González-Muñoz et al. [2003] have shown that barite production may be directly bacterially mediated and suggest that bacteria may enhance barite production by providing nucleation sites for crystal growth. Alternative pathways suggest that barite precipitation is biologically mediated, debating the specific role of different planktonic organisms. In the surface layer, incorporation of Ba in the celestite ($SrSO_4$) skeleton of acantharians and active barite precipitation during skeleton dissolution has been involved by Bernstein et al. [1998] and Bernstein and Byrne [2004]. However, work by Esser and Volpe [2002] and Ganeshram et al. [2003]

argues against acantharians as the main source of biogenic barium in the upper water column. Experimental work on diatom cultures has shown Ba-uptake in diatoms to be relatively small and insufficient to sustain the Ba contents and fluxes in the deeper ocean [Dehairs et al., 1980; Sternberg et al., 2005]. It fits with results presented in Chapter 5, excluding diatoms as significant consumers of Ba. (**ii**) Moreover, next to uncertainties linked to the barite precipitation itself, the calibration of the meso-Ba_{xs} proxy needs to be refined. For instance, the choice of the Ba_{xs} background, called $Ba_{residual}$ as given in Eq. 1 (Chapter 1), is crucially important in the translation of Ba_{xs} fluxes into C mineralization rates. This background signal at zero oxygen consumption, i.e. zero organic C demand, depends of the saturation state of the water for $BaSO_4$. For the S.O. south of the PF, shown by Monnin et al. [1999] and Monnin and Cividini [2006] to be saturated for $BaSO_4$ from surface to 2500 m, this residual Ba_{xs} is close to 180 pM [Dehairs et al., 1997]. Saturation index calculations are a means to estimate the saturation state of barite in various environments and to refine the Ba_{xs} background. Moreover, the relationship relating meso-Ba_{xs} to O_2 consumption as established by Shopova et al. [1995] and Dehairs et al. [1997] in the PF region of the S.O. (see Eq.2; Chapter 1) need also to be tested in other environments, as well as to other modes of carbon utilization assessment.

Objectives

[135] In this section, we investigated particulate biogenic Ba_{xs} in order to better validate and calibrate the meso-Ba_{xs} proxy, to make it a powerful tracer of the C mineralization. We confronted the major results from KEOPS (Indian sector) and EIFEX (Atlantic sector) cruises in the Southern Ocean and also compared them to VERTIGO 1 & 2 cruises in the North Pacific. We examined the details of Ba_{xs} profiles in the biogeochemical and hydrodynamical contexts of the different study areas. Especially we discussed the behavior of Ba_{xs} vs. biomass parameters, planktonic communities, bacterial activity, other trace and major elements, export production and sediment traps. Particular attention was put on investigating the impact of natural and artificial Fe-amended blooms on mesopelagic C mineralization. Ocean fertilizations are a means to assess possible changes in the magnitude and efficiency of particle transport, key to any assessment of the atmospheric CO_2 modulation. We also investigated the relations between Ba_{xs} and acantharians, to better understand which role acantharians could play in the barite formation process. Moreover, we compiled the whole Ba_{xs} data we dispose of (Southern Ocean & North Pacific data) and discussed them in a broader context. Have we come closer toward a 'generic'

proxy for twilight zone organic carbon mineralization? Where are we in valuing what controls transport on sinking particles between surface and deep ocean? We attempted to define whether certain regions or type of environments (biogeochemical divides) in the Southern Ocean have characteristics in common or are more critical than other for C export and mineralization, and in some extent to potential pCO_2 and deeper C sequestration.

Chapter outline

[136] Overall, this third section has attempted to improve our understanding on the particulate biogenic Ba_{xs}-barite formation process, its fate in the water column and its calibration in order to better constrain estimation of C mineralization fluxes. The issue of barite precipitation constitutes the limiting keys for robust application of the Ba proxies for reconstructing modern and past ocean C export. Moreover, a quantitative representation of mineralization processes is integral to every simulation of the S.O.'s role in the global carbon cycle. First (Chapter 7), we studied the impact of an artificial iron fertilization on mesopelagic C mineralization (EIFEX). Particulate Ba_{xs} evolution in the upper 1000 m water column was followed over a 37-day observation period in a fertilized eddy. Secondly (Chapter 8), we followed the fate of a natural iron-induced bloom and the associated flux of sinking particles at intermediate layers (KEOPS). The extent of particulate Ba_{xs} contents in the upper mesopelagic zone was examined at contrasting stations in the natural fertilized water and in the surrounding HNLC waters. Thirdly (Chapter 9), we confronted the Ba_{xs} proxy approach with other modes of carbon utilization assessment (VERTIGO 1 & 2). We compared Ba_{xs}-based mesopelagic C mineralization fluxes from two contrasting locations (oligotrophic and mesotrophic stations) to bacterial carbon demand and POC flux decrease with depth obtained from NBST's (Neutrally Buoyant Sediment Trap). Fourthly (Chapter 10), we confronted particulate Ba_{xs}, barite, Sr and Ca with acantharians distribution and Ba/Sr skeleton contents, in order to shed light on the potential role of acantharians in the barite formation process (EIFEX). Finally, in a General discussion, we provide a brief overview of the whole results presented in Section 3.

Chapter 7

Mesopelagic C mineralization in artificial iron fertilization conditions

Foreword

[137] To understand present day ocean C sequestration and to valuate potential strategies for enhancing sequestration, one means consists in assessing possible changes in the efficiency of particles transport via iron fertilization. Iron fertilization of the ocean is widely discussed as a possible strategy for extracting CO_2 from the atmosphere. Here in Chapter 7, we present changes in mesopelagic C mineralization processes as a result of artificial iron fertilization (EIFEX experiment).

SUMMARY

[138] Mesopelagic carbon (C) mineralization was determined during the European Iron Fertilization Experiment (EIFEX) in the Southern Ocean, by measuring changes in excess particulate biogenic barium (Ba_{xs}) over a 37-day observation period. Mesopelagic Ba_{xs} (meso-Ba_{xs}; 150-1000 m) revealed that before the iron was released, the site was already sustaining a significant vertical flux of particles leading to C mineralization. Following 35 days after fertilization, meso-Ba_{xs} provided evidence of changes in surface particulate export and of enhanced, fast mineralization processes up to 1000 m. However, both export and mineralization decreased at the end of the experiment. Total C mineralization, which mainly occurred in the lower part of the mesopelagic zone (500-1000 m), increased more than 5-fold during EIFEX, reaching fluxes of 91 $mgC/m^2/d$. Such mineralization rates, however, are not particularly high compared to other values reported for Southern Ocean summer conditions. During EIFEX, considering the respective total export and mineralization maxima around day 34, calculations indicate that the C mineralized in the 150-1000 m depth layer accounted for 11% of the surface export at 150 m, suggesting that a substantial amount of exported carbon reached deep in the water column. However, unexpected similarities and phase lags between stations located both inside and outside of the fertilized patch, indicated that eddy dynamics were determinant in setting particle patterns on a broad spatial scale exceeding the extent of the fertilization, thereby homogenizing the signals of mesopelagic mineralization.

7.1. INTRODUCTION

[139] The Southern Ocean (S.O.) plays a key role in regulating the climate system and is recognized as an oceanic body particularly sensitive to climate change [Sarmiento et al., 1998]. Model results indicate that it acts as a sink for atmospheric CO_2, mainly due to phytoplankton uptake [Takahashi et al., 2002]. Like other High Nutrient Low Chlorophyll (HNLC) areas, primary production in the S.O. is mostly limited by the micro-nutrient iron, as has been unequivocally demonstrated by artificial mesoscale iron enrichment experiments (IronEx, SOIREE, EisenEX, SEEDS, SOFeX and SERIES cruises; Boyd et al., 2000, 2004; Gervais et al., 2002; Buesseler et al., 2004, 2005; de Baar et al,. 2005), confirming former phytoplankton incubation trials [Martin and Fitzwater, 1988; Hutchins and Bruland, 1998; Takeda, 1998]. All iron enrichment experiments showed an enhancement of primary production associated with a shift in the structure of the phytoplankton community towards larger diatoms [De Baar et al., 2005]. However, due to the short duration of these experiments, the fate of the Fe-induced phytoplankton blooms was poorly recorded. Indeed, an increase in export production as a result of the iron addition was only reported for SOFeX [Buesseler et al., 2005]. However, in assessing whether artificial iron fertilization in the Southern Ocean could be a means of sequestering C deeper in the water column and mitigate the atmospheric CO_2 increase resulting from the anthropogenic activities [Martin, 1990], the magnitude of the export is not the only important parameter to infer this sequestration [Sarmiento et al., 2004-a, 2004-b]. Indeed, the fate of the C exported under such iron fertilization experiments is largely overlooked although mineralization in mesopelagic waters (150-1000 m) is responsible for the release of most of the C exported from the surface mixed layer (0-150 m) [Lampitt and Antia, 1997; Martin et al., 1987; Sarmiento et al., 1993; Suess, 1980].

[140] Chapter 7 aims to understand the impact of an artificial iron-induced bloom in terms of mesopelagic mineralization processes. Changes in mesopelagic Ba_{xs} (150-1000 m) in response to the addition of iron were examined during the European Iron Fertilization Experiment, EIFEX [Smetacek, 2005], carried out in the Atlantic sector of the S.O.; stations were monitored over a 37-day observation period. We expand on these results with a detailed analysis of the time series evolution of meso-Ba_{xs} in the context of the biogeochemistry of the fertilized area, and in terms of its implication in quantifying carbon fluxes. The

present work is part of a multi-pronged approach which aims to determine the fate of an iron-induced bloom and associated sinking particles. The goal is to help in deciphering whether or not C export and sequestration increase significantly as a result of iron fertilization in the ocean.

7.2. EXPERIMENT

[141] EIFEX (cruise ANT XXI/3 of R/V Polarstern; 21 Jan.-25 Mar. 2004) was carried out in a mesoscale cyclonic eddy located in a meander of the Polar Front. The physical setting of the experiment is described by Strass et al. [2005]. The water mass in the eddy, centered at roughly 50°S-2°E, was characteristic of the Antarctic Circumpolar Current (low temperature, HNLC conditions) and showed iron depletion (0.08-0.2 nM; Hoffmann et al., 2006). 7 tones of iron sulphate were added to an area of 150 km^2 on February 12-13 after an initial sampling to determine the pre-fertilization conditions; T= -1 reflects the conditions before the iron release, which occurred on day zero (T0). A second iron release into the previously fertilized patch was undertaken on February 26-27 (day 12). The outcome of the fertilizations was monitored over 35 days after the initial iron release. Samples were collected at stations both inside and outside the iron-fertilized patch (hereafter referred to as IN and OUT stations, respectively), though all stations reported in this study were located inside the eddy. IN and OUT patch stations were defined by surface parameters (e.g. photosynthetic activity Fv/Fm, Fe, Chl a and pCO_2 data).

[142] During EIFEX, Chl a concentrations had increased more than fivefold by day 25 and then decreased toward the end of the experiment, while particulate organic matter followed a similar pattern, declining after day 29. These findings indicate the demise of the iron-induced bloom [Hoffmann et al., 2006]. The massive increase in Chl a concentrations was mainly due to the growth of long chain-forming diatoms [Assmy et al., in preparation]. A deep and fast export has been clearly characterized during EIFEX, as revealed by surface sediment [Sachs et al., in preparation] and ^{234}Th [N. Savoye, unpublished data; Strass et al., in preparation] data.

[143] Sampling of suspended matter for particulate Ba measurements were performed at T= -1, one day prior the first iron infusion and subsequently at the IN stations (on days 10, 21, 28, and 36) and the OUT stations (on days 11, 26 and 34). During EIFEX, the particulate biogenic Ba, Ba_{xs}, represented more

than 96% of total particulate Ba. As revealed by SEM-EMP (scanning electron microscopy-electron microprobe) analysis, barite-$BaSO_4$ crystals accounted for up to 100% of the meso-Ba_{xs} during EIFEX (see further Chapter10).

7.3. RESULTS

Particulate biogenic Ba_{xs} profiles

[144] Mesopelagic particulate biogenic Ba_{xs} profiles (150-1000 m) were measured at IN and OUT patch stations over a 37-day observation period (Figure 7.1). Upper 150 m Ba_{xs} data are discussed further in Chapter 10; we report that non-barite particles comprised nearly the whole surface Ba_{xs} signal; in surface waters Ba is expected to be mainly adsorbed on or incorporated into biologically derived materials [Cardinal et al., 2005]. Here, we focus on the mesopelagic zone where most of the mineralization of exported C is thought to take place [Martin et al., 1987; Sarmiento et al., 1993] and where the meso-Ba_{xs} signal is mainly composed of barite [Dehairs et al., 1980; see also Chapter 10]. Before the first iron infusion (T= -1), a clear meso-Ba_{xs} maximum was present between 300 and 400 m. A similar finding was observed recurrently in the 150-500 m depth layer during previous Southern Ocean cruises, although the maximum value observed in this study (reaching 1150 pM) was quite high compared to previous studies [Dehairs et al., 1992, 1997; Cardinal et al., 2001, 2005; see also Chapter 3]. This meso-Ba_{xs} content value indicates high mineralization of sinking particles. Because there is a time delay of a few days/weeks between C export event and the build-up of meso-Ba_{xs} maximum [Cardinal et al., 2005], this mineralization must be associated with a bloom that occurred before the start of the EIFEX experiment. This is consistent with several other independent parameters like export production and fCO_2 data [Strass et al., in preparation]. After the first iron infusion, a decrease in the meso-Ba_{xs} maximum was observed within the first 10 days at IN-patch stations. However, Ba_{xs} contents between 250 and 600 m were still as high as 485 pM. Deeper in the water column, concentrations of Ba_{xs} decreased to 180 pM at 1000 m. From day 10 to 36 (at IN-patch stations), the meso-Ba_{xs} maximum at 400 m tended to dissipate and Ba_{xs} increased in the deeper mesopelagic domain (up to 1000 m). This was a striking and rather unusual feature for S.O. Ba_{xs} profiles. By the end of the 37-day observation period, meso-Ba_{xs} at IN-patch stations was rather homogeneous between 300 and 1000 m. A similar trend of increasing Ba_{xs} contents in the deeper mesopelagic zone was also observed at OUT-patch stations.

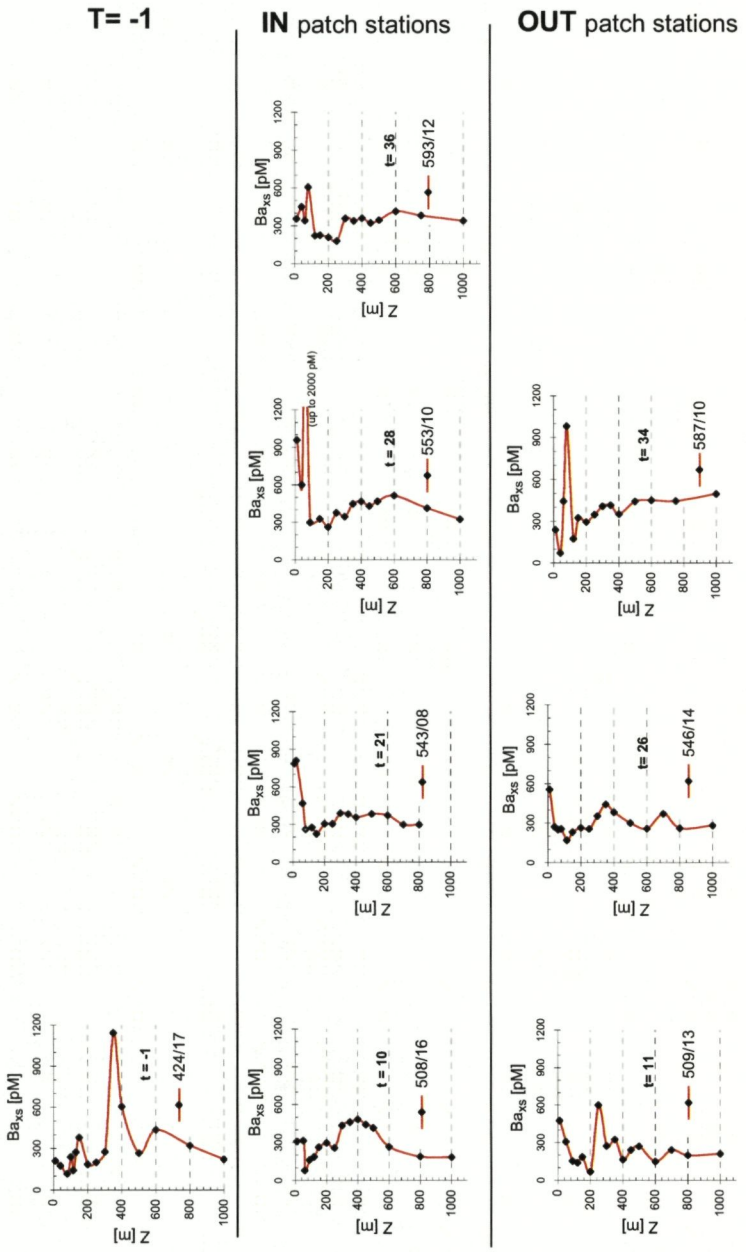


Figure 7.1: Particulate biogenic Ba_{xs} profiles (pM; 0-1000 m) at T=-1, IN-patch and OUT-patch stations during EIFEX.

Depth-weighted average values of Ba_{xs}

[145] We quantified temporal changes in meso-Ba stocks from the time series data. As mentioned above, Ba_{xs} contents between 150 and 500 m decreased with time, while between 500 and 1000 m, contents appeared to increase. We will now consider temporal meso-Ba_{xs} changes over both these depth layers in more detail. Ba_{500} and Ba_{1000} (depth-weighted average values integrated over 150-500 and 500-1000 m, respectively) are reported in Figure 7.2 for both IN and OUT stations; data are given in Table 7.1. As depicted in the water column profiles, Ba_{500} was high at the start of the experiment (T= -1) and decreased within the first 11 (OUT) and 21 (IN) days, reflecting the dissipation of the initial meso-Ba_{xs} maximum (Figure 7.2-a). Then, depth weighted average values increased slightly with time and decreased again by the very end of the experiment. Note that Ba_{500} obtained at day 28 at IN-patch stations (390 pM) was lower in magnitude to those naturally occurring before the iron infusion (452 pM; T= -1). In contrast, the Ba_{1000} decrease stopped at day 10 (IN) and day 11 (OUT) and then, notably, increased until days 28 and 34 for IN and OUT stations, respectively. After reaching a maximum of 432 and 460 pM at IN and OUT stations, respectively, Ba_{1000} finally decreased once again until day 36 at IN-patch stations (Figure 7.2-b). Ba_{500} and Ba_{1000} maximum values during EIFEX (at T= -1, as well as at days 28 for IN stations and 34 for OUT stations) were relatively small in comparison to other values reported for S.O. summer conditions (i.e. 500 to 600 pM; Dehairs et al., 1992, 1997; Cardinal et al., 2001, 2005; see also Chapter 3 and Chapter 8).

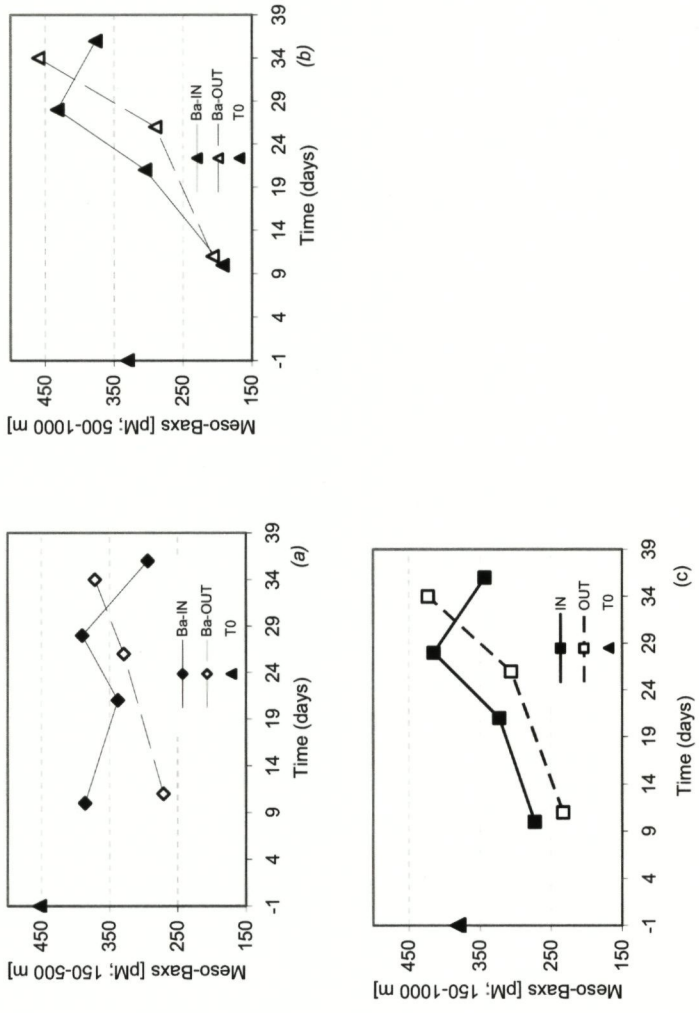


Figure 7.2: Mesopelagic Ba_{xs} depth-weighted average values (pM) over a 37-day observation period during EIFEX; integration between (a) 150-500 m, (b) 500-1000 m and (c) 150-1000 m.

	Station	Time (days)	Meso-Ba_{xs} [pM]			C remineralization [mgC/m^2/d]
			150-500m	*500-1000m*	*150-1000m*	*150-1000m*
	424/17	-1	452	330	381	78
IN patch	508/16	10	386	193	273	31
	543/08	21	338	305	323	40
	553/10	28	390	432	415	92
	593/12	36	294	377	343	61
OUT patch	509/13	11	271	207	233	14
	546/14	26	329	290	306	45
	587/10	34	371	460	423	96

Table 7.1: Depth-weighted average values of mesopelagic Ba_{xs} (pM; 150-500m, 500-1000 m and 150-1000 m) and C mineralization fluxes (mgC/m^2/d; 150-1000 m) at T= -1, IN-patch and OUT-patch stations during EIFEX.

[146] Considering now meso-Ba_{xs} depth weighted values integrated between 150-1000 m, IN and OUT stations showed a similar progression of the Ba_{xs} signal throughout the experiment, though OUT stations lagged behind by 5 to 6 days (Figure 7.2-c). Such similarities in Ba_{xs} stocks may have resulted from particle sedimentation patterns and eddy dynamics (see discussion below). Noteworthy are also the Ba_{xs} depth-weighted average values which increased faster at days 21 (IN stations) and 26 (OUT stations) and decreased after day 28 (IN patch stations) as outlined above. This fits with temporal trends of Chl a and particulate biogenic matter concentrations at 20-m depths (i.e. POC, PON, POP and bPSi) [Hoffmann et al., 2006], which both showed a distinct dip at day 21 and a decline after days 25 at IN stations that was associated with an increase of export of particles [N. Savoye, unpublished data; Strass et al., in preparation]. Between days 10 and 21 (at IN-patch stations), meso-Ba_{xs} increased slightly (Figures 7.2-c), reflecting enhanced mesopelagic remineralization processes, while the export flux at 150 m remained high [N. Savoye, unpublished data; Strass et al., in preparation]. In Figures 7.2-a,-b, it is obvious that Ba_{xs} between 150-1000 m was mainly driven by Ba_{1000}. Comparisons between T= -1, Ba_{500}, and Ba_{1000} integrated values (Table 7.1) indicated that at IN-patch stations, Ba_{500} decreases between T= -1 and day 21 equaled Ba_{1000} increases between days 10 and 21. It is thus possible that until day 21 the remineralization signal of the pre-infusion bloom was still ongoing. In addition, the decline of the different biomass parameters in the mixed layer at the end of the experiment indicates that field observations extended beyond the iron-induced bloom maximum and that we witnessed the decay of the bloom [Hoffmann et al., 2006]. The concordance of the variation of meso-Ba_{xs} stocks suggests rapid changes in particle export and of enhanced and fast mesopelagic mineralization processes up to 1000 m in response to the iron fertilization, followed by their decline toward the end of the

experiment as well. Ba_{xs} depth-integrated values (150-1000 m) were translated into C mineralization rates using Equations 1 and 2 given in Chapter 1. Data are reported in Table 7.1 for both IN and OUT stations; the remineralized C ranged from 14 to 96 $mgC/m^2/d$.

7.4. DISCUSSION

Fate of exported organic material during EIFEX

[147] The pattern of mineralization described above can be explained by superposition of two events of particle sedimentation: slow sedimentation from the natural pre-fertilization bloom and fast sedimentation from the bloom that was stimulated by artificial iron supply. The slow sedimentation is evident from the opposite temporal developments of IN patch Ba_{xs} stocks in the layers between 150-500 and 500-1000 m (Figure 7.2), as well as by the downward propagation of the pre-fertilization mesopelagic Ba_{xs} maximum seen in Figure 7.1, which also flattens and broadens during the 5 weeks of the experiment. The fast sedimentation event is suggested by the temporal Ba_{xs} stock increase, which occurs between days 21 and 34 in both layers 150-500 and 500-1000 m depth. Our results thus indicate that biogenic materials from the induced-bloom were quickly transported deeper into the mesopelagic zone, within just a few days after first indications of particle export were observed in the mixed layer [N. Savoye, unpublished data; Strass et al., in preparation]. Our data provide further information on the location and extent of C mineralization, which mainly occurred deep in the mesopelagic zone (500-1000 m) rather than in the upper mesopelagic zone (150-500 m) as observed under natural conditions [Cardinal et al., 2001, 2005; see also Chapter 3 and Chapter 5]. However, the maximum C mineralization flux reached at day 28 (IN; 92 $mgC/m^2/d$; Table 7.1) is not particularly high when compared with other values reported for Southern Ocean summer conditions (up to 140 $mgC/m^2/d$ in the Indian sector; see Chapter 3). Moreover, unexpected similarities in mineralization fluxes at mesopelagic depths between IN- and OUT-patch stations suggested that particle export at OUT-patch stations was likely impacted by the fertilization. In contrast, OUT-patch surface waters did not show any impact of fertilization, and were distinct by phytoplankton communities, particulate organic materials and Chl a values which remained more or less at the pre-fertilization level [Hoffman et al., 2006]. The same holds for export production which stayed high but relatively constant in the mixed layer at OUT-patch stations and increased only slightly during the experiment [N. Savoye, unpublished data; Strass et al., in preparation]. That

mesopelagic waters sampled at OUT stations have been influenced by the Fe-fertilized patch (i.e. by mixed layer waters with high POC concentration) can be the consequence of the eddy circulation, in which the speed of rotation changes with depth. In the simplest example where the speed decreases linearly with depth from highest values at the surface to zero at the sea floor, a patch in the mixed layer would drift over the slower moving layers below. Therefore, deeper "OUT" layers should also receive particles from "IN" surface waters but with a longer time lag than "IN" deep layers. We remind that the label "IN" and "OUT-patch" stations was defined using surface parameters, which don't describe the conditions at mesopelagic depths. The vanishing differences between IN and OUT-patch casts in C mineralization and the unusual Ba_{xs} profiles (i.e. homogeneous meso-signals of IN and OUT stations spreading up to 1000 m) would thus result from deeper mesopelagic horizontal mixing. This explanation fits with results from Assmy et al. [in preparation], who found clear differences in diatom abundances between IN and OUT stations up to 350 m, while deeper differences are less distinct. Moreover, these authors report high and similar abundances of empty and broken diatoms frustules down to 3500 m both IN and OUT-side the patch, emphasizing the impact of the eddy vertical shear on the distribution of particles. It results that mesopelagic carbon mineralization fluxes at both IN and OUT stations should be considered to reflect the system's response to iron addition during EIFEX.

[148] As outlined above, the present work is part of a multi-pronged approach whose target is the fate of an iron-induced bloom and associated sinking particles. In particular, our approach is based on the comparison between Ba_{xs}-based C mineralization and ^{234}Th-based export production; ^{234}Th data are discussed in more details in Strass et al. [in preparation]. Briefly, these authors report that export production at 150 m was high at T= -1 and that fluxes at both IN and OUT stations remained high and constant during the first 21 days (referred to as the first period) of the experiment. Day 21 is considered as the switch over between the situation before and after the impacts of the fertilization (as reported from ^{234}Th data; N. Savoye, unpublished data; Strass et al., in preparation). These authors also indicate that while at OUT-patch stations the export production increased slightly from day 17 to day 34, at IN-patch stations it decreased to negative flux at days 20-24. A huge increase was observed from day 24 to day 32, this increase corresponding to a massive sinking of large diatoms [Assmy et al., in preparation]. To estimate the fraction of C carried on material exported from the mixed layer that was mineralized at mesopelagic

depths during EIFEX, we compared total C mineralization to total export production (Figure 7.3). The total export production is given by the weighted average of IN plus OUT fluxes to the water column underlying the drifting fertilized patch. A drift of the patch in the mixed layer relative to the deeper layers results from the vertical shear in the circular flow of the eddy. Relative to the sea floor, the trace of the drifting patch resembles a ring whose area is roughly four times the area of the fertilized patch [Strass et al., in preparation], suggesting a dilution factor of 2 for the export flux from the fertilized patch. The total C mineralization was calculated between days 11 and 36 by the same way as total C export production.

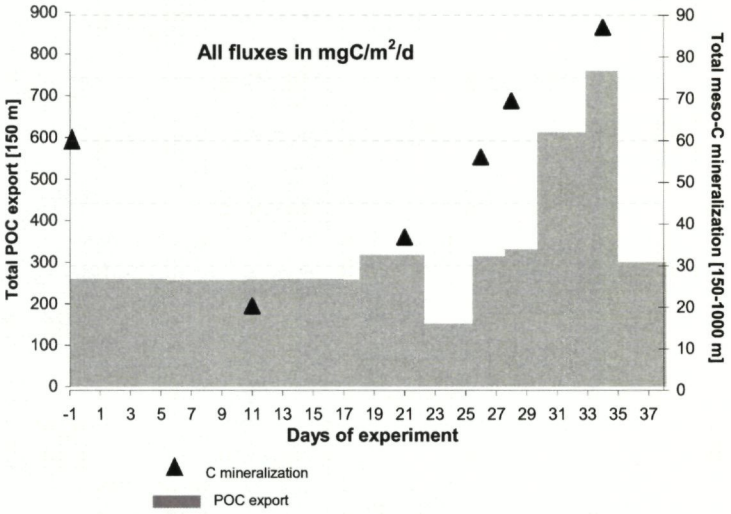


Figure 7.3: Total C mineralization (150-1000 m) and total export production (0-150 m) fluxes (mgC/m²/d) over a 37-day observation period during EIFEX.

From Figure 7.3, the agreement in timing between the two independent estimates emphasizes the speed of C export and mineralization processes during EIFEX. Considering the respective total export and mineralization maxima, calculations indicate that total mineralization in the 150-1000 m depth layer accounts at day 34 for 14% of the surface export at 150 m, which suggests a large fraction of the export is transported below 1000 m. Moreover, integrating total C mineralization fluxes from day 11 to 21 (first period; see above) and from day 21 to 34, reveal that the mineralized C increased from 5 to 20% of the total export, indicating higher export vs. remineralization ratio following the fertilization. Comparison of C export and remineralization for EIFEX is however subject to some uncertainty,

due to the mismatch of sampling times and a rather coarse temporal resolution of the latter. Overall, such findings corroborate other observations from EIFEX, such as an increase of the particle load in the depth range 1000-3000 m evident from optical data [Strass et al., in preparation] as well as measurements in the nepheloid layer and surface sediments, which indicate that highly reactive biogenic particles directly related to the fertilization experiment reached the bottom [Sachs et al., in preparation].

Deeper mesopelagic mineralization induced by iron fertilization?

[149] The finding that the effect of iron addition during EIFEX led to a fast and deep mesopelagic C mineralization has several important implications. It indicates that the iron fertilization not only enhanced particle flux within the fertilized surface water [Strass et al., in preparation], it also significantly influenced the fate of these sinking particles once they left the upper layers. Our results suggest that ~15% of biogenic materials exported from the induced bloom were quickly remineralized down to a depth of 500-1000 m in the mesopelagic zone (Figure 7.2). It implies that export of materials might also have extended beyond these intermediate depths, such findings being corroborated by sediment data [Sachs et al., in preparation].

[150] These results would indicate that artificial iron fertilization has potential implications for large-scale ocean fertilization as a means of long-term C sequestration. In natural systems in the S.O., C mineralization between 150-500 m could explain 60 to 90 % of the carbon carried on sinking particles from the upper layers [see Chapter 8; Cardinal et al., 2005]. Actually there is evidence of complete mesopelagic mineralization during summer in the Australian sector (CLIVAR SR3 transect) of the PFZ whereas the spring remineralization is 40% of the New Production for the same area [Cardinal et al., 2005]. Our observations at T= -1, just prior to the fertilization, indicate a very similar mesopelagic mineralization rate (33%). This would imply that blooms are less prone to remineralization probably as the result of their fast and intense characteristics, leaving less time for mesopelagic mineralization to occur. Compared to natural blooms, the Fe induced bloom of EIFEX seems to have a C mineralized vs. export ratio even lower (11% at day 34). However, as revealed by the shape of Ba_{xs} profiles and the similarities between meso-Ba_{xs} stocks at IN and OUT stations, the results we presented appear influenced also by the eddy dynamics. We can rule out that the eddy used as the experimental site for EIFEX had such a dominant impact on the vertical transport of biogenic matter as the one Mediterranean eddy

described by van Haren et al. [2006], which was considered responsible for the convective transport of fresh material from the surface layer down to the bottom at around 3000 m within a few days. The density structure of the eddy occupied during EIFEX was monitored throughout the experiment and always found to be stably stratified, precluding convection, and the eddy itself was observed to persist with rather unchanged rotational velocity beyond the end of the experiment, excluding the slumping of isopycnals as a possible mechanism for the vertical transport of matter [Strass et al., in preparation]. We nevertheless consider highly possible that mineralization rates determined during EIFEX are not solely representative of the direct impact of iron fertilization, and we do not claim representativeness of our results for the whole Southern Ocean regarding the efficiency of mineralization vs. export as an indicator of potential C sequestration. It should be stressed in particular that even if the remineralization vs. export ratio at the end of EIFEX appears to be favorable for deep C sequestration, such event was short and the excess in export flux (from ^{234}Th data in Strass et al., in preparation) not very intense.

Chapter 8

Mesopelagic C mineralization in the Kerguelen Plateau region

Foreword

[151] Next to the artificial fertilization experiment presented in the previous chapter, a natural iron fertilization survey (KEOPS cruise) was carried out on the Kerguelen Plateau region, a sector where natural iron inputs from sediment sustain over-months massive blooms. In Chapter 8, we examine mesopelagic C mineralization at contrasting stations located on and off the Kerguelen Plateau, respectively in the fertilized waters during the bloom period and in the surrounding HNLC waters.

SUMMARY

[152] We report on the distribution of excess, non-lithogenic particulate barium (Ba), a proxy for twilight zone mineralization of organic matter, in the Kerguelen Plateau area during the late austral summer of 2005. This study was part of a broader investigation focusing on natural iron fertilization controlling the characteristic and recurrent phytoplankton blooms in the region. The Plateau area contrasted strongly with the off-shelf HNLC area. Plateau stations had quite high excess of Ba contents (up to 5000 pM) in surface waters which coincided with enhanced phytoplankton biomasses. However, it had a lower mesopelagic excess of Ba contents when compared to the off-shelf stations. Particulate excess Ba in the twilight zone (125-450 m depth layer) proved to be significantly set by the vertical distribution of bacterial activity, with higher particulate Ba contents in situations where significant bacterial activity extended deeper in the water column. These observations are in agreement with the role of excess biogenic particulate Ba as a proxy of twilight zone organic matter mineralization. Using a transfer function established during earlier work, we calculated organic carbon mineralization rates and weighed these against other carbon fluxes (primary production, bacterial carbon demand), including carbon export from the 125 m horizon (^{234}Th method). Off-shelf HNLC stations had a larger fraction of the organic carbon production exported and subsequently mineralized in the mesopelagic waters (125-450 m). Plateau stations had a smaller fraction of produced carbon exported, but this fraction appeared less prone to mineralization in the twilight zone and therefore had potential to reach the (shallow, ~500 m) seafloor.

8.1. INTRODUCTION

[153] Present-day evidence that iron (Fe) limits ocean primary production in high-nutrient-low-chlorophyll (HNLC) regions [Martin et al., 1990, 1994; Coale et al., 1996] focused interest on ocean fertilization as a C sequestration tool. As outlined in the previous chapter, recent large scale experiments demonstrated the role of iron in enhancing the S.O. phytoplankton biomass and production. However, determining to what extent fertilization could modify the actual export of sinking particulate organic carbon (POC) to the deep ocean is far from being comprehensively achieved. This is partly due to the short term over which the observations were made, thus precluding extrapolation to longer time scales. Moreover, the magnitude of the export increase is not the only parameter which is important in inferring the degree of C sequestration [Sarmiento et al., 2004]. Indeed, the efficiency of the biologic pump in exporting and routing C toward longer term sequestration is mainly set in the intermediate layers (mesopelagic zone). In Chapter 7 we showed that the artificial fertilization performed in an eddy of the Polar Front provided evidence of changes in surface particulate export and of enhanced, fast mineralization processes up to 1000 m. However, clues also surfaced that eddy dynamics were determinant in setting particle patterns on a broad spatial scale exceeding the extent of the fertilization, thereby homogenizing the signals of mesopelagic mineralization.

[154] Next to the artificial fertilization experiments outlined in Chapter 7, a natural iron fertilization survey (KEOPS cruise; Kerguelen: Ocean and Plateau compared Study) was conducted during the late austral summer 2005 on the Kerguelen Plateau, southeast of the Kerguelen Islands and northeast of Heard Island (Indian sector of the S.O.). The Kerguelen Plateau is characterized by recurrent and predictable massive blooms [Blain et al., 2001], as sustained by Fe inputs from shelf sediments. During KEOPS, the Kerguelen Plateau thus served as a laboratory to study the effect of natural iron fertilization on ecosystems functioning and C cycling [Blain et al., 2007]. Contrasting with short term artificial Fe experiments, special emphasis was placed on the potential of the Kerguelen Plateau and margin system for deep C sequestration. Therefore, the present work focuses on mineralization of particulate organic matter in the mesopelagic zone, as assessed from the distribution of excess, biogenic particulate barium (Ba_{xs}). The mesopelagic (meso-) Ba_{xs} distribution was followed at contrasted settings in iron fertilized waters above the Kerguelen Plateau and off-shelf HNLC waters.

8.2. SAMPLING

[155] During the KEOPS cruise in the Kerguelen Plateau region (19 Jan. - 13 Feb. 2005; R/V Marion Dufresne), 8 stations were sampled for particulate barium (Ba_p) along 3 transects (A, B and C) crossing the Kerguelen Plateau and extending into the off-shelf deep ocean (Figure 8.1).

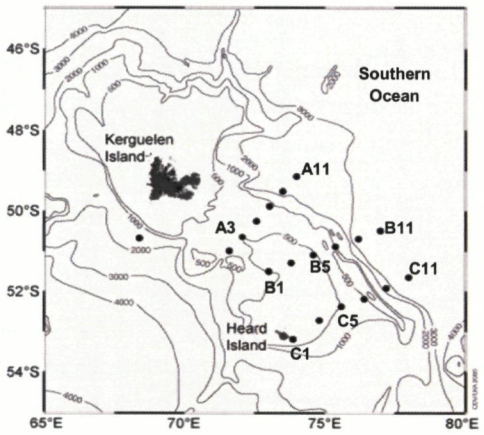


Figure 8.1: Map of the Kerguelen Plateau study area showing the 3 transects A, B, C with stations location.

All stations were located south of the Polar Front (PF). Since the bloom in this area appears remarkably constrained by the bathymetry of the Plateau [Blain et al., 2001, 2007] and thus to potential iron supply, the focus during KEOPS was on two contrasting sites in particular- station A3 (located on the Plateau in the core of the bloom; 50.62°S, 72.07°E) and C11 (located off-shelf in typical of HNLC waters; 51.65°S, 78.00°E). A3 and C11 were sampled 3 times (24/01, 03/02 and 12/02) and 2 times (26/01 and 5/02) respectively for Ba_p; the other stations were visited once. Here, the different repeats of A3 and C11 consist in the 3rd, 4th and 5th visits for A3 (the two first visits of A3 were not sampled for Ba_p), and in the 1st and 2nd visits for C11, respectively. In the following, we use both the station and CTD numbers to refer to stations.

8.3. RESULTS

[156] Particulate Ba_{xs} concentrations are reported in Table 8.1. At most sites, particulate biogenic Ba_{xs} represented >95 % of total particulate Ba.

However, lithogenic Ba was particularly high at shallow plateau stations such as C1-100 with 78 to 87% of total particulate Ba (Table 8.1). At station B5-60 and to a lesser extent station C5-91, lithogenic Ba reached up to 20% of total Ba_p, especially in approach of the seafloor (at 526 m and 550 m, respectively). Therefore, we expect that subtracting the lithogenic Ba fraction induced a larger error on the Ba_{xs} numbers at B5 and at C1 and C5 at some discrete depths; at the other stations the lithogenic fraction was very small (<5%) and thus the impact on the precision of the Ba_{xs} results was minimal.

[157] At plateau stations A3 and B1, Ba_{xs} concentrations in the upper 125 m were quite high (>1000 pM), while margin and off-shelf stations had Ba_{xs} concentrations ≤400 pM (see contrast in Figure 8.2 between stations A3-119 and B11-50). The very high Ba_{xs} contents reached in the surface layer at A3 (up to 5900 pM; 50 m cast 73; Table 8.1) are quite unusual, though similar values were occasionally observed in earlier S.O. studies [Dehairs et al., 1992, 1997; see also Chapter 7]. Furthermore at A3, significant temporal changes in Ba_{xs} content occurred. Depth weighted average concentrations (DWAv; Table 8.2) of Ba_{xs} in the upper 125 m first increased from 578 (CTD 32; Jan. 24th) to 4125 pM (CTD 73; Feb. 3rd), but subsequently decreased to 2493 pM (CTD 119; Feb 12th).

Transect A

A3-32 (bottom depth: 525 m)

Niskin	Depth	Baxs [pM]	% Baxs/Bap	Al [nM]
22	10	576	95	21.9
20	31	142	90	11.9
18	50	1355	98	20.3
16	74	557	99	5.8
14	100	436	97	8.3
12	124	274	96	8.4
10	150	408	96	13.9
8	199	190	94	9.0
6	249	320	95	13.6
5	300	420	96	13.4
3	348	412	94	18.0
2	399	536	92	32.6
1	451	630	91	47.4

A3-73 (bottom depth: 525 m)

Niskin	Depth	Baxs [pM]	% Baxs/Bap	Al [nM]
24	10	2800	100	5.5
21	50	5930	100	4.6
20	74	5814	100	3.4
18	99	2249	99	17.3
17	125	3213	99	12.4
15	150	269	96	8.2
14	199	330	99	3.2
13	249	255	96	7.2
11	298	231	99	1.2
10	349	335	94	16.3
9	399	564	98	8.5
8	450	825	99	8.1

A3-119 (bottom depth: 525 m)

Niskin	Depth	Baxs [pM]	% Baxs/Bap	Al [nM]
23	12	517	98	6.1
21	30	1766	100	4.4
19	51	2638	100	8.3
17	75	4115	100	8.1
14	101	2826	99	11.1
11	150	287	98	4.5
9	200	255	97	6.7
8	250	306	96	10.7
6	299	403	96	11.9
5	349	304	97	8.2
3	400	493	96	14.3
2	449	356	93	19.1

A11-11 (bottom depth: 2600 m)

Niskin	Depth	Baxs [pM]	% Baxs/Bap	Al [nM]
24	8	59	86	7.2
23	30	272	96	9.2
21	76	152	91	11.1
20	101	99	89	9.5
19	125	267	95	10.8
18	150	546	91	40.3
17	199	146	93	7.7
10	249	437	95	17.3
9	300	252	94	12.8
8	349	393	94	17.7
6	448	564	90	46.7
5	499	521	95	18.8
4	549	275	88	28.0
3	648	338	94	16.5
2	798	387	93	23.0

Transect B

B1-68 (bottom depth: 400 m)

Niskin	Depth	Baxs [pM]	% Baxs/Bap	Al [nM]
24	10	306	97	7.0
22	50	2761	100	6.9
18	74	2918	100	4.3
17	100	352	98	4.2
13	126	282	98	4.9
12	152	334	98	4.6
11	199	308	95	10.9
7	249	472	95	19.5
6	297	1013	96	31.9

B5-60 (bottom depth: 526 m)

Niskin	Depth	Baxs [pM]	% Baxs/Bap	Al [nM]
24	11	418	92	25.4
22	51	286	93	16.5
21	76	324	93	18.1
20	99	289	93	16.1
19	126	239	91	17.6
18	149	228	84	31.3
14	200	298	80	54.8
10	249	105	79	20.9
9	299	556	88	57.3
5	349	560	90	45.5
4	400	700	81	120.6
1	451	199	81	34.6

B11-50 (bottom depth: 3270 m)

Niskin	Depth	Baxs [pM]	% Baxs/Bap	Al [nM]
24	11	186	98	2.9
20	99	134	100	0.4
16	151	306	98	3.5
14	200	128	98	2.2
11	250	547	95	19.7
9	299	798	97	16.4
8	350	589	99	3.4
4	400	548	99	6.2
3	453	458	99	3.6

Transect C

C1-100 (bottom depth: 140 m)

Niskin	Depth	Baxs [pM]	% Baxs/Bap	Al [nM]
24	10	596	23	1523
21	30	578	23	1420
17	49	552	20	1674
12	76	386	19	1221
10	102	359	13	1838
5	119	323	13	1573
4	131	573	20	1686

C5-91 (bottom depth: 550 m)

Niskin	Depth	Baxs [pM]	% Baxs/Bap	Al [nM]
24	11	127	96	3.8
22	50	130	95	4.6
21	75	100	100	0.0
20	100	162	96	4.9
19	124	227	96	7.1
18	149	422	95	15.0
17	198	335	93	18.2
16	250	423	88	42.4
15	298	444	91	32.2
14	348	505	95	18.8
13	398	557	98	8.3
12	450	429	80	77.3
1	498	403	81	68.2

C11-42 (bottom depth: 3350 m)

Niskin	Depth	Baxs [pM]	% Baxs/Bap	Al [nM]
24	9	386	98	4.6
21	49	370	98	4.5
19	75	181	98	3.1
17	98	241	98	4.2
16	125	410	99	2.4
14	150	234	99	1.4
13	199	314	98	5.7
12	250	503	98	8.2
10	301	292	98	3.3
8	400	221	98	2.7
7	450	368	98	6.7
6	499	246	99	1.1
5	550	688	97	17.0
4	649	336	97	7.7
3	798	519	98	7.9

C11-83 (bottom depth: 3350 m)

Niskin	Depth	Baxs [pM]	% Baxs/Bap	Al [nM]
24	11	317	98	5
20	50	218	96	7
19	74	96	98	1
18	99	218	97	5
15	150	237	98	4
13	249	450	98	5
11	300	450	99	2
9	349	528	99	3
8	399	502	99	3
7	449	1051	98	13
5	548	357	99	2
4	649	484	99	2
3	798	431	98	6

Table 8.1: Excess biogenic particulate Ba (Ba_{xs}; pM) and particulate Al (nM) at KEOPS stations. $\%Ba_{xs}/Ba_p$ represents the non-lithogenic fraction of the total particulate Ba signal.

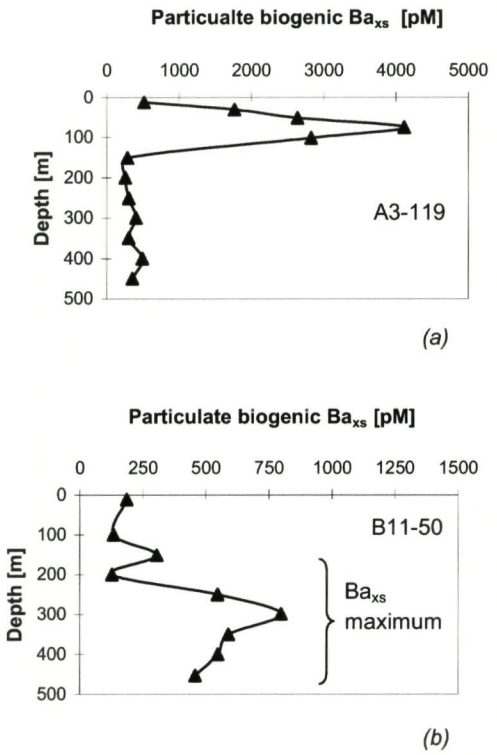


Figure 8.2: Profile of excess biogenic particulate Ba (Ba_{xs}; pM) at stations A3-119 and B11-50.

[158] The upper mesopelagic layer (125-450 m) at the margin and off-shelf stations (C5, C11, B5 and B11) shows the characteristic broad Ba_{xs} maximum (as illustrated in Figure 8.2-b for station B11-50) with concentrations reaching between 500 and 1050 pM at discrete depths (Table 8.1). Mesopelagic Ba_{xs} values exceeding 1000 pM have been recorded previously in the complex frontal region of the Crozet-Kerguelen Basin (see Chapter 3). While at station C11, DWAv Ba_{xs} values for the 125-450 m layer increased from 309 pM (CTD 42; Jan 26th) to 493 pM (CTD 83; Feb 6th) over a 10 day period; at station A3, Ba_{xs} contents remained rather stable over a 19 day period and even displayed a slight decrease from 401 pM (CTD 32; Jan 24th) to 342 pM (CTD 119; Feb 12th) (Table 8.2). The lowest and highest DWAv mesopelagic Ba_{xs} values during KEOPS were both observed at station C11 (309 and 493 pM for CTD 42 and 83 respectively). At station B11, the DWAv mesopelagic Ba_{xs} content was also quite high (474 pM), being only slightly lower than the value at station C11-83. Overall, it is interesting to note that the highest mesopelagic Ba_{xs} contents (>450 pM) were reached in

off-shelf environments (C11, B11), while margin and shelf environments demonstrated lower mesopelagic Ba_{xs} values (≤ 400pM at all A3 casts; B5). C5 served as an exception, reaching ~450 pM. This is opposite to the situation in the upper 125 m layer, which demonstrated higher Ba_{xs} contents at plateau stations compared to margin and off-shelf stations.

Station	Seafloor [m]	0-125 m	125-450 m
A3_32	525	578	401
A3_73	525	4125	370
A3_119	525	2493	342
A11_11	2600	171	391
B1_68	400	1458	-
B5_60	526	322	403
B11_50	3270	157	474
C1_100	140	468	-
C5_91	550	140	447
C11_42	3350	315	309
C11_83	3350	219	493

Table 8.2: Depth weighted average Ba_{xs} contents (pM) in the 0 to 125 m and the 125 to 450 m (= upper mesopelagic) depth layers.

8.4. DISCUSSION

Plateau vs. off-shelf environments

[159] Primary production at A3 was high (864-1872 $mgC/m^2/d$) compared to C11 (216-384 $mgC/m^2/d$) (data from B. Griffith in Lefèvre et al., in review), but at both these stations the bloom was mainly sustained by diatoms. These consisted of large cells at A3 and smaller cells at C11 [Armand et al., in review]. At A3, the Ba_{xs} signal in the upper 125 m during the different repeats (data in Tables 8.1 and 8.2) followed the variations in primary productivity, Chl_a [Uitz et al., pers. comm.], and BSi variations [Mosseri and Quéguiner, in review]. Thus while at plateau stations, higher biological activities were reflected by the higher Ba_{xs} contents in the upper 125 m (stations A3, B1), at margin and off-shelf sites (stations C5, A11, B11, C11) lower surface Ba_{xs} contents were in agreement with the lower biological activity at these sites. Based on SEM-EMP (scanning electron microscopy-electron microprobe) investigations, Stroobants et al. [1991] conclude that particulate Ba_{xs} in the surface waters is dispersed over different biogenic, non-barite phases (see also Cardinal et al., 2005 and further Chapter 10) while in the mesopelagic water column, on the contrary, Ba_{xs} is mainly composed of discrete barite particles, as shown earlier by Dehairs et al. [1980]. Though it is not yet totally clear how the surface and mesopelagic Ba_{xs} signals are

linked, current belief is that the mesopelagic Ba_{xs}, carried mainly by barite, is precipitated within $BaSO_4$ saturated micro-environments (i.e. aggregates, pellets), which are Ba-enriched because of the composition of the particles composing the micro-environment [Bishop, 1988], and/or which take up dissolved Ba up from the medium while sinking from the surface mixed layer and degrading with time [Collier et al., 1984; Dehairs et al., 2000; see also Chapters 5 and 6]. Mesopelagic barite micro-crystals persist in $BaSO_4$ saturated waters, their stocks reflecting the intensity of the mesopelagic mineralization process [Dehairs et al., 1997]. In contrast to the situation for the surface layer (upper 125 m), our observations indicate that the off-shelf environments (stations C11-83 and B11) give rise to higher mesopelagic Ba_{xs} contents compared to the plateau sites A3 and B5. Thus, the most intense mesopelagic mineralization appears to be taking place in the off-shelf environment. Our results furthermore suggest a significant increase of mesopelagic mineralization over time at off-shelf station C11, while at plateau station A3 the system seems to evolve at steady state.

Mesopelagic Ba_{xs} and bacterial production

[160] Previous studies have highlighted the relationship between mesopelagic Ba_{xs} contents and organic matter mineralization [Dehairs et al., 1980; 1992; 1997; Cardinal et al., 2005]. Therefore, we expect mesopelagic Ba_{xs} content to be related to bacterial activity. During KEOPS, assessment of bacterial production (BP) was mostly limited to the upper 200 m (^{3}H-leucine method; Christaki et al., in review), prohibiting a direct comparison with mesopelagic Ba_{xs} contents. However, we suspected that vertical gradients of integrated bacterial production in the upper 200 m could also possibly provide information on the potential for significant BP to extend to depths exceeding 200 m, as was observed during recent work in the North Pacific [Dehairs et al., in preparation-b]. The underlying rationale is that steep, shallow gradients of integrated BP presumably indicate efficient, close to complete mineralization within the upper 200 m of the water column with relatively little organic matter left for consumption by bacteria deeper in the water column. On the contrary, weak gradients of integrated BP in the upper 200 m would indicate that significant bacterial activity is still ongoing at depths exceeding 200 m.

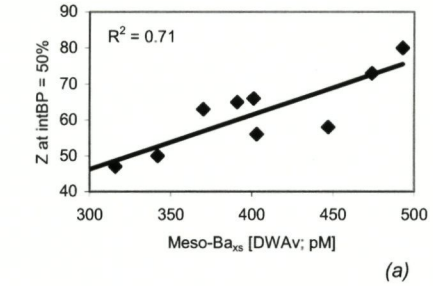
[161] For KEOPS, we verified several regressions in order to check whether the depth to which significant bacterial production extends is somehow related with the Ba_{xs} content in the upper mesopelagic (125-450 m) (Table 8.3). Depth weighted (125–450 m) average mesopelagic Ba_{xs} was plotted vs. (1) water

column height wherein 50% of the 200 m integrated BP takes place, and (2) the ratio of integrated BP in the upper 200 m over integrated BP in the upper 125, 100, 80 m and the mixed layer (ML). DWAv mesopelagic Ba_{xs} appears significantly correlated ($p<0.05$) with the water layer where 50% of the upper 200 m integrated BP occurs (see also Figure 8.3-a) and the ratio of 200 m over 125 (see also Figure 8.3-b), 100, and 80 m integrated BP. However, it is not significantly correlated with the ratio of 200 m over ML depth integrated BP (Table 8.3). These observations suggest indeed that systems where bacterial activity extends well below the mixed layer (i.e. high ratio of 200 m over 125, 100 and 80 m integrated BP) are more efficiently exporting organic matter to greater depths for subsequent mineralization in the mesopelagic region. An implication of such a scenario is that it is the general plankton community parameters (species composition, cell sizes, phytoplankton biomass...) in the surface layer that define whether export of mineralizable material will be shallow or deep, and that bacteria merely follow the food.

Linear regression (y=b+ax)	R^2	b	a	p
BPintZ = 50% of BPint200m vs. Meso-Ba_{xs}	0.712	0.709	0.152	0.0043
Ratio of BPint200m over BPint125m vs. Meso-Ba_{xs}	0.551	0.788	0.0010	0.0225
Ratio of BPint200m over BPint100m vs. Meso-Ba_{xs}	0.452	0.764	0.0016	0.0474
Ration of BPint200m over BPint80m vs. Meso-Ba_{xs}	0.539	0.711	0.0026	0.0242
Ratio of BPint200m over /BPint ML vs. Meso-Ba_{xs}	0.171	0.240	0.0047	0.2687*

* not significant

Table 8.3: Regression of the upper water column depth where 50% of the integrated bacterial production (BP) in the upper 200 m is achieved versus mesopelagic Ba_{xs} contents and regressions of integrated BP gradients in the upper 200 m vs. 125, 100, 80 and mixed layer depth versus mesopelagic Ba_{xs} content.



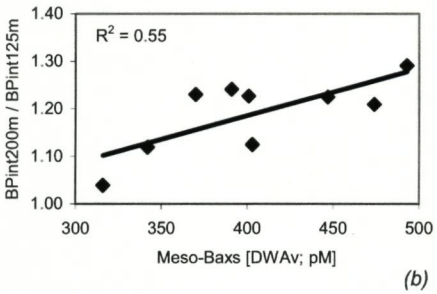


Figure 8.3: (a) Regression of upper water column depth where 50% of the integrated bacterial production (BP) in the upper 200 m is achieved versus depth weighted average (DWAv) mesopelagic excess particulate Ba (Ba_{xs} in pM); (b) regression of the ratio of upper 200 m integrated BP over upper 125 m integrated BP versus depth weighted average (DWAv) mesopelagic Ba_{xs} (pM).

Mesopelagic C mineralization vs. PP, BCD and EP

[162] We translated Ba_{xs} DWAv into C fluxes using Equations 1 and 2 (see methods section). Saturation index calculation (SI; Monnin and Cividini, 2006), confirmed that the upper mesopelagic water (125-450 m) in the whole study area is in equilibrium with barite (0.9<SI<1.1) (Figure 8.4-a); 180 pM were thus taken as representative of the Ba_{xs} background, i.e. the Ba_{xs} content at zero mineralization. Moreover, calculations indicated that there is a return to undersaturation of the water column at depths of about 1500 m (Figure 8.4-b). In the upper 125 m, on-shelf and margin stations also presented undersaturation at discrete depths (Figure 8.4-a).

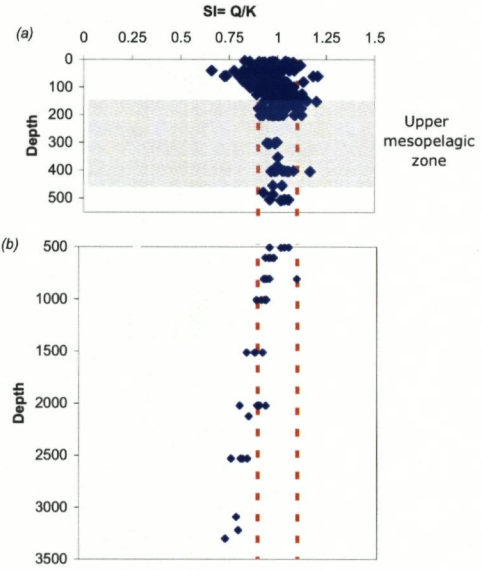


Figure 8.4: Saturation index (SI) of barite in the upper 500 m water column (*a*) and between 500 and 3500 m (*b*).

[163] In Table 8.4 we compare mineralization integrated over the 125-450 m depth layer with primary production (PP) integrated over the euphotic layer (^{14}C-incorporation data from B. Grifftith in Lefèvre et al., in review and ^{13}C-incorporation data from N. Garcia in Mosseri and Quéguiner, in review), bacterial carbon demand (BCD; calculated as BP/BGE, with a mean BGE bacterial growth efficiency= 20% as determined for A3-73) integrated over the upper 200 m (data from Obernosterer et al., in review), and export of carbon from the 125 m horizon (EP; ^{234}Th method, data from Savoye et al., accepted). Ba_{xs}, PP, BCD and EP were not always analyzed for the same CTD casts, but data were obtained for casts sampled close by in time and space. Mesopelagic mineralization values range between 21 and 48 mgC m^{-2} d^{-1}. Such mineralization fluxes are similar to those observed during summer in the PFZ in the Crozet – Kerguelen basin and along 145°E [Cardinal et al., 2001; see also Chapter 3].

All fluxes in mgC/m²/d

Station	PP [1]	BCD[2]	EP [3]	Mesopelagic remin. [4]		
Ba cast	*euphotic layer*	*0-200 m*	*125 m*	*150-450 m*	%	Meso-remin. [4] vs. EP [3]
A3-32	1872	1705	264	34		13
A3-73	1644	830	223	29		13
A3-119	864	1005	266	25		9
A11-11	1400*	1170	216	32		15
B5-60	1250*	765	140	34		24
B11-50	250*	265	106	45		42
C5-91	350*	235	74	41		55
C11-42	384	340	114	21		18
C11-83	216	261	124	48		39

1 PP= Primary Production, based on ^{14}C-incorporation (data from B. Griffith, in Lefèvre et al., in review)

* PP based on ^{13}C-incorporation(data from N. Garcia, in Mosseríe and Quéguiner, in review)

2 BCD= Bacterial Carbon Demand; from Obernoster et al. (in review) and Christaki et al. (in review)

3 EP= Export Production, based on ^{234}Th data; from Savoye et al. (in review)

4 Mesopelagic remineralization, based on meso-Ba_{xs} data

Table 8.4: Comparison of Ba_{xs} based mesopelagic C mineralization with primary production (PP), bacterial carbon demand (BCD) and export production (EP); all fluxes in mgC m^{-2} d^{-1}.

[164] Our observations indicate that the largest mesopelagic mineralization (up to 48 mgC m^{-2} d^{-1}) occurs in the less productive off-shelf region (stations C11-83 and B11), while the highly productive A3 site is characterized by lower mineralization rates (25 mgC m^{-2} d^{-1} at A3-119) (Table 8.4). Furthermore, the off-shore site C11 shows the most drastic change over time, from lowest mesopelagic mineralization on January 26th to highest on February 6th (from 21 to 48mg C m^{-2} d^{-1}). Though export of C (EP) from the 125

m horizon is twice as large at A3 compared to C11, it represents only ~20% of PP at A3, while at C11 it represents approximately 45% of PP (Table 8.4). Moreover at C11, while EP remains relatively stable over a 10 day period, the remineralization flux more than doubled over that same period. Also at C11, a larger fraction (from 18 to 39%) of the carbon exported out of the upper 125 m was remineralized in the 125-450 m depth layer; at A3 mineralization in the 125-450 m layer ranged only between 9 and 13% (Table 8.4). This indicates that on the plateau, a larger fraction of organic carbon exported from the upper 125 m crosses the mesopelagic layer and probably reaches the seafloor at ~525 m. Thus, although the system above the plateau (station A3) is exporting in a less efficient manner than the off-shelf system (station C11), the transfer efficiency of the exported matter through the mesopelagic layer at A3 is larger than at C11 (see illustration in Figure 8.5). This appears to be related to the vertical distribution of the bacterial activity, itself significantly linked to the plankton biomasses. Mosseri and Quéguiner [in review] report that the phytoplankton community at A3 (predominantly larger diatoms) was mainly utilizing (during the 5th visit) ammonium produced from organic nitrogen remineralization by an active community of bacteria [Christaki et al., in review] and mesozooplankton [Carlotti et al., in review]. This agrees with the picture drawn above indicating that significant shallow mineralization occurs above the plateau together with more efficient transfer through the mesopelagic layer of the organic matter that escaped shallow mineralization. The latter could result from the fact that larger particles composed of large diatoms (Chaetoceros spp. and Eucampia Antarctica; Armand et al., in review) and sinking aggregates and fecal pellets [Ebersbach and Trull, in review] are present at A3. Such conditions would likely favor fast and deep export, short-circuiting mesopelagic processing of organic matter. On the contrary at C11, small diatoms (Fragilariopsis pseudonana) were predominant [Armand et al., in review] with zooplankton biomass being less, thus providing for relatively more important mesopelagic mineralization.

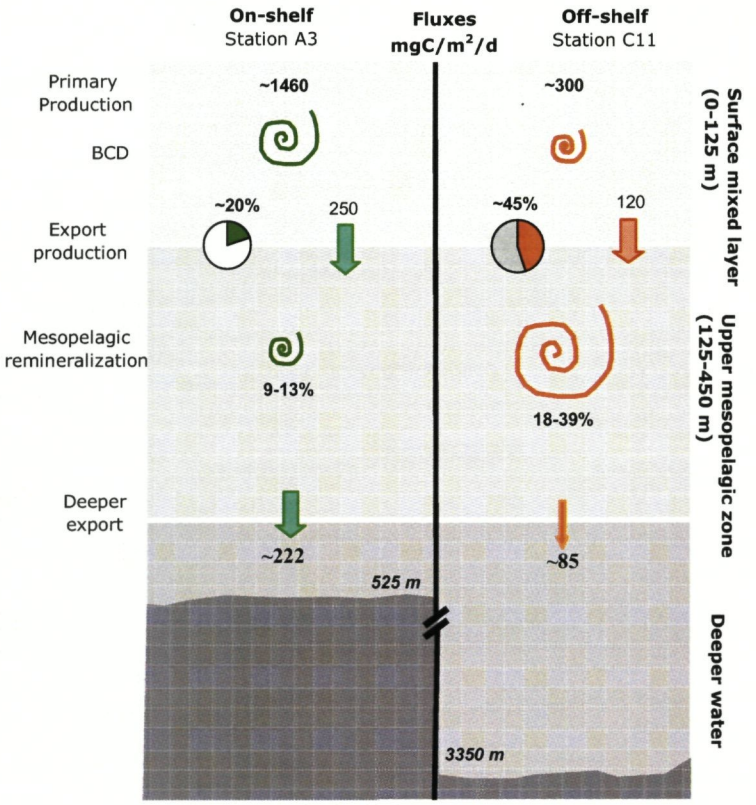


Figure 8.5: Illustration of the Plateau (A3) vs. off-shelf (C11) environments functioning.

8.5. CONCLUDING REMARKS

[165] Particulate biogenic Ba_{xs} distribution in the mesopelagic waters appears closely tuned by bacterial production in the overlying water column. The general picture emerging is that bacterial production which extends deeper in the water column generally sustains larger mesopelagic Ba_{xs}, as opposed to bacterial production restrained to a shallower surface layer. With mesopelagic particulate Ba_{xs} reflecting organic matter mineralization, our findings indicate that the off-shelf open ocean east of the Kerguelen Plateau is a region of relatively more important deep water column processing of exported matter as compared to the plateau. Thus, the fate (mesopelagic mineralization) of organic carbon exported from the upper water column of the Kerguelen Plateau area is quite different between the shelf region proper and the margin, open ocean region. Indeed,

though the primary production above the shelf area between Heard Island and Kerguelen is strongly boosted by a natural supply of iron, the fraction of PP exported from the upper 125 m is smaller for the shelf system as compared to the open ocean system [Savoye et al., accepted]. This probably results from significant mineralization within the upper layer of the water column, leaving material available for export that is less prone to mesopelagic mineralization (125-450 m). As a result, the on-shelf system provides for a more efficient delivery of organic carbon below 450 m in the water column, as compared to the open ocean HNLC system, despite the fact the export ratio (export production vs. primary production) is lower (see Figure 8.5).

Chapter 9

Twilight zone organic C mineralization in the North Pacific

Foreword

[166] Based in the statement that what grows up must fall down, Chapter 7 and Chapter 8 investigated the potential impact of climate change on plankton and carbon export. These studies are part of a multi-pronged approach whose target is the fate of iron-induced bloom and associated sinking particles; the goal being to refine the issue of significant, or not, carbon sequestration by ocean fertilization. Here in Chapter 9, we leave the Southern Ocean for the North Pacific (VERTIGO 1 & 2 cruises) and focus on determining more specifically what controls the magnitude and efficiency of the particle transport: what is the fate of sinking particles leaving the upper ocean and what factors influence mineralization length scales.

SUMMARY

[167] Suspended matter profiles were obtained for the oligotrophic station ALOHA (Hawaii) and the mesotrophic subarctic Pacific station K2, using CTD rosette with Niskin bottles and a Multiple Unit Large Volume Filtration System (MULVFS). While at ALOHA the excess (i.e. non-lithogenic) Ba profiles obtained via repeated sampling, showed remarkable consistency between the sampling systems as well as little variability over a period of three weeks, suggesting that the system was close to being at steady state, more variability and higher excess Ba (Ba_{xs}) concentrations were observed for K2. Both at ALOHA and K2 Ba concentrations were low (<50 pM) in the upper mixed layer (70 m), but increased through the upper mesopelagic waters (down to 500 m) where average concentrations reached 160 and 400 pM at ALOHA and K2, respectively. Below 500 m, down to 1000 m (the deepest waters sampled), concentrations remained fairly unchanged at ALOHA but decreased at K2, thereby producing a clear barium maximum in the mesopelagic waters at the latter site. This distribution reflects production of particulate Ba (shown for other systems to be carried mainly be micro-crystalline barite) to take place below the upper mixed layer and to be ongoing in the twilight zone, as recently emphasized in Van Beek et al. [2007]. This general picture is quite similar to what has been observed for other oceanic systems where this production of excess Ba has been linked to export and mineralization of organic matter. We compared Ba_{xs} signals in the 150 to 500 m mesopelagic depth interval with integrated bacterial carbon demand and POC flux decrease (i.e microbial and zooplankton C demand) as obtained from Neutrally Buoyant Sediment Trap (NBST) deployments over the same depth interval. Particulate Ba_{xs} correlated well with bacterial production and carbon demand, highlighting the potential for the development of a transfer function relating Ba_{xs} and bacterial carbon demand. Furthermore, application of a different transfer function, relating mesopelagic Ba_{xs} and oxygen consumption, was in good agreement (though slightly lower) with carbon demand based on bacterial production. Finally the comparison between carbon demand calculated from Ba_{xs} (and bacterial production) with POC flux decrease over depth from NBST's showed good agreement in 3 out of 4 cases. For one situation at K2, carbon demand exceeded POC flux decrease from NBST. However, carbon demand was positively correlated with NBST POC fluxes at 500 m when normalized to the 150 m fluxes. Overall, these results indicate that mineralization at ALOHA site was more intense and was mainly confined to the upper 100 m, while at K2 site, proportionally more material was exported to deeper layers where it fuelled deep heterotrophic activity as reflected by enhanced particulate Ba_{xs} contents.

9.1. INTRODUCTION

[168] This work is part of the VERTIGO (VERtical Transport In the Global Ocean) research effort which focuses on the processes controlling the efficiency of particle export between the surface and deep ocean. During VERTIGO, several approaches to assess carbon export and mineralization fluxes were compared at two contrasting locations in the Pacific where large differences in magnitude of particle flux, composition of sinking and suspended particles and remineralization length scales were expected: (**1**) the oligotrophic Hawaii Ocean Time series station ALOHA (22°45'N-158°W; see Karl et al., 1996) sampled during June–July 2004 and (**2**) the High Nutrient Low Chlorophyll Japanese time station K2 located near the centre of the subarctic gyre (47°N-161°W) and sampled during July-August 2005. The approaches included new production [Elskens et al., in preparation], particles flux assessment via neutrally buoyant sediment trap (NBST) devices [Buesseler et al., in press, Stanley et al., 2004], ^{234}Th deficit [Buesseler et al., in preparation], bacterial and zooplankton carbon demand [Van Mooy et al., in preparation; Steinberg et al., in preparation]. Earlier work has shown that mesopelagic accumulation of particulate biogenic Ba, present mainly as barite, does reflect mineralization of exported organic matter in the twilight zone [Dehairs et al., 1980; 1992; 1997]. We took the opportunity offered by the VERTIGO research effort to confront the particulate Ba proxy approach with two other modes of carbon utilization assessment: bacterial carbon demand and POC flux decrease with depth obtained from NBST's (the interest in NBST is in that it drifts with the currents, thus eliminating hydrodynamic effects which can lead to particle sorting and flux biases).

9.2. SITES DESCRIPTION

[169] The contrasts between the ALOHA and K2 sites are large regarding strength and source characteristics (carbonate vs. silicate predominance) of the biological pump [Buesseler et al., in preparation, in press]. ALOHA is an oligotrophic site, characterized by low chlorophyll, low f-ratios and low upper ocean export fluxes. Coccolithophorids were present at ALOHA site but a diatom community actually dominated the biomass of test producing phytoplankton [Silver et al., in preparation]. At the subarctic mesotrophic K2 site, characterized by high surface nutrients, including silica [Talley, 1999], diatoms were the dominant group [Silver et al., in preparation]. New production estimates at both sites indicate larger potential for export at K2 compared to ALOHA [Elskens et al.,

in preparation]. Bacteria and zooplankton biomasses at K2 were significantly higher at K2 than at ALOHA [Steinberg et al., submitted].

9.3. RESULTS

[170] Suspended matter was sampled for particulate Ba, Sr and Ca analyses using Niskin bottles (see Chapter 1) and also by in-situ filtration using filter holders (holding 47 mm Nuclepore membranes of 0.4 µm porosity) mounted on side arms of Multiple Unit Large Volume Filtration Systems (MULVFS; Bishop et al., 1985). In-situ pumping lasted between 3 and 5 hours and seawater volumes filtered through the side arm filter holders ranged between 10 (upper water column) and 40 L (at 1000 m).

[171] Figure 9.1 shows the averaged Ba_{xs} profiles obtained at both sites.

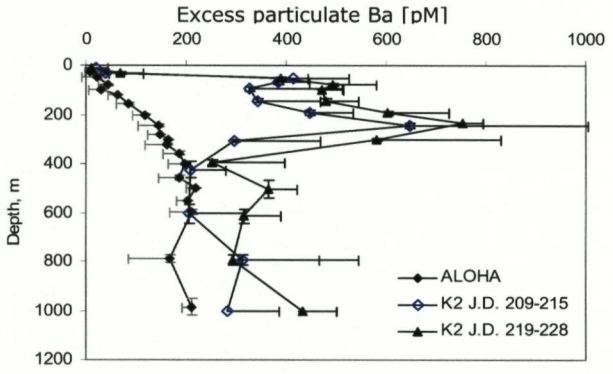


Figure 9.1: Reconstituted average profiles of excess particulate Ba at ALOHA and K2 sites; for ALOHA all cast were averaged (7 casts); for K2 averages shown are those for casts taken during NBST deployment 1 (Julian day 209 to 215; 5 casts) and 2 (Julian day 219 to 228; 5 casts). Error bars are 1 SD.

At ALOHA the average Ba_{xs} profile (based on 5 CTD casts and 2 MULVFS casts) shows concentrations to increase with depth from about 30 pM in the upper 100 m to 200 pM between 400 and 600 m. Below 500 m concentrations remain close to the maximum value. Variability of the Ba_{xs} content over 3 weeks time is relatively small at ALOHA. At station K2 average profiles are shown for the first (Jul. 28^{th} – Aug. 3^{rd}; 3 CTD and 2 MULVFS casts) and second half (Aug. 8^{th} – 14^{th}; 3 CTD and 2 MULVFS casts) of the occupation period, to highlight the Ba_{xs} increase with time. Surface water Ba_{xs} contents at K2 are also very low (<50 pM)

but increase sharply with depth to reach maximum values between 200 and 400 m and contrasting with a more gradual Ba_{xs} increase with depth at ALOHA. The very low surface water Ba_{xs} contents at ALOHA and K2 contrast with observations for the Southern Ocean where occasionally very high values, even exceeding 1000 pM, have been reported for the surface mixed layer [Dehairs et al., 1997; Cardinal et al., 2001; Chapters 3 and 7] and which in at least one situation was associated with presence of large numbers of $SrSO_4$ secreting acantharia (see Chapter 10). At K2 the subsurface Ba_{xs} maximum appears subdivided into a shallow maximum around 50 to 80 m, just below the Chl-a maximum located at 50 to 60 m [Boyd et al., in preparation], reaching up to 490 pM and a deeper but larger maximum between 150 and 400 m reaching up to 650 pM (see Figure 1). At depths >300 m, average Ba_{xs} contents decrease again to range between 200 and 400 pM during the first half of the observation period and between 250 and 430 pM during the second half. Overall variability of the Ba_{xs} contents was much larger at K2 than at ALOHA, in agreement with more dynamic conditions of water mass circulation and of ecosystem functioning at K2. Over the period of study the ALOHA site remained confined inside an anticyclonic vortex [Siegel et al., in preparation], a condition which probably contributed to maintaining a relatively stable production regime. At K2, the currents in the upper 500m (Oyashio current) were consistently in eastward direction [Siegel et al., in preparation], and larger day to day variability of suspended matter composition might be related with variability in productivity and community composition upstream of the sampled area. Also, a substantial shift in phytoplankton cell size and primary production occurred during the occupation of the K2 site [Boyd et al., in preparation; Elskens et al., in preparation]. These contrasting conditions in subsurface and mesopelagic waters between ALOHA and K2 likely reflect differences in export and mineralization regimes between both environments.

[172] In contrast to Ba_{xs}, particulate Sr and Ca contents are highest in the upper 50 m (ALOHA: up to 850 pM and 39 nM, respectively) and decrease with depth (Figure 9.2). While surface water Sr concentrations at ALOHA significantly exceed those at K2 (850 vs 230 pM, respectively), deeper in the water column (>100 m) Sr contents are similar between both sites. Overall Sr at K2 shows little variability with depth. The overall low particulate Sr content at ALOHA and K2 (<1 nM), compared to the 10 times higher concentrations during a situation with abundant acantharia (see Chapter 10), suggests that acantharia were not present in significant numbers at the North pacific sites studied here. Ca contents are more similar between both sites, though values at ALOHA clearly

exceed those at K2 (in particular see 50-150 m depth region in Figure 9.2). Al contents vary considerably at K2 (from <0.1 to an exceptional 63 nM), but in general concentrations are low in the surface waters (<5 nM) and increase with depth (Figure 9.1). Al concentrations at ALOHA do not reach such high values (<15 nM) and neither do Al profiles exhibit an increase with depth as observed at K2.

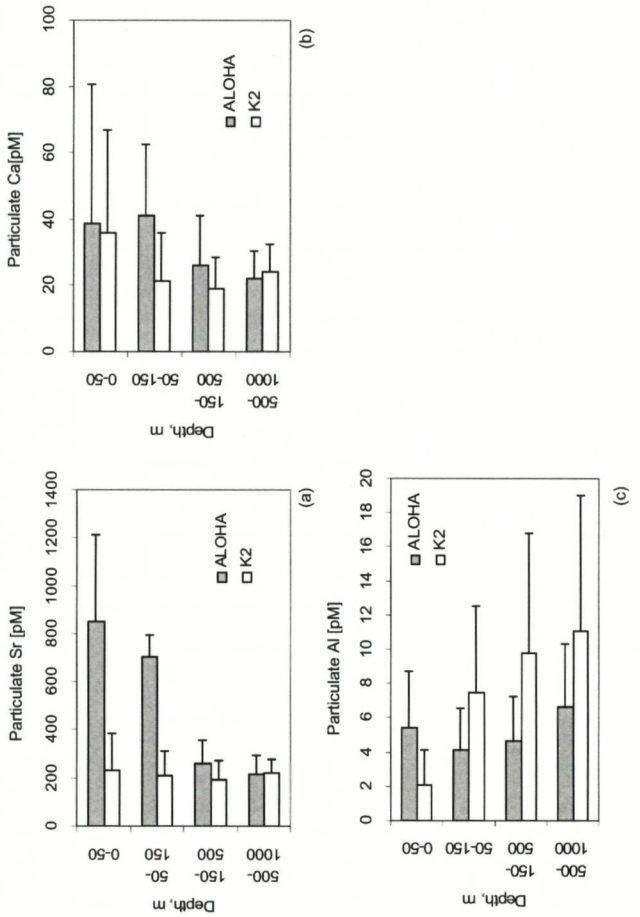


Figure 9.2: ALOHA (grey bars) and K2 (white bars) sites. Depth weighted average particulate (*a*) Sr(nM), (*b*) Ca (nM), (*c*) Al (pM); concentrations in the 0to 50 m, 50 to 150 m, 150 to 500 m and 500 to 1000 m depth regions. Data shown are averages of all casts; error bar = 1 SD (ALOHA: 7 casts; K2: 10 casts).

9.4. DISCUSSION

Comparing subsurface and mesopelagic Ba_{xs} contents at ALOHA and K2

[173] Figure 9.1 illustrates the large differences in concentrations and profile shapes between ALOHA and K2 sites, which are particularly salient in the subsurface and mesopelagic waters. The upper mesopelagic Ba_{xs} signal is low and stable over time at ALOHA, while at K2 signals are larger, more variable and there is a tendency toward higher values during station occupation (Figures 9.1 and 9.3). Considering that the Ba_{xs} signal is related with export and degradation of organic matter [Dehairs et al., 1992, 1997] our data indicate more intense production, export and processing of exported organic material in the HNLC subarctic Pacific as compared to the oligotrophic subtropical ALOHA site. This is in agreement with significantly higher biomasses, productivities and POC export fluxes reported for K2 [data from Saitoh/Okamoto; Buesseler et al., in press; Boyd et al., in preparation; Elskens et al., in preparation]. On the other hand, the trend of increasing Ba_{xs} over time at K2 (a 66% increase on average; Figure 9.3) is not observed for Chl-biomass in the upper 200 m (Chl varies but there is no clear temporal trend; 37.5 µg l^{-1} ± 5.6; data from Saitoh/Okamoto), nor for primary production, with average column integrated primary production actually decreasing from 530 mgC m^{-2} d^{-1} (Julian day 209 to 215) to 365 mgC m^{-2} d^{-1} (Julian day 219 to 228) [Boyd et al., in preparation].

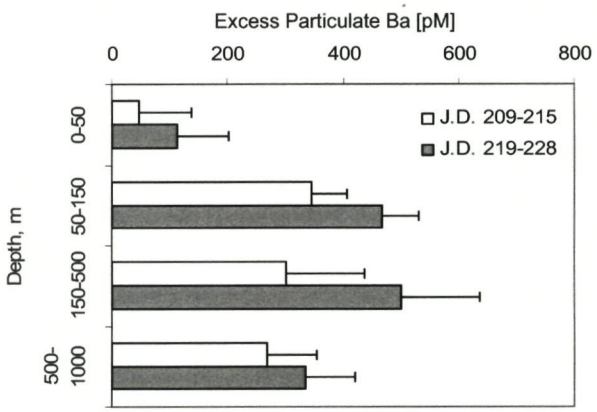


Figure 9.3: Station K2: temporal evolution of depth weighted average excess Ba concentrations (pM; erro bars represent 1 s.d) in the 0 to 50 m, 50 to 150 m, the 150 to 500 m and the 500 to 1000 m layers of the water column, for cast sampled during the first (Julian day 209 to 215; 5 cast: white bars) and the second NBST deployment (Julian day 219 to 228; 5 casts; grey bars).

[174] Also, at K2 average Sr and Ca contents in surface and mesopelagic waters decrease during occupation of the site (9 and 27% on average, respectively; Figure 9.4), thus more in agreement with the primary productivity temporal trend.

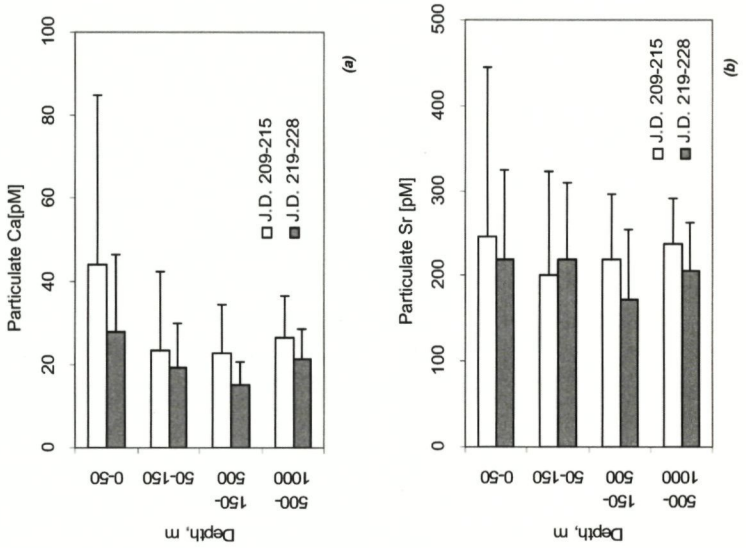


Figure 9.4: Station K2. Average Ca (nM; a) and Sr (pM; b) in the upper 0 to 50 m, 50 to 150 m, 150 to 500 m and 500 – 1000 m layers of the water column, for casts sampled during the first (Julian days 209 to 215; 5 casts; white bars) and the second NBST deployment (Julian days 219 to 228; 5 casts; grey bars). Error bars represent 1 SD.

Particulate Al (data not shown), on the contrary, behaves differently from Sr and Ca and shows a 26% increase during occupation of the K2 site, thereby following Ba_{xs}. These observations highlight the peculiar condition of Ba_{xs} which in essence is not carried with other biogenic phases such as carbonate and celestite (acantharia), but is most likely present essentially as microcrystalline barite, as observed for other oceanic systems. Since former S.O. work on Ba_{xs} in fine suspended matter has indicated that mesopelagic processing of exported material as reflected by Ba_{xs} has a phase lag relative to the upper ocean processes [Dehairs et al., 1997; Cardinal et al; 2001; 2005], we do not expect mesopelagic Ba_{xs} to be in phase with surface water biomass and production. In the following we will check whether there is any relationship between Ba_{xs} and bacterial activity, as our observations in the S.O. suggest.

Ba_{xs} contents and bacterial production

[175] Bacterial production (BP) determined using [^{3}H]-thymidine (TdR) incorporation incubations conducted at atmospheric pressure and in situ temperature [Fuhrmann and Azam, 1982]. BP was calculated from TdR conversion factors of 2.10^{18} cells mol^{-1} and a carbon conversion factor of 15 fgC $cell^{-1}$; these values approximate the median of those published for bacterial communities in surface waters [Ducklow, 2000]. While the influence of pressure on BP conversion factors have not yet been systematically examined, there is no a priori reason to expect that they should vary with depth and conversion factors for surface communities are commonly applied to the mesopelagic. However, the TdR incorporation rates derived from incubation conducted at atmospheric pressure may underestimate true rates, and thus, the BP rates we present here are conservative. Bacterial carbon demand (BCD) was calculated using a bacterial growth efficiency (BGE) range of 0.15 [delGiorgio and Cole, 2000; Ducklow, 2000; Steinberg et al., in preparation], which is also derived from published values for surface bacterial communities. Bacterial production data shown here are discussed in Steinberg et al. [in preparation] and Van Mooy et al. [in preparation]; details on the incubation protocols and assumptions regarding conversions factors and BGE will be found in these papers.

[176] For comparison with Ba_{xs} we will only consider BP data for casts reaching 1000 m, i.e. the deepest depth sampled for Ba_{xs}. The column (1000 m) integrated BP values are not very different between ALOHA and K2 sites (overall range is between 69 and 97 $mgC/m^2/d$) with K2 values even being slightly lower (69 and 93 $mgC/m^2/d$) than ALOHA values (83 and 98 $mgC/m^2/d$). However, there is a clear difference between both sites in terms of surface to deep gradients in BP. At ALOHA this gradient is steep and most of the BP is localized in the upper 100m (Figure 9.5), while at K2 significant BP goes on deeper in the water column. We note that upper 100 m integrated BP relates inversely with depth-weighted average Ba_{xs} in mesopelagic waters (150 to 500 m depth layer; Figure 9.6-a), suggesting that intensive bacterial mineralization in the upper part of the water column (the case for ALOHA) leaves little organic material to be decomposed (thereby forming barite) in the mesopelagic waters below. At K2 a less steep BP gradient reflects significant bacterial activity to extend deeper in the water column.

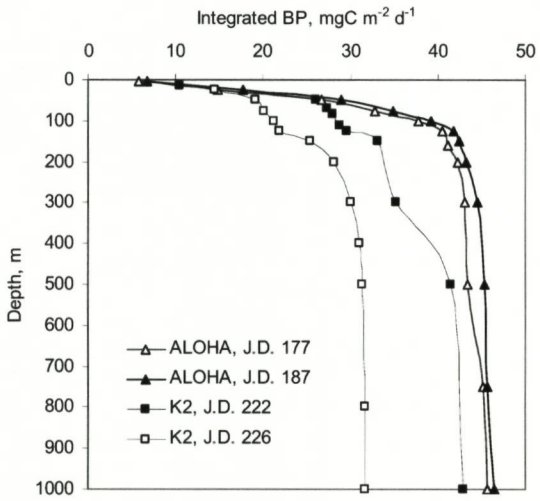


Figure 9.5: Profiles of integrated bacterial production (mgC/m^2/d) in upper 1000 m at stations ALOHA (open triangles, Julian day 117; closed triangles, Julian day 187) and K2 (closed squares, Julian day 222; open squares, Julian day 226). Data from Van Mooy et al. [in preparation].

[177] In the following we focus specifically on the 150 to 500 m depth interval where the K2 mesopelagic Ba_{xs} maximum is located and where the NBST's were deployed. Figure 9.6-b compares the integrated BP values with depth weighted average Ba_{xs} values for the 150 to 500m depth interval at ALOHA and K2. Clearly, both variables appear highly correlated: increasing BP leads to increasing Ba_{xs} concentration in mesopelagic waters. Though only 4 casts were suited for direct comparison between BP and Ba_{xs} content we were nevertheless tempted to calculate the relationship translating mesopelagic Ba_{xs} into bacterial organic carbon demand. Taking a BGE value of 0.15 into account, the following linear regression between mesopelagic Ba_{xs} and bacterial carbon demand (BCD) holds: $Ba_{xs} = 5\ BCD - 40$ (with Ba_{xs} in pM and BCD in mg C m^{-2} d^{-1}). In essence this equation reflects that a given mesopelagic Ba_{xs} concentration is maintained as a result of a certain bacterial organic carbon consumption rate. In earlier work on the Southern Ocean we proposed a simple relationship between mesopelagic Ba_{xs} and the rate of oxygen consumption deduced from a 1D advection-diffusion model applied on highly resolved, precise oxygen profiles [Shopova et al., 1996; Dehairs et al., 1997; see Chapter 1]. It is tempting to compare the outcome of that S.O. relationship based on oxygen consumption with the one deduced here, based on bacterial carbon demand.

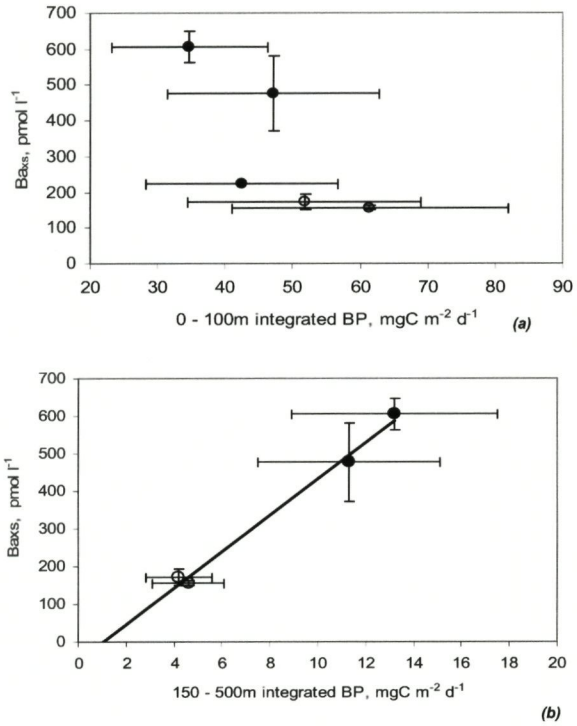


Figure 9.6: ALOHA and K2 sites; (*a*) depth weighted average excess particulate Ba (pM) in the 150 to 500 depth layer (data points are averages of two casts; error bars represent 1 SD) compared with bacterial production ($mgC/m^2/d$) integrated over the upper 100 m (each data point represents a single cast with error bars representing the BP ranges based on different values for bacterial activity conversion coefficient; see text); (*b*) comparison between bacterial production integrated over the 150 to 500 m domain and the depth weighted average excess particulate Ba content (Ba_{xs}, pM). ALOHA, open circles; K2, closed circles.

[178] In earlier work in the Southern Ocean we proposed a simple relationship between mesopelagic Ba_{xs} and the rate of oxygen consumption deduced from a 1D advection-diffusion model applied on highly resolved, precise oxygen profiles [Shopova et al., 1996; Dehairs et al., 1997]. It is tempting to compare the outcome of that S.O. relationship based on oxygen consumption with the one deduced here, based on bacterial carbon demand. For K2 such a comparison with the S.O. system seems warranted, since both systems have diatoms as a dominant component of the phytoplankton community [Silver et al., in preparation] and since water temperatures in the mesopelagic layer are similar (typically ranging between 1.5 and 3.5°C). ALOHA of course is quite different with

higher temperatures, a larger temperature gradient through the upper mesopelagic (typically 8 to 22°C), and hosting a quite different algal community with diatoms present, but dominated by nano and picoplankton and including nitrogen fixers [Silver et al., in preparation]. We will nevertheless assume the S.O. transfer function relating mesopelagic Ba_{xs} content with oxygen consumption applies also for this sub-tropical North Pacific environment. The transfer function for O_2 demand (and thus C demand) based on Ba_{xs} requires subtraction of a background Ba_{xs} value (i.e. residual Ba at zero C demand), a value which is likely dependent on the $BaSO_4$ saturation state of the ambient sea water. For S.O. waters, known to be saturated for $BaSO_4$ [Monnin et al., 1999; Monnin and Cividini, 2006] this Ba_{xs} residual is about 200 pM [Dehairs et al., 1997]. North Pacific waters, on the contrary, appear undersaturated for $BaSO_4$ in their upper 1000 m [Monnin et al., 1999]. We checked possible differences in saturation between both sites. Dissolved Ba concentrations in the upper 500 m at ALOHA are about half those observed at K2 (30 to 45 nM and 65 to 97 nM, respectively) (not shown; pers. data). Calculated $BaSO_4$ saturation conditions for ALOHA indicate undersaturation in the upper 500 m while at K2 saturation seems to be reached in the upper mesopelagic (Figure 9.7; C. Monnin, pers. communication). To take these differences in saturation conditions into account we considered a smaller Ba_{xs} residual value (0 to 50 pM) at ALOHA than at K2 (100 to 150 pM; see Table 9.1).

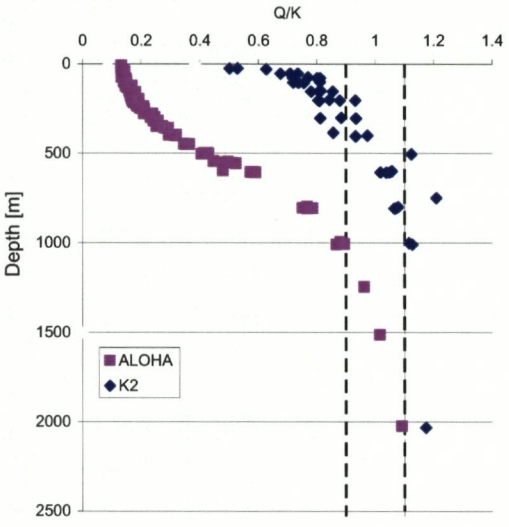


Figure 9.7: SI for K2 and ALOHA

[179] Table 9.1 compares calculations of carbon demand based on bacterial activity and own mesopelagic Ba_{xs} content. It appears that both approaches converge quite well and yield similar magnitudes of carbon demand, though Ba_{xs} based carbon demand is generally closer to the lower end of the BCD range. Considering the uncertainty on the different conversion factors utilized in both calculations this similarity is nevertheless remarkable and emphasizes the usefulness of Ba_{xs} in fine suspended matter as proxy of organic matter degradation in the twilight zone. In the next section we investigate the relationship between mesopelagic Ba_{xs} and the NBST POC fluxes.

Site Timing	**Bacterial Carbon demand** [1] $mgC/m^2/d$	**C min. based on Ba_{xs}** [2] $mgC/m^2/d$
ALOHA		
J.D. 177	19-56	22 – 31 *
J.D. 187	20-61	19 – 28 *
K2		
J.D. 223	50-151	58 – 67 **
J.D. 226	58-175	81 – 89 **

min-max data

[1] calculated as BP/0.15

[2] calculated as [127/175]*[(Ba_{xs} – residual)/17200)], from Dehairs et al. [1997]

* residual Ba_{xs} taken as 50 and 0 pM, resp.

** residual Ba_{xs} taken as 150 and 100 pM, respectively

Table 9.1: ALOHA and K2 sites: Carbon demand over the 150 to 500 m depth region, based on bacterial carbon demand and mesopelagic Ba_{xs} content; comparison is based on individual casts which were different for BP and Ba, but were sampled within a day's interval. BP data from Steinberg et al. [in preparation] and Van Mooy et al. [in preparation].

Mesopelagic Ba_{xs} and NBST POC fluxes

[180] Based on the POC fluxes recorded by neutrally buoyant sediment traps (NBST) Buesseler et al. [in press, in preparation] report lower transfer efficiencies (i.e. the ratio of 500 m PC flux over 150 m POC flux) at ALOHA compared to K2. This condition is reflected by a larger 'Martin-curve' b-value [Martin et al., 1987] of 1.3 for ALOHA compared to a value of 0.5 for K2 [Buesseler et al., in review]. Higher b-values at ALOHA reflect the fact that the combined microbial and zooplankton communities there are tuned for rapid turn-over of the exported material, leaving little material for deeper export and resulting in a short mineralization length scale. At K2 the combined microbial and zooplankton specific activity is less efficient, allowing for organic matter to escape, thereby increasing the mineralization length scale. Overall the condition of larger POC fluxes and increased transfer efficiencies to deeper waters at K2 translates into larger mesopelagic Ba_{xs} inventories there as compared to ALOHA.

[181] In Table 9.2 we compare C demand calculated from mesopelagic Ba_{xs} in the 150 to 500 m layer with loss in POC flux as recorded by the NBST's between 150 and 500 m [Buesseler et al., in review] for ALOHA and K2 sites. Note that the Ba_{xs}-based C demand calculations in Table 9.2 are based on averages of several casts sampled during the respective NBST deployments, while the earlier comparisons with bacterial carbon demand (see Table 9.1) are on a cast by cast basis.

Site Event Timing	**NBST ΔPOC flux[1]** (150-500m) $mgC/m^2/d$	**C min. based on Ba_{xs}** (150-500m) $mgC/m^2/d$	**New production[2]** $mgC/m^2/d$
ALOHA			
depl #1: J.D. 178 - 182	14.4	20 – 29 ± 4** (3)	30
depl #2: J.D. 186 - 191	14.4	19 – 28 ± 1** (4)	30
K2			
depl # 1: J.D. 209 - 215	33	27 – 36 ± 22*** (5)	151
depl # 2: J.D. 219 - 225	10	64 – 73 ± 18*** (5)	72

[1] NBST POC flux data from Buesseler et al. [in preparation]

[2] New production data from Elskens et al. [in preparation]

** residual Ba_{xs} taken as 50 and 0 pM, resp.

*** residual Ba_{xs} taken as 150 and 100 pM, resp.

Table 9.2: ALOHA and K2 sites: Estimates of POC mineralization between 150-500 m; comparison between NBST POC flux decrease (ΔPOC flux) and C demand based on excess Ba; Ba values shown are averages for several casts (n) sampled during the duration of the NBST deployments.

POC flux decreases with depth recorded by the traps must reflect the combined effects of bacterial and zooplankton carbon demands, with BCD being estimated to account only about half of this (i.e. 55% and 65% of total carbon demand at K2 and ALOHA respectively; Steinberg et al., submitted). Since earlier work suggests mesopelagic Ba_{xs} is more likely associated with bacterial activity rather than with zooplankton grazing and respiration [Stroobants et al., 1990; Dehairs et al., 1992; Cardinal et al., 2001, 2005] we do not a priori expect a good coherence between both approaches. However, the values of both approaches are quite similar, at least for ALOHA and the first NBST deployment at K2 (Table 9.2). This does not hold for the second NBST deployment at K2 with Ba_{xs}-based mesopelagic mineralization exceeding several times trap recorded POC loss between 150 and 500 m (Table 9.2). Mesopelagic Ba_{xs} increased over time at K2, while NBST POC fluxes decreased following new production which decreased two-fold (from 151 to 72 mgC m^{-2} d^{-1}; Elskens et al., in preparation and see Table 9.2). We now investigate some possible scenarios offering a possible explanation for this discrepancy.

[182] Between both NBST deployments at K2 the contribution of larger phytoplankton (>20 µm) to primary production decreased from 30 to 19% [Boyd et al., in preparation] possibly inducing the observed decrease of POC flux during the second NBST deployment. We are uncertain whether this same condition of increased contribution of smaller sized phytoplankton to primary production would have inversely affected the mesopelagic Ba_{xs} stock. It is likely though that decreased phytoplankton cell sizes would rather favor water column organic matter accumulation as opposed to sinking thereby enhancing mesopelagic mineralization and yielding increased Ba_{xs} contents. However, at K2 the mesopelagic transfer efficiency, T_{eff} (i.e. ratio of 500 m POC flux over 150 m POC flux), is 46% and 55% for deployment #1 and #2, respectively [Buesseler et al., in preparation]. Thus the fact that flux attenuation for both NBST deployments at K2 is similar and even slightly less during the second NBST deployment at K2, speaks against enhanced mineralization during the 2nd NBST deployment. We notice furthermore that mesopelagic Ba_{xs} contents relate positively with the 500 m NBST POC fluxes normalized to the 150 m POC fluxes, including the 2nd NBST trap data at K2 (Figure 9.8), contrasting with the comparison based on absolute POC flux values discussed above.

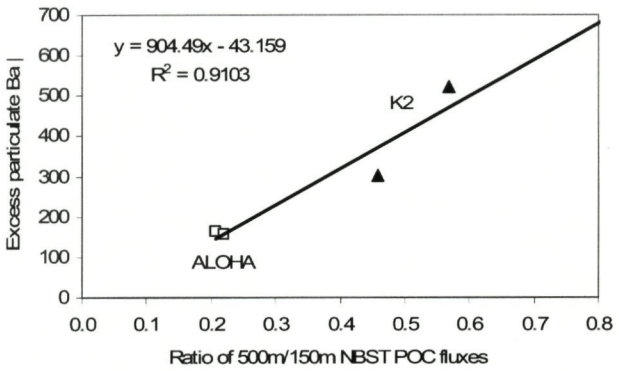


Figure 9.8: ALOHA and K2 sites. Depth weighted average excess particulate B (150-500 m) compared with ratio of NBST POC flux at 500 m over POC flux at 150 m.

[183] This then suggests mesopelagic Ba_{xs} to be related with the ecosystem's mode of operation, such as for instance trophic structure and relative importance of the microbial loop, and not necessarily with magnitude of contemporaneous carbon export flux (which is smaller during the second NBST deployment at K2). Finally, we note that next to Ba_{xs}, also Al contents in the upper 500 m increased over time at K2 (data not shown), maybe indicating advection of fine suspended matter (aluminosilicates and probably organic matter as well) less susceptible to fast sinking. Indeed during the entire occupation of the K2 site strong westerly currents prevailed [Siegel et al., in preparation] possibly advecting material from the nearby Kamtchaka and Sea of Okhotsk continental shelves and sills [Lam and Bishop, in review].

[184] Though at this point no fully satisfactory explanation can be offered to account for the discrepancy between Ba_{xs} based mesopelagic mineralization and POC flux decrease during the second deployment at K2, available results nevertheless sustain the idea that export of POC is carried essentially by two categories of particles. **(i)** A first category consisting of large and fast sinking aggregates such as fecal pellets which are dependent on the relative importance of zooplankton in the trophic structure (a condition that did remain relatively constant between NBST deployment 1 & 2 at K2 [Steinberg et al., in review], and which sustain an attenuation profile that is rather independent of export magnitude (b-values don't change over time). IRS trap results indicate that up to 70% of the POC flux at K2 was carried by fast sinking particles (sinking speeds exceeding 105m d^{-1}; Trull et al., in review), emphasizing the significance of this

category of particles in setting the POC flux profile. **(ii)** A second category would consist of phytoplankton cells not selected for by the grazers since of smaller size and forming aggregates which sink more slowly since smaller and less densely packed than fecal pellets. These may thereby partially escape collection by the traps. Though barite has been identified inside large sized fecal pellets [Dehairs et al., 2000] we expect that it rather are the more slowly sinking, less dense aggregates which are the major loci of barite formation [Stroobants et al., 1990]. Since these slower sinking particles appear not to represent the major component of POC flux recorded by the traps, coherence between water column Ba_{xs} inventory based and trap flux attenuation based mineralization need not necessarily exist.

9.5. CONCLUDING REMARKS

[185] This work investigated particulate Ba contents in the upper 1000m of the water column at two North Pacific sites (the oligotrophic ALOHA and the HNLC K2 time series sites) which contrast strongly in terms of carbon production and export. It appears that the vertical distributions of particulate non-lithogenic Ba (i.e. excess Ba or Ba_{xs}) in the water column also are quite contrasted with higher mesopelagic Ba_{xs} contents for the more productive K2 system which also supports higher organic carbon export. We observed mesopelagic Ba_{xs} contents to be closely correlated with bacterial carbon demand, providing a relationship which converges with the one relating mesopelagic Ba_{xs} to O_2 consumption rate established during earlier work. This offers prospects for better constraining mineralization of particulate organic matter exported to the twilight zone. Differences in respiration and degradation rates by the heterotrophic communities between ALOHA and K2 sites, next to the mass-effect of exported POC (which is larger at K2), are responsible for the differences in mesopelagic Ba_{xs} contents between both sites. For equal POC export we expect that more Ba_{xs} is produced in the mesopelagic waters in situations where the specific activity of the heterotrophs at the bottom of the upper mixed layer is not too high, leaving organic matter for deeper export and continued (slower) breakdown. However, it is also possible that the observed differences in mesopelagic heterotrophic activity between both sites in fact directly result from differences in export intensity between both sites with lower export fluxes *in se* (case of ALOHA) leading to more efficient re-mineralization by the heterotrophs (i.e. heterotrophs are adapted to the prevailing export regime and the least food there is the more efficient heterotrophs are in consuming it).

Chapter 10

Particulate Ba_{xs}, barite and acantharians

Foreword

[186] In this chapter we return in the Southern Ocean and we investigate an alternative scenario of barite precipitation in the water column, by which barite could be biologically mediated. We confront particulate Ba_{xs}, barite, Sr and Ca from suspended matter with acantharians distribution and Ba/Sr skeleton contents, in order to shed light on the potential role of acantharians in the barite formation process (EIFEX).

SUMMARY

[187] Particulate biogenic Ba, Sr and Ca and barite crystal contents from suspended matter were compared with acantharian water column distribution and individual Ba/Sr acantharian skeleton ratio during the European Iron Fertilization Experiment (EIFEX) in the Southern Ocean. In the upper 150 m, results indicate that the particulate biogenic Ba_{xs} signal is almost free from barite ($BaSO_4$) particles and follows the same evolution as biomass parameters, implying that Ba is incorporated in or adsorbed onto biologically derived (biogenic) particles of which acantharians could account up to 96% of Ba contents. In contrast, in the mesopelagic zone (150-1000 m), particulate biogenic Ba_{xs} is mainly composed of micro-crystalline barite. Calculation estimates indicate that acantharian-associated Ba in the upper 150 m and between 150-500 m, if entirely transformed into barite- an unlikely condition- and dispersed in the 150-1000 m and 150-500 m layers respectively, could explain up to 18 and 10% of the mesopelagic Ba_{xs} contents, respectively. Our results indicate that acantharians are probably not the major source of particulate Ba-barite in the water column. They support the hypothesis that mesopelagic Ba_{xs} is mostly built-up as the result of biogeochemical processes within aggregates and its usefulness as a proxy of mesopelagic C remineralization processes as recently strengthened by Dehairs et al. [in preparation-b] and in Chapter 8 and Chapter 9.

10.1.INTRODUCTION

[188] Micro-crystalline barite ($BaSO_4$) is an ubiquitous component of suspended matter in the open ocean [Dehairs et al., 1980]. At the start of Section 3 we presented the potential mechanisms of barite formation in the water column. The scenario debated is that inside micro-environments (biogenic aggregates), Ba subtraction from solution, oxidation of organic sulfur and/or release of biogenic Ba or Sr (from e.g. acantharian celestite) could lead to barite precipitation. Here, we will test the hypothesis that barite could be directly or indirectly biologically mediated. Indeed, while Bernstein et al. [1992; 1998] and Bernstein and Byrne [2004] report that incorporated Ba in the celestite skeletons of acantharians could lead to barite precipitation during skeleton dissolution, Esser and Volpe [2002] and Ganeshram et al. [2003] provided evidence that acantharians are not a prerequisite for the formation of barite. Both possible main barite formation loci (acantharian or decaying plankton) are not just limited to the upper mixed layer but are likely to occur also in waters below. Because of the high solubility of celestite ($SrSO_4$) in the water column [Bernstein et al., 1987; Prieto et al., 2003] and the use of sampling techniques consistently underestimating acantharian abundance [Michaels et al., 1995], their quantitative importance in the barite precipitation process remains unclear. Next to their potential impact on the strontium and barium cycles, Michaels et al. [1995] also suggested that acantharian could significantly contribute to total C fluxes in the surface mixed layer (~upper 150 m). Quantification of acantharian abundance and the temporal variability of their distribution would thus seem integral to any study of C budget, particularly in the Southern Ocean. The role of acantharian has too often been ignored, even if they are ubiquitous and abundant, normally surpassing foraminiferans and siliceous radiolarians in numbers [Michaels, 1988, 1995; De Deckker et al., 2004].

[189] Based on the association of barite formation with bacterial degradation of organic matter, the meso-Ba_{xs} signal is used to date as an indirect proxy for mesopelagic mineralization of exported biogenic material [Dehairs et al., 1997, in preparation-b; Cardinal et al., 2001, 2005; see also Chapter 9]. Next to this application, Ba-based proxies (e.g. total barium, Ba_{xs}, Ba-barite) in marine sediments should reflect aggregates that have been exported to the seafloor (i.e. not remineralized in the intermediate zone) and are therefore used for (paleo)-productivity reconstitutions [Dehairs et al., 1991; Dymond et al., 1992; Paytan et

al., 1993; Gingele and Dahmke, 1994; François et al., 1995; Bonn et al., 1998; Murray et al., 2000; Eagle et al., 2003; Gonneea and Paytan, 2006]. However, the issues outlined above lead to questions about quantitative use of the Ba proxies; better constraining the barite formation process in the water column is thus crucial for any of their applications [De Deckker et al., 2004; Bernstein and Byrne, 2004; Anderson et al., 2005]. Indeed, if barite results mainly from bacterial degradation of organic matter, sedimentary barite could be related to surface production and meso-Ba_{xs} to C remineralization using an empirical relationship relating Ba_{xs} to O_2 consumption rates [Shopova et al., 1995; Dehairs et al., 1997], but if barite formation appears to be driven by acantharian, sedimentary barite would reflect productivity via the corresponding acantharians population growth, and meso-Ba_{xs}, as translated into C mineralization fluxes, would underestimate total mineralization processes. It is thus important to quantify which part acantharian-derived Ba could really supply to the water column Ba_{xs} signal.

[190] The present chapter aims at contributing toward a better understanding of the potential role of acantharian in the Ba and Sr dynamics. We report results from the European Iron Fertilization Experiment (EIFEX), carried out in the Atlantic sector of the Southern Ocean (S.O.). Here, we compare particulate Ba, Sr, Ca and barite crystals from suspended matter, with the acantharian water column distribution and their individual Ba/Sr skeleton contents; stations were monitored for a 37-day observation period with focus on the upper 1000 m of the water column.

10.2.EXPERIMENT

[191] EIFEX (cruise ANT XXI/3 of R/V *Polarstern*; 21 Jan.-25 Mar. 2004) was carried out in a mesoscale cyclonic eddy located in a meander of the Polar Front. The physical setting of the experiment is described by Strass et al. [2005]. The water mass in the eddy, centered at roughly 50°S-2°E, was characteristic of the Antarctic Circumpolar Current (low temperature, HNLC conditions) and showed iron depletion (0.08-0.2 nM; Hoffmann et al., 2006). 7 tones of iron sulphate were added to an area of 150 km^2 on February 12-13 after an initial sampling to determine the pre-fertilization conditions; T= -1 reflects the conditions before the iron release, which occurred on day zero (T0). A second iron release into the previously fertilized patch was undertaken on February 26-27 (day 12). The outcome of the fertilizations was monitored over 36 days after the

initial iron release. Samples were collected at stations both inside and outside the iron-fertilized patch (hereafter referred to as IN and OUT stations, respectively), though all stations reported in this study were located inside the eddy. IN and OUT patch stations were defined by surface parameters (e.g. photosynthetic activity Fv/Fm, Fe, Chl a and pCO_2 data).

[192] During EIFEX, Chl a concentrations had increased more than fivefold by day 25 and then decreased toward the end of the experiment, while particulate organic matter followed a similar pattern, declining after day 29. These findings indicate the demise of the iron-induced bloom [Hoffmann et al., 2006]. The massive increase in Chl a concentrations was mainly due to the growth of long chain-forming diatoms [Assmy et al., in preparation]. A deep and fast export has been clearly characterized during EIFEX, as revealed by surface sediment [Sachs et al., in preparation] and ^{234}Th [data from N. Savoye in Strass et al., in preparation] data.

10.3.RESULTS

Particulate biogenic Ba_{xs}

[193] Particulate biogenic Ba_{xs} distribution was followed over a 37-day observation period during EIFEX (Figure 10.1). Profiles in the mesopelagic zone (150-1000 m) have been discussed in Chapter 7. We showed that while at T= -1, the Ba_{xs} profile displayed a typical mesopelagic maximum between ~200 and 500 m (reflecting the occurrence of a previous naturally induced bloom), the latter decreased within the first 21 days. Subsequent Ba_{xs} profiles exhibited relatively high and homogeneous mesopelagic contents spreading up to 1000 m; the same trend was observed at OUT stations from day 11 to 34. Moreover, we reported that the differentiation between "IN" and "OUT"-patch stations (based in surface parameters) does not hold for conditions at mesopelagic depths: particulate biogenic Ba_{xs} particles were highly influenced by the eddy dynamics, leading to the spreading of the mesopelagic particles originating from the patch to a wider area within the eddy.

[194] Profiles in the upper 150 m present a different trend (Figure 10.1). Ba_{xs} contents in the surface layer increased from T= -1 (~200 pM) to day 28 (IN) reaching up to 950 and 2000 pM in the very surface and at 80 m, respectively. Subsequent values decreased again to ~400 pM at the end of the experiment (day 36). OUT patch profiles in the upper 150 m also have increasing Ba contents

which reached a maximum at day 34 at 80 m (~1000 pM). The occurrence of such high subsurface Ba_{xs} contents (e.g. at day 28 IN and day 34 OUT), has been reported earlier by Dehairs et al. [1997] and in Chapter 8 for the PFZ in the Atlantic (from 1000 to 9100 pM) and Indian (from 1355 to 6000 pM) sectors of the Southern Ocean.

[195] During EIFEX, depth weighted average Ba_{xs} values (DWAv; Table 10.1-a) range from 197 to 732 pM (integration between 0-150 m) and from 271 to 452 pM (integration between 150-500 m); note that integrations were made on these two depth layers in order to allow direct confrontation with the Sr, Ca and acantharian data sets. IN-patch DWAv values highlight the large differences between the surface and mesopelagic Ba_{xs} signal, with higher values found in the upper 150 m. OUT patch, DWAv differences between the 0-150 and 150-500 m integrated signals are smaller.

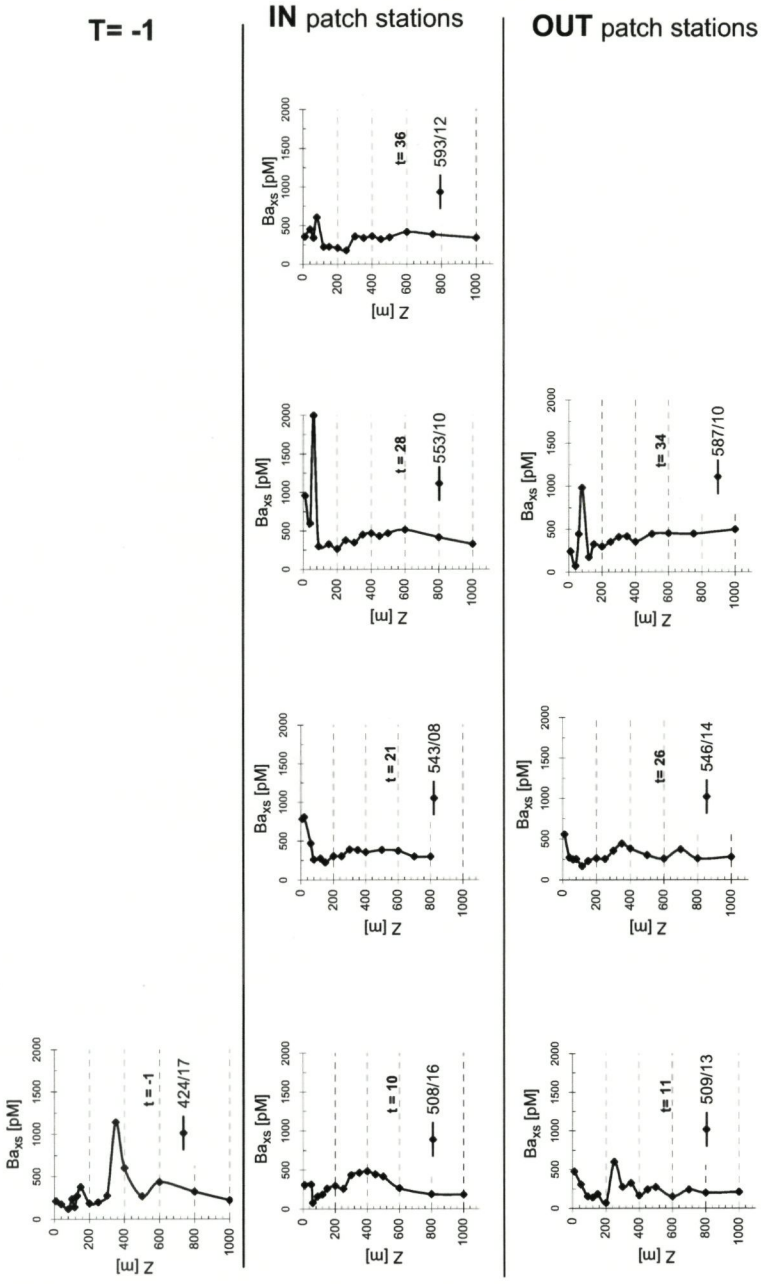


Figure 10.1: Particulate biogenic Ba_{xs} profiles (pM; 0-1000 m) during EIFEX.

Table 10.1: Depth-weighted average values for Ba_{xs} (pM), Sr_p (nM) and Ca_p (nM) (a; 0-150 and 150-500 m) and for <50 µm, >50µm and total acantharians (b; indiv/m^3; 0-150 and 150-350 m), during EIFEX.

(a)

	Station	Time (d)	Ba_{xs} [pM] 0-150m	Ba_{xs} [pM] 150-500m	Sr_p [nM] 0-150m	Sr_p [nM] 150-500m	Ca_p [nM] 0-150m	Ca_p [nM] 150-500m	Sr/Ca 0-150m	Sr/Ca 150-500m
	424/17	-1	197	452	2.4	0.48	41.0	42.9	0.047	0.012
IN	508/16	10	238	386	3.6	0.41	51.8	27.2	0.060	0.016
patch	543/08	21	495	338	26.7	0.50	98.5	4.5	0.067	0.027
	553/10	28	732	390	11.9	0.76	165.1	33.2	0.108	0.026
	593/12	36	377	294	9.0	0.56	119.3	27.0	0.086	0.026
OUT	509/13	11	244	271	6.1	0.15	68.9	11.9	0.070	0.012
patch	546/14	26	265	329	3.6	0.40	52.6	32.2	0.069	0.012
	587/10	34	390	371	3.8	0.49	59.7	28.9	0.065	0.018

(b)

	Station	Time (d)	Acanth.<50 µm [indiv/m^3] 0-150m	Acanth.<50 µm [indiv/m^3] 150-350m	Acanth.>50 µm [indiv/m^3] 0-150m	Acanth.>50 µm [indiv/m^3] 150-350m	Total Acanth [indiv/m^3] 0-150m	Total Acanth [indiv/m^3] 150-350m
	424/17	-1	23249	5066	31947	5068	55197	10182
IN	508/16	10	42824	1994	36662	1241	79486	3236
patch	543/08	21	44586	6766	75532	4755	120118	11520
	553/10	28	42362	6877	50204	2634	92566	9511
	593/12	36	31342	5360 *	50098	3944 *	81440	9305 *
OUT	509/13	11	37147	2283	35949	2081	73095	2170
patch	546/14	26	22254	3981	15892	1282	38145	5263
	587/10	34	25151	4014 *	24377	2710 *	49528	6724 *

** Integration done between 150-500 m*

Particulate Sr and Ca

[196] Particulate Sr and Ca depth profiles are shown in Figure 10.2; depth weighted average values are reported in Table 10.1-a. IN patch contents are high in the upper 150 m (from 6 to 23 nM for Sr_p and from 30 to 530 nM for Ca_p) but decrease sharply deeper in the water column where values are more uniform and low, ranging from ~0.1 to 0.6 nM for Sr_p (Figure 10.2-a) and from ~5 to 30 nM for Ca_p (Figure 10.2-b), in general agreement with other observations in the Southern Ocean [e.g. Dehairs et al., 1992; Cardinal et al., 2001]. Sr_p contents in the upper 150 m increased from T= -1 to day 28 when they reach maximum values in subsurface (~23 nM at 60 m). Ca_p profiles are quite similar to those of Sr_p and also reach maximum values (up to ~530 nM) at day 28. OUT patch profiles, on the contrary, show lower surface Sr_p and Ca_p contents, decreasing from day 11 to 34. Sr_p depth weighted average values range from 2.4 to 26.7 nM (integration between 0-150 m) and from 0.48 to 0.76 nM (integration between 150-500 m). Ca_p DWAv values range from 41 to 165 nM (0-150 m) and from 4.5 to 42.9 nM (150-500 m) (Table 10.1-a). As for Ba_{xs}, DWAv for Sr_p and Ca_p emphasize the expected differences IN patch between the surface and mesopelagic signals, with particularly high values found in the upper 150 m.

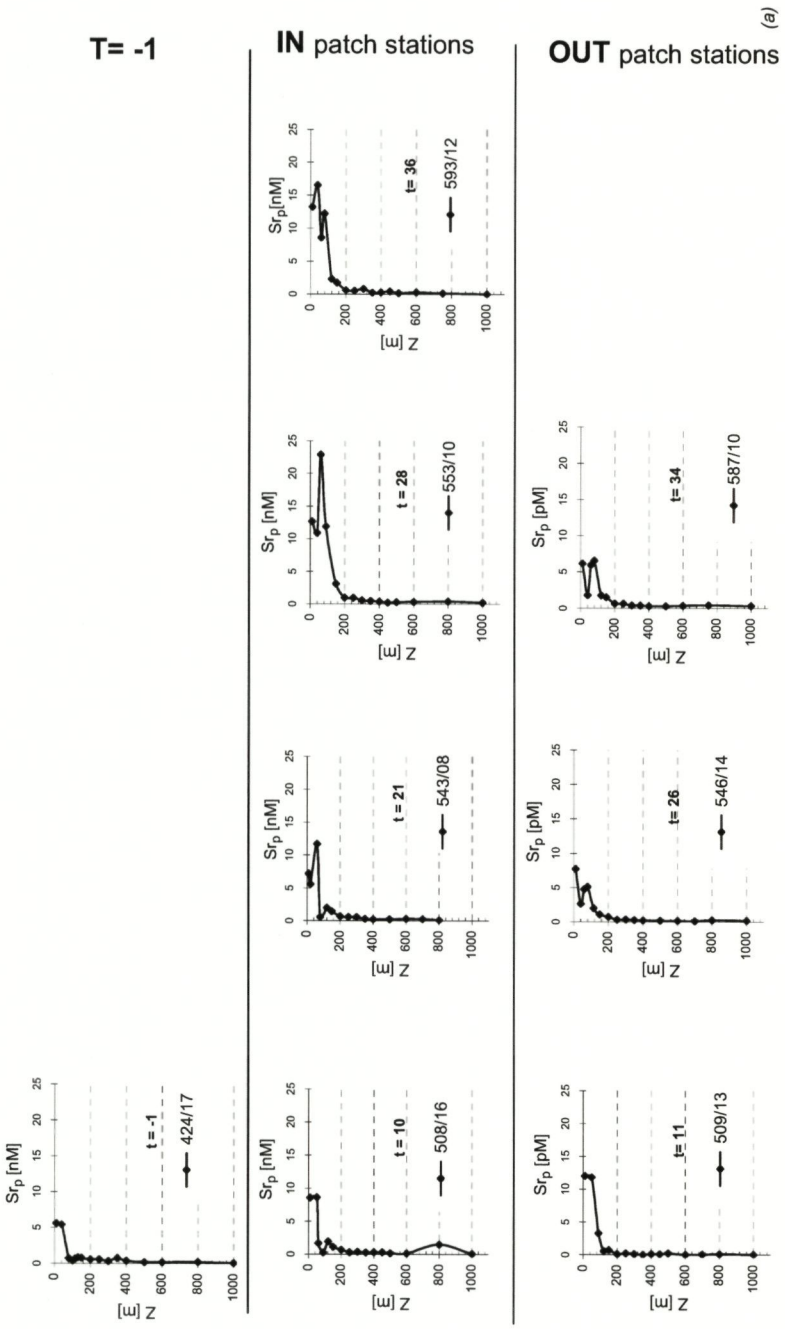


Figure 10.2-a: Particulate Sr_p profiles (nM; 0-1000m) during EIFEX.

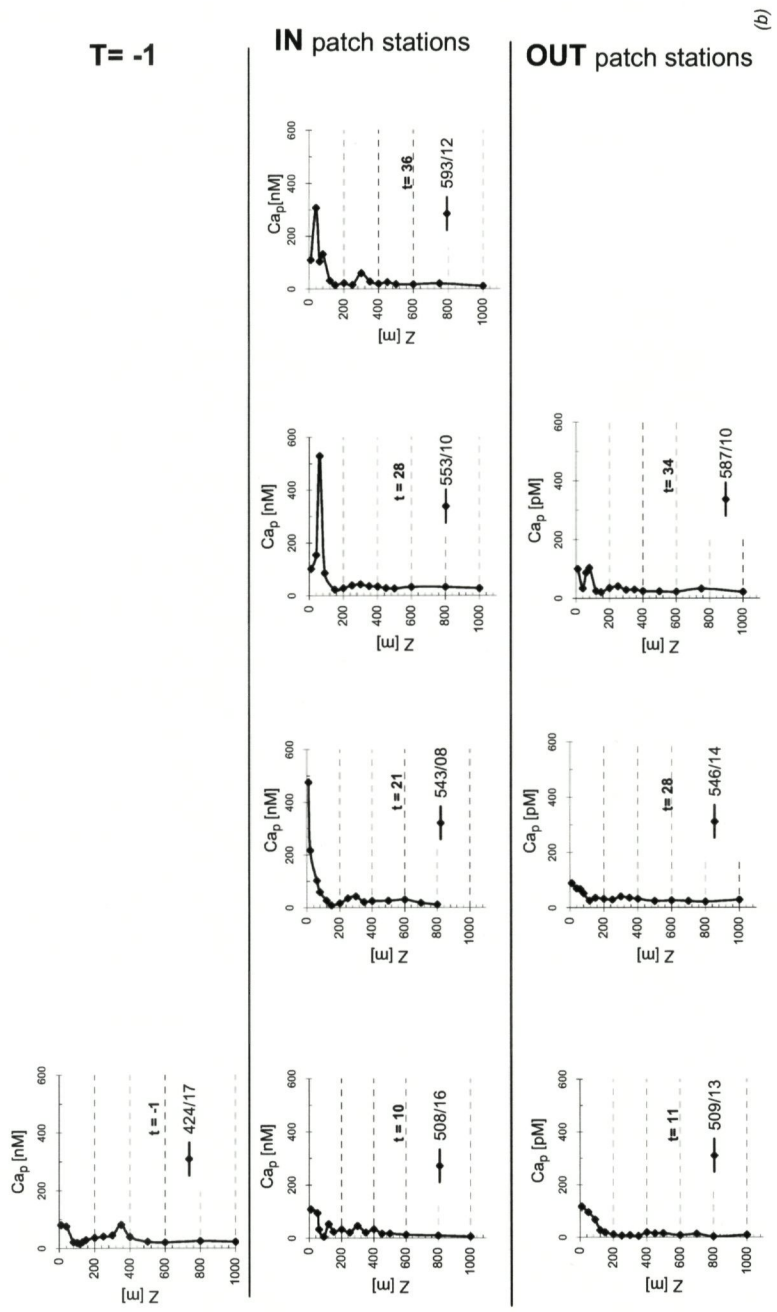


Figure 10.2-b: Particulate Ca_p profiles (nM; 0-1000m) during EIFEX.

Barite particles in suspended matter

[197] In Table 10.2 we report EMPA analyses of discrete Ba particles identified as barite ($BaSO_4$) at 6 depths in the water column and confront them to particulate biogenic Ba_{xs} data for filtered suspended matter. In suspended matter, Ba_{xs} at these 6 depths accounts for >97% of the total particulate Ba. In surface water, where the Ba_{xs} signal exceeds the one in the mesopelagic zone (see also Figure 10.1 and Table 10.1-a), EMPA analysis reveals discrete barite particles are a minor component. In fact, no barite crystals were spotted at 20 m and 90 m, and at 80 m crystals were scarce, accounting for less than 2% of the Ba_{xs} signal. Clearly in surface matters non-barite particles appear to control Ba_{xs}. In the mesopelagic zone on the contrary, barites are abundant, showing close agreement with total Ba_{xs} at 400 and 1000 m but exceeding Ba_{xs} at 800 m (see discussion below). The meso-Ba_{xs} signal could thus be entirely explained by barite particles, in agreement with previous observations of Dehairs et al. [1980] and Stroobants et al. [1991]. During EIFEX, discrete barite particles size ranges on average from 0.71 to 1.06 µm in diameter, similar to earlier observations by Dehairs et al. [1980].

			ICP-MS	%	EPMA			%
Station	Day	Depth [m]	Ba_{xs} [pM]	Ba_{xs}/Ba_p	**Ba-barite [pM]**	Diam µm	Stdev	Barite/Ba_{xs}
543/08 *IN*	21	20	793	99	**0**	-	-	0
587/10 *OUT*	34	80	982	97	**22**	0.82	0.57	2
553/10 *IN*	28	90	299	97	**0**	-	-	0
546/14 *OUT*	26	400	383	99	**420**	1.06	0.62	110
509/13 *OUT*	11	800	199	99	**460**	0.84	0.54	231
546/14 *OUT*	26	1000	280	98	**300**	0.71	0.32	107

Table 10.2: Contribution (%) of Ba-rich particles identified as barite to the Ba_{xs} signal at 6 depths in the water column.

Acantharian distribution

[198] Distribution of acantharian with depth is shown in Figure 10.3 for specimens <50 µm and >50 µm; depth weighted average values are given in Table 10.1-b. The temporal acantharians distribution during EIFEX is discussed in more detail in Henjes et al. [in review]. Briefly, acantharians were most abundant in the upper 150 m ($P<0.05$, Mann-Whitney U-test) and showed a marked decrease below the pycnocline. Mean integrated densities for <50 µm acantharians reached maximum values up to 44,586 (day 21) and 37,147 (day 11) indiv.m^{-3} IN and OUT-patch, respectively. >50 µm acantharians reached maximum values up to 75,532 (day 21) and 35,949 (day 11) indiv.m^{-3}, IN and OUT-patch, respectively (Table 10.1-b). Below 150 m, acantharians are scarce in both size classes (Figure 10.3; Table 10.1-b). IN-patch, initial abundance of total

acantharians (<50 µm and >50 µm) in the upper 150 m increased markedly (twofold) over the first 21 days of the experiment and then decreased slightly towards the end of the experiment. OUT-patch, total acantharian abundance increases only slightly over the first 11 days of EIFEX and decreases thereafter below initial values. The maximum abundance of total acantharians (159,000 indv. m^{-3} at day 21, 60 m depth) exceeds these reported by Michaels et al. [1995] in the Sargasso Sea by a factor of five. They are also 4 times higher than maximum abundances from a previous iron fertilization experiment (EisenEx) conducted in the PFZ during spring 2000 [Henjes et al., in review]. This will have several important implications for further acantharian-derived Ba-barite estimations (see below) compared to previous studies using average values never reaching more than 30,000 acantharians m^{-3} [Bernstein and Byrne, 2004; De Deckker et al., 2004]. Moreover, the increase of acantharian abundance inside the fertilized patch corresponds to the increase in Chl a. Their ability to almost triple population abundance in 16 days is remarkable and would qualify them as an indicator of productivity [Henjes et al., in review].

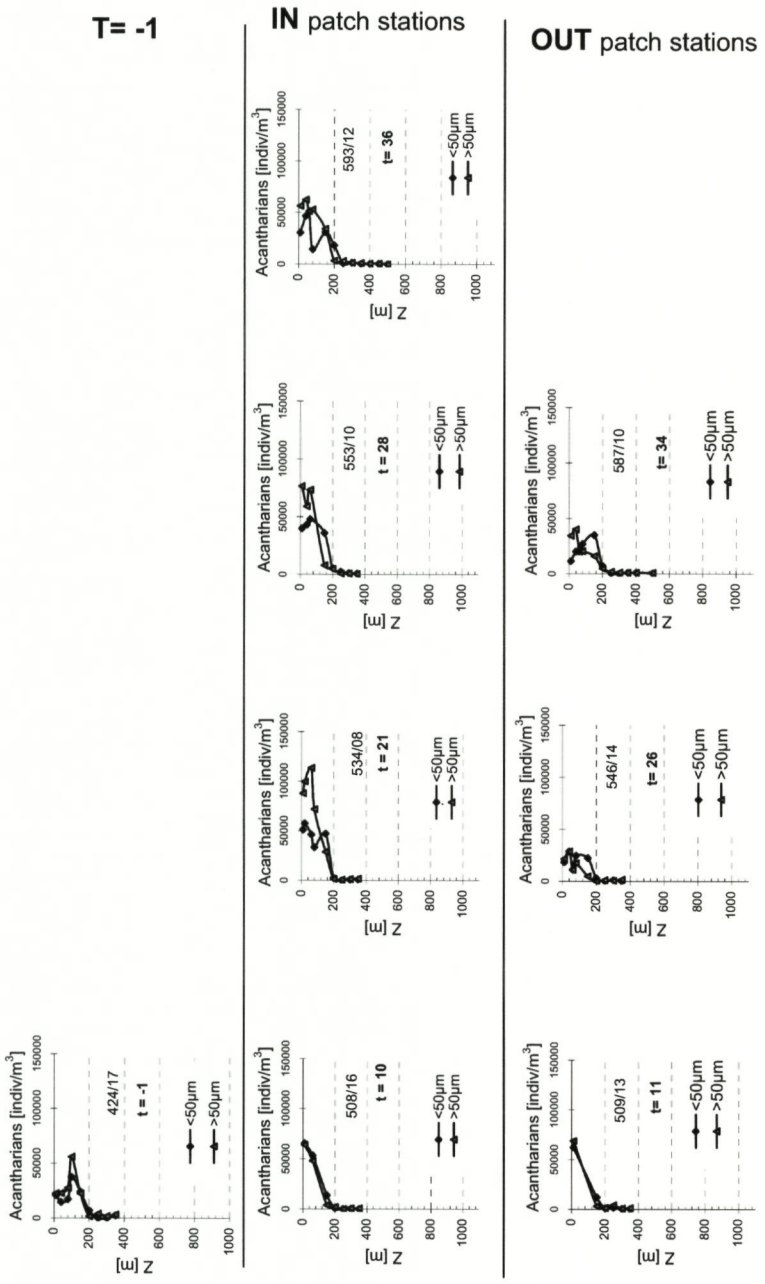


Figure 10.3: <50 µm (full diamonds) and >50 µm (open triangles) acantharians abundance profiles (indiv/m^3; 0-1000m) during EIFEX.

Acantharian Ba/Sr molar ratio

[199] Ba and Sr contents per acantharian range from 1.65 to 15.9 pmoles and from 28 to 626 pmoles respectively (Table 10.3). Bishop et al. [1977] reported individual Sr contents around 200 pmoles and Bernstein et al. [1998] reported values ranging from 1 to 270 pmol for Ba and from 137 pmol to 22 nmol for Sr. We observe a broad range of Ba/Sr molar ratios (0.008-0.135; Figure 10.4) with 3 samples showing particularly high ratios (stations 420, 421' and 423', see italic data in Table 10.3). When excluding these, ratios range from 7.8 $x10^{-3}$ to 4.2 $x10^{-2}$ with a mean value of 2.1± 1 $x10^{-2}$, which is significantly higher than the average acantharian mole fraction of 2.6 $x10^{-3}$ (min. and max.= 6.1 $x10^{-4}$ and 2.5 $x10^{-2}$, respectively) reported by Bernstein et al. [1998].

Stations	Date	Day	Nbr. Indiv.	pmol/indiv. Sr	pmol/indiv. Ba	Ba/Sr
390	28/1/04	-15	2	208.7	5.3	0.0253
391	29/1/04	-14	2	199.4	4.3	0.0214
391'	29/1/04	-14	2	130.1	4.7	0.0361
391"	29/01/04	-14	2	248.0	4.5	0.0181
420	*2/04/04*	-10	*6*	*96.3*	*9.1*	*0.0947*
421	3/02/04	-9	3	64.0	2.7	0.0418
421'	*3/02/04*	-9	*4*	*28.1*	*3.5*	*0.1251*
422	6/02/04	-6	4	195.0	7.0	0.0361
423	7/02/04	-5	3	168.1	2.6	0.0156
423'	*7/02/04*	-5	*3*	*54.3*	*7.3*	*0.1352*
423"	7/02/04	-5	4	161.6	3.6	0.0221
423"'	8/02/04	-4	9	62.6	1.6	0.0256
514	29/02/04	17	6	152.4	1.8	0.0115
514'	29/02/04	17	5	207.6	2.1	0.0101
514"	29/02/04	17	2	626.3	5.1	0.0081
539	03/03/04	20	5	234.1	3.0	0.0127
545	08/03/04	25	4	169.1	2.7	0.0160
545'	08/03/04	25	4	168.3	3.4	0.0200
546	09/03/04	26	4	598.9	4.7	0.0078
546'	09/03/04	26	6	353.3	4.9	0.0139
553	11/03/04	28	3	472.7	3.8	0.0079
553'	12/03/04	28	2	168.5	2.5	0.0150
553"	11/03/04	28	4	497.9	13.8	0.0277
577	15/03/04	32	4	190.6	3.5	0.0186
577'	15/03/04	32	4	153.1	5.8	0.0376
587	17/03/04	34	5	249.8	2.6	0.0105
591	20/03/04	35	5	236.2	4.3	0.0184
591	19/03/04	35	7	214.6	7.8	0.0363
593	20/03/04	36	5	284.0	6.8	0.0240
593'	21/03/04	36	1	464.2	15.9	0.0343

Table 10.3: Acantharians Ba and Sr (pmol/indiv.) contents in surface specimens.

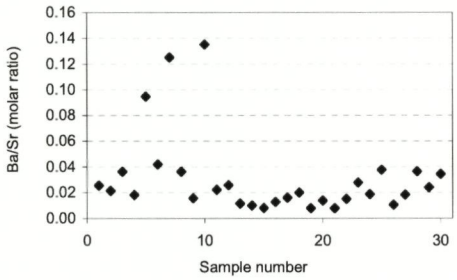


Figure 10.4: Acantharians Ba/Sr molar ratio in surface specimens.

10.4.DISCUSSION

Particulate biogenic Ba_{xs} and barite

[200] In the mesopelagic zone, EMPA results indicate that barites are abundant, showing close agreement with total Ba_{xs} at 400 and 1000 m but exceeding by a factor of more than 2 Ba_{xs} values at 800 m (Table 10.2). Similar differences up to 250% have been reported for suspended matter samples from mesopelagic depths by Sternberg et al. [accepted]. To estimate Ba contents by EMPA we considered the mass of Ba of equivalent sphere and pure barite particles (see section 2), which could in part lead to overestimate the Ba contents. Moreover, we also considered that the particles were homogenously spread over the filter area, whereas the total surface scanned during EMPA represents only a very small fraction (<0.2‰) of the whole filter, thus multiplying the imprecision. So, we caution the EMPA results are rather semi-quantitative.

[201] It is not yet totally clear to date how the surface and mesopelagic Ba_{xs} signals are linked. Cardinal et al. [2005] report that the mixed layer Ba_{xs} contents are not correlated with mesopelagic Ba_{xs}. Dehairs et al. [1980] and Stroobants et al. [1991] showed that Ba_{xs} is mainly composed of barite at mesopelagic depths, but not in surface waters, which is confirmed in this study by EMPA analyses. These results are strengthened by recent works of Dehairs et al. [in preparation] (see also Chapter 8 and Chapter 9) comparing mesopelagic Ba_{xs} and bacterial production, and providing evidences of the strong link between barite formation and mineralization processes of exported materials at mesopelagic depths. Here, results emphasize that even being higher than in the mesopelagic zone and presenting particularly high peaks in subsurface, the Ba_{xs} signal in the upper 90 m is not composed by barite crystals. Thus, the hypothesis that barite formation could be mainly driven by acantharians does not stand for

surface waters; this hypothesis will be tested further below at mesopelagic depths, where the Ba_{xs} signal is mainly composed of barite. Moreover, results also indicate that the Ba_{xs} signal in the upper 150 m (Figure 10.1; Table 10.1) follows the same evolution as biomass parameters (e.g. particulate organic materials and Chl a; Hoffman et al., 2006), which confirms that Ba_{xs} be mainly incorporated in or adsorbed onto biologically derived particles at these depths [Cardinal et al., 2005]. Overall, our findings emphasize that in the surface mixed layer, non-lithogenic Ba_{xs} is accounted by other biogenic carriers than barite, such as detrital organic matter and opal, carbonate or celestite skeletons. See further below calculations of the contribution of acantharian-derived Ba to this surface Ba_{xs} signal.

Sr/Ca ratio in suspended matter

[202] Figure 10.5 displays the Sr/Ca ratio versus depth for all stations; values range between 5 and 164 mmol/mol. In the upper 150 m, values are particularly high (>50 mmol/mol) and then decrease with increasing depth. It has been reported that Sr/Ca for biogenic calcite ranges between 1 and 3 mmol/mol (Stoll and Schrag, 1999 for coccolithophorids; Graham et al,. 1982 for planktonic foraminifera) and for organic material between 10 and 40 [Martin and Knauer, 1973]. Our results reveal the following:

(**1**) Sr/Ca mole ratios are higher than those recorded for calcite, implying a minor contribution of coccolithophorids and/or foraminifera to this signal. This hypothesis fits with results from Henjes et al. [in review]. These authors reported that total foraminifera (juvenile and mature forms) abundance showed no increase inside and outside the fertilized patch during EIFEX and ranged between 11 and 20 $\times 10^5$ ind. m^{-2} (integrated over 150 m depth). Total foraminifera were more abundant in the upper 150 m of the water column IN and OUT patch and showed a clear decrease in abundance below the mixed layer. In Assmy et al. [in preparation], authors reported abundances of coccolithophores, found in 10 or 20 m depth, decreasing from initially 32 $\times 10^3$ cells l^{-1} to 27 $\times 10^3$ cells L^{-1} after 36 days inside the fertilized patch; abundances during EIFEX were a factor six lower than during the previous experiment EisenEx [Assmy et al., in review];

(**2**) Sr/Ca mole ratios are particularly high (>50 mmol/mol) in the upper 150 m, exceeding those reported for other areas in the Southern Ocean [Cardinal et al., 2001]. Such high ratios indicate a preferential enrichment in Sr and would suggest that it is the presence of acantharians that affect these ratios in surface

water. This hypothesis seems valid, as reported by depth-weighted average values of Sr_p vs. acantharians (Table 10.3). The relation is particularly good when comparing Sr_p and >50 µm acantharians integrated between 0-150 m (R^2=0.83; Figure 10.6-a).

(**3**) Below 150 m, Sr/Ca values are similar to those recorded for organic material, suggesting organic matter is a major carrier of the Sr/Ca ratios in the mesopelagic zone [Martin and Knauer, 1973; Cardinal et al., 2001].

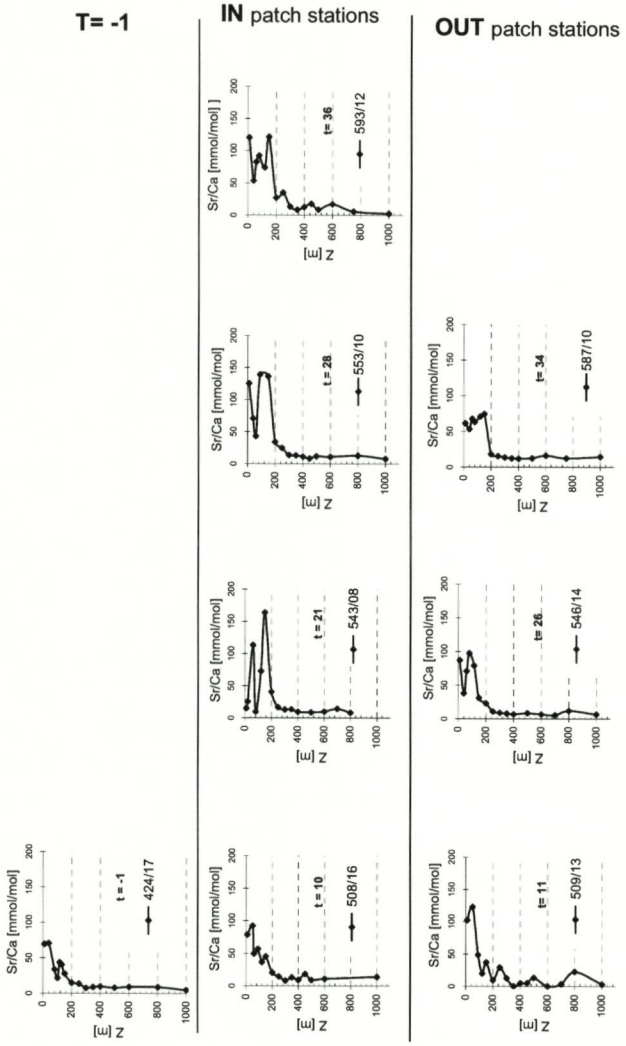


Figure 10.5: Suspended matter Sr/Ca profiles (mmol/mol) during EIFEX.

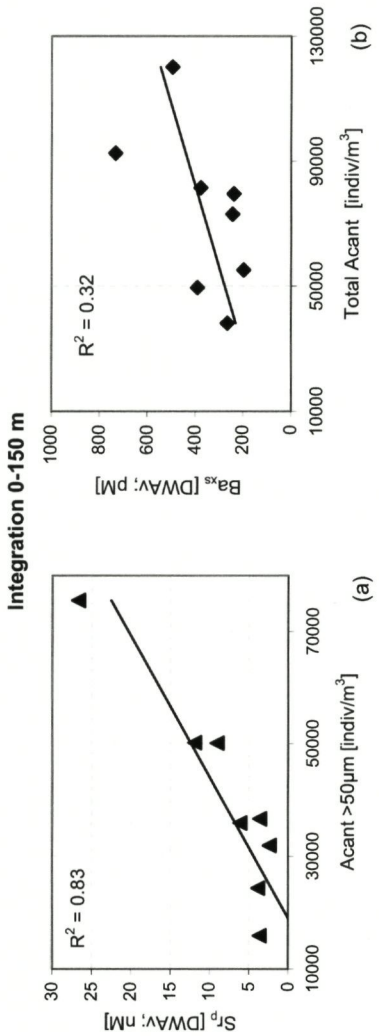


Figure 10.6: Sr_p DWAv vs >50µm acantharian and Ba_{xs} DWAv vs. Total acantharian in the upper 150 m water column.

Ba carried by acantharians

[203] We first wondered whether upper 150 m acantharian-derived Ba could explain the surface particulate Ba_{xs} signal (non barite particles). It implies to consider that the whole particulate Ba_{xs} contents in the surface layer are adsorbed on or incorporated into the acantharian celestite ($SrSO_4$) skeletons. When comparing Ba_{xs} DWAv vs. total acantharians between 0-150 m (Figure

10.6-b; values are reported in Table 10.3), the relation is not very good (R^2= 0.32) compared to what is obtained for the relationship between Sr_p and acantharians (Figure 10.6-a). Now, when multiplying the mean Ba content per acantharians (5 pmol/indiv; Table 10.3) by the mean acantharian abundance (73,700 indiv/m^3; 0-150 m, Table 10.1), calculations indicate that the acantharian-derived Ba could account for 96% of the upper 150 m Ba_{xs} signal, thus essentially accounting for all excess Ba.

[204] Next, we calculated the contribution of upper 150 m acantharians-derived Ba to the mesopelagic (150-1000 m) particulate biogenic Ba_{xs} signal (barite particles). Here we assume that the entire Ba contents carried by acantharian in the surface layer are transferred into barite - a maximalized estimate- to the intermediate depth layers. Considering the same mean Ba content per acantharians and acantharian abundance given above, calculations indicate that the acantharian-associated Ba in the upper 150 m, if entirely translocated into barite and now re-distributed into the 150-1000 m layer (850 m), could account for 18% of the 150-1000 m mesopelagic Ba_{xs} contents. Unless the Ba_{xs} turn-over rate of the upper 150 m is faster than the one in the mesopelagic layer merely inducing an accumulation effect of Ba_{xs} in the latter, it seems unlikely that acantharians leaving in surface water are the major source of Ba-barite in the mesopelagic layers. Moreover, when considering that the individual Ba/Sr molar ratio from acantharians sampled in surface also applies for the same acantharian genera at mesopelagic depths, calculations indicate that the 150-500 m acantharian-derived Ba could account for 10% of the meso-Ba_{xs} signal over the same depth layer.

[205] Overall, results indicate that while acantharian-Ba contents can entirely explain the Ba_{xs} signal in surface water, even if there is no particular relationship between the Ba_{xs} and acantharian evolution in the upper 150 m during EIFEX, the contribution at mesopelagic depths, through significant, appears not a major source to barite formation. Moreover, we outlined above that acantharian abundance in the upper 150 m during EIFEX exceeds up to a factor of five previous data reported in literature, while Ba_{xs} data were in good accordance, which indicates that the acantharians-Ba contribution, again, could be considered as an upper estimate, and emphasizes that acantharians are not the key factor controlling the Ba_{xs} signal and barite formation in the water column.

General discussion- Section 3

GENERAL DISCUSSION - Section 3

[206] The main objective of Section 3 was to better constrain mesopelagic Ba_{xs}, to make it a robust tool to trace C mineralization processes. In particular we examined the particulate biogenic Ba_{xs} signal in various and contrasted environments in terms of surface biologic pump and fate of exported biogenic material. Our work will have several important implications for the use of the Ba proxy (see General conclusion). Here, we discuss in a broader context the insight on the Ba-barite formation process, Ba_{xs} proxy calibration and meso-C mineralization extent that our various studies (Chapter 7 to 10) provided.

On the particulate biogenic Ba_{xs}-barite formation process

[207] The scenario of open Ocean Ba_{xs}-barite formation process we investigated in this dissertation stipulates that the particulate biogenic Ba_{xs} precipitates inside micro-environments (e.g. aggregates of exported biogenic materials) [Dehairs et al., 1980, Stroobants et al., 1991]. In these micro-environments, Ba subtraction from solution (hypothesis tested in Section 2) and/or release of biogenic Ba or oxidation of organic sulfur during organic matter degradation are put forward as the probable processes leading to $BaSO_4$ super saturation. Previous studies have highlighted the relationship between mesopelagic Ba_{xs} contents and organic matter mineralization [Dehairs et al., 1980, 1992, 1997; Cardinal et al., 2005]. Here, we report that the particulate excess Ba in the twilight zone during KEOPS is tuned by the vertical distribution of bacterial activity, with higher particulate Ba_{xs} contents in situations where significant bacterial production (BP) extends deeper in the water column, i.e. systems which more efficiently export organic matter to greater depths for subsequent mineralization in the mesopelagic region. During VERTIGO similar results were obtained with intense bacterial mineralization concentrated in the upper part of the water column leaving little organic material to be decomposed (thereby forming barite) in the mesopelagic water below.

[208] We also investigated the alternative scenario implying Ba_{xs}-barite production to result from direct biological mediation. In particular we debated the relations between particulate biogenic Ba_{xs}, barite and acantharians. Bernstein et al. [1998] and Bernstein and Byrne [2004] proposed that incorporation of Ba in the celestite ($SrSO_4$) skeleton of acantharian could lead to barite precipitation during skeleton dissolution. On the contrary, Esser and Volpe [2002] and Ganeshram et al. [2003] provided evidence that acantharians are not a prerequisite for the formation of barite. In our study we show that non-barite

particles comprise nearly the whole mixed layer Ba_{xs} signal (the latter sometimes higher exceeds concentrations at mesopelagic depths; KEOPS, EIFEX). This suggests that the surface water Ba_{xs} signal is mainly adsorbed on or incorporated into biologically derived materials (biogenic aggregates and carbonate, opal or celestite skeletons). We also observed that Ba_{xs} in surface waters follows the variations of Chl a, productivity, biomass, BSi and particulate organic materials (KEOPS, EIFEX). While Ba_{xs} in the surface layer appears dispersed over different biogenic, non barite phases, at mesopelagic depths Ba_{xs} is mainly composed of barite particles (EIFEX), as previously observed by Dehairs et al. [1980]. We calculated whether acantharian-derived Ba could explain the surface and mesopelagic Ba_{xs} signals. In the first case we considered that the whole particulate Ba_{xs} contents in the surface layer are adsorbed on or incorporated into the acantharian celestite ($SrSO_4$) skeletons, while in the second case we assumed that the entire Ba content carried by acantharian in the surface layer is transferred into barite -an unlikely situation- to the intermediate depth layers. Results reveal that, even if quantitatively the Ba carried by acantharians could explain the entire Ba_{xs} contents in the upper 150 m, the relationship between their distribution and evolution during EIFEX is not so good (R^2=0.32). Moreover, at mesopelagic depths, only up to 18% of the Ba_{xs} signal would be potentially supplied by acantharians. Acantharian-derived Ba is thus not the major source of particulate Ba-barite in the water column.

[209] Overall, from these different studies, results strengthen that particulate biogenic Ba_{xs}, present as barite micro-crystals at mesopelagic depths, reflects the intensity of C mineralization processes. Results moreover stress the robustness of the scenario by which barite in the intermediate layers is formed during degradation of exported biogenic materials. Formation of barite via Ba release from biogenic Ba carrier would only account for a small part of the mesopelagic signal, while the major part would be formed through Ba subtraction from solution and oxidation of organic sulfur during organic matter degradation. Moreover, no evidence is actually found that the surface and mesopelagic Ba_{xs} signals are linked [see also Cardinal et al., 2005].

On the Ba_{xs} proxy calibration

[210] As reported in Chapter 1, the meso-Ba_{xs} stock is translated into POC fluxes by using a relationship empirically relating mesopelagic Ba_{xs} to the rate of O_2 consumption. This relationship, deduced from a 1D advection-diffusion model applied on highly resolved, precise oxygen profiles (see Eq. 1, 2), was

established for the PF region of the S.O. by Shopova et al. [1995] and Dehairs et al. [1997]. The choice of the Ba_{xs} background, called $Ba_{residual}$ in Eq.1 (Chapter 1) is quite crucial. This background signal at zero oxygen consumption, i.e. zero organic C demand, depends of the saturation state of the water for $BaSO_4$. For the S.O. south of the PF, shown by Monnin et al. [1999] and Monnin and Cividini [2006] to be saturated for $BaSO_4$ from surface to 2500 m, this residual Ba_{xs} is close to 180 pM [Dehairs et al., 1997]. Saturation index calculations performed during KEOPS confirmed that in the upper mesopelagic water (125-450 m) – where we convert Ba_{xs} fluxes into C mineralization rates - water is in equilibrium with barite ($0.9<SI<1.1$). However, for the North pacific- where we assume that the transfer function could also apply- differences in saturation appear. ALOHA water is undersaturated in the upper 500 m while at K2 saturation is close to being reached. These differences were thus taken into account and we considered a smaller Ba_{xs} residual value (0 to 50 pM) at ALOHA than at K2 (100 to 150 pM), both being lower than the one used for EIFEX and KEOPS (180 pM; from Dehairs et al., 1997).

[211] Next to the Ba_{xs} background choice, the relationship relating meso-Ba_{xs} to O_2 consumption should also be refined and tested in other environments, as well as to other modes of carbon utilization. We checked it in the North Pacific (VERTIGO) by comparing Ba_{xs}-based mesopelagic C mineralization to bacterial carbon demand (BCD) and POC flux decrease with depth obtained from NBST's (Neutrally Buoyant Sediment Trap). Ba_{xs}-based mesopelagic C mineralization correlates well with both BCD and NBST flux differences. Moreover, the quite good correlation between C mineralization and BCD highlights the potential for the development of a complementary transfer function relating Ba_{xs} to bacterial production (BP). The linear regression given during VERTIGO reflects that a given meso-Ba_{xs} concentration is maintained as a result of a certain bacterial organic consumption rate. Similar results are obtained during KEOPS. Overall, both approaches (BCD and NBST fluxes) converge quite well when comparing with Ba_{xs}-based C mineralization. Considering the uncertainty on several conversion factors utilized in both calculations, the similarities are nevertheless remarkable and emphasize the usefulness of Ba_{xs} in fine suspended matter as proxy of organic matter degradation in the twilight zone. Moreover, these results also reveal that the actual transfer function applies for various environments, be it that correct assessment of Ba_{xs} background is done before.

Remineralization vs. export ratio

[212] The multi-pronged approach discussed in this dissertation aims to determine the fate of exported sinking biogenic materials following bloom development. The outcome of the C exported, not only dependant on the magnitude of the export, is significantly modified by conditions at intermediate layers. Contrasted systems were studied in Section 3, from the oligotrophic and mesotrophic sites in the North Pacific, to the artificial Fe fertilized eddy and the natural Fe-enriched Kerguelen Plateau in the HNLC PF region of Southern Ocean.

[213] First during EIFEX, following Fe fertilization the meso-Ba_{xs} signal provides evidence of rapid changes in particulate Ba export and of enhanced, fast and deep mesopelagic mineralization. However, only ~15% of the biogenic materials exported at 150 m are quickly mineralized down to a depth of 500-1000 m, suggesting a large fraction of the C export is transported deeper. It contrasts with natural systems where C mineralization mainly occurs in the upper mesopelagic zone (150-500 m; ANTARES-4, SAZ-98, CLIVAR SR3) and accounts for 60 to near 100% of the C carried on sinking particles (KEOPS, SAZ-98, ALOHA). We also observe that C mineralization rates during EIFEX (~92 $mgC/m^2/d$; 150-1000 m) are not particularly high when compared with other values reported for S.O. summer conditions (up to 140 $mgC/m^2/d$, 150-1000 m, ANTARES-4). Even though EIFEX data might be in part influenced by the eddy dynamics, mineralization rates obtained during KEOPS for the iron fertilized area above the Kerguelen Plateau present a quite similar trend. Indeed, while Plateau stations (in the bloom strongly boosted by natural supply of iron) have a smaller fraction of the produced C exported (~20%), but this fraction appears less prone to mineralization (9-13%) and therefore has potential to reach deeper, off-shelf HNLC stations have a larger fraction of the C production exported (~45%) and subsequently mineralized (18-39%) in the upper mesopelagic zone (125-400 m). Mineralization fluxes at off-stations (up to 48 $mgC/m^2/d$; 150-450 m) are similar to those observed for the same depths layer during ANTARES-4. Overall EIFEX and KEOPS results suggest that blooms are less prone to mesopelagic mineralization, probably as the result of the fast and intense surface productivity, C export and role of grazers, leaving less time for mesopelagic mineralization to occur. Potential explanations are the presence during EIFEX and KEOPS (On-shelf) of larger particles composed of larger diatoms and of more abundant sinking aggregates and fecal pellets (KEOPS On-shelf) which thus would favor fast and deep export, short-circuiting mesopelagic processing of organic matter. On the contrary, at off-shelf HNLC stations (KEOPS) the predominance of small

diatoms and lower zooplankton biomass provides for relatively more important deeper mesopelagic mineralization. Then, when confronting the oligotrophic (ALOHA) and subarctic mesotrophic (K2) sites in the North Pacific, it appears that respiration and degradation rates by heterotrophic communities at ALOHA were more intense and were mainly confined to the upper 100 m, while at K2, proportionally more material was left for export to deeper layers where it fuelled deep bacterial activity and induces enhanced particulate Ba_{xs} contents. The contrast between ALOHA and K2 was large regarding strength and source characteristics of the biological pump, with more intense production, export and processing of exported plankton material at K2 compared to ALOHA.

[214] Now, comparison between SAZ-98 and CLIVAR SR3 [Section 2; see also Cardinal et al., 2001, 2005] indicates an inverse latitudinal trend between deep-ocean flux and mesopelagic Ba_{xs} contents (Figure I) as suggested during KEOPS between On- and Off-shelf stations. Although the SAZ shows highest deep export, the mesopelagic Ba_{xs} build-up is lowest there. The PFZ, on the other hand, has the lowest deep-ocean flux, but a large mesopelagic Ba_{xs} build-up. These conditions potentially reflect the importance of $CaCO_3$ mineral ballast north of the PF and a more intense mineralization in the mesopelagic waters in the PF where diatoms dominate, in general agreement with the conclusions by François et al. [2002] and Klaas and Archer [2002] that $CaCO_3$ is the important controller of deep export flux, rather than opal.

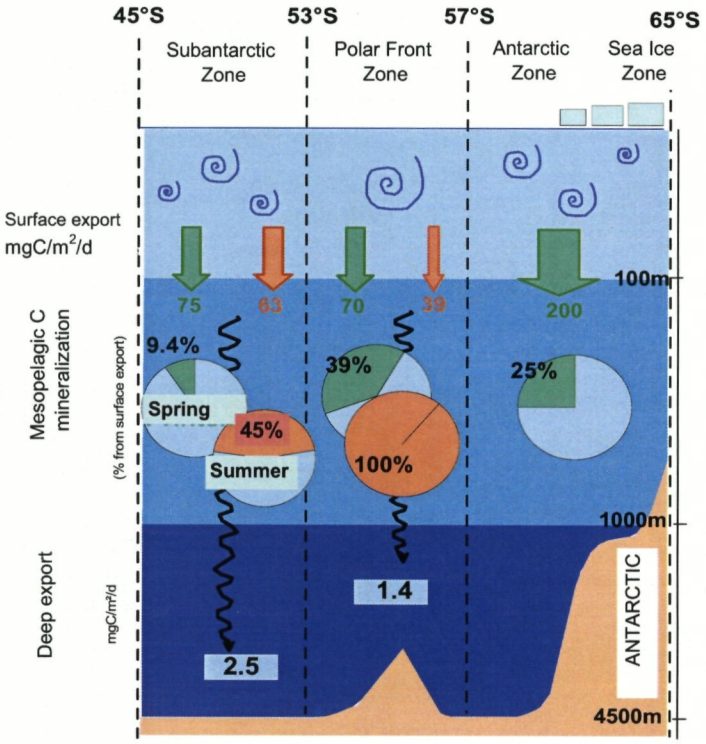


Figure I: C export and mineralization fluxes during CLIVAR (spring) and SAZ-98 (summer).

[215] Overall, as revealed by the meso-Ba_{xs} distribution in the various environments studied, it is actually difficult to define a single, global response in mineralization processes following bloom developments (Figure J). The extent of mesopelagic C mineralization appears closely linked to the combination of both the intensity and nature of the bloom, the distribution of bacterial activity and grazing pressure and the type of biogenic material exported.

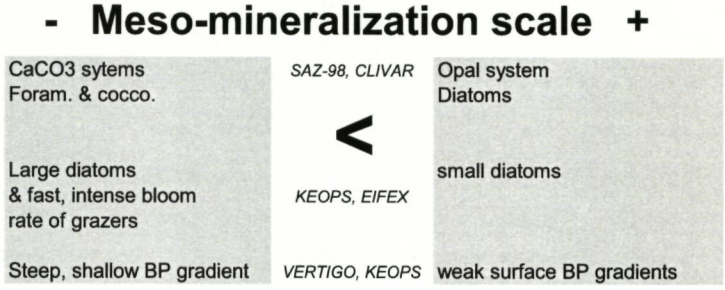


Figure J: The different factors potentially influencing mineralization processes.

At the Southern Ocean's scale

[216] Recent work by Marinov et al. [2006] shows that different regions of the Southern Ocean have very different impacts on the biological pump. Remember that the fronts are delimited by specific hydrodynamics and biogeochemical conditions. As outlined above, predicting meso-C mineralization processes is not an easy task. Nevertheless, when comparing fluxes at the S.O.'s scale, it appears that certain environments are more subject to intense mesopelagic C mineralization than other (in absolute values). It is especially the case in the SAF-PFZ regions of the various sectors of the Southern Ocean (Figure K-a) where depth weighted average Ba_{xs} values (150-500 m) reach up to 500-600 pM. The Ba_{xs} background ranges around 180 nM as reported by Dehairs et al. [1997] and in general, Ba_{xs} DWAv are higher in summer compared to spring (Figure K-b).

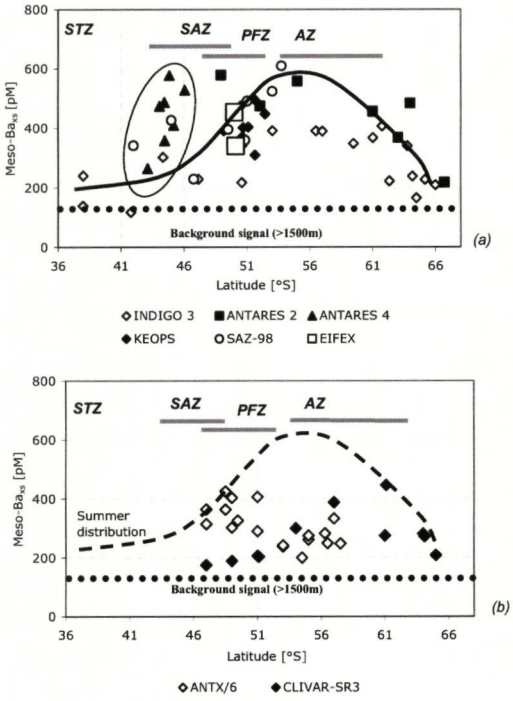


Figure K: Latitudinal distribution of meso-Ba_{xs} in the Southern Ocean during summer (a) and spring (b).

[217] Moreover, we also observe that in the Crozet Basin and Kerguelen Plateau region (Indian sector), mesopelagic (150-500 m) Ba_{xs} maxima (i.e. intense C mineralization) concord quiet well with negative CO_2 fluxes (i.e.

atmospheric CO_2 sink) (Figure L). These observations fit with particular productivity enhancement due to dynamics conditions along fronts [Arrigo et al., 1998; Fiala et al., 1998; Moore et al., 1999; Landry et al., 2002] and to natural iron supply from the sediment in the area [Blain et al., 2001; 2007]. The biological pump and undergoing C export and mineralization at intermediate depths appears thus more intense in these areas.

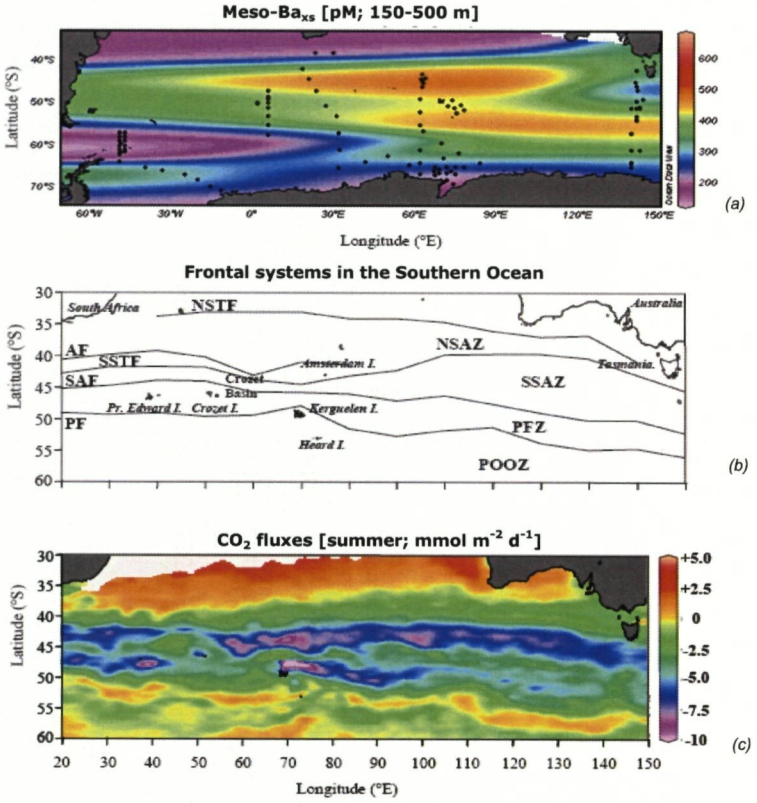


Figure L: Synoptic view of (a) Meso-Ba_{xs} distribution; (b) Fronts location; (c) summer CO_2 fluxes (CO_2 data courtesy of B. Delille, 2006).

[218] Overall, this third section provided major improvements in the validation and calibration of the meso-Ba_{xs} proxy in the Southern Ocean, to make it a powerful tracer of the C mineralization. It also allowed a better evaluation of the processes controlling transport of sinking particles between surface and deep ocean; several important implications of these results for the use of Ba proxy will be discuss further (see General conclusion).

General conclusion

GENERAL CONCLUSION

[219] The present section provides an integrated overview of obtained results. Where relevant, some gaps in the current knowledge will be pointed out, along with suggestions for future research. In Section 2 (Chapters 3 to 6), we investigated which exact process (physical and/or biogeochemical control) acts upon the Ba_d distribution to value the proxy-role of dissolved Ba in the global Ba-barite dynamics. In Section 3 (Chapters 6 to 10), we better constrained our understanding of the spatio-temporal variability of mesopelagic Ba_{xs} to make it a robust tool to trace C mineralization processes. The results obtained have several important implications for the application of the Ba proxy:

(**1**) We showed how the surface to deep and north to south positive gradient of Ba_d in the water column results from the particle-solute Ba dynamics, driven by the intensity of particulate organic matter mesopelagic mineralization, the $BaSO_4$ saturation state of the S.O. and the general circulation. In particular, we provided and confirmed evidences that Ba_d, silicate and alkalinity distributions are not mechanistically coupled, that local Ba_d enrichments and depletions are significant in the upper 1000 m and that Ba_{xs} formation/dissolution was causing these features. The implications of an uncoupling of the Ba and alkalinity cycles are that the Ba/Ca ratios in carbonates (e.g. benthic foraminifera; Lea and Boyle, 1989; Lea, 1993, 1995) are not a robust proxy for paleo-alkalinity reconstruction [Jeandel et al., 1996; Rubin et al., 2003];

(**2**) Our findings about Ba_d depletions at mesopelagic depths strengthen the scenario of barite precipitation being linked to micro-environments. Indeed, Ba_d subtraction from ambient solution during degradation of biogenic matter and resulting in barite formation induces a measurable impact (depletion) on Ba_d profiles and can explain the Ba_d gradient between surface and 1000 m. However, considering the differences in turn-over rate between the two Ba phases and since missing dissolved Ba quantities (Ba_d depletions) are not balanced by equivalent increases in the mesopelagic particulate phase, this situation implies sinking of particle associated Ba to depths >1000 m. This makes it unlikely that Ba_d can be directly used to quantitatively reconstruct Ba_{xs};

(**3**) In situations where the parametric optimum multi-parameter (POMP) model indicates that the non-conservative part of the Ba_d signal is minimal, the possibilities exist to use Ba_d as a water mass tracer. In particular Ba_d could serve

as a further tracer of water mass pathway when combined to a multi-proxies approach (e.g. Nd, Th, Ra and other trace elements). This approach is of interest for the KEOPS survey (Jan.-Feb. 2005) on the Kerguelen Plateau (Indian sector) to understand the water mass circulation in this area and to determine the possible origin of Fe enrichment there;

(**4**) Feeding the existing dissolved Ba data bank with new data will help in better assessing the barite saturation state in the open Ocean. It will in turn allow the estimation of the large scale distribution of the Ba_{xs} residuals via the POMP approach, thus highlighting areas where mesopelagic particulate biogenic Ba_{xs} is formed, thereby contributing to identifying area of intense mineralization of organic C;

(**5**) We showed that particulate biogenic Ba_{xs} contents in the twilight zone are tuned by the vertical distribution of bacterial activity and thus that the meso-Ba_{xs} build-up clearly reflects degradation intensity of exported biogenic materials, as was suggested by earlier work [Dehairs et al., 1997; Cardinal et al., 2001, 2005] but never demonstrated until now. Further systematic comparison between Ba_{xs} and bacterial production and respiration is thus required to develop a transfer function relating Ba_{xs} and bacterial carbon demand. Therefore, during the upcoming SAZ-SENSE expedition (Australian sector; Jan.-Feb. 2007) we will investigate in a systematic way Ba excess distribution and bacterial activity for the same sites and depth. In parallel, oxygen consumption from direct O_2 measurements from insitu incubated seawater and from long term incubations will also be performed;

(**6**) We showed that while acantharian-associated Ba can account for the near totality of surface particulate biogenic Ba_{xs} (i.e. non barite particles; Ba_{xs} being adsorbed on or incorporated into biogenic materials), acantharia can only account for a few percent of the mesopelagic Ba_{xs} (barite particles) content. Acantharia are thus not the major source of barite in the water column. We also confirmed that diatoms are not significant consumers of Ba. Active biological mediation appears not to be the major control setting the barite water column distribution. Understanding the processes leading to the Ba_{xs}–barite formation in the water column is crucial for a correct use of the Ba_{xs} proxy in paleoproductivity studies (e.g. reconstructing modern and past ocean C export from sedimentary barite). Indeed, the fact that acantharian celestite does not control water column barite precipitation (the release of biogenic Ba in acantharia containing aggregates

would only account for a few % of the barite), corroborates conclusions about sedimentary barite being related to surface production. In the case of acantharia control on barite formation, sedimentary barite would not reflect primary productivity, but only acantharia activity.

(**7**) The most probable scenario of open Ocean mesopelagic Ba_{xs}-barite formation process we retain is the one involving micro-environments (i.e. aggregates of exported biogenic materials). Inside these, Ba subtraction from solution combined with oxidation of organic sulfur during organic matter degradation would lead to barite precipitation. This process appears to occur at any depth, as has recently been shown in Van Beek et al. [2007]. However, a certain category of aggregates (finer suspended matter, <50 µm) is preferentially decomposed in the mesopelagic region, releasing the barite crystals formed. Here, translation of particulate biogenic Ba_{xs} into C fluxes is a powerful tool to estimate mesopelagic mineralization rate. Complementary investigations on elemental and isotopic composition (e.g. Sr, Rd; Paytan et al., 1993, 1996-b; Van Beek et al., 2007) of barite crystals is suspended matter, and variability of barite spatio-temporal distribution would be a way to gain further insight into the barite formation process [Bertram and Cohen, 1997; Monnin et al., 2006; Robin et al., 2006; Van Beek et al., 2007]. The fact that the origin of Ba_{xs} remains not fully resolved results also in part from our limitated understanding of what controls the particle flux in the twilight zone. To enable further progress, the latter issue requires reliable flux and particle characterization data within the twilight zone.

(**8**) We highlighted that the mineralization process in response to bloom development can be multiple. The outcome of the C export is linked to the combinations of various factors. Among these, we showed that systems where calcium carbonate producing plankton is significant (north of Polar Front) were prone to more important deep export than systems dominated by diatoms where intense mineralization usually occurs at mesopelagic depths. Moreover, in diatom dominated systems thriving in Fe replete conditions (Kerguelen Plateau), we showed that blooms were less prone to mesopelagic C mineralization when surface productivity is particularly intense and the materials exported composed by larger diatoms and fast sinking pellets. On the contrary, mesopelagic processing of organic matter appeared higher in systems dominated by smaller diatoms, lower grazing pressure and deeper bacterial activity. Thus, for up-coming studies, we advocate time-series and seasonally resolved systematic

multi-proxy process studies targeting a mechanistic understanding of biogeochemical processes at mesopelagic depths;

(**9**) We finally showed that at the Southern Ocean's scale, mesopelagic Ba_{xs}-based C mineralization rates are particularly intense in the SAZ and PF areas, coinciding with regions of known atmospheric CO_2 sink. Frontal systems, well known to enhance productivity, seem also to be site of higher mineralization processes at intermediate layers. However, only a systematic comparison of these fluxes with the C export from the surface mixed layer will allow to determine whether these areas are also sites of potential, deep C sequestration;

References

ANDERSON R.F. and G. Winckler (2005). Problems with paleoproductivity proxies. Paleoceanography, 20(3): doi:10.1029/2004PA001107

ANTIA A.N., W. Koeve, G. Fischer, T. Blanz, D. Schulz-Bull, J. Scholten, S. Neuer, K. Kremling, J. Kuss, R. Peinert, D. Hebbeln, U. Bathmann, M. Conte, U. Fehner and B. Zeitzschel (2001). Basin-wide particulate carbon flux in the Atlantic Ocean: Regional export patterns and potential for atmospheric CO_2 sequestration. Global Biogeochemical Cycles, 15(4): 845-862

ARMAND L.K., B. Queguiner and V. Barthaux. Summer phytoplankton community response on the Kerguelen Plateau during the KEOPS program: biomass and diversity. In review, Deep-Sea Research II

ARMSTRONG R.A., C. Lee, J.I. Hedges, S. Honjo and S.G. Wakeham (2002). A new, mechanistic model for organic carbon fluxes in the ocean based on the quantitative association of POC with ballast minerals. Deep-Sea Research Part Ii-Topical Studies in Oceanography, 49(1-3): 219-236

ARRIGO K.R., D. Worthen, A. Schnell and M.P. Lizotte (1998). Primary production in Southern Ocean waters. Journal of Geophysical Research-Oceans, 103(C8): 15587-15600

ASSMY et al., EIFEX, in preparation, Nature

ASSMY P., Henjes J., C. Klaas and V. Smetacek. Mechanisms determining species dominance in a phytoplankton bloom induced by the iron fertilization experiment EisenEx in the Southern Ocean. In review, Deep-Sea Research

BATTLE M., M.L. Bender, P.P. Tans, J.W.C. White, J.T. Ellis, T. Conway and R.J. Francey (2000). Global carbon sinks and their variability inferred from atmospheric O-2 and delta C-13. Science, 287(5462): 2467-2470

BENDTSEN J., C. Lundsgaard, M. Middelboe and D. Archer (2002). Influence of bacterial uptake on deep-ocean dissolved organic carbon. Global Biogeochemical Cycles, 16(4):

BERELSON W.M. (2002). Particle settling rates increase with depth in the ocean. Deep-Sea Research Part Ii-Topical Studies in Oceanography, 49(1-3): 237-251

BERNSTEIN R.E. and R.H. Byrne (2004). Acantharians and marine barite. Marine Chemistry, 86(1-2): 45-50

BERNSTEIN R.E., R.H. Byrne and J. Schijf (1998). Acantharians: a missing link in the oceanic biogeochemistry of barium. Deep-Sea Research Part I-Oceanographic Research Papers, 45(2-3): 491-505

BERNSTEIN R.E., R.H. Byrne, P.R. Betzer and A.M. Greco (1992). Morphologies and Transformations of Celestite in Seawater - the Role of Acantharians in Strontium and Barium Geochemistry. Geochimica Et Cosmochimica Acta, 56(8): 3273-3279

BERTRAM M.A. and J.P. Cowen (1997). Morphological and compositional evidence for biotic precipitation of marine barite. Journal of Marine Research, 55(3): 577-593

BISHOP J.K.B. (1988). The Barite-Opal-Organic Carbon Association in Oceanic Particulate Matter. Nature, 332(6162): 341-343

BISHOP J.K.B., R. Collier, J.M. Edmond and D.R. Ketten (1977). Chemistry and Vertical Flux of Particulate Matter Collected by Large Volume Insitu Filtration of Surface Most 1500 M in Galapogos Region of Equatorial Pacific Ocean. Transactions-American Geophysical Union, 58(12): 1172-1172

BISHOP J.K.B., D. Schupack, R.M. Sherrell, M. Conte (1985). A multiple unit large volume in situ filtration system (MULVFS) for sampling oceanic particulate matter in mesoscale environments. In: Zirino, A. (Ed.) Mapping Strategies in Chemical Oceanography, Advances in Chemistry Series, Vol. 209. American Chemical Society, Washington, DC, pp. 155-175

BLAIN S., B. Quéguiner et al. (2007). Impacts of natural iron fertilisation on C sequestration in the Southern Ocean. Nature, doi:10.1038/05700

BLAIN S., P. Treguer, S. Belviso, E. Bucciarelli, M. Denis, S. Desabre, M. Fiala, V.M. Jezequel, J. Le Fevre, P. Mayzaud, J.C. Marty and S. Razouls (2001). A biogeochemical study of the island mass effect in the context of the iron hypothesis: Kerguelen Islands, Southern Ocean. Deep-Sea Research Part I-Oceanographic Research Papers, 48(1): 163-187

BONN W.J., F.X. Gingele, H. Grobe, A. Mackensen and D.K. Futterer (1998). Palaeoproductivity at the Antarctic continental margin: opal and barium records for the last 400 ka. Palaeogeography Palaeoclimatology Palaeoecology, 139(3-4): 195-211

BOULYGA S.F., J. Heilmann and K.G. Heumann (2005). Isotope dilution ICP-MS with laser-assisted sample introduction for direct determination of sulfur in petroleum products. Analytical and Bioanalytical Chemistry, 382(8): 1808-1814

BOYD P.W., R.H. Goldblatt and P.J. Harrison (1999). Mesozooplankton grazing manipulations during in vitro iron enrichment studies in the NE subarctic Pacific. Deep-Sea Research Part Ii-Topical Studies in Oceanography, 46(11-12): 2645-2668

BOYD P.W., A.J. Watson, C.S. Law, E.R. Abraham, T. Trull, R. Murdoch, D.C.E. Bakker, A.R. Bowie, K.O. Buesseler, H. Chang, M. Charette, P. Croot, K. Downing, R. Frew, M. Gall, M. Hadfield, J. Hall, M. Harvey, G. Jameson, J. LaRoche, M. Liddicoat, R. Ling, M.T. Maldonado, R.M. McKay, S. Nodder, S. Pickmere, R. Pridmore, S. Rintoul, K. Safi, P. Sutton, R. Strzepek, K. Tanneberger, S. Turner, A. Waite and J. Zeldis (2000). A mesoscale phytoplankton bloom in the polar Southern Ocean stimulated by iron fertilization. Nature, 407(6805): 695-702

BOYD P.W., C.S. Law, C.S. Wong, Y. Nojiri, A. Tsuda, M. Levasseur, S. Takeda, R. Rivkin, P.J. Harrison, R. Strzepek, J. Gower, R.M. McKay, E. Abraham, M. Arychuk, J. Barwell-Clarke, W. Crawford, D. Crawford, M. Hale, K. Harada, K. Johnson, H. Kiyosawa, I. Kudo, A. Marchetti, W. Miller, J. Needoba, J. Nishioka, H. Ogawa, J. Page, M. Robert, H. Saito, A. Sastri, N. Sherry, T. Soutar, N. Sutherland, Y. Taira, F. Whitney, S.K.E. Wong and T. Yoshimura (2004). The decline and fate of an iron-induced subarctic phytoplankton bloom. Nature, 428(6982): 549-553

BOYD P.W., VERTIGO, in preparation, Deep Sea Research II

BOYD P.W. and T. Trull (in press). Understanding the export of biogenic particles in oceanic waters: Is there consensus? Progress In Oceanography, 72(4): 276-312

BROECKER W.S. (1974). No a Conservative Water-Mass Tracer. Earth and Planetary Science Letters, 23(1): 100-107

BROECKER W.S. and T.H. Peng (1982). Tracer in the sea. Lamont-Doherty Geological Observatory, Columbia University, Eldigio Press, New York, 690 pp

BRULAND K.W. and R.P. Frank (1983). Trace Metals in Sea Water. Eds Wong, C. S., Boyle, E., Bruland, K. W., Burton, D. & Goldberg, E., Plenum, New York: 415–426

BUESSELER K.O., A.F. Michaels, D.A. Siegel and A.H. Knap (1994). A 3-Dimensional Time-Dependent Approach to Calibrating Sediment Trap Fluxes. Global Biogeochemical Cycles, 8(2): 179-193

BUESSELER K.O., J.E. Andrews, S.M. Pike and M.A. Charette (2004). The effects of iron fertilization on carbon sequestration in the Southern Ocean. Science, 304(5669): 414-417

BUESSELER K.O., J.E. Andrews, S.M. Pike, M.A. Charette, L.E. Goldson, M.A. Brzezinski and V.P. Lance (2005). Particle export during the southern ocean iron experiment (SOFeX). Limnology and Oceanography, 50(1): 311-327

BUESSELER K.O. et al., VERTIGO, in preparation, Deep Sea Research II

CARDINAL D., F. Dehairs, T. Cattaldo and L. Andre (2001). Geochemistry of suspended particles in the Subantarctic and Polar Frontal Zones south of Australia: Constraints on export and advection processes. Journal of Geophysical Research-Oceans, 106(C12): 31637-31656

CARDINAL D., N. Savoye, T.W. Trull, L. Andre, E.E. Kopczynska and F. Dehairs (2005). Variations of carbon rernineralisation in the Southern Ocean illustrated by the Ba-xs proxy. Deep-Sea Research Part I-Oceanographic Research Papers, 52(2): 355-370

CARLOTTI F. et al.. Mesozooplankton size structure and biomass above the Kerguelen Plateau (Southern Ocean) during KEOPS. In review, Deep-Sea Research II

CHAN L.H., D. Drummond, J.M. Edmond and B. Grant (1977). Barium Data from Atlantic Geosecs Expedition. Deep-Sea Research, 24(7): 613-649

CHOW T.J. and E.D. Goldberg (1960). On the marine geochemistry of barium. Geochimica et Cosmochimica Acta 20: 192-198

CHRISTAKI U., Van Wambeke F., Obernosterer, I. , Catala P., Malits A., Weinbauer M., Ruiz, Natural iron fertilization above the Kerguelen Plateau (Southern Ocean): Spatial and temporal variability of microbial food web structure. In review, Deep-Sea Research II

COALE K.H., K.S. Johnson, S.E. Fitzwater, R.M. Gordon, S. Tanner, F.P. Chavez, L. Ferioli, C. Sakamoto, P. Rogers, F. Millero, P. Steinberg, P. Nightingale, D. Cooper, W.P. Cochlan, M.R. Landry, J. Constantinou, G. Rollwagen, A. Trasvina and R. Kudela (1996). A massive phytoplankton bloom induced by an ecosystem-scale iron fertilization experiment in the equatorial Pacific Ocean. Nature, 383(6600): 495-501

COLLIER R. and J. Edmond (1984). The Trace-Element Geochemistry of Marine Biogenic Particulate Matter. Progress in Oceanography, 13(2): 113-199

DE BAAR H.J.W., P.W. Boyd, K.H. Coale, M.R. Landry, A. Tsuda, P. Assmy, D.C.E. Bakker, Y. Bozec, R.T. Barber, M.A. Brzezinski, K.O. Buesseler, M. Boye, P.L. Croot, F. Gervais, M.Y. Gorbunov, P.J. Harrison, W.T. Hiscock, P. Laan, C. Lancelot, C.S. Law, M. Levasseur, A. Marchetti, F.J. Millero, J. Nishioka, Y. Nojiri, T. van Oijen, U. Riebesell, M.J.A. Rijkenberg, H. Saito, S. Takeda, K.R. Timmermans, M.J.W. Veldhuis, A.M. Waite and C.S. Wong (2005). Synthesis of iron fertilization experiments: From the iron age in the age of enlightenment. Journal of Geophysical Research-Oceans, 110, C09S16, doi:10.1029/2004JC002601

DE BRAUWERE A., S.H.M. Jacquet, F. de Ridder, F. Dehairs, R. Pintelon, J. Schoukens and W. Baeyens (2007). Water mass distributions in the Southern Ocean derived from a parametric analysis of mixing water masses. Journal of Geophysical Research-Oceans, 112, C02021, doi:10.1029/2006JC003742

DEHAIRS F., R. Chesselet and J. Jedwab (1980). Discrete Suspended Particles of Barite and the Barium Cycle in the Open Ocean. Earth and Planetary Science Letters, 49(2): 528-550

DEHAIRS F., N. Stroobants and L. Goeyens (1991). Suspended Barite as a Tracer of Biological-Activity in the Southern-Ocean. Marine Chemistry, 35(1-4): 399-410

DEHAIRS F., A. de Brauwere, S.H.M. Jacquet, et al.. Dissolved Barium in the southern Ocean along 6°W and 30°E. In preparation-a

DEHAIRS F., Goeyens L., Stroobants N., Bernard P., Goyet C., Poisson A. and Chesselet R. (1990). On suspended barite and the oxygen minimum in the Southern Ocean. Global Biogeochemical Cycles, 4(1): 85-102

DEHAIRS F., W. Baeyens and L. Goeyens (1992). Accumulation of Suspended Barite at Mesopelagic Depths and Export Production in the Southern-Ocean. Science, 258(5086): 1332-1335

DEHAIRS F., S.H.M. Jacquet, D. Cardinal, J. Bishop et al.. Particulate Ba and mesopelagic C remineralization at stations ALOHA and K2 during VERTIGO 1 and 2. In preparation-b, Deep Sea Research II

DEHAIRS F., D. Shopova, S. Ober, C. Veth and L. Goeyens (1997). Particulate barium stocks and oxygen consumption in the Southern Ocean mesopelagic water column during spring and early summer: Relationship with export production. Deep-Sea Research Part Ii-Topical Studies in Oceanography, 44(1-2): 497-516

DEHAIRS F., N. Fagel, A.N. Antia, R. Peinert, M. Elskens and L. Goeyens (2000). Export production in the Bay of Biscay as estimated from barium - barite in settling material: a comparison with new production. Deep-Sea Research Part I-Oceanographic Research Papers, 47(4): 583-601

DEL GIORGIO P.A. and J.J. Cole (2000). Bacterial growth efficiency and energetics. Microbial Ecology of the Oceans, Plenum Press: 289-325

DELILLE B., 2006. Inorganic carbon dynamics and air-ice-sea CO2 fluxes in the open and coastal waters of the Southern Ocean, Ph.D thesis

DEDECKKER P. (2004). On the celestite-secreting Acantharia and their effect on seawater strontium to calcium ratios. Hydrobiologia, 517: 1-13

DUCKLOW H. (2000). Bacterial production and biomass in the oceans. Microbial Ecology of the Oceans, ed. D.L. Kirchman, Wiley & Sons, pp 85-152

DYMOND J., E. Suess and M. Lyle (1992). Barium in deep-sea sediment: a geochemical proxy for paleoproductivity. Paleoceanography, 9 (2): 163-181

EAGLE M., A. Paytan, K.R. Arrigo, G. van Dijken and R.W. Murray (2003). A comparison between excess barium and barite as indicators of carbon export. Paleoceanography, 18(1):

EDMOND J.M. (1974). Dissolution of Carbonate and Silicate in Deep Ocean. Deep-Sea Research, 21(6): 455-480

EPPLEY R.W. and B.J. Peterson (1979). Particulate Organic-Matter Flux and Planktonic New Production in the Deep Ocean. Nature, 282(5740): 677-680

EBERSBACH F. and T.W. Trull. Sinking particle properties from polyacrylamide gels during KEOPS: controls of carbon export in an area of persistent natural iron inputs in the Southern Ocean. In review, Limnology and Oceanography

ELSKEN M. et al., VERTIGO, in preparation, Deep Sea Research II

ESSER B.K. and A.M. Volpe (2002). At-sea high-resolution chemical mapping: extreme barium depletion in North Pacific surface water. Marine Chemistry, 79(2): 67-79

FALKNER K.K., G.P. Klinkhammer, T.S. Bowers, J.F. Todd, B.L. Lewis, W.M. Landing and J.M. Edmond (1993). The Behavior of Barium in Anoxic Marine Waters. Geochimica Et Cosmochimica Acta, 57(3): 537-554

FALKNER K.K., R.W. Macdonald, E.C. Carmack, and T. Weingartner (1994). The Potential of Barium as a Tracer of Arctic Water Masses. Geophysical Monograph, 85, 63-76, Washington DC

FIALA M., M. Semeneh and L. Oriol (1998). Size-fractionated phytoplankton biomass and species composition in the Indian sector of the Southern Ocean during austral summer. Journal of Marine Systems, 17(1-4): 179-194

FIALA M., B. Delille, C. Dubreuil, E. Kopczynska, K. Leblanc, J. Morvan, B. Queguiner, S. Blain, C. Cailliau, P. Conan, R. Corvaisier, M. Denis, M. Frankignoulle, L. Oriol and S. Roy (2003). Mesoscale surface distribution of biogeochemical characteristics in the Crozet Basin frontal zones (South Indian Ocean). Marine Ecology-Progress Series, 249:1-14

FIELDING S., N. Crisp, J.T. Allen, M.C. Hartman, B. Rabe and H.S.J. Roe (2001). Mesoscale subduction at the Almeria-Oran front - Part 2. Biophysical interactions. Journal of Marine Systems, 30(3-4): 287-304

FRANCOIS R., S. Honjo, S.J. Manganini and G.E. Ravizza (1995). Biogenic Barium Fluxes to the Deep-Sea - Implications for Paleoproductivity Reconstruction. Global Biogeochemical Cycles, 9(2): 289-303

FRANCOIS R., S. Honjo, R. Krishfield and S. Manganini (2002). Factors controlling the flux of organic carbon to the bathypelagic zone of the ocean. Global Biogeochemical Cycles, 16, 10.1029/2001GB001722

FRANCOIS R., M.A. Altabet, E.F. Yu, D.M. Sigman, M.P. Bacon, M. Frank, G. Bohrmann, G. Bareille and L.D. Labeyrie (1997). Contribution of Southern Ocean surface-water

stratification to low atmospheric CO2 concentrations during the last glacial period. Nature, 389(6654): 929-935

FRESNEL J., P. Galle and P. Gayral (1979). Résultats de la microanalyse des cristaux vacuaolaires chez deux Chromophytes unicellulaires marines: Exanthemachrysis gayraliae, Pavlova sp. (Prymnésiophycées, Pavlovacées). C. R. Acad. Sc. Paris, 288D, 823-825.

FREYDIER R., B. Dupre and M. Polve (1995). Analyses by Inductively-Coupled Plasma-Mass Spectrometry of Ba Concentrations in Water and Rock Samples - Comparison between Isotope-Dilution and External Calibration with or without Internal Standard. European Mass Spectrometry, 1(3): 283-291

GANESHRAM R.S., R. Francois, J. Commeau and S.L. Brown-Leger (2003). An experimental investigation of Barite formation in seawater. Geochimica Et Cosmochimica Acta, 67(14): 2599-2605

GERVAIS F., U. Riebesell and M.Y. Gorbunov (2002). Changes in primary productivity and chlorophyll a in response to iron fertilization in the Southern Polar Frontal Zone. Limnology and Oceanography, 47(5): 1324-1335

GINGELE F. and A. Dahmke (1994). Discrete Barite Particles and Barium as Tracers of Paleoproductivity in South-Atlantic Sediments. Paleoceanography, 9(1): 151-168

GOLDBERG E.D. and G.O.S. Arrhenius (1958). Chemistry of Pacific pelagic sediments, Geochimica Et Cosmochimica Acta 13:153-212

GONNEEA M.E. and A. Paytan (2006). Phase associations of barium in marine sediments. Marine Chemistry, 100(1-2): 124-135

GONZALEZ-MUNOZ M.T., B. Fernandez-Luque, F. Martinez-Ruiz, K. Ben Chekroun, J.M. Arias, M. Rodriguez-Gallego, M. Martinez-Canamero, C. de Linares and A. Paytan (2003). Precipitation of barite by Myxococcus xanthus: Possible implications for the biogeochemical cycle of barium. Applied and Environmental Microbiology, 69(9): 5722-5725

GOODAY A.J., J.M. Bernhard and S.S. Bowser (1995). The Taxonomy and Ecology of Crithionina-Delacai Sp-Nov, an Abundant Large Agglutinated Foraminifer from Explorers-Cove, Antarctica. Journal of Foraminiferal Research, 25(4): 290-298

GOVINDARAJU K. (1994). Compilation of Working Values and Sample Description for 383 Geostandards. Geostandards Newsletter 18

GOYET C., C. Beauverger, C. Brunet and A. Poisson (1991). Distribution of Carbon-Dioxide Partial-Pressure in Surface Waters of the Southwest Indian-Ocean. Tellus Series B-Chemical and Physical Meteorology, 43(1): 1-11

GOYET C., C. Coatanoan, G. Eischeid, T. Amaoka, K. Okuda, R. Healy and S. Tsunogai (1999). Spatial variation of total CO2 and total alkalinity in the northern Indian Ocean: A novel approach for the quantification of anthropogenic CO2 in seawater. Journal of Marine Research, 57(1): 135-163

GRAHAM D.W., M.L. Bender, D.F. Williams and L.D. Keigwin (1982). Strontium-Calcium Ratios in Cenozoic Planktonic-Foraminifera. Geochimica Et Cosmochimica Acta, 46(7): 1281-1292

GRAHAM W.M., S. MacIntyre and A.L. Alldredge (2000). Diel variations of marine snow concentration in surface waters and implications for particle flux in the sea. Deep-Sea Research Part I-Oceanographic Research Papers, 47(3): 367-395

GUAY C.K. and K.K. Falkner (1997). Barium as a tracer of Arctic halocline and river waters. Deep-Sea Research Part Ii-Topical Studies in Oceanography, 44(8): 1543-1569

HENJES J., P. Assmy, C. Klaas and V. Smetacek. Response of the larger protozooplankton to an iron-induced phytoplankton bloom in the Polar Frontal Zone of the Southern Ocean (EisenEx). In review, Deep-Sea Research I

HOFFMANN L.J., I. Peeken, K. Lochte, P. Assmy and M. Veldhuis (2006). Different reactions of Southern Ocean phytoplankton size classes to iron fertilization. Limnology and Oceanography, 51(3): 1217-1229

HONJO S. (1996). Fluxes of particles to the interior of the open oceans. In: Ittekkot, V., Sch.afer, P., Honjo, S., Depetris, P.J. (Eds.), Particle Flux in the Ocean, SCOPE, Vol. 57. Wiley, New York: 91–254

HONJO S. and S.J. Manganini (1996). Annual biogenic particle fluxes to the interior of the North Atlantic Ocean; studied at 34jN 21jW and 48jN 21jW. In: Milliman, J.D. (Ed.), Topical Studies in Oceanography, JGOFS: The North Atlantic Bloom Experiment. Pergamon, Oxford: 587– 607

HOPPE H.G. and S. Ullrich (1999). Profiles of ectoenzymes in the Indian Ocean: phenomena of phosphatase activity in the mesopelagic zone. Aquatic Microbial Ecology, 19(2): 139-148

HOPWOOD J.D., S. Mann and A.J. Gooday (1997). The crystallography and possible origin of barium sulphate in deep sea rhizopod protists (Xenophyophorea). Journal of the Marine Biological Association of the United Kingdom, 77(4): 969-987

HUTCHINS D.A. and K.W. Bruland (1998). Iron-limited diatom growth and Si : N uptake ratios in a coastal upwelling regime. Nature, 393(6685): 561-564

JACKSON G.A. and A.B. Burd (2002). A model for the distribution of particle flux in the mid-water column controlled by subsurface biotic interactions. Deep-Sea Research Part Ii-Topical Studies in Oceanography, 49(1-3): 193-217

JACQUET S.H.M., A. de Brauwere, F. De Ridder and F. Dehairs. Investigating dissolved barium behavior in the Southern Ocean using a parametric mixing model, In review, Geophysical Research Letters.

JACQUET S.H.M., F. Dehairs, M. Elskens, N. Savoye and D. Cardinal (2007). Barium cycling along WOCE SR3 line in the Southern Ocean. In press, Marine Chemistry

JACQUET S.H.M., F. Dehairs and S. Rintoul (2004). A high resolution transect of dissolved barium in the Southern Ocean. Geophysical Research Letters, 31, L14301, doi:10.1029/2004GL20016

JACQUET S.H.M., F. Dehairs, D. Cardinal, J. Navez and B. Delille (2005). Barium distribution across the Southern Ocean frontal system in the Crozet-Kerguelen Basin. Marine Chemistry, 95(3-4): 149-162

JACQUET S.H.M., F. Dehairs, N. Savoye, I. Obernosterer, U. Christaki, C. Monnin and D. Cardinal. Mesopelagic organic carbon mineralization in the Kerguelen Plateau region tracked by biogenic particulate Ba. Accepted, Deep Sea Research II

JACQUET S.H.M., J. Henjes, F. Dehairs, A. Maeyer-Vorobiec, N. Savoye and D. Cardinal. Particulate barium, barite and acantharians in the Southern Ocean during the European Iron Fertilization Experiment (EIFEX). In review, Journal of Geophysical Reseach-Biogeosciences

JACQUET S.H.M., N. Savoye, F. Dehairs, I. Vöge, V. Strass and D. Cardinal, Mesopelagic carbon mineralization during the European Iron Fertilization Experiment (EIFEX). Accepted, Global Biogeochemical Cycles

JEANDEL C., J.K. Bishop and A. Zindler (1995). Exchange of Neodymium and Its Isotopes between Seawater and Small and Large Particles in the Sargasso Sea. Geochimica Et Cosmochimica Acta, 59(3): 535-547

JEANDEL C., K. Tachikawa, A. Bory and F. Dehairs (2000). Biogenic barium in suspended and trapped material as a tracer of export production in the tropical NE Atlantic (EUMELI sites). Marine Chemistry, 71(1-2): 125-142

JEANDEL C., B. Dupre, G. Lebaron, C. Monnin and J.F. Minster (1996). Longitudinal distributions of dissolved barium, silica and alkalinity in the western and southern Indian Ocean. Deep-Sea Research Part I-Oceanographic Research Papers, 43(1): 1-31

KARL D.M., J.R. Christian, J.E. Dore, D.V. Hebel, R.M. Letelier, L.M. Tupas and C.D. Winn (1996). Seasonal and interannual variability in primary production and particle flux at Station ALOHA. Deep-Sea Research Part Ii-Topical Studies in Oceanography, 43(2-3): 539-568

KLAAS C. and D.E. Archer (2002). Association of sinking organic matter with various types of mineral ballast in the deep sea: Implications for the rain ratio. Global Biogeochemical Cycles, 16(4): 1116

KLINKENBERG H., W. VanBorm and F. Souren (1996). A theoretical adaptation of the classical isotope dilution technique for practical routine analytical determinations by means of inductively coupled plasma mass spectrometry. Spectrochimica Acta Part B-Atomic Spectroscopy, 51(1): 139-153

KLINKHAMMER G.P. and L.H. Chan (1990). Determination of Barium in Marine Waters by Isotope-Dilution Inductively Coupled Plasma Mass-Spectrometry. Analytica Chimica Acta, 232(2): 323-329

KRIEST I. and G.T. Evans (1999). Representing phytoplankton aggregates in biogeochemical models. Deep-Sea Research Part I-Oceanographic Research Papers, 46(11): 1841-1859

KUMAR M.D. and Y.H. Li (1996). Spreading of water masses and regeneration of silica and Ra-226 in the Indian Ocean. Deep-Sea Research Part Ii-Topical Studies in Oceanography, 43(1): 83-110

LAMBORG et al., VERTIGO, in preparation, Deep Sea Research II

LAMPITT R.S. and A.N. Antia (1997). Particle flux in deep seas: regional characteristics and temporal variability. Deep-Sea Research Part I-Oceanographic Research Papers, 44(8): 1377-1403

LAMPITT R.S., K.F. Wishner, C.M. Turley and M.V. Angel (1993). Marine Snow Studies in the Northeast Atlantic-Ocean - Distribution, Composition and Role as a Food Source for Migrating Plankton. Marine Biology, 116(4): 689-702

LANDRY M.R., K.E. Selph, S.L. Brown, M.R. Abbott, C.I. Measures, S. Vink, C.B. Allen, A. Calbet, S. Christensen and H. Nolla (2002). Seasonal dynamics of phytoplankton in the Antarctic Polar Front region at 170 degrees W. Deep-Sea Research Part Ii-Topical Studies in Oceanography, 49(9-10): 1843-1865

LEA D. and E. Boyle (1989). Barium Content of Benthic Foraminifera Controlled by Bottom-Water Composition. Nature, 338(6218): 751-753

LEA D.W. (1993). Constraints on the Alkalinity and Circulation of Glacial Circumpolar Deep-Water from Benthic Foraminiferal Barium. Global Biogeochemical Cycles, 7(3): 695-710

LEA D.W. (1995). A Trace-Metal Perspective on the Evolution of Antarctic Circumpolar Deep-Water Chemistry. Paleoceanography, 10(4): 733-747

LEBLANC K., B. Queguiner, M. Fiala, S. Blain, J. Morvan and R. Corvaisier (2002). Particulate biogenic silica and carbon production rates and particulate matter distribution in the Indian sector of the Subantarctic Ocean. Deep-Sea Research Part Ii-Topical Studies in Oceanography, 49(16): 3189-3206

LEFÈVRE D., C. Guige and I. Obernosterer. The Balance Between Autotrophic and Heterotrophic Processes During a Phytoplankton Bloom Induced By Natural Fertilisation Above The Kerguelen Plateau (Southern Ocean). In review, Deep-Sea Research II

LEE C. (2004). Transformations in the "Twilight Zone" and beyond. Marine Chemistry, 92(1-4): 87-90

LI Y.H., T.L. Ku, G.G. Mathieu and Wolgemut.K (1973). Barium in Antarctic Ocean and Implications Regarding Marine Geochemistry of Ba and Ra-226. Earth and Planetary Science Letters, 19(3): 352-358

LO MONACO C., N. Metzl, A. Poisson, C. Brunet and B. Schauer (2005). Anthropogenic CO2 in the Southern Ocean: Distribution and inventory at the Indian-Atlantic boundary (World Ocean Circulation Experiment line I6). Journal of Geophysical Research-Oceans, 110, C06010, doi:10.1029/2004JC002643

LONGERICH H.P., B.J. Fryer and D.F. Strong (1987). Determination of Lead Isotope Ratios by Inductively Coupled Plasma-Mass Spectrometry (Icp-Ms). Spectrochimica Acta Part B-Atomic Spectroscopy, 42(1-2): 39-48

LONGHURST A.R., A.W. Bedo, W.G. Harrison, E.J.H. Head, D.D. Sameoto (1990). Vertical flux of respiratory carbon by oceanic diel migrant biota. Deep-Sea Research 37(4): 685-694

LOUREY M.J. and T.W. Trull (2001). Seasonal nutrient depletion and carbon export in the Subantarctic and Polar Frontal Zones of the Southern Ocean south of Australia. Journal of Geophysical Research-Oceans, 106(C12): 31463-31487

LUTZ M., R. Dunbar and K. Caldeira (2002). Regional variability in the vertical flux of particulate organic carbon in the ocean interior. Global Biogeochemical Cycles, 16(3): doi:10.1029/2000GB001383

MACINTYRE S., A.L. Alldredge and C.C. Gotschalk (1995). Accumulation of Marine Snow at Density Discontinuities in the Water Column. Limnology and Oceanography, 40(3): 449-468

MACKAS D.L., K.L. Denman and A.F. Bennett (1987). Least-Squares Multiple Tracer Analysis of Water Mass Composition. Journal of Geophysical Research-Oceans, 92(C3): 2907-2918

MARINOV I., A. Gnanadesikan, J.R. Toggweiler and J.L. Sarmiento (2006). The Southern Ocean biogeochemical divide. Nature, 441(7096): 964-967

MARTIN J.H. (1990). Glacial-interglacial CO2 change: The iron hypothesis. Paleoceanography, 5: 1–13

MARTIN J.H. and G.A. Knauer (1973). Elemental Composition of Plankton. Geochimica Et Cosmochimica Acta, 37(7): 1639-1653

MARTIN J.H., G.A. Knauer, D.M. Karl and W.W. Broenkow (1987). Vertex - Carbon Cycling in the Northeast Pacific. Deep-Sea Research Part a-Oceanographic Research Papers, 34(2): 267-285

MARTIN and Fitzwater (1988). Nature, 331, 341-343 doi:10.1038/331341a0

MARTIN J.H., K.H. Coale, K.S. Johnson, S.E. Fitzwater, R.M. Gordon, S.J. Tanner, C.N. Hunter, V.A. Elrod, J.L. Nowicki, T.L. Coley, R.T. Barber, S. Lindley, A.J. Watson, K. Vanscoy, C.S. Law, M.I. Liddicoat, R. Ling, T. Stanton, J. Stockel, C. Collins, A. Anderson, R. Bidigare, M. Ondrusek, M. Latasa, F.J. Millero, K. Lee, W. Yao, J.Z. Zhang, G. Friederich, C. Sakamoto, F. Chavez, K. Buck, Z. Kolber, R. Greene, P. Falkowski, S.W. Chisholm, F. Hoge, R. Swift, J. Yungel, S. Turner, P. Nightingale, A. Hatton, P. Liss and N.W. Tindale (1994). Testing the Iron Hypothesis in Ecosystems of the Equatorial Pacific-Ocean. Nature, 371(6493): 123-129

MCMANUS J., W.M. Berelson, D.E. Hammond and G.P. Klinkhammer (1999). Barium cycling in the North Pacific: Implications for the utility of Ba as a paleoproductivity and paleoalkalinity proxy. Paleoceanography, 14(1): 53-61

METZL N., F. Louanchi and A. Poisson (1998). Seasonal and interannual variations of sea surface carbon dioxide in the subtropical Indian Ocean. Marine Chemistry, 60(1-2): 131-146

METZL N., B. Tilbrook and A. Poisson (1999). The annual fCO(2) cycle and the air-sea CO2 flux in the sub-Antarctic Ocean. Tellus Series B-Chemical and Physical Meteorology, 51(4): 849-861

MICHAELS A.F. (1988). Vertical-Distribution and Abundance of Acantharia and Their Symbionts. Marine Biology, 97(4): 559-569

MICHAELS A.F., D.A. Caron, N.R. Swanberg, F.A. Howse and C.M. Michaels (1995). Planktonic Sarcodines (Acantharia, Radiolaria, Foraminifera) in Surface Waters near Bermuda - Abundance, Biomass and Vertical Flux. Journal of Plankton Research, 17(1): 131-163

MILLERO F.J., K. Lee and M. Roche (1998). Distribution of alkalinity in the surface waters of the major oceans. Marine Chemistry, 60(1-2): 111-130

MONNIN C. and D. Cividini (2006). The saturation state of the world's ocean with respect to (Ba,Sr)SO4 solid solutions. Geochimica Et Cosmochimica Acta, 70(13): 3290-3298

MONNIN C., C. Jeandel, T. Cattaldo and F. Dehairs (1999). The marine barite saturation state of the world's oceans. Marine Chemistry, 65(3-4): 253-261

MOORE J.K., M.R. Abbott, J.G. Richman, W.O. Smith, T.J. Cowles, K.H. Coale, W.D. Gardner and R.T. Barber (1999). SeaWiFS satellite ocean color data from the Southern Ocean. Geophysical Research Letters, 26(10): 1465-1468

MOSSERI J. and B.Queguiner. The biogenic silica cycle during austral summer in the Southern Ocean: contrast between naturally Fe-enriched and HNLC waters south of Kerguelen Islands. In review, Deep Sea Research II

MURRAY R.W. and M. Leinen (1993). Chemical-Transport to the Sea-Floor of the Equatorial Pacific-Ocean across a Latitudinal Transect at 135-Degrees-W - Tracking Sedimentary Major, Trace, and Rare-Earth Element Fluxes at the Equator and the Intertropical Convergence Zone. Geochimica Et Cosmochimica Acta, 57(17): 4141-4163

NAVEZ J., F. Dehairs and T. Cattaldo (1999). Isotope Dilution ICP-MS Measurement of Barium in Sea Water: Improvement of the Accuracy with a New Approach to Correct for Mass Bias. Colloquium Spectroscopicum Internationale XXXI, September 5-10, Ankara, Turkey

NODDER S.D. and A.M. Waite (2001). Is Southern Ocean organic carbon and biogenic silica export enhanced by iron-stimulated increases in biological production? Sediment trap results from SOIREE. Deep-Sea Research Part Ii-Topical Studies in Oceanography, 48(11-12): 2681-2701

NODDER S.D., M.A. Charette, A.M. Waite, T.W. Trull, P.W. Boyd, J. Zeldis and K.O. Buesseler (2001). Particle transformations and export flux during an in situ iron-stimulated algal bloom in the Southern Ocean. Geophysical Research Letters, 28(12): 2409-2412

OBERNOSTERER I., U. Christaki, D. Lefèvre, P. Catala, F. Van Wambeke and P. Lebaron. Rapid bacterial mineralization of organic carbon produced during a phytoplankton bloom induced by natural iron fertilization in the Southern Ocean. In review, Deep Sea Research II

ORSI A.H., G.C. Johnson and J.L. Bullister (1999). Circulation, mixing, and production of Antarctic Bottom Water. Progress in Oceanography, 43(1): 55-109

ÖSTLUND H., H. Craig, W. Broecker and D. Spencer (1987). GEOSECS Atlantic, Pacific and Indian Ocean Expeditions. Vol 7n Shore-based Data and Graphics, NSF, Washington, DC

PARK Y.H. and L. Gamberoni (1997). Cross-frontal exchange of Antarctic Intermediate Water and Antarctic Bottom Water in the Crozet Basin. Deep-Sea Research Part Ii-Topical Studies in Oceanography, 44(5): 963-986

PARK Y.H., L. Gamberoni and E. Charriaud (1993). Frontal Structure, Water Masses, and Circulation in the Crozet Basin. Journal of Geophysical Research-Oceans, 98(C7): 12361-12385

PARK Y.H., E. Charriaud, P. Craneguy and A. Kartavtseff (2001). Fronts, transport, and Weddell Gyre at 30 degrees E between Africa and Antarctica. Journal of Geophysical Research-Oceans, 106(C2): 2857-2879

PARK Y.H., R.T. Pollard, J.F. Read and V. Leboucher (2002). A quasi-synoptic view of the frontal circulation in the Crozet Basin during the Antares-4 cruise. Deep-Sea Research Part Ii-Topical Studies in Oceanography, 49(9-10): 1823-1842

PASSOW U. and C.L. De la Rocha (2006). Accumulation of mineral ballast on organic aggregates. Global Biogeochemical Cycles, 20, GB1013, doi:10.1029/2005GB002579

PAYTAN A. and M. Kastner (1996-a). Benthic Ba fluxes in the central Equatorial Pacific, implications for the oceanic Ba cycle. Earth and Planetary Science Letters, 142(3-4): 439-450

PAYTAN A., M. Kastner, E.E. Martin, J.D. Macdougall and T. Herbert (1993). Marine Barite as a Monitor of Seawater Strontium Isotope Composition. Nature, 366(6454): 445-449

PAYTAN A., W.S. Moore and M. Kastner (1996-b). Sedimentation rate as determined by Ra-226 activity in marine barite. Geochimica Et Cosmochimica Acta, 60(22): 4313-4319

POISSON A., Schauer B. and Brunet C. (1990). Les rapports de campagnes à la Mer, MD53/INDIGO 3 à bord du 'Marion Dufresne', 3 janvier-27 février 1987; Pub. 87-01, Fascicule 2, 269pp; Les Publications de la Mission de Recherche de Terres Australes et Antarctiques Françaises, Paris.

PORTER K.G. and Y.S. Feig (1980). The Use of Dapi for Identifying and Counting Aquatic Microflora. Limnology and Oceanography, 25(5): 943-948

RATHBONE C. and B. Griffiths. NASA ocean colour web, global 8 day mean chlorophyll composites. Feldman, G. C., C. R. McClain, Ocean Color Web, SeaWiFS Reprocessing 5, NASA Goddard Space Flight Center. Eds. Kuring, N., Bailey, S. W. http://oceancolor.gsfc.nasa.gov/, with graphical processing by Chris Rathbone, CSIRO Marine and Atmospheric Research, 2006

READ J.F. and R.T. Pollard (1993). Structure and Transport of the Antarctic Circumpolar Current and Agulhas Return Current at 40-Degrees-E. Journal of Geophysical Research-Oceans, 98(C7): 12281-12295

RINTOUL S.R. and J.L. Bullister (1999). A late winter hydrographic section from Tasmania to Antarctica. Deep-Sea Research Part I-Oceanographic Research Papers, 46(8): 1417-1454

RINTOUL S.R. and T.W. Trull (2001). Seasonal evolution of the mixed layer in the Subantarctic Zone south of Australia. Journal of Geophysical Research-Oceans, 106(C12): 31447-31462

RINTOUL S.R. and S. Sokolov (2001). Baroclinic transport variability of the Antarctic Circumpolar Current south of Australia (WOCE repeat section SR3). Journal of Geophysical Research-Oceans, 106(C2): 2815-2832

RINTOUL S.R., J.R. Donguy and D.H. Roemmich (1997). Seasonal evolution of upper ocean thermal structure between Tasmania and Antarctica. Deep-Sea Research Part I-Oceanographic Research Papers, 44(7): 1185-1202

ROBIN E., C. Rabouille, G. Martinez, I. Lefevre, J.L. Reyss, P. van Beek and C. Jeandel (2003). Direct barite determination using SEM/EDS-ACC system: implication for constraining barium carriers and barite preservation in marine sediments. Marine Chemistry, 82(3-4): 289-306

ROSENBERG M., Rintoul S., Bray S., Curran C. and N. Johnston. Aurora Australis Marine Science Cruise AU0103, CLIVAR-SR3 Transect - Oceanographic Field Measurements and Analysis. ACE-CRC, Hobart, unpublished report

ROSMAN P.D.P. and J.R. Taylor (1998). Isotope compositions of the elements 1997, Pure & Appl. Chem., 70: 217-235

RUBIN S.I., S.L. King, R.A. Jahnke and P.N. Froelich (2003). Benthic barium and alkalinity fluxes: Is Ba an oceanic paleo-alkalinity proxy for glacial atmospheric CO_2? Geophysical Research Letters, 30(17), 10.1029/2003GL017339

RUSHDI A.I., J. McManus and R.W. Collier (2000). Marine barite and celestite saturation in seawater. Marine Chemistry, 69(1-2): 19-31

SACHS et al., EIFEX, in preparation, Nature

SARMINETO J.L., J. Dunne and R.A. Armstrong (2004). Do we understand the Ocean's Biological Pump? U.S. JGOFS Newsletter, 12(4), 1-5

SARMIENTO J.L., T.M.C. Hughes, R.J. Stouffer and S. Manabe (1998). Simulated response of the ocean carbon cycle to anthropogenic climate warming. Nature, 393(6682): 245-249

SARMIENTO J.L., N. Gruber, M.A. Brzezinski and J.P. Dunne (2004). High-latitude controls of thermocline nutrients and low latitude biological productivity. Nature, 427(6969): 56-60

SARMIENTO J.L., R.D. Slater, M.J.R. Fasham, H.W. Ducklow, J.R. Toggweiler and G.T. Evans (1993). A Seasonal 3-Dimensional Ecosystem Model of Nitrogen Cycling in the North-Atlantic Euphotic Zone. Global Biogeochemical Cycles, 7(2): 417-450

SARMIENTO J.L., J.R. Toggweiler and R. Najjar (1988). Ocean Carbon-Cycle Dynamics and Atmospheric Pco2. Philosophical Transactions of the Royal Society of London Series a-Mathematical Physical and Engineering Sciences, 325(1583): 3-21

SAVOYE N., T. Trull, S.H.M. Jacquet, J. Navez and F. Dehairs. ^{234}Th-derived export fluxes during a natural iron fertilization experiment (KEOPS). Accepeted with minor modifications, Deep Sea Research II

SCHNETZER A., D.K. Steinberg (2002-a). Natural diets of vertically migrating zooplankton in the Sargasso Sea. Marine Biology, 141: 89-99

SCHNETZER A., D.K. Steinberg (2002). Active transport of particulate organic carbon and nitrogen by vertically migrating zooplankton in the Sargasso Sea. Marine Ecology Progress Series, 234: 71-84

SCHLITZER R., Ocean Data View, http://www.awi-bremerhaven.de/GEO/ODV, 2003

SCHNEIDER B., J. Karstensen, A. Oschlies and R. Schlitzer (2005). Model-based evaluation of methods to determine C : N and N : P regeneration ratios from dissolved nutrients. Global Biogeochemical Cycles, 19, doi:10.1029/2004GB002256

SHERIDAN C.C., C. Lee, S.G. Wakeham and J.K.B. Bishop (2002). Suspended particle organic composition and cycling in surface and midwaters of the equatorial Pacific Ocean. Deep-Sea Research Part I-Oceanographic Research Papers, 49(11): 1983-2008

SHOPOVA D., F. Dehairs and W. Baeyens (1995). A Simple-Model of Biogeochemical Element Distribution in the Oceanic Water Column. Journal of Marine Systems, 6(4): 331-344

SIEGEL D.A. and W.G. Deuser (1997). Trajectories of sinking particles in the Sargasso Sea: modeling of statistical funnels above deep-ocean sediment traps. Deep-Sea Research Part I-Oceanographic Research Papers, 44(9-10): 1519-1541

SIEGEL et al., VERTIGO, in preparation, Deep Sea Research II

SILVER et al., VERTIGO, in preparation, Deep Sea Research II

SIMON M., H.P. Grossart, B. Schweitzer and H. Ploug (2002). Microbial ecology of organic aggregates in aquatic ecosystems. Aquatic Microbial Ecology, 28(2): 175-211

SMETACEK V. (2005), Fahrtabschnitt ANT XXI/3 Kapstadt - Kapstadt (21.01.04 - 25.03.04), 1. Introduction, Reports on Polar and Marine Research, 500: 3–7

SOKOLOV S. and S.R. Rintoul (2002). Structure of Southern Ocean fronts at 140 degrees E. Journal of Marine Systems, 37(1-3): 151-184

STANLEY R.H.R., K.O. Buesseler, S.J. Manganini, D.K. Steinberg and J.R. Valdes (2004). A comparison of major and minor elemental fluxes collected in neutrally buoyant and surface-tethered sediment traps. Deep-Sea Research Part I-Oceanographic Research Papers, 51(10): 1387-1395

STECHER H.A. and M.B. Kogut (1999). Rapid barium removal in the Delaware estuary. Geochimica Et Cosmochimica Acta, 63(7-8): 1003-1012

STEMMANN L., G.A. Jackson and G. Gorsky (2004). A vertical model of particle size distributions and fluxes in the midwater column that includes biological and physical processes - Part II: application to a three year survey in the NW Mediterranean Sea. Deep-Sea Research Part I-Oceanographic Research Papers, 51(7): 885-908

STERNBERG E., C. Jeandel, E. Robin and M.Souhaut. Seasonnal cycle of suspended barite in the Mediterranean Sea: aggregates vs acantharians, Accepted, Geochimica Cosmichimica acta

STERNBERG E., D.G. Tang, T.Y. Ho, C. Jeandel and F.M.M. Morel (2005). Barium uptake and adsorption in diatoms. Geochimica Et Cosmochimica Acta, 69(11): 2745-2752

STEINBERG et al., VERTIGO, in preparation, Deep Sea Research II

STOLL H.M. and D.P. Schrag (2000). Are seawater Sr/Ca variations preserved in Quaternary foraminifera? *Geochimica and Cosmochimica Acta,* 1999.

STRASS et al., EIFEX, in preparation, Nature

STRASS V., B. Cisewski, S. Gonzales, H. Leach, K.-D. Loquay, H. Prandke, H. Rohr and M. Thomas (2005). The physical setting of the European Iron Fertilization Experiment 'EIFEX' in the Southern Ocean. Reports on Polar and Marine Research, 500: 15–49

STROOBANTS N., F. Dehairs, L. Goeyens, N. Vanderheijden and R. Vangrieken (1991). Barite Formation in the Southern-Ocean Water Column. Marine Chemistry, 35(1-4): 411-421

SUESS E. (1980). Particulate Organic-Carbon Flux in the Oceans - Surface Productivity and Oxygen Utilization. Nature, 288(5788): 260-263

TAKAHASHI T., S.C. Sutherland, C. Sweeney, A. Poisson, N. Metzl, B. Tilbrook, N. Bates, R. Wanninkhof, R.A. Feely, C. Sabine, J. Olafsson and Y. Nojiri (2002). Global sea-air CO2 flux based on climatological surface ocean pCO(2), and seasonal biological and temperature effects. Deep-Sea Research Part Ii-Topical Studies in Oceanography, 49(9-10): 1601-1622

TAKEDA S. (1998). Influence of iron availability on nutrient consumption ratio of diatoms in oceanic waters. Nature, 393(6687): 774-777

TAYLOR J.R., K.K. Falkner, U. Schauer and M. Meredith (2003). Quantitative considerations of dissolved barium as a tracer in the Arctic Ocean. Journal of Geophysical Research-Oceans, 108(C12):

TAYLOR S.R. and S.M. McLennan (1985). The continental crust: its composition and evolution. Blackwell Scientific Publications, 312pp

TENDAL O.S. and A.J. Gooday (1981). Xenophyophoria (Rhizopoda, Protozoa) in Bottom Photographs from the Bathyal and Abyssal Ne Atlantic. Oceanologica Acta, 4(4): 415-422

TOMCZAK M. (1981), A multi-parameter extension of temperature/salinity diagram techniques for the analysis of non-isopycnal mixing, Prog. Oceanog., 10: 147-171

TOMCZAK M. and D.G.B. Large (1989). Optimum Multiparameter Analysis of Mixing in the Thermocline of the Eastern Indian-Ocean. Journal of Geophysical Research-Oceans, 94(C11): 16141-16149

TOOLE J.M. and B.A. Warren (1993). A Hydrographic Section across the Subtropical South Indian-Ocean. Deep-Sea Research Part I-Oceanographic Research Papers, 40(10): 1973-2019

TRULL T., S.R. Rintoul, M. Hadfield and E.R. Abraham (2001-c). Circulation and seasonal evolution of polar waters south of Australia: Implications for iron fertilization of the

Southern Ocean. Deep-Sea Research Part Ii-Topical Studies in Oceanography, 48(11-12): 2439-2466

TRULL T.W. and L. Armand (2001-b). Insights into Southern Ocean carbon export from the delta C-13 of particles and dissolved inorganic carbon during the SOIREE iron release experiment. Deep-Sea Research Part Ii-Topical Studies in Oceanography, 48(11-12): 2655-2680

TRULL T.W., S.G. Bray, S.J. Manganini, S. Honjo and R. Francois (2001-a). Moored sediment trap measurements of carbon export in the Subantarctic and Polar Frontal Zones of the Southern Ocean, south of Australia. Journal of Geophysical Research-Oceans, 106(C12): 31489-31509

UTERMÖHL H. (1958). Zur Vervollkommnung der quantitativen Phytoplankton-Methodik. Mitt. Int. Ver. Limnol. 9, 1-38

VAN BEEK P., R. Francois, M. Conte, J.L. Reyss, M. Souhaut and M. Charette (2007). Ra-228/Ra-226 and Ra-226/Ba ratios to track barite formation and transport in the water column. Geochimica Et Cosmochimica Acta, 71(1): 71-86

VAN BEEK P., J.L. Reyss, P. Bonte and S. Schmidt (2003). Sr/Ba in barite: a proxy of barite preservation in marine sediments? Marine Geology, 199(3-4): 205-220

VAN ESPEN P. and K. Janssens (1992). "Spectrum Evaluation", Chap. 4 of the "Handbook of X-ray Spectrometry", (R. Van Grieken, A. Marcowicz, eds.), Marcel Dekker, New York, (ISBN 0-8247-8483-9)

VAN ESPEN P. (1984). Analytica and chimica Acta, 165:31-49

VAN HAREN H., C. Millot and I. Taupier-Letage (2006). Fast deep sinking in Mediterranean eddies. Geophysical Research Letters, 33, L04606, doi:10.1029/2005GL025367

VAN MOOY et al., VERTIGO, in preparation, Deep Sea Research II

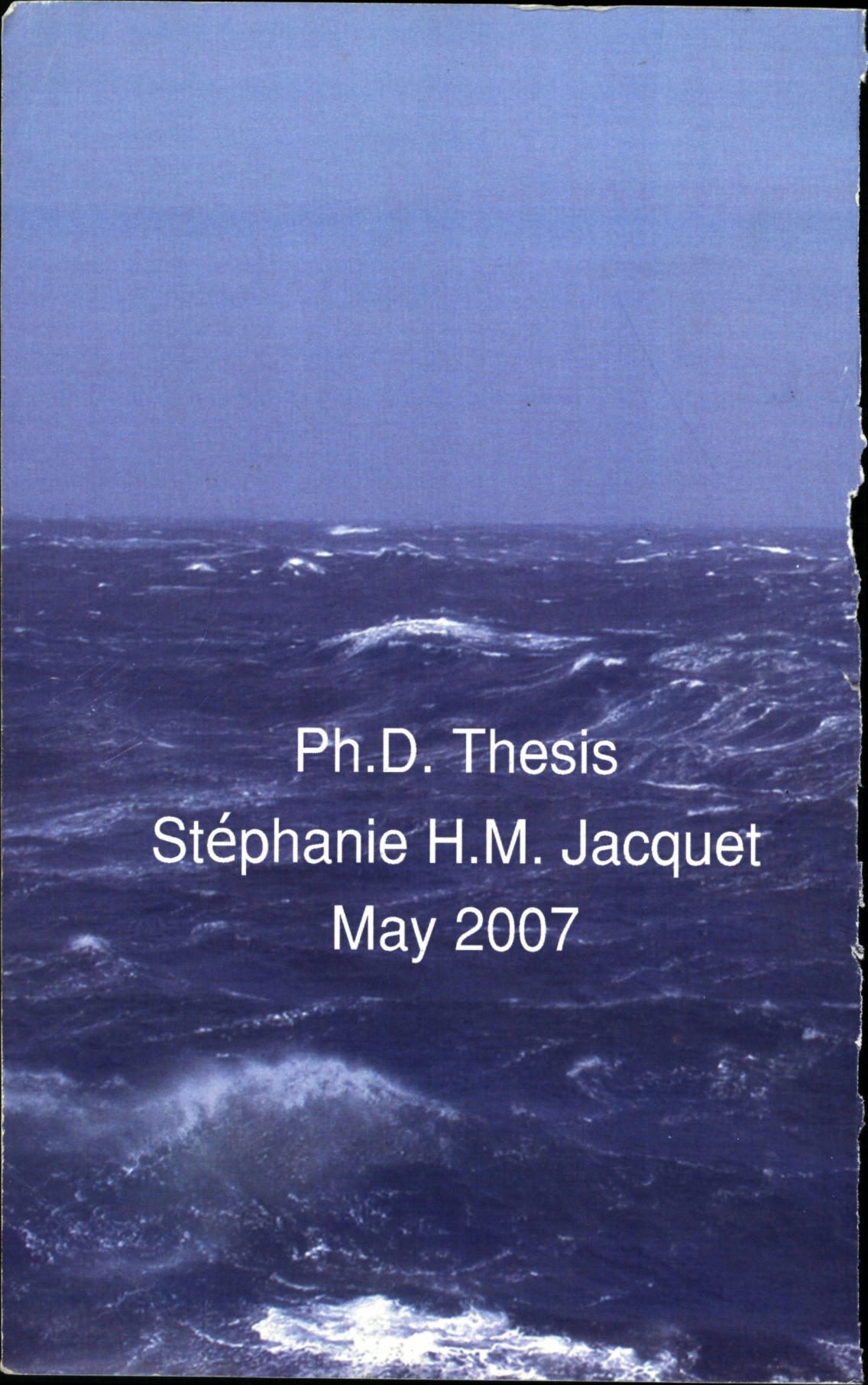
YAREMCHUK M., N.L. Bindoff, J. Schroter, D. Nechaev and S.R. Rintoul (2001). On the zonal and meridional circulation and ocean transports between Tasmania and Antarctica. Journal of Geophysical Research-Oceans, 106(C2): 2795-2814

YOU Y., J.R.E. Lutjeharms, O. Boebel and W.P.M. de Ruijter (2003). Quantification of the interocean exchange of intermediate water masses around southern Africa. Deep-Sea Research Part Ii-Topical Studies in Oceanography, 50(1): 197-228

YU E.F., R. Francois, M.P. Bacon, S. Honjo, A.P. Fleer, S.J. Manganini, M.M.R. van der Loeff and V. Ittekot (2001). Trapping efficiency of bottom-tethered sediment traps estimated from the intercepted fluxes of Th-230 and Pa-231. Deep-Sea Research Part I-Oceanographic Research Papers, 48(3): 865-889

WEBSTER, Methods in Geochemistry, in:A.A;Smales , L.R. Wagner (Eds), Interscience, new York, 1960, pp202-246

WOLGEMUTH K. and W.S. Broeker (1970). Barium in seawater. Earth and Planetary Sciences Letter, 8: 372–378


Ph.D. Thesis
Stéphanie H.M. Jacquet
May 2007